Design, Synthesis and Evaluation of Novel Chromone Analogues as Pancreatic Lipase Inhibitors for Obesity Treatment

THESIS

Submitted in partial fulfilment
of the requirements for the degree of
DOCTOR OF PHILOSOPHY

by

AUTI PRASHANT SAVLERAM
ID. No. 2019PHXF0057P

Under the Supervision of
Prof. PAUL ATISH TULSHIRAM

BITS Pilani
Pilani | Dubai | Goa | Hyderabad | Mumbai

BIRLA INSTITUTE OF TECHNOLOGY & SCIENCE, PILANI
PILANI-333031 (RAJASTHAN) INDIA

2024

Dedicated to My Family

DECLARATION

I hereby declare that the thesis work entitled **'Design, Synthesis and Evaluation of Novel Chromone Analogues as Pancreatic Lipase Inhibitors for Obesity Treatment'** is an original piece of research work carried out under the guidance of Prof. Paul Atish Tulshiram in the Department of Pharmacy, Birla Institute of Technology and Sciences (BITS PILANI), Pilani campus. This thesis has not been submitted by me for the award of any other degree of any other University/Institute.

Auti Prashant Savleram

2019PHXF0057P

Research scholar

BITS PILANI, Pilani campus

ACKNOWLEDGEMENTS

The Ph.D. journey was like a roller coaster ride for me with lots of excitement, numerous challenges, and uncertainties. Really, this journey has transformed me in many aspects, and I firstly thank almighty GOD for giving me the strength to fight and not letting me give up throughout my tenure. Another deepest gratitude towards my real god, i.e. my parents. What to say about them really, they have sacrificed a lot for our happiness and at whatever position I am today is because of them. The Ph.D. journey was tough but made easy with the support of many people who came into my life and made it possible. I would like to express my deepest gratitude towards such exceptional individuals.

First and foremost, I would like to thank my supervisor Dr. Atish Tulshiram Paul for his constant support, guidance, and encouragement. Sometimes, there were emotional breakdowns and continuous failures, but his trust and emotional support were memorable. We have achieved our expected research goals. In addition to this, he helped me become a good human being. He helped me to develop the skills to solve the problems. He has always given us the freedom to research, and I really appreciate it.

I am grateful to Prof. V. Ramgopal Rao, Vice-Chancellor, BITS Pilani, Pilani Campus, Prof. R.N. Saha and Souvik Bhattacharyya (Former Vice-Chancellor, BITS, Pilani), Prof. Sudhir Kumar Barai (Director, BITS Pilani, Pilani Campus), Prof. Ashoke K. Sarkar (Ex-Director, BITS Pilani, Pilani Campus), Prof. S. K. Verma (Dean, Administration), and Prof. Shamik Chakraborty (Associate Dean, AGSRD), Prof. Jitendra Panwar (Former Associate Dean, AGSRD) for their academic and administration support to perform this research work.

Besides my advisor, I would like to thank my Doctoral Advisory Committee members Prof. Hemant R Jadhav and Prof. S Murugesan. Their insightful comments and suggestions always broaden the perspectives related to research. My whole-hearted gratitude to Dr. Anil Jindal, Convener, Departmental Research Committee, Department of Pharmacy, BITS Pilani, Pilani Campus, Prof. Anil Gaikwad, Head, Dept. of Pharmacy, BITS Pilani, Pilani Campus and Prof. Hemant R. Jadhav (Former Head, Dept of Pharmacy, BITS Pilani, Pilani Campus) for their support and encouragement. My sincere thanks to all the faculty members for their encouragement throughout my association with Department of Pharmacy, BITS, Pilani.

I would like to acknowledge the Department of Science and Technology, Science and Engineering Research Board (DST-SERB) and Department of Science and Technology, Innovation in Science Pursuit for Inspired Research (INSPIRE) for providing the fellowship

I always believe that friendship is a relationship that is one of the purest relations. I really appreciate the support of many of the friends, namely Mr. Mukesh, Miss. Maravajjala Kavyasree, Mr. Imran Ansari, Mr. Amit Sharma. Also, another true relation, without her I can't imagine my life in BITS, thank you Miss. Tejashree Waghule, who came as a friend and became my life partner. Really Thank you to stand positively as a pillar in every situation. Thank you is really not enough for her support.

Two energetic senior-come-friend, Mr. Ginson George and Miss. Pracheta Sengupta who were always there to look towards me. Thank you Ginson sir for supporting me in lab related activities and for taking care of me. Pracheta Ma'am really thanks for your patient teaching, only because of you it was possible for me to get real understanding of the various studies.

I would like particularly to acknowledge the contribution of my lab members Mrs. Nisha Yadav, Mrs. Karnam Sriravali, Mr. Utkarsha Jagtap, Mr. Samarth Dwiwedi, Miss. Lavanya B for their support. Also, how to forget our M. Pharmacy students, starting with Mr. Arjun Jeswani, Miss. Radhika Prabhu (Energetic Bestiee), Miss. Vijeta Kumari, Miss. Shweta Shinde (Our Placement Co-ordinator) and Miss Sakshi Jagetiya (Bestiee) for their friendly gesture and for making the lab energetic.

I would like to thank the Central Animal facility members, especially Dr. Sushil K Yadav, (Senior Vet. In-charge) and staff members, Mr. Vishal, Mr. Shyam, Mr. Mukesh for their assistance during my work and their friendly behaviour.

I am extremely lucky to have a great company of research scholars of the Department of pharmacy and chemistry. It was a great opportunity to observe and learn a lot from them and I sincerely acknowledge to all.

I am thankful to the administrative staff, Mr. Puran Singh, Mr. Vikas Kumar Agrawal, Mr. Laxman Kumar, Mr. Ram Suthar, Mr. Naveen Rana, Mr. Tarachand Saini, Mr. Mahender, Mr. Abhishek and Mr. Sandeep Ruidas for their continuous support.

Auti Prashant Savleram Sulochana

ABSTRACT

Obesity is a chronic relapsing condition characterized by the excessive deposition of dietary fat in the body and it is now considered as one of the most critical global health issues. Surprisingly, the demography of obese and overweight population is higher as compared with the malnutrition population. Its prevalence is increasing day by day at an alarming rate. Looking at such a pandemic nature of obesity, a proper strategy is essential to combat the current situation. Pharmacotherapy of obesity consists of drugs that act on various targets. Majority of these drugs act on the central nervous system (CNS), resulting in numerous side effects. Inhibition of fat digestion is one of the peripheral targets. For the digestion of dietary fat, pancreatic lipase (PL) is the principal enzyme responsible for 56% of dietary fat digestion. Thus, through inhibition of PL, obesity condition can be prevented by inhibiting further fat deposition in the body.

For the development of small molecule inhibitors, natural products are always an inspiration and numerous phytochemicals have been identified for their PL inhibitory potential. These can be divided into various classes such as polyphenols, saponins, alkaloids, benzofurans, etc. Among those chemical classes, majority of the PL inhibitors were found to be of polyphenolic origin (42% of total natural PL inhibitors). Many of these polyphenolic PL inhibitors are found to have a chromone ring as a bioactive heterocycle. While a vast amount of literature is available on chromone-based natural PL inhibitors, there is no single report on synthetic chromone-based PL inhibitors with a rational design approach. Also, looking at the importance of heterocyclic scaffolds, many of the heterocycles, namely indole, carbazole, thiazolidinedione, quinazolinone, and coumarin have been utilized for the development of novel PL inhibitors. Looking at the potential of chromone heterocycle and to fill the gap in PL inhibitory research, in this study we aimed to design and synthesize chromone-based PL inhibitors, with their *in vitro* screening, followed by *in vivo* anti-obesity testing of the topmost analogue.

For the design of novel PL inhibitors, chromone (being an electron-rich moiety) was fixed for either interacting with lid domain or Arg256 amino acids. Further, the acrylate fragment was utilized to interact with Ser152 (catalytic amino acid). Another aromatic or heteroaromatic ring was attached with the spacer (linker length of 1/2/ 3 carbon atoms). Such designed prototypes were docked in the PL active site (PDB ID: 1LPB). The results were encouraging in terms of docking score and amino acid interactions for the prototypes with the 1 and 2

carbon atom linkers (n =1,2). The prototype with the linker length of 3 carbon atoms (n =3) failed to exhibit significant interactions with active site amino acids. By considering such observations, a series I of **24** analogues (with linker length of 1 carbon atom) was synthesized through a suitable synthetic scheme. Among these analogues **5ad** and **5am** were the most potent with IC$_{50}$ values of 5.82 ± 0.933, 5.16 ± 0.287 µM, respectively. Through enzyme kinetics study, the analogue **5am** was found to exhibit a competitive mode of inhibition with K_i value of 2.003 µM. The fluorescence quenching study also confirmed the binding of analogue **5am** at a single binding site of PL enzyme. The analogue **5am** was further subjected to molecular dynamics simulation for 100 ns. It was found to be stable with RMSD value in the range of 2.4-6.4 Å.

Further, the series I analogues were optimized by increasing the linker length to 2carbon and 3carbon. It was hypothesized that increased spacer distance would lead to better opportunities for both chromone and aromatic/heteroaromatic moieties for their respective interactions at the PL active site. Through *in vitro* results the linker length of 2 carbon atoms was found to be efficient with analogue **6aa** (IC$_{50}$ of 16.01 ± 0.274 µM) being more potent as compared to the analogues with linker length of 1 carbon atom (**5aa**; IC$_{50}$ = 25.27 ± 0.550 µM) and 3 carbon atom (**8aa**; IC$_{50}$ = 31.49 ± 1.363 µM). Thus, series II was synthesized by keeping the linker length of 2 carbon atoms with various substituents on chromone and aromatic moieties. Among the **29** analogues of series II, **6fj** and **6gj** were found to exhibit potential PL inhibitory activities of 4.92 ± 1.398, 4.23 ± 0.747 µM, respectively. With K_i value of 1.601 µM, the analogue **6gj** was also inhibited PL with competitive mode. Through molecular dynamics simulation study, the protein was found to deviate with maximum RMSD of 5 Å and ligand RMSD was found to deviate up to 6 Å till 60 ns, that was found to elevate from 60-100 ns. Such results explain moderate stability of the complex and hence further optimization will lead to better stability of the complex.

Finally, the optimized III series was developed by modifying the 2-carbon atom linker (n =2) of series II analogues (**6aa-6gj**). The linker was modified by the substitution of an aromatic moiety and a keto substituent. Such optimization was performed to maximize the interactions (aromatic and H-bonding) and binding of inhibitors at the PL active site. Delightedly, the proposed prototype analogue **10aa** was found to bind at the active site more efficiently, as evidenced by the good MolDock score of -168.33 kcal/mol. With such positive results, we have synthesized a series of **18** analogues with EDG, EWG and bulkier substituents. A total of 6 analogues were found to exhibit IC$_{50}$ values in the range of 1.24 - 2.76 µM. The

analogue **10gb** was the most potent among all the series of analogues with IC_{50} of 1.24 ± 0.296 µM. The analogue **10gb** also exhibited fluorescence quenching with a static mechanism and was capable of binding PL at one binding site. Through enzyme kinetics studies, analogue **10gb** was found to exhibit K_i value of 0.554 µM with a competitive nature of inhibition. In molecular dynamics simulation of 100 ns, the ligand RMSD was found to deviate from 5-8 Å. Also, the protein molecule exhibited the RMSD value less than 4.5 Å. Such RMSD values are within the range, that proves the stability of the ligand-protein complex.

Finally, a total of 6 best potent PL inhibitory analogues from all three series were screened for in silico ADMET prediction using Swiss ADME and ProTox-2 web servers. Many of the analogues including topmost analogue **10gb** were found to be metabolically stable and devoid of any toxicities. Further, the analogue **10gb** was tested for *in vivo* anti-obesity activity, utilizing HFD-induced obesity model in mice. The model was developed by feeding HFD to *Swiss albino* mice and the induction of obesity was checked by weekly body weight and serum triglyceride, cholesterol, HDL cholesterol measurement. Through OTTT analysis, doses of 10 mg/kg (LD) and 20 mg/kg (HD) of **10gb** were selected for the treatment of HFD-induced obese mice. After the induction of obesity, 4-week treatment of **10gb** (HD, LD) and orlistat (10 mg/kg) was initiated. After the 4-week treatment, the weight of treatment groups (**orlistat** and **10gb**) was found to be lower than the DC group. Also, there was a normalization of spiked levels of triglycerides, total cholesterol and LDL cholesterol in the case of treatment groups. In addition to it, the triglyceride excretion caused by **10gb** was also proved through faecal triglyceride measurement, confirming its PL inhibitory action. After the histopathological examination of liver and adipose tissue, hepatic fibrosis and lipid accumulation with the increase in size of adipocytes were observed for DC group (HFD without treatment). Such changes were found to normalized in case of orlistat and **10gb** (HD) treatment groups. Such results proves equal effectivity of analogue **10gb** (10 mg/kg, 20 mg/kg) as orlistat (10 mg/kg) in the management of the obesity condition.

Table of Contents

List of Figures

pharmacophoric features

List of Tables

List of Schemes and Formulae

#	Title	Page No.
Scheme 2.1	Synthesis of 3-Formylchromone via Vilsmeier-Haack reaction	20
Scheme 4.1	Synthesis of designed acrylate linked chromone analogues (**5aa-5fm**)	63
Scheme 5.1	Synthesis of designed Chromone-3-acrylic acid ester analogues (**6aa-gj**, **8aa-ac**)	91
Scheme 6.1	Synthetic scheme for acrylate linked chromone analogues (**10aa-ka**, **10ab-gb**)	120
Formula 3.1	Percentage inhibition	54
Formula 3.2	Stern−Volmer equation	54
Formula 3.3	Modified Stern−Volmer equation	55
Formula 7.1	Low-density lipoprotein-cholesterol	146

List of Abbreviations and Symbols

%	Percentage
% CV	Percent coefficient of variation
% RSD	Percent relative standard deviation
% v/v	Percent volume by volume
% w/v	Percent weight by volume
Å	Angstrom unit
°C	Degree celsius
δ	Delta
μg	Microgram
μL	Microliter
μM	Micromolar
4-NPB	4-nitrophenyl butyrate
5-HT_{2C}	5-Hydroxytryptamine type 2C receptor
ADMET	Absorption, Distribution, Metabolism, Excretion and Toxicity
AOM	Anti-Obesity Medication
BBB	Blood Brain Barrier
BMI	Body Mass Index
CB_1	Cannabinoid type 1 receptor
CHARMM	Chemistry at Harvard Macromolecular Mechanics
CNS	Central Nervous System
Conc.	Concentration
CYP	Cytochrome P
Da	Dalton
DCM	Dichloromethane
DMF	Dimethyl formamide
DMSO	Dimethyl sulfoxide
e.g.	Example
ESI	Electrospray ionization

eV	Electron volt
FDA	Food and drug administration
FTIR	Fourier Transform Infrared
G	gram
GABA	Gamma aminobutyric acid
GI	Gastro-Intestinal
GLP-1	Glucagon like peptide type 1 receptor
h	Hour
HCl	Hydrochloric acid
HDL	High-density lipoproteins
HFD	High Fat Diet
HPLC	High Performance Liquid Chromatography
HR-MS	High Resolution Mass Spectrometry
i.e	That is
IC_{50}	Half maximal inhibitory concentration
ICH	International Conference on Harmonization
IEAC	Institutional animal ethics committe
Kcal/mol	Kilocalorie per mole
Kg	kilogram
KOH	Potassium hydroxide
LCMS	Liquid Chromatography Mass Spectrometry
LD_{50}	Half maximal Lethal Dose
LDL	Low-density lipoproteins
m.p.	Melting point
MD	Molecular Dynamics
mg	Milligram
min	Minutes
mL	Millilitre
mM	Millimolar

MM2	Molecular Mechanics 2
MUP	Methoxyundecyl phosphinic acid
ng	Nanogram
NMR	Nuclear Magnetic Resonance
NP	Natural Product
NPD	Normal Pellet Diet
NPT	No. of atoms, Pressure and Temperature
ns	not significant
NVT	No. of atoms, Volume and Temperature
OTTT	Oral Triglyceride Tolerance Test
PDB	Protein Data Bank
Pgp	P-glycoprotein
PL	Pancreatic lipase
RMSD	Root Mean Square Deviation
rpm	Rotations per minute
RSD	Relative Standard Deviation
RT	Room Temperature
S.E.M	Standard error of mean
SD	Standard Deviation
TC	Total cholesterol
TCM	Traditional Chinese Medicine
TEA	Triethylamine
TG	Triglycerides
THF	Tetrahydrofuran
TLC	Thin Layer Chromatography
US	United States
UV	Ultraviolet
WHO	World Health Organization
WHR	Waist-Hip Ratio

CHAPTER 1

INTRODUCTION

CHAPTER 1

1. Introduction

1.1. Obesity

Obesity is a condition in which there is fat deposition to such an extent that it can have potential effects on health. According to the National Institute of Health (NIH), overweight and obesity is an excessive accumulation of fat (globally, regionally and in organs) that increases risk for adverse health outcomes. It has grown up to epidemic proportions, as over 4 million people die each year because of being obese. Out of the global population, more than 1.9 billion adults are overweight and 650 million are obese. As per the reports of the year 2020, 39 million children under the age group of 5 were either overweight or obese. As per WHO European Regional Obesity Report 2022, almost 60% of adults and one in three children are affected by overweight and obesity in the European region.[1] More than 135 million Indians are affected by obesity and related complications. According to ICMR-INDIAB study in 2015, the prevalence rate of obesity varies from 11.8% to 31.3%.[2] It is also forecasted that the prevalence of obesity in India will triple from 2010 to 2040.[3]

There is a high risk of obesity and its associated comorbidities, including type 2 diabetes, hypertension, ischemic heart disease, fatty liver disease, cancer, etc.[4,5] Such problems are more in developing countries due to the consumption of food with high calorific value (i.e. unhealthy food habits), sedentary lifestyle, lack of financial and health care support, etc.[6,7] Various risk issues associated with obesity are outlined in **Figure 1.1.** Also, the impact of obesity on non-communicable diseases like viral infection has been identified. Recently, in the case of obese population, the rate of patients hospitalised and ill due to COVID-19 was found to be significantly high.[8,9] Overweight and obesity are determined using body mass index (BMI), independent of the stature of the population. Globally, a BMI > 30 kg/m^2 defines generalized obesity, BMI > 40 kg/m^2 denotes extreme obesity.
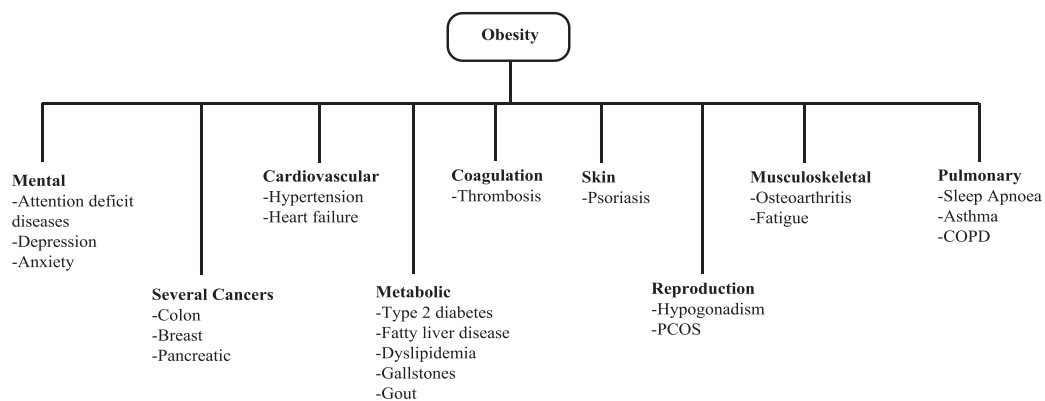
Figure 1.1. Risk factors associated with obesity

CHAPTER 1

1.1.1. Causes of Obesity

It is a known fact that obesity is caused due to an imbalance between energy consumption and energy expenditure, but the etiology of obesity is highly complex with genetic, physiological, environmental, psychological, socio-economic factors involved.[10,11] As detailed in **Figure 1.2**, there are many causes of obesity including food environment, decreased physical activity, infection, endocrine disruptors, drug-induced weight gain, sleep debt, etc. Consumption of diet enriched in fat is the main cause of obesity, along with decreased physical activities.

Apart from energy intake and expenditure, the weight gain is also contributed by several commonly used medications including psychotropic medications, diabetic treatments, antihypertensives, steroid hormones & contraceptives, antihistamines, protease inhibitors, etc.[12] There is no underlying mechanism proven for drug-induced obesity.
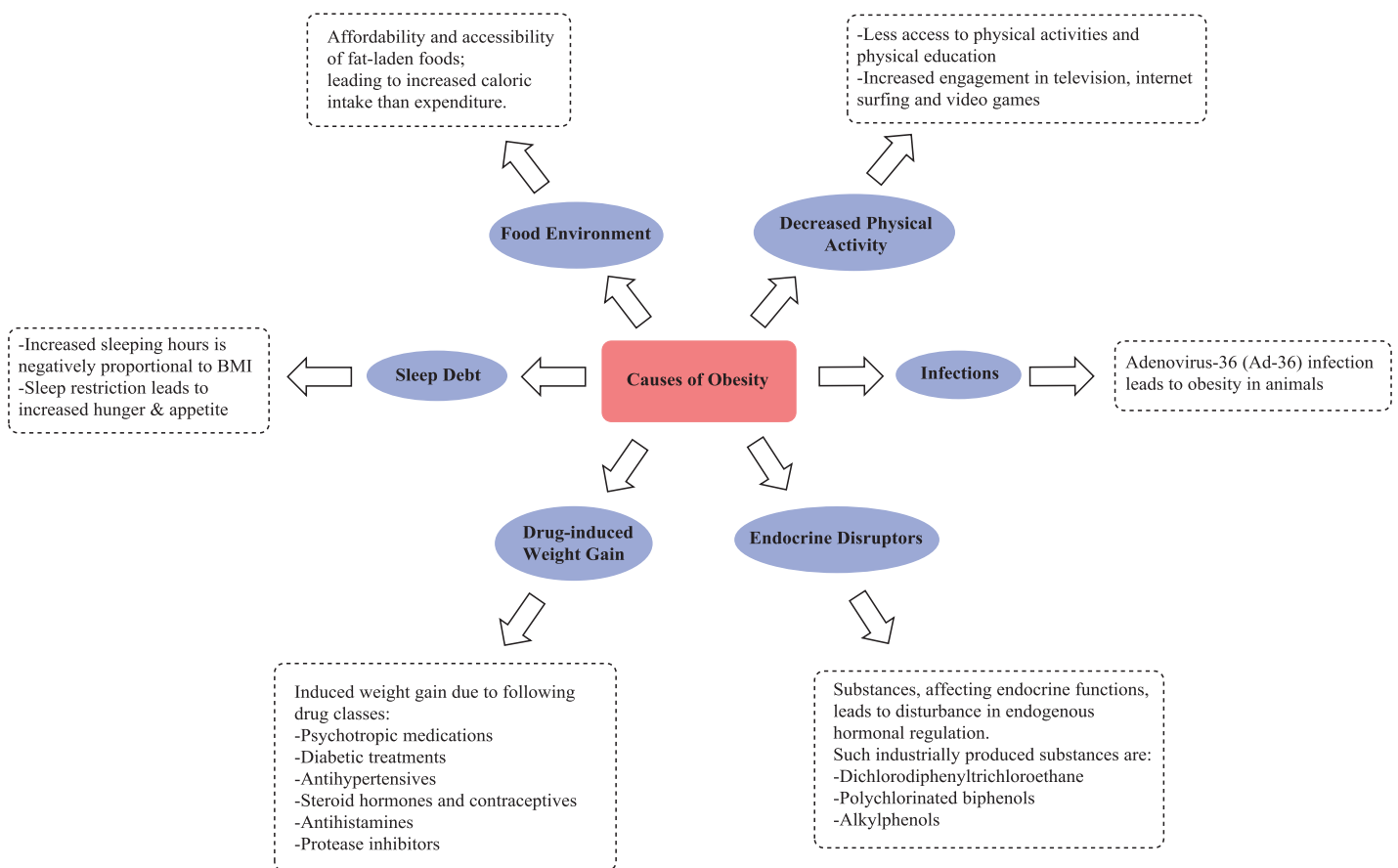
Figure 1.2. Various factors responsible for obesity

It is only an observation that the long-term treatment of above-mentioned classes of drugs lead to obesity. Sleep debt is also associated with weight gain, as studies have shown the

negative correlation of extended sleep on BMI.[13,14] Some industrially produced substances such as dichlorodiphenyltrichloroethane, some polychlorinated bisphenols, etc. can affect the endocrine function, leading to hormonal imbalance can also cause obesity.[15] The studies on animals, has proven that the Adenovirus-36 (Ad-36) infection leads to obesity. [16]

1.1.2. Prevention and Treatment of Obesity

As the obesity condition is so prevalent and difficult to treat, it is important to prevent the condition rather than treatment. For the prevention of overweight and obesity, one should eat according to their nutritional needs with regular physical exercise and check weight regularly. For nutrition, the consumption of low energy density food (food with high water and fibre content) should be more as compared with high energy density ones (food with high fat and sugar). For subjects, who are unable to control their weight through diet and exercise solely, various treatment options are available that are listed below:

A) Dietary Therapy

It is a long-term therapy, carried out by the counselling of nutritional specialist. The main aim of the programme is to reduce fat and carbohydrate consumption, while providing with necessary nutritional supply. For body weight reduction, the energy deficit of around 500-600 kcal/day is required, that will result in 0.5 Kg/week of weight loss.

B) Increased Exercise

For effective weight loss, more than 150 min/week of exercise is required with energy consumption of 1200-1800 kcal/week. [17]

C) Behaviour Modification

Behaviour modification may help the obese and overweight individual through counselling, self-monitoring, stress management, stimulus control, reinforcement techniques, rewarding changes in behaviour, social support and relapse prevention training. [18]

D) Anti-Obesity Medications

Anti-Obesity medications (AOMs) are required for those subjects who are unable to manage the weight using lifestyle modifications such as exercise, diet, behaviour modification or combination of all. There are limited number of drugs that are in clinical use and many of the AOMs are withdrawn due to life threatening adverse effects. Currently, Phentermine, Semaglutide, Liraglutide, Phentermine-Topiramate combination, Naltrexone-Bupropion combination and Orlistat are the drugs that are clinically available as AOM. Except Orlistat,

all the listed drugs target the CNS pathways. The AOMs and lifestyle modification should be combined to experience increased efficacy of the treatment.

E) Surgical Intervention

In case of extremely obese patients, the surgical intervention is more effective for body fat reduction, improvement in obesity related disease and reduction in mortality rate. Surgical treatment is indicated according to BMI of patients, that is as follows:

- Grade III obesity: BMI $\geq$ 40 kg/m^2
- Grade II obesity: BMI $\geq$ 35 kg/m^2 and with significant co-morbidities
- Grade I obesity: BMI in between 30-35 kg/m^2, in patients with Type-2 diabetes (Special case)

1.1.3. Pharmacotherapeutic Targets for Treatment of Obesity

Obesity condition is associated with the feedback system in the body. Hence, the individual sites in such feedback system serves as a target for obesity treatment. Medicinal agents that have been investigated, constitutes lipase inhibitors [19,20], mitochondrial uncouplers,[21,22] sympathomimetics, seretonergic agonists [23], and cannabinoid receptor agonists. [24,25]

The investigational anti-obesity agents are divided into following categories[26] namely,

A) CNS agents (Affecting neurotransmitters and neural ion channels)

- Antidepressants: Bupropion
- Selective 5-HT$_{2C}$ agonist: Lorcaserin
- antiseizure agents: Topiramate
- Dopamine antagonists: Ecopipam
- Cannabinoid receptor-1 (CB-1) antagonists: Rimonabant

B) Agents affecting leptin/insulin/central nervous system pathways

- Leptin analogues
- Leptin transport and/or Leptin receptor promoters
- Ciliary neurotrophic factor, neuropeptide Y and agouti-related peptide antagonists
- Pro-opiomelanocortin and cocaine & amphetamine regulated transcript promoters
- α-melanocyte-stimulating hormone analogues: MC4-NN2-0453
- Melanocortin-4 receptor agonists: Setmelanotide
- Agents that affect insulin metabolism/activity: PPAR- γ antagonists

C) Gastrointestinal-neural pathway agents

- Agents that increase cholecystokinin activity
- Agents increasing glucagon-like peptide-1 (GLP-1) activity
- Agents increasing protein YY3-36 activity
- Ghrelin antagonists
- Amylin analogues: Cagrilintide

D) Agents increasing resting metabolic rate

- Selective β-3 stimulators/agonist
- Uncoupling protein homologues
- Thyroid receptor agonists

E) Agents blocking nutrient absorption

- Pancreatic Lipase inhibitors: Orlistat

F) Other agents
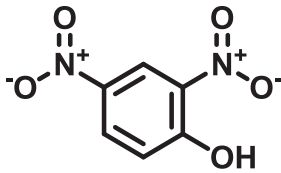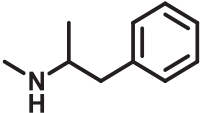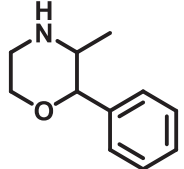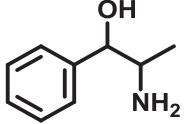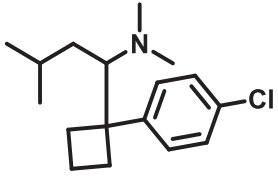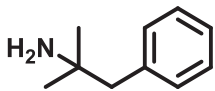
- Melanin concentrating hormone receptor (MChR) antagonists
- Phytostanol analogues
- Amylase inhibitors
- Corticotropin releasing hormone agonists
- Fatty acid synthesis inhibitors

1.1.4. Anti-obesity Medications: Approval and Current Status
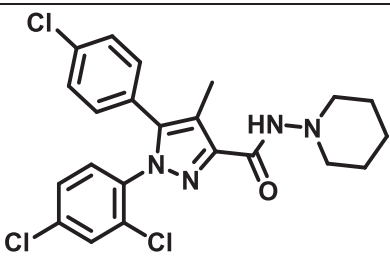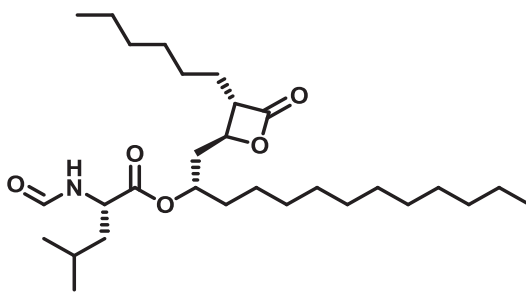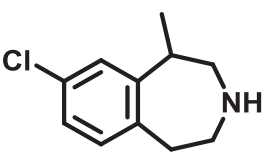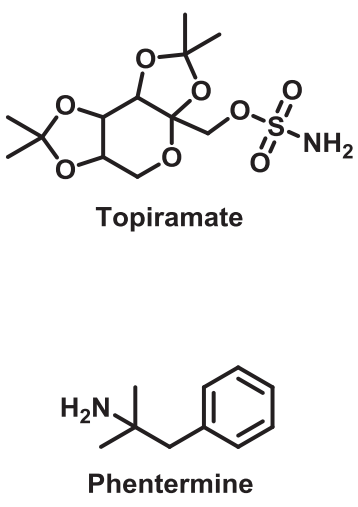
Pharmacotherapy of obesity has a very long history, as many of the promising drugs were withdrawn due to adverse effects. Various anti-obesity medications (AOMs) such as, amphetamines, thyroid hormones, dinitrophenol (DNP) and rainbow pills were withdrawn due to serious adverse effects, shortly after their approval. **Table 1.1** highlights the list of approved AOMs along with their adverse effects, structure, category and approval period.
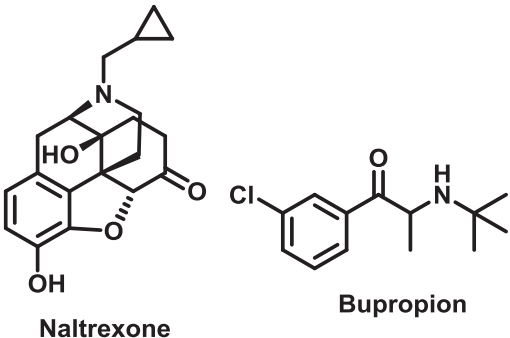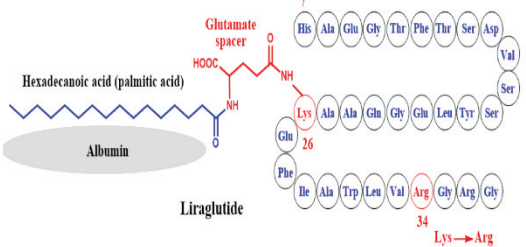
Table 1.1 List of approved AOMs with their structures and adverse effects [27]

Drug	Structure	Approval	Side effects
Mitochondrial uncoupler			
DNP		1933–1938 (USA)	Hyperthermia, tachycardia, fever, tachypnoea, death
Sympathomimetics			
Methamphetamine		1947–1979 (USA)	High risk for abusiveness and addiction
Phenmetrazine		1956–present (USA)	Nausea, diarrhoea, dry mouth
Phenylpropanolamine		1960–2000 (USA)	Haemorrhagic stroke
Sibutramine (10mg, OD)		1997–2010 (USA, EU)	Non-fatal myocardial infarction and stroke (in individuals with pre-existing CVD)
Phentermine (15–30mg, OD, oral)		1959–present (USA, only for short-term use)	Palpitations, elevated blood pressure
Polypharmacy			
Rainbow pills	Amphetamines, Diuretics, Laxatives, Thyroid hormones Digitalis, Benzodiazepines, Barbiturates, Potassium, Corticosteroids, Antidepressants	1940-1960 (USA)	Insomnia, palpitations, anxiety, increase in heart rate and blood pressure, death

CB1 receptor blocker			
Rimonabant (20mg, OD)		2006–2009 (EU)	Depression, suicidal ideation
Pancreatic lipase inhibitor			
Orlistat (120mg TID, oral)		1999–present (USA, EU)	Liver injury, gastrointestinal symptoms
5-HT$_2$C serotonin agonist			
Lorcaserin (10mg, BID, oral)		2012–2020 (USA)	Depression, suicidal ideation, palpitations, gastrointestinal symptoms, increased cancer risk
Sympathomimetic/anticonvulsant			
Phentermine / topiramate ER (with titration) (15mg/92mg, OD, oral)	**Topiramate** **Phentermine**	2012–present (USA)	Depression, suicidal ideation, cardiovascular events, memory loss, birth defects

Opioid receptor antagonist/dopamine and noradrenaline reuptake inhibitor		
Naltrexone SR / bupropion SR (with titration) (32mg/360mg, BID, oral)		2014–present (USA, EU)	Seizures, palpitations, transient blood pressure elevations
GLP1R agonists		
Liraglutide (with titration) (3.0mg, OD, subcutaneous injection)		2014–present (USA, EU)	Nausea/vomiting, diarrhoea, constipation, pancreatitis, gallstones
Semaglutide (2.4mg, once weekly, subcutaneous injection)		2021 (USA)	Nausea/vomiting, diarrhoea, constipation

1.2. Targeting Pancreatic Lipase for Obesity Treatment

1.2.1. Role of PL in Lipid Digestion

In the western world, dietary fat is an important energy source, constituting about 30-40% of daily caloric intake.[28] Almost 90% of the dietary fat comprises of TAG that get digested into monoacylglycerol and free fatty acids, followed by its absorption into the systemic circulation (**Figure 1.3**). In 1849, it was proved that the pancreas is responsible for the digestion of fats due to its ability to hydrolyze the ester of long chains of fatty acid, chemically known as triacylglycerol (TAG). It was also discovered that to get absorbed into the systemic circulation (through penetration of the intestinal barrier) and to be used as an energy source, TAG should get hydrolyzed into free fatty acids.[29] Lipases are a group of

enzymes from the carboxylesterase class, responsible for TAG hydrolysis. PL also known as TAG acyl hydrolase is an important fat-digesting enzyme, responsible for almost 56% of dietary fat digestion.[30] PL is stored in zymogen granules, present in the apical pole of acinar cells and gets secreted based on the body's demand along with pro-colipase.

The effective digestion of dietary lipids starts in the stomach where the preduodenal lipases play a role. The amount of lipids digested by preduodenal lipases is less. Such partially digested emulsion form is then emptied in the duodenum, where it is mixed with the pancreatic juice having PL enzyme. In the duodenum, the PL hydrolyzes the ester linkage present in the TAG, leading to the formation of monoacylglycerol and free fatty acid molecules.[31] The bile salts are then secreted by the gall bladder, that helps in the emulsification of digested fatty acids following which the digested fatty acids gets transferred into the small intestine followed by its systemic absorption.[32] After the resynthesis into TAG, it will get deposited in the form of adipose tissue. For energy expenditure, the deposited TAG will then hydrolyze and the obtained fatty acid molecule will be utilized for ATP generation. The excessive deposition of TAG will lead to overweight and obesity. The detailed mechanism of TAG digestion is described in **Figure 1.3**.
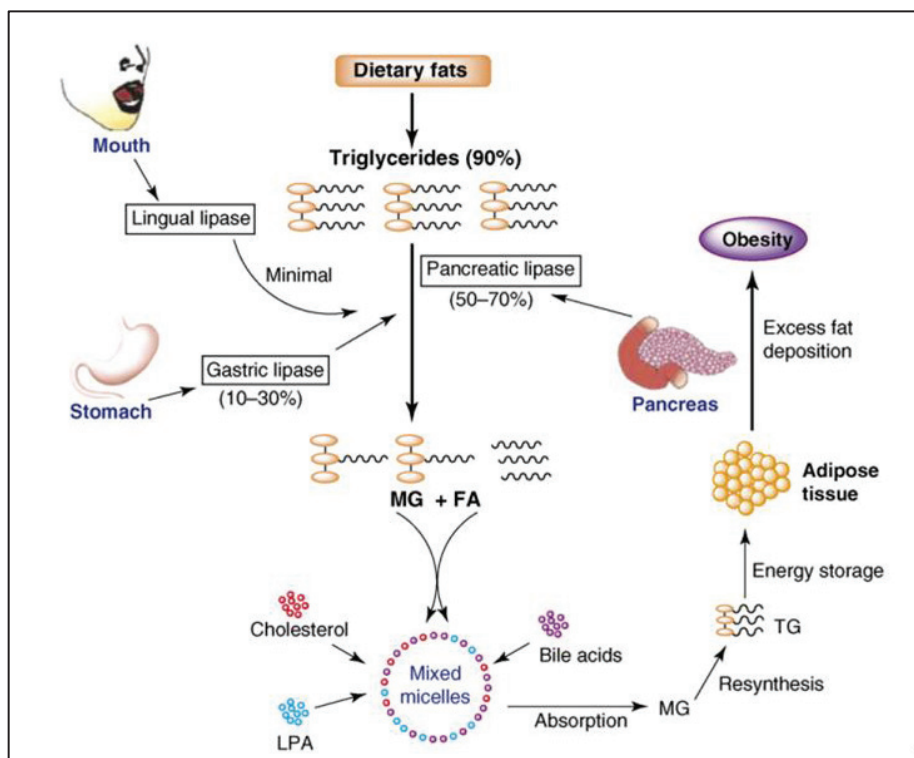
Figure 1.3. Mechanism of pancreatic lipase inhibition for obesity treatment

1.2.2. Structure of Human Pancreatic Lipase (HPL)

The structure of HPL was first solved by Winkler *et al.*, with the observation that the HPL consists of a large *N*-terminal domain with 1-336 amino acid residues and smaller C-terminal domain with 337-449 amino acids. [33] The primary structure was determined by the analysis of cDNA clones, isolated from human pancreas cDNA library. The human protein showed 86% and 68% homology with porcine and canine PL, respectively. For the determination of X-ray structure of HPL, crystallization was performed using the hanging-drop vapour-diffusion method.

It is proven from the studies that the catalytic Serine is prevented from reaching the solvent surface by one or more loops that should be rearranged for an easy access to the substrate molecule. To study the catalytic site of PL enzyme, a phosphonate inhibitor with C11 alkyl chain was synthesized by Tilbeurgh *et al.*[34] It was then followed by the formation of single crystal of PL-colipase complex, that inhibited by C11 alkyl phosphonate. The crystals were found to diffract X-rays with 2.46 Å resolution. After final refinement to the structure, the protein was found to be surrounded by 1 covalent inhibitor (two enantiomers), 1 Ca^{+2} ion, 293 water molecules and 5 detergent molecules. The PL enzyme was found to exist in two conformations, i.e., open and closed form (**Figure 1.4**) and for the catalytic action, the open conformation is required. The mechanism of opening and closing is still unknown.
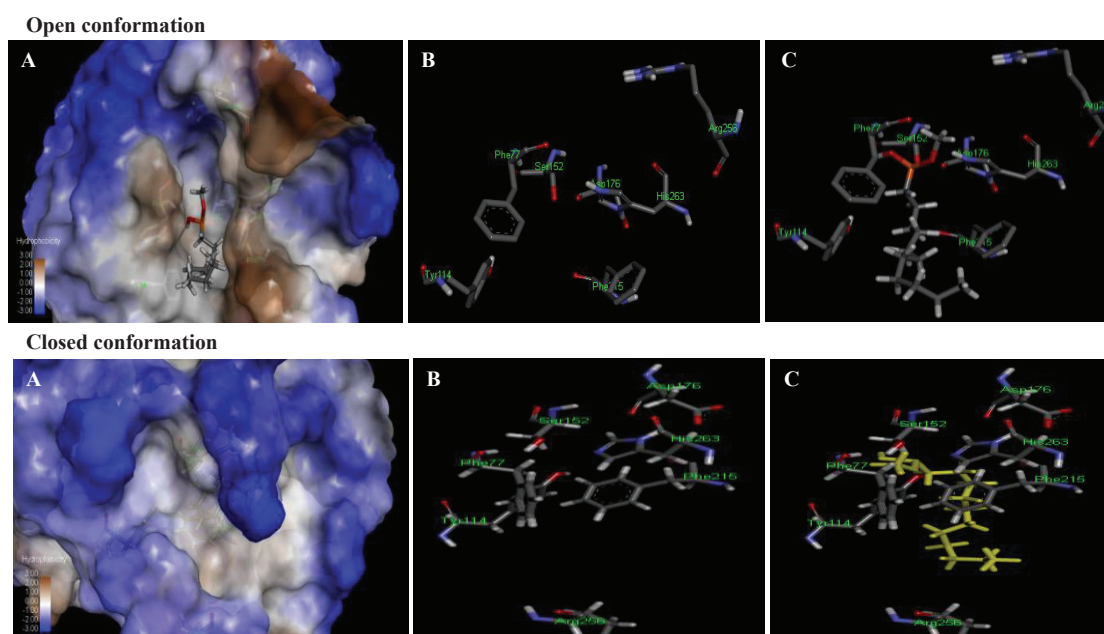
Figure 1.4. Representation of open and closed lid forms of human PL. A – hydrophobic surface representing the open and closed lid conformations (in brown); B – Amino acid alignment in the active site; C-ligand present in the active site, yellow represents the ligand in active site (represent the steric hindrance by closed conformation)

The structure of TAG consists of a glycerol molecule on which 3 fatty acid molecules forms an ester linkage. The PL enzyme catalyses the breakdown of such ester linkage, leading to the generation of fatty acids. For such catalytic function, the PL consists of catalytic triad with **Serine152–Histidine263–Aspartate176** amino acids. This triad is conserved throughout the lipase family and it is same as that present in other serine proteases. As the endogenous substrate (TAG) reaches PL enzyme, following changes appears [35]:

A) Without the presence of any substrate, the PL enzyme will be in closed conformation. In such conformation the *N*-terminal domain (commonly known as Lid domain) covers the active site of an enzyme. The β5 domain helps in maintaining the loop to be closed, *via* van der Waal's interactions.

B) After the contact of TAG molecule, the β5 domain moves away from the lid domain, leading to its opening (open conformation).

C) As β5 domain moves, it will create the oxyanion hole, that helps in the stabilization of an intermediate formed during the reaction. It is constituted by aromatic (Phe77, Tyr114 and Phe215) and aliphatic amino acids (Pro180, Leu202, Ile209), thereby making it hydrophobic.

D) The carbonyl carbon is then facilitated by two acyl-binding sites in β9 domain to react with Ser152 amino acid. One acyl side chain will interact with the oxyanion hole and the other side chain with the hydrophobic groove formed by lid domain amino acids (residues 251-259) and Ile78 of β5 domain. Such domino process results in the hydrolysis of triacylglycerol moiety. It was observed that the contact of Leu213 and Phe215 of β9 domain increases the stabilization of lipid-hydrolysis product.

1.2.3. PL Inhibition in the Treatment of Obesity

PL is the principal enzyme responsible for fat digestion. Thus, by its inhibition, TAG will remain intact and will not get absorbed through small intestine due to its larger size. The unabsorbed TAGs will then get excreted through feces. Hence, through the use of PL inhibitors, there will not be any build-up of TAG, and subsequent obesity condition. The PL inhibitor treatment along with physical exercise may lead to combustion of deposited fat and further complete cure from the obesity condition.

Orlistat is the only drug approved by US-FDA for the management of obesity, that acts *via* PL inhibitory mechanism. [36,37] As shown in **Figure 1.5**, the structure of orlistat consists of a lactone ring, attached with two long chain alkyl groups. The highly strained lactone ring

helps in covalent modification of catalytic Ser152 amino acid residue, present at the active site of PL enzyme. Orlistat is available with brand names of **ALLI** and **XENICAL** as 60 mg or 120 mg capsule, that needs to be taken three times a day, after meal. It is advised to take the drug along with multivitamins and fish oil, as orlistat tend to inhibit the absorption of certain fats and fat soluble vitamins.[38]

Another molecule, having benzoxazinone scaffold has completed its phase III clinical trial and has been approved by Japanese Ministry of Health, Family and Welfare in year 2013.[39,40] Till now there are no reports available on its US-FDA approval.

Orlistat
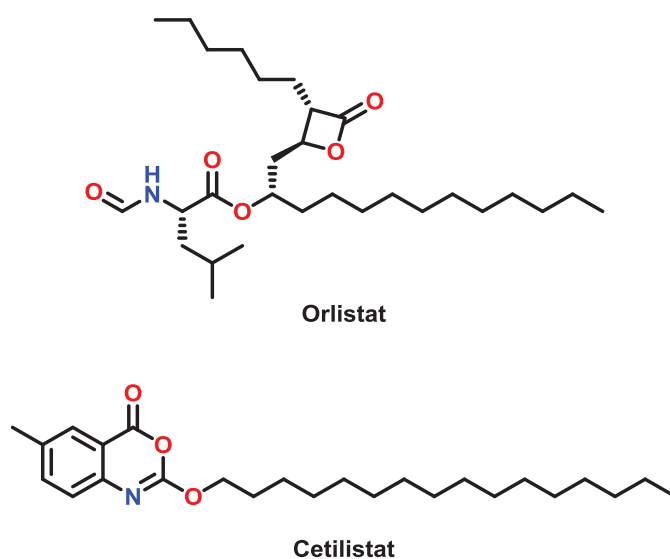
Cetilistat

Figure 1.5. Structure of orlistat and cetilistat

References

(1)   *WHO   European   Regional   Obesity   Report   2022.* https://www.who.int/europe/publications/i/item/9789289057738 (accessed 2024-2-06).

(2)   Ahirwar, R.; Mondal, P. R. Prevalence of obesity in India: A systematic review. *Diabetes Metab. Syndr. Clin. Res. Rev.* **2019**, *13* (1), 318–321.

(3)   Luharid, S.; Timaeus, I. M.; Jonesid, R.; Cunninghamid, S.; Patel, S. A.; Kinra, S.; Clarke, L.; Houben, R. Forecasting the prevalence of overweight and obesity in India to 2040. *PLoS One* **2020**, *15* (2), 1–17.

(4)   Durán, P. Body-mass index in 2.3 million adolescents and cardiovascular death in adulthood. *Arch. Argent. Pediatr.* **2016**, *114* (6), 2430–2440.

(5)   Bjerregaard, L. G.; Jensen, B. W.; Ängquist, L.; Osler, M.; Sørensen, T. I. A.; Baker, J. L. Change in overweight from childhood to early adulthood and risk of type 2 diabetes. *N. Engl. J. Med.* **2018**, *378* (14), 1302–1312.

(6)   Yanovski SZ. Overweight, obesity, and health risk. *Arch. Intern. Med.* **2000**, *160* (7), 898–904.

(7)   Padwal, R.; Li, S. K.; Lau, D. C. W. Long-term pharmacotherapy for overweight and obesity: A systematic review and meta-analysis of randomized controlled trials. *Int. J. Obes.* **2003**, *27* (12), 1437–1446.

(8)   Petrilli, C. M.; Jones, S. A.; Yang, J.; Rajagopalan, H.; O'Donnell, L.; Chernyak, Y.; Tobin, K. A.; Cerfolio, R. J.; Francois, F.; Horwitz, L. I. Factors associated with hospital admission and critical illness among 5279 people with coronavirus disease 2019 in New York city: Prospective cohort study. *BMJ.* **2020**, *369*, 1–15.

(9)   Zhao, X.; Gang, X.; He, G.; Li, Z.; Lv, Y.; Han, Q.; Wang, G. Obesity increases the severity and mortality of influenza and covid-19: A systematic review and meta-analysis. *Front. Endocrinol.* **2020**, *11*, 595109.

(10)   Aronne, L. J.; Nelinson, D. S.; Lillo, J. L. Obesity as a disease state: A new paradigm for diagnosis and treatment. *Clin. Cornerstone* **2009**, *9* (4), 9–29.

(11)   Wright, S. M.; Aronne, L. J. Causes of obesity. *Abdom. Imaging* **2012**, *37* (5), 730–732.

(12)   Aronne, L. J.; Segal, K. R. Weight gain in the treatment of mood disorders. *J. Clin.*

Psychiatry **2003**, *64* (8), 22–29.

(13) Gangwisch, J. E.; Malaspina, D.; Boden-Albala, B.; Heymsfield, S. B. Inadequate sleep as a risk factor for obesity: Analyses of the nhanes. *Sleep* **2005**, *28* (10), 1289–1296.

(14) Spiegel, K.; Tasali, E.; Penev, P.; Van Cauter, E. Brief communication: Sleep curtailment in healthy young men is associated with decreased leptin levels, elevated ghrelin levels, and increased hunger and appetite. *Ann. Intern. Med.* **2004**, *141* (11), 846–850.

(15) Keith, S. W.; Redden, D. T.; Katzmarzyk, P. T.; Boggiano, M. M.; Hanlon, E. C.; Benca, R. M.; Ruden, D.; Pietrobelli, A.; Barger, J. L.; Fontaine, K. R.; Wang, C.; Aronne, L. J.; Wright, S. M.; Baskin, M.; Dhurandhar, N. V.; Lijoi, M. C.; Grilo, C. M.; DeLuca, M.; Westfall, A. O.; Allison, D. B. Putative contributors to the secular increase in obesity: Exploring the roads less traveled. *Int. J. Obes.* **2006**, *30* (11), 1585–1594.

(16) Atkinson, R. L.; Dhurandhar, N. V.; Allison, D. B.; Bowen, R. L.; Israel, B. A.; Albu, J. B.; Augustus, A. S. Human adenovirus-36 is associated with increased body weight and paradoxical reduction of serum lipids. *Int. J. Obes.* **2005**, *29* (3), 281–286.

(17) Donnelly, J. E.; Blair, S. N.; Jakicic, J. M.; Manore, M. M.; Rankin, J. W.; Smith, B. K. Appropriate physical activity intervention strategies for weight loss and prevention of weight regain for adults. *Med. Sci. Sports Exerc.* **2009**, *41* (2), 459–471.

(18) Hainer, V.; Toplak, H.; Mitrakou, A. Treatment modalities of obesity: What fits whom? *Diabetes Care* **2008**, *31* (Supplement_2), S269–S277.

(19) Davidson, M. H.; Hauptman, J.; DiGirolamo, M.; Foreyt, J. P.; Halsted, C. H.; Heber, D.; Heimburger, D. C.; Lucas, C. P.; Robbins, D. C.; Chung, J.; Heymsfield, S. B. Weight control and risk factor reduction in obese subjects treated for 2 years with orlistat: A randomized controlled trial. *J. Am. Med. Assoc.* **1999**, *281* (3), 235–242.

(20) Weintraub, M.; Sundaresan, P. R.; Cox, C. Long-term weight control study. *Clin. Pharmacol. Ther.* **1992**, *51* (5), 619–633.

(21) Tainter, M. L.; Stockton, A. B. Cutting, W. C. Use of dinitrophenol in obesity and related conditions a progress report. *J. Am. Med. Assoc.* **1933**, *101* (19), 1472–1475.

(22) Tainter, M. L.; Cutting, W. C.; Stockton, A. B. Use of dinitrophenol in nutritional

disorders. *Am. J. Public Heal. Nations Heal.* **1934**, *24* (10), 1045–1053.

(23) Alphin, R. S.; Ward, J. W. Anorexigenic effects of fenfluramine hydrochloride guinea pigs, and dogs. *Toxicol. Appl. Pharmacol.* **1969**, *14* (1), 182–191.

(24) Van Gaal, L. F.; Rissanen, A. M.; Scheen, A. J.; Ziegler, O.; Rössner, S. Effects of the cannabinoid-1 receptor blocker rimonabant on weight reduction and cardiovascular risk factors in overweight patients: 1-year experience from the rio-europe study. *Lancet* **2005**, *365* (9468), 1389–1397.

(25) Després, J.-P.; Golay, A.; Sjöström, L. Effects of rimonabant on metabolic risk factors in overweight patients with dyslipidemia. *N. Engl. J. Med.* **2005**, *353* (20), 2121–2134.

(26) Bays, H. E. Current and investigational antiobesity agents and obesity therapeutic treatment targets. *Obes. Res.* **2004**, *12* (8), 1197–1211.

(27) Müller, T. D.; Clemmensen, C.; Finan, B.; Dimarchi, R. D.; Tschöp, M. H. Anti-obesity therapy: From rainbow pills to polyagonists. *Pharmacol. Rev.* **2018**, *70* (4), 712–746.

(28) Ros, E. Intestinal absorption of triglyceride and cholesterol: Dietary and pharmacological inhibition to reduce cardiovascular risk. *Atherosclerosis* **2000**, *151* (2), 357–379.

(29) Chapus, C.; Rovery, M.; Sarda, L.; Verger, R. Minireview on pancreatic lipase and colipase. *Biochimie* **1988**, *70* (9), 1223–1233.

(30) Birk, R. Z.; Brannon, P. M. Regulation of pancreatic lipase by dietary medium chain triglycerides in the weanling rat. *Pediatr. Res.* **2004**, *55* (6), 921–926.

(31) Zhu, G.; Fang, Q.; Zhu, F.; Huang, D.; Yang, C. Structure and function of pancreatic lipase-related protein 2 and its relationship with pathological states. *Front. Genet.* **2021**, *12*, 693538.

(32) Brownlee, I. A.; Forster, D. J.; Wilcox, M. D.; Dettmar, P. W.; Seal, C. J.; Pearson, J. P. Physiological parameters governing the action of pancreatic lipase. *Nutr. Res. Rev.* **2010**, *23* (1), 146–154.

(33) Winkler, F. K.; D'Arcy, A.; Hunziker, W. Structure of human pancreatic lipase. *Nature* **1990**, *343* (6260), 771–774.

(34) Egloff, M.-P.; Marguet, F.; Buono, G.; Verger, R.; Cambillau, C.; Van Tilbeurgh, H. A

2.46 Å resolution structure of the pancreatic lipase-colipase complex inhibited by a c11 alkyl phosphonate. *Biochemistry* **1995**, *34* (9), 2751–2762.

(35) Miled, N.; Canaan, S.; Dupuis, L.; Roussel, A.; Rivière, M.; Carrière, F.; De Caro, A.; Cambillau, C.; Verger, R. Digestive lipases: From three-dimensional structure to physiology. *Biochimie* **2000**, *82* (11), 973–986.

(36) Srivastava, G.; Apovian, C. M. Current pharmacotherapy for obesity. *Nat. Rev. Endocrinol.* **2018**, *14* (1), 12–24.

(37) Pilitsi, E.; Farr, O. M.; Polyzos, S. A.; Perakakis, N.; Nolen-Doerr, E.; Papathanasiou, A. E.; Mantzoros, C. S. Pharmacotherapy of obesity: Available medications and drugs under investigation. *Metabolism.* **2019**, *92*, 170–192.

(38) Liu, T. T.; Liu, X. T.; Chen, Q. X.; Shi, Y. Lipase inhibitors for obesity: A review. *Biomed. Pharmacother.* **2020**, *128*, 110314.

(39) Tiwari, S. S.; Mukesh, S.; Sangamwar, A. T.; Talluri, M. V. N. K. In vivo metabolic investigation of cetilistat in normal versus pseudo-germ-free rats using UPLC-QToF MS/MS and in silico toxicological evaluation of its metabolites. *Biomed. Chromatogr.* **2020**, *34* (8), 4860–4870.

(40) Adis Medical Writers. Current and investigational anti-obesity drugs help reduce weight and offer additional benefits, but more effective options are needed. *Drugs Ther. Perspect.* **2020**, *36* (1), 12–16.

CHAPTER 2

LITERATURE REVIEW & GAPS IN EXISTING RESEARCH

CHAPTER 2

2. Literature Review & Gaps in Existing Research

2.1. Importance of Heterocyclic Scaffolds in Drug Discovery

In the field of medicinal chemistry, heteroatoms play a vital role as they constitute several pharmaceutical drugs and excipients. Heterocyclic compounds are the cyclic system with at least one heteroatom in it. The compounds containing various heteroatoms, such as nitrogen, oxygen, sulfur, phosphorus, iron, magnesium, selenium etc. are reported.[1,2] Heterocycles are the most important division of organic chemistry with an ever growing research interest due to their medicinal and industrial applications.[3] According to various reports, more than 85% of active pharmaceutical ingredients contain heterocyclic motifs, reflecting their critical role in the process of drug design.[4] In the case of biological systems, endogenous biomolecules such as DNA, RNA, chlorophyll, haemoglobin, vitamins, etc. consist of various heterocycles. Also, there are many biologically active macromolecules such as vitamins, hormones, antibiotics, sugars and pigments, containing heterocyclic scaffolds. Among the various heterocyclic classes, the contribution of Nitrogen-containing heterocycles (quinoline, indoles, pyrroles, pyrrolidines, etc.) is more towards the development of medicinal agents.

Apart from *N*-containing heterocycles, *O*-heterocycles also contribute well in the process of drug discovery and development.[5] Fosfomycin, an anti-bacterial agent contains oxirane heterocycle. Also, (-)-Ovalicin, a fungal product with 2 oxirane rings, shows angiogenesis inhibitory potential for inhibiting solid tumor growth.[6] Paclitaxel is another example of an oxygen-containing four-membered heterocyclic drug used as an anti-cancer agent.[7] One of the loop diuretics, Furosemide contains furan ring and is used in treatment of edema as a drug of choice.[8] Warfarin, a well-known anti-coagulant contains coumarin nucleus in it.

Another important oxygen-containing heterocycle is chromone, commonly known as, 4*H*-1-benzopyran-4-one.[9] The chromone ring system is the core nucleus of many of the flavonoids (an important class of secondary metabolite in plants), such as flavones and isoflavones. Hence, there is a significant importance of chromone-containing analogues as pharmacological agents. Many of the natural and synthetic analogues with chromone scaffold have been reported for various medicinal properties such as antibacterial, antifungal, neuroprotective, antiviral, etc.[10-14] Various drugs of chromone origin that are either approved or are in clinical trials are depicted in **Figure 2.1**.
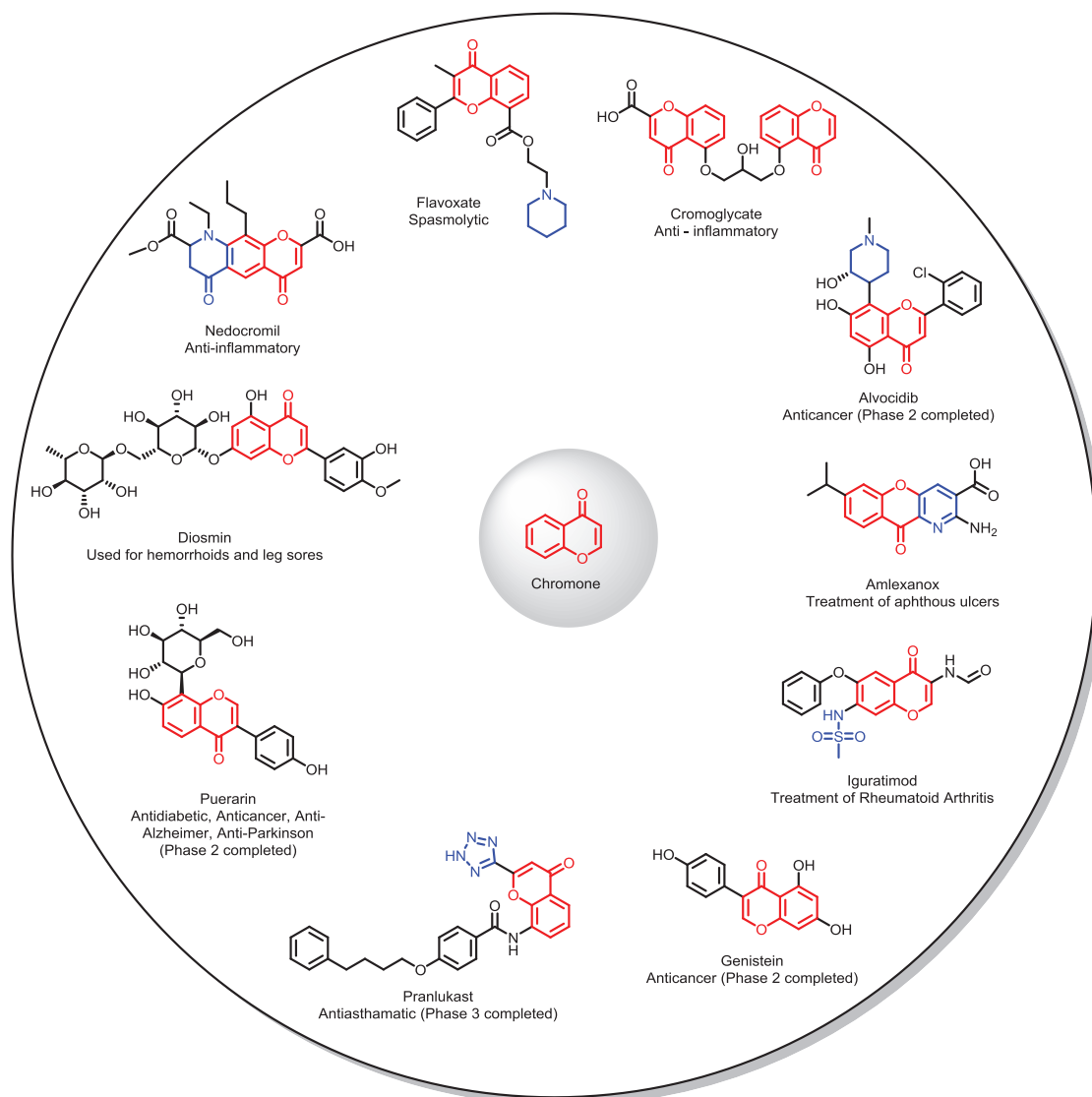
Figure 2.1. Chromone containing analogues approved by US-FDA and in clinical trials against various diseases

For the synthesis of such privileged chromone analogues, 3-Formylchromone is considered as a well-known precursor. For the synthesis of 3-Formylchromone, Vilsmeier-Haack reaction is utilized[15]). As shown in **Scheme 2.1**, 2'-Hydroxyacetophenone reacts with DMF in the presence of POCl$_3$ to get a condensed product known as 3-Formylchromone.

Scheme 2.1. Synthesis of 3-Formylchromone via Vilsmeier-Haack reaction

CHAPTER 2
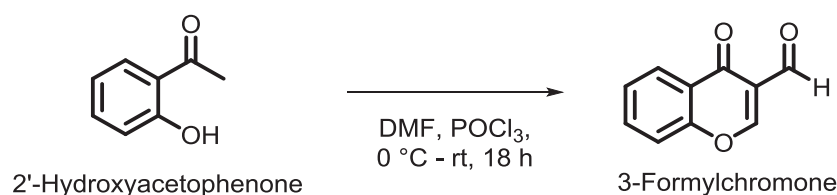
2.2. Chromone Containing Heterocyclic Hybrid Analogues as Medicinal Agents

Recently, much of the research has gone into the development of independent entities with multiple functions, known as hybrid drugs. Molecular hybrids can be defined as drugs designed by the combination of two or more bioactive fragments for the treatment of a particular disease.[16] Hence in various reports, more than one heterocyclic scaffolds were incorporated in a single molecule for the effective targeting of a particular disease. By the consideration of a diverse activity profile of chromone heterocycle, many of the researchers have reported hybrid analogues with variety of heterocycles and drug molecules. In further section, various examples of chromone containing hybrid analogues are represented with biological activities in the field of obesity, diabetes, cancer, microbial infections and Alzheimer's disease.

2.2.1. Anti-obesity Hybrids

Obesity can be defined as a complex, multifactorial metabolic disease, caused by an excessive deposition of fat, thereby presenting the risk to human health.[17] As the obesity condition is associated with variety of severe comorbidities, it should not be considered as a cosmetic problem. In particular, it is associated with the development of type-2 diabetes mellitus, coronary heart disease, osteoarthritis, respiratory complications, etc.[18] Treatment of obesity consists of dietary restrictions, exercise, surgery and pharmacotherapy. Pharmacotherapy involves appetite suppression, preventing fat absorption, modulation of fat storage and increase in thermogenesis.

Drugs targeting orexigenic and anorectic neuropeptide receptors, can be a potential target, supressing the food intake. Melanin-concentrating hormone-1 receptor (MCHR1) is one of the orexigenic neuropeptide receptors, used for targeting obesity condition.[19] MCH, a cyclic nonadeca-peptide, expressed in lateral hypothalamus and *zona incerta*, acts as a natural substrate for MCHR1 receptor. MCH is proven to increase body weight in rats, by stimulating the food intake, hence the inhibition of MCHR1 with small molecules is considered as one of the potential strategies to control obesity.[20]

In the continuous search for anti-obesity agents, many small molecules have been designed for the potential inhibition of MCHR1. In one of the reports by Lynch *et al*., chromone carboxamide based analogues have been synthesized by the incorporation of the dihydropyridine functionality (**Figure 2.2**).[21] Amongst the synthesized chromone-2-carboxamide analogues, analogue **1** was found to show potent MCHR1 inhibition with an

IC_{50} of 0.003 µM. Also, analogue **1** was found to be orally effective in the reduction of body weight in the DIO mouse model. However through toxicity studies, it was found to show QT interval prolongation in concentration-dependent manner. Through investigation, it was found to be the result of human ether-a-go-go-related gene (hERG) channel inhibition (IC_{50} of 15.1 µM).

To overcome such side effect without affecting the MCHR1 inhibitory potential, the 3,4-methylenedioxy phenyl moiety was replaced with a variety of heterocycles (benzofuran, benzothiazole, indole, benzoxazole, coumarin, etc.).[22] All the analogues were screened for MCHR1 as well as hERG inhibition. Many of them were found to be potent MCHR1 antagonist but were also found to have an affinity for hERG Ca^{+2} ion channel. The hybrid analogue **2**, possessing coumarin heterocycle was found to have selective MCHR1 inhibition (IC_{50} of 0.001 µM) with less affinity toward hERG (IC_{50} of 51.1 µM).
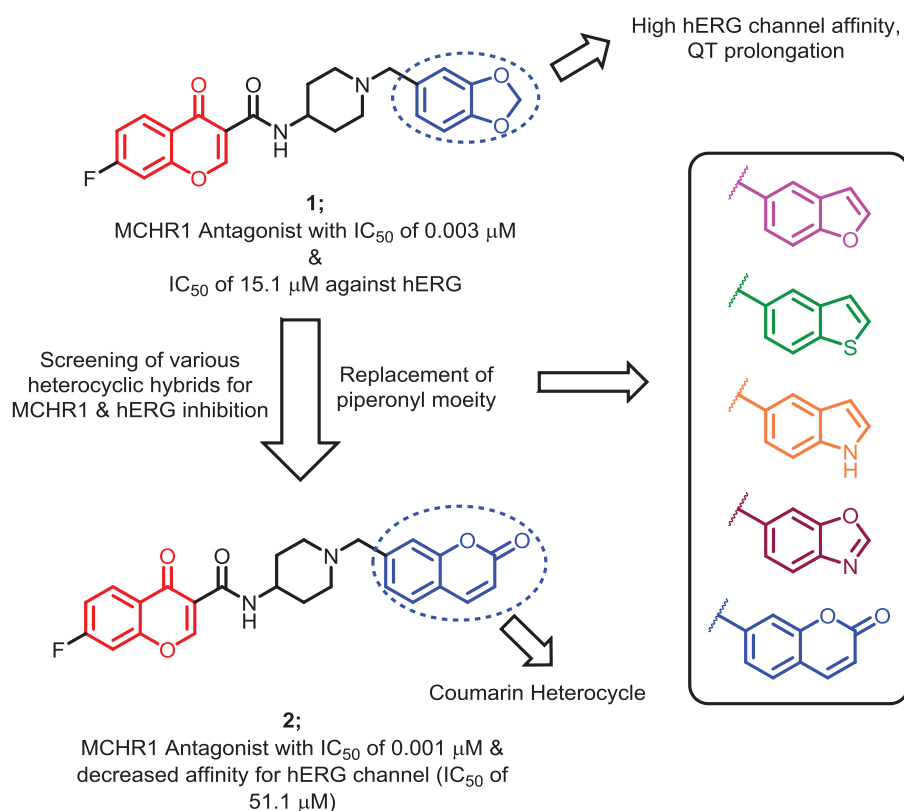
Figure 2.2. Chromone-based MCHR1 antagonist (1) and its modification (2)

2.2.2. Anti-Diabetic Hybrids

Diabetes mellitus is a chronic condition characterized by hyperglycemia, leading to serious complications. Depending upon its cause, it can be classified as Type-1 and Type-2 diabetes mellitus. Type-2 diabetes is common among the human population. α-glucosidase, a membrane-bound enzyme is responsible for the digestion of carbohydrates. It hydrolyzes the

glycosidic bond present in polysaccharides and converts it to glucose that will then get absorbed into the systemic circulation.[23] Hence, to decrease the systemic level of glucose, α-glucosidase can be inhibited, leading to low rate of carbohydrate absorption and subsequently leading to decreased postprandial hyperglycemia.

Isatin is an important heterocycle, present in a variety of alkaloids, drugs, pesticides and various pharmaceutical reagents.[24,25] Many of the isatin derivatives have been found to exhibit a variety of biological activities, such as antibacterial, antiviral, anticancer, antidiabetic, etc.[26–29] Also, many of the isatin-containing hybrids have been synthesized and evaluated for their α-glucosidase inhibitory potential (**Figure 2.3**).[30–32] Due to such a variety of biological activities, the chromone and isatin containing hybrid analogues have been designed and synthesized for α-glucosidase inhibitory potential.[33] Many of the synthesized analogues were active against the α-glucosidase enzyme, but the analogue with 7-hydroxy substituent on chromone and 4-bromobenzyl group at $N1$ of isatin was found to be more potent (analogue **3** with IC_{50} of 3.18 μM) than the other analogues.

In another study by Wang *et al.*, chromone and hydrazine moieties were hybridized by considering the desired fragments required for the binding at the active site of the α-glucosidase enzyme (**Figure 2.3**).[34] From the synthesized analogues, **4** was the most potent α-glucosidase inhibitory analogue, with an IC_{50} value of 20.1 μM. After SAR analysis, it was observed that the phenyl hydrazine moiety was essential for the inhibitory potential. Replacement of it by benzylhydrazide leads to diminished activity. Also, the replacement of phenyl group by other heterocycles led to decreased potential. The sulfonamido moiety at the *para* position of the phenyl group of hydrazides was found to be important.

3;
R^1 = 4-Bromobenzyl; R^2 = OH;
IC_{50} = 3.18 μM against
α-glucosidase enzyme

4;
R = Sulfonamido;
IC_{50} = 20.1 μM against α-glucosidase enzyme
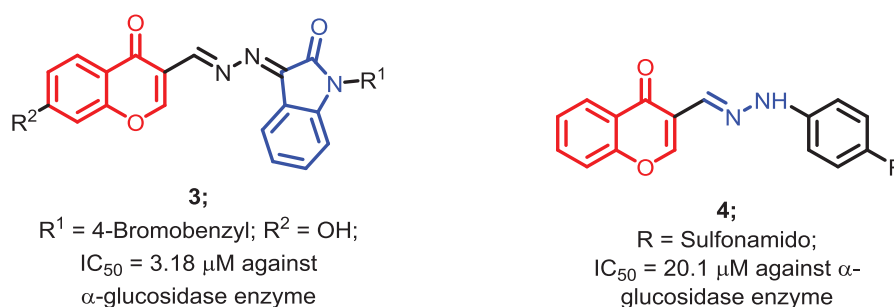
Figure 2.3. Chromone, isatin and hydrazone containing α-glucosidase inhibitory hybrid analogues as anti-diabetic agents

2.2.3. Anti-Cancer Hybrids

Using a hybrid drug design approach, many of the chromone-containing hybrids namely, chromone-imidazole, chromone-pyrimidine, chromone-pyrazole, etc., have been designed,

synthesized and evaluated for their potential as anti-cancer agents. In a study by Kantankar *et al.*, chromone and dihydropyrimidinone containing hybrid analogues were designed as anti-cancer agents.[35] The resulting hybrid analogues were synthesized *via* a modified Biginelli reaction. Among them, analogue **5** showed potent anti-cancer activity on A549 and HeLa cell lines (IC$_{50}$ of 6.86, 6.29 μM, respectively) (**Figure 2.4**). The analogue **5** was found to be comparatively potent as compared with cisplatin (IC$_{50}$ of 5.84, 8.41, 10.78 μM against A549, HeLa and K562 cell lines, respectively).

Yavuz *et al.* synthesized chromeno-pyrimidine hybrid analogues as anti-cancer agents[36] by looking at the potential of chromone, pyrimidine and hydrazone fragments.[37–39] Two cancer cell lines namely, HepG2 and MDA-MB-231 (human breast cancer cell line) were utilized for screening the analogues for anti-cancer activity, using MTT assay. More than half of the synthesized analogues were found to be potent against both cell lines. Amongst all, analogue **6** was found to exhibit the best activity with an IC$_{50}$ value of 13.56 μM against the HepG2 cell line (**Figure 2.4**). Raju *et al.* have also developed chromone and tetrahydropyrimidine-based hybrid analogues by utilizing the Biginelli reaction.[40] All the analogues were screened for their cytotoxicity profile using MTT assay. As shown in **Figure 2.4**, analogue **7** was found to have greater % inhibition on A549, SK-N-SH and HeLa cancer cell lines (47.6%, 56.0%, 60.6%, respectively), as compared with standard drug Doxorubicin (55.0%, 31.8%, 86.5%, respectively).

Chromone-Dihydrpyrimidinone Hybrids

5;
R^1 = R^2 = H, R^3 = OMe;
IC$_{50}$ = 6.86, 6.29 μM,
against A549 and HeLa cell lines, respectively.

Chromone-Pyrimidine Hybrid

6;
R^1 = H, R^2 = 2,4-dimethoxy;
IC$_{50}$ = 13.56 μM; against HepG2 cell line

Chromone-Tetrahydropyrimidine Hybrid

7;
47.6, 56.0, 60.6% Inhibition against A549, SK-N-SH and HeLa cancer cell lines
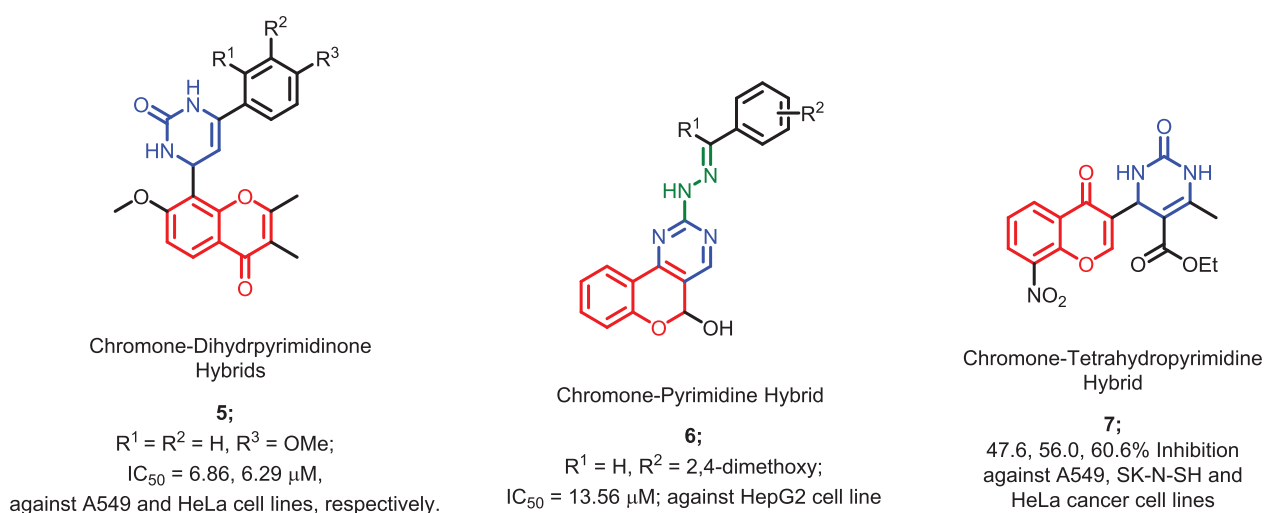
Figure 2.4. Anti-cancer hybrids of chromone with dihydropyrimidine, pyrimidine and tetrahydropyrimidine heterocycles

Inspired by the synergistic anti-cancer potential of various natural products, the chromone moiety (e.g. genistein and quercetin) was clubbed with that of imidazole (bioisostere of the terminal aryl group of curcumin) by Chen *et al.*[41] The analogue 8 with IC_{50} values of 1.8, 3.0, 1.0 µM against PC-3, DU-145, LNCaP cell lines, respectively was found to be the most potent analogue of the series when compared with Curcumin (25.4, 26.2, 12.1 µM), genistein (68.6, >100, 37.4 µM) and quercetin (>100, >100, 45.5 µM) (**Figure 2.5**).

Recently, Shatokhin *et al.* developed a mild, metal-free, moisture-tolerant, two-step methodology for the synthesis of chromone-benzimidazole hybrids with sterically hindered phenolic fragments.[42] MTT assay was used for the cytotoxicity screening of the synthesized analogues. The analogue **9** showed comparable cytotoxic activity (IC_{50} of 1.9 & 1.2 µM) as that of standard drug doxorubicin (IC_{50} of 0.9 µM) against HCT116 (Human colon cancer cells) and MCF7 (Breast cancer) cell lines, respectively. To evaluate the antioxidant potential of the synthesized analogues, a DPPH assay was performed and analogue **10** (IC_{50} of 0.18 µmol/ml) was found to have better antioxidant potential as compared with other analogues (**Figure 2.5**).

Chromone-imidazole hybrid analogue

8;
IC_{50} of 1.8, 3.0 & 1.0 µM,
against PC-3, DU-145 & LNCaP cell lines

Chromone-Benzimidazole hybrid analogue

9:
R^1 = F, R^2 = R^3 = H;
IC_{50} of 1.9, 1.2 µM,
against HCT116 and MCF7
cancer cell lines

10;
R^1 = R^2 = R^3 = H;
IC_{50} of 0.18 µmol/mL,
obtained from DPPH assay
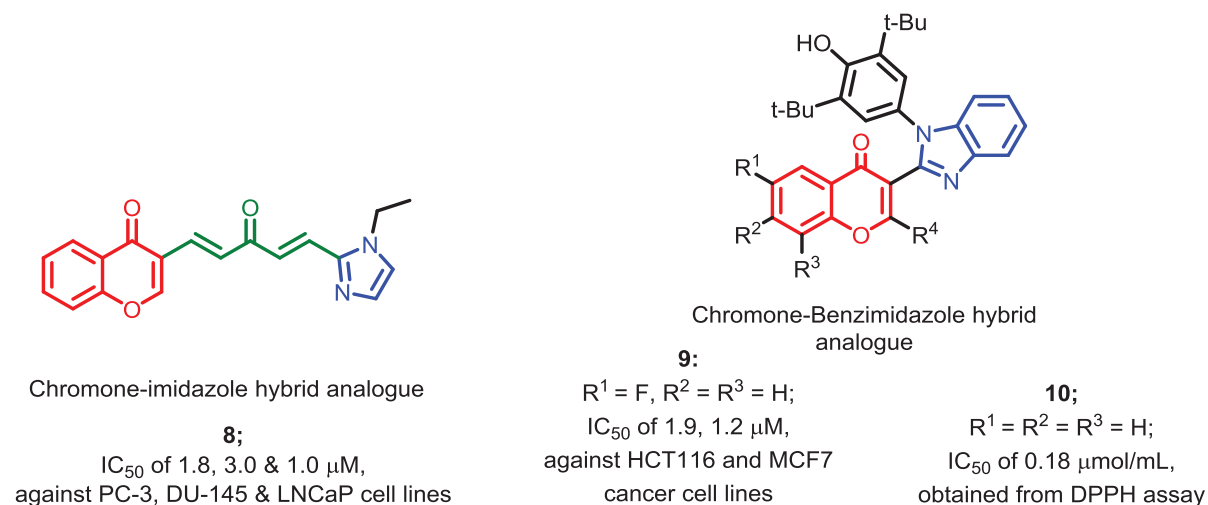
Figure 2.5. Anti-cancer hybrids of chromone with imidazole and benzimidazole heterocycles

2.2.4. Anti-microbial Hybrids

The introduction of antimicrobial agents into the clinic for effective treatment of infectious diseases has been considered a landmark in medical science. Looking at the rising cases of microbial drug resistance, the appropriate use of existing antimicrobials and the development of new agents is warranted.[43] There are many reports of chromone-containing hybrids with

various heterocycle namely, azoles, furanchalcone, pyrimidine, etc. Few of them are represented below.

In one of the studies by *Cano et al.*, Ugi-azide reaction was utilized for the synthesis of chromone and tetrazole-based hybrid analogues as potential antimicrobials. Those analogues were tested against pathogenic bacteria (*Pseudomonas aeruginosa* and *Staphylococcus aureus*), protozoan (*Entamoeba histolytica)*, and human fungal pathogens (*Sporothrix schenckii*, *Candida albicans*, and *Candida tropicalis*).[44] All the analogues were found active in liquid culture media, whereas analogue **11** was found to exhibit the potent antifungal activity in solid media against *C. tropicalis* at the concentration of 6.25 μg/μL. For the evaluation of the antibacterial potential of the synthesized hybrid analogues, Minimum Inhibitory Concentration (MIC) and Minimum Bactericidal Concentration (MBC) were determined. With the MIC of 40 μg/mL, the iodinated analogue **12** showed the highest potency against *S. aureus*. The fluorinated analogue **13** was found to be highly active against *P. aeruginosa* (MIC of 20 μg/mL). From the results of the antibacterial study, preliminary SAR was derived, and halogen substituents were found to be effective in increasing the antibacterial potential. Also, the halogenated analogues **12** (IC_{50} = 61.7 μg/mL) and **14** (IC_{50} = 69.5 μg/mL) exhibited greater inhibitory potential against *E. histolytica* (**Figure 2.6**).

In another study, chromone-pyrimidine hybrids with antibacterial and antifungal pharmacophoric features were designed (**Figure 2.6**).[45] For the anti-bacterial screening of the synthesized analogues, the classical paper disk method was utilized against *S. aureus, S. abony, S. epidermidis* and *E. coli*. The presence of electron-withdrawing groups were found to have a positive effect on antibacterial potential, as analogue **15**, with chloro substitution, was found to be the most potent antibacterial of the series (Zone of inhibition of 13, 18, 14 and 10 mm against *S. aureus, S. abony, S. epidermidis* and *E. coli*, respectively. Analogue **16** was the most active amongst the series (Zone of inhibition of 34 mm against *C. albicans*), having a potent activity profile as that of griseofulvin (Zone of inhibition of 10 mm against *C. albicans*).

Chromone-tetrazole hybrid analogues

11: R= F; R^1 = R^2 = R^4 = H; R^3 = Cl; R^5 = t-Bu;
Antifungal activity against *C. tropicalis*
at the conc. of 6.25 µg/µL
12: R= H; R^1 = I; R^2 = R^3 = R^4 = H; R^5 = t-Bu;
MIC of 40 µg/mL, against *S. aureus*;
IC$_{50}$ = 61.7 µg/mL against *E. histolytica*
13: R= F; R^1 = R^2 = R^3 = R^4 = H; R^5 = t-Bu;
MIC of 20 µg/mL against *P. aeruginosa*
14: R= F; R^1 = H; R^2 = R^3 = R^4 = OMe; R^5 = Cy;
IC$_{50}$ = 69.5 µg/mL against *E. histolytica*

Chromone - Pyrimidine Hybrids

☐ : Antibacterial Pharmacophore Site
☐ : Antifungal Pharmacophore Site

15: R^1 = Cl; R^2 = H; R^3 = Cl; X = S
(Zone of inhibition of 13, 18, 14 and 10 mm
against *S. aureus*, *S. abony*, *S. epidermidis*
and *E. coli*, respectively)
16: R^1 = Cl; R^2 = H; R^3 = Cl; X = O
Zone of inhibition of 34 mm against *C. albicans*

Figure 2.6. Chromone-containing hybrids with tetrazole and pyrimidine heterocycles as anti-bacterial and anti-fungal agents

Triclosan analogues have been found to possess many biological activities, including antimicrobial activity against malaria, tuberculosis, etc. Also, triclosan-quinoline hybrids were recently developed and tested against axenic and intracellular amastigotes of *L. panamensis* with EC$_{50}$ < 24 µg/mL.[46] Looking at the design features of such hybrids, in the work by Otero *et al.*, 4 chromone-triclosan hybrids were designed and synthesized to check their potential against leishmaniasis.[47] The analogues **17** & **18** showed 94.1 & 91.0 % inhibition as well as EC$_{50}$ of 2.7 and 7.5 µM against intracellular amastigotes of *L. (V) panamensis* (**Figure 2.7**). The potency of the analogues **17** & **18** were comparable with the standard drug Amphotericin B (% inhibition of 69.1 and EC$_{50}$ of 0.1 µM). The length of the alkyl chain played an important role in the activity profile. There was an inverse relation between the increased chain length and leishmanicidal activity.

Due to the prominent antimycobacterial activity of triazole heterocycle, it has been combined with the chromone scaffold (**Figure 2.7**) with the purpose of increasing potency of the existing antitubercular triazole moieties by Nalla *et al.*[48] *In vitro* antitubercular screening of the analogues was performed using Microplate Alamar Blue Assay (MABA) method against *Mycobacterium tuberculosis* H37Rv (ATCC27294). The analogue **19,** with the substitution of (tridecan-1-ol)yl on a triazole ring, was found to be the most potent among the series with MIC of 1.56 µg/mL. It was found to have 4.8 times higher potency than standard drug ethambutol (MIC of 7.64 µg/mL).

Chromone - triclosan Hybrids

17: n = 1; EC$_{50}$ = 2.7 μM
18: n = 2; EC$_{50}$ = 7.5 μM
against intracellular amastigotes of
L. (V) panamensis

Chromone-Triazole Hybrids

19;

R = Tridecan-1-ol
MIC of 1.56 μg/mL against
Mycobacterium tuberculosis H37Rv
(ATCC27294)
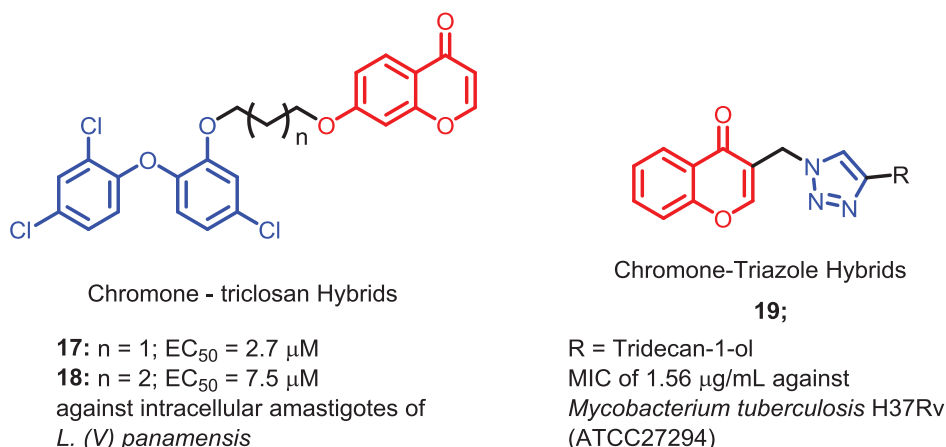
Figure 2.7. Chromone containing anti-tubercular hybrids with triclosan and triazole heterocycles

In the search for potential candidate for the treatment of cutaneous Leishmaniasis and Chagas disease, the chromone and quinoline-containing hybrids were designed by Coa *et al.*[49] The antileishmanial activity was performed on intracellular amastigotes of *L. (V) panamensis*, while intracellular amastigotes of *T. cruzi* were used for the determination of trypanocidal activity. Among many of the active analogues, analogue **20** was found to be the most potent analogue against both *L. (V) panamensis* and *T. cruzi* (IC$_{50}$ of 6.11, 4.09 μg/mL, respectively) (**Figure 2.8**).

In a study by Garcia *et al.,* chromone and furanchalcone were hybridized for the treatment of leishmaniasis and Chagas disease.[50] Among the synthesized analogues, **21** was the best active analogue, with EC$_{50}$ values of 46.00 and 25.58 μM against *L. (V.) panamensis* and *T. cruzi*, respectively (**Figure 2.8**).

Chromone-Quinoline Hybrids

20; n = 2;
EC$_{50}$ of 6.11 μg/mL against
L. (V) panamensis &
EC$_{50}$ of 4.09 μg/mL against *T. cruzi*

Chromone-Furanchalcone Hybrids

21; n = 9;
EC$_{50}$ of 46.00, 25.58 μM against *L. (V.)
panamensis and T. cruzi* respectively
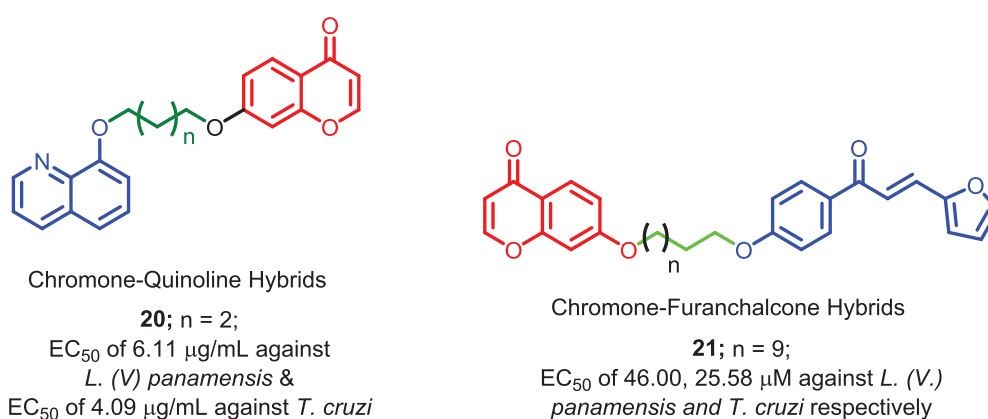
Figure 2.8. Chromone-containing hybrids with quinoline and furanchalcone heterocycles as Leishmanicidal agents

2.2.5. Anti-Alzheimers Hybrids

Alzheimer's disease (AD) is a slowly progressive neurodegenerative disease that is the most common cause of dementia. The disease is characterized by neurofibrillary tangles and neuritic plaques due to the accumulation of amyloid β peptide in the affected area of the brain.[51] For drug development towards AD, enzymes namely acetylcholinesterase (AChE), butyrylcholinesterase (BuChE) and monoamine oxidase (MAO) are most validated targets.[52] Various hybrid analogues of chromone with pyridine, indole, donepezil, etc. have been reported for simultaneous targeting of multiple enzymes for the effective treatment of AD.

Lipoic acid, a naturally occurring antioxidant found in plants and animals, has the ability to control the progression of AD *via* various mechanisms such as decreasing oxidative stress, inflammation and Aβ plaque formation, increasing the levels of ACh, etc.[53] Many hybrid analogues have been synthesized, e.g. Lipocrine, which is a hybrid of lipoic acid and tacrine with potent neuroprotective activity.

Taking into consideration such facts, chromone (with neuroprotective potential) has been clubbed with lipoic acid by Baleh *et al*. to get the hybrids with potential cholinesterase (ChEs) inhibitory activity.[54] All the analogues were found to have poor AChE inhibition with IC_{50} values greater than 100 μM, except analogue **22** with moderate potential (IC_{50} of 56.50 μM). As shown in **Figure 2.9**, analogue **23** (IC_{50} of 7.55 μM) was found to be potent against BuChE enzyme, as compared with donepezil (IC_{50} of 4.01 μM). Kinetic study of the most potent analogue **23**, revealed its mixed mode of inhibition, suggesting the binding of analogue with both catalytic active site (CAS) and peripheral anionic site (PAS) of AChE. Thioflavin T (ThT) analysis of analogue **23** concluded its 13% inhibition of Aβ aggregation, as compared with Donepezil (22% inhibition) at 100 μM concentration. The antioxidant activity of analogue **23** was also determined using Dichloro-dihydro-fluorescein diacetate (DCFH-DA) assay. The results indicated concentration-independent inhibition of analogue **23** in intracellular reactive oxygen species (ROS) production in PC12 cells.

22;
n = 4; R = 7-F
IC_{50} of 56.50 μM against AChE

23;
n = 4
IC_{50} of 7.55 μM against BuChE
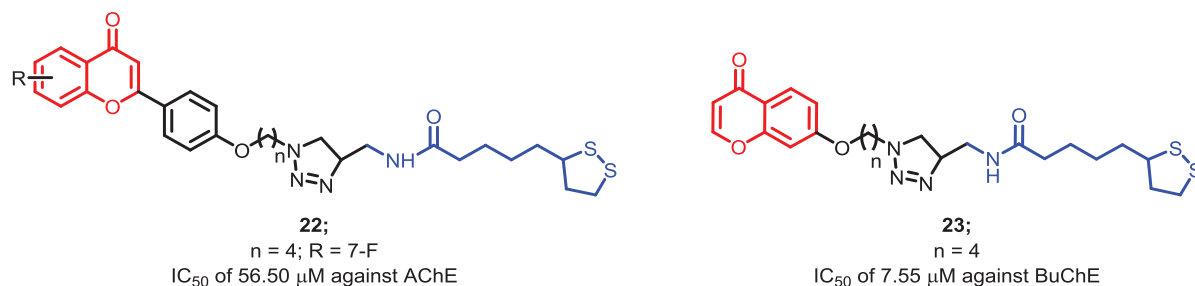
Figure 2.9. Chromone and Lipoic acid-based hybrid analogues as ChE inhibitors

Due to various biological properties of aminophosphonate, including antileishmanial[55], antialzheimer's[56] and antimicrobial[57,58] properties, *N*-substituted α-aminophosphonates-bearing chromone hybrids were designed by Shaikh *et al.*[59] Ellman's method was utilized for the *in vitro* screening of anticholinesterase activity. Most of the synthesized analogues were found to be selective against AChE as compared with BuChE, with selectivity index ranging from 1.49 to 139.81. The most potent hybrid analogue **24** was found to possess mixed inhibition, with an IC_{50} value of 0.103 µM, against the AChE enzyme. It was 2 times more potent as compared with tacrine (IC_{50} of 0.289 µM). DPPH (2,2-Diphenyl-1-picrylhydrazyl) and H_2O_2 scavenging assays were performed as the scavenging of H_2O_2 is necessary for the neuroprotective action. The analogue **24** was found to have the highest radical and H_2O_2 scavenging activity with IC_{50} of 45.61 and 55.52 µM, respectively (**Figure 2.10**).

There are many pyridinium analogues with ChE inhibitory, neuroprotective and anti-amyloid aggregation activities.[60,61] Looking at such biological potential, the pyridine heterocycle was clubbed with the biologically active chromone heterocycle by Abdpour *et al.*[62], considering the desired features essential for AChE and BuChE inhibition. For BuChE inhibition, the analogue **25** was found to be the most potent inhibitor (IC_{50} of 0.006 µM), whereas, the analogue **26** was found to be potent against the AChE enzyme, with IC_{50} of 0.71 µM. Further, the inhibitory effect of analogues **25** and **26** on AChE and self-induced Amyloid-β aggregation was determined. Both the analogues were found to inhibit A-β aggregation with 36.6 & 21.8% inhibition for **25 & 26**, respectively. (**Figure 2.10**), that was much better as compared with the standard drug Donepezil (26.9% inhibition).
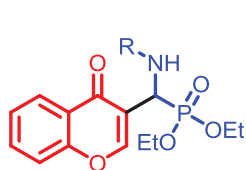
Chromone-aminophosphonate Hybrids

24;
R = 1-(4-Methoxyphenyl)ethyl
IC_{50} of 0.103 µM against AChE,
IC_{50} of 45.61 µM against DPPH &
55.52 µM against H_2O_2
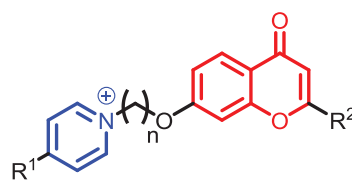
Chromone-Pyridine Hybrids

25;
n = 3; R^1 = Et; R^2 = 4-Methoxyphenyl
IC_{50} of 2.5 µM and 0.006 µM against
AChE and BuChE, respectively.

26;
n = 4; R^1 = H; R^2 = 4-Chlorophenyl
IC_{50} of 0.71 µM and 1.5 µM against AChE
and BuChE, respectively.

Figure 2.10. Chromone hybrids with aminophosphonate and pyridine as ChEs inhibitors

Along with ChEs, MAO-B also plays an important role in neuronal dysfunction, leading to the development of AD.[63,64] Recent studies have shown the importance of MAO-B inhibitors (ladostigil and rasagiline) in inhibition of Aβ aggregation, antiapoptotic activity and

neuroprotection.[65,66] Through the hybridization of chromone and indole heterocycles, MAO-B selective hybrids were designed, synthesized, and evaluated for their inhibitory potential. Many of the analogues were effective, inhibiting MAO-A and MAO-B enzymes. Analogue **27** was found to have IC_{50} of 0.15 μM against MAO-B enzyme, with poor inhibitory action on MAO-A enzyme (IC_{50} > 100 μM) with MAO-B selectivity > 670 (**Figure 2.11**).

In the research by Wang *et al*., the chromone scaffold with MAO-B inhibitory potential[67,68] was linked with the benzylpiperidine moiety of donepezil *via* amide linker.[69] Amongst all, analogue **28** was found to have a balanced potential against AChE & BuChE, with IC_{50} of 0.37 and 5.24 μM, respectively. Activities were compared with the standard drug Donepezil (IC_{50} of 0.032, 2.47 μM against AChE and BuChE, respectively). It was also effective against the hMAO-B enzyme (IC_{50} of 0.272 μM), with the highest MAO-B selectivity of 247, over MAO-A enzyme (**Figure 2.11**). For MAO-B inhibition, it was found to be highly potent as compared with the iproniazid (IC_{50} of 6.93 μM).

In a study by Angona *et al*. Ugi reaction was utilized to incorporate selective fragments of donepezil and melatonin with the chromone heterocycle for ChEs and MAO dual inhibition.[70] The hBuChE and hAchE were used for the screening of synthesized hybrid analogues using Ellman's protocol. The MAO inhibitory activity was performed using hMAO-A & hMAO-B enzymes and kynuramine as a substrate. Amongst all the synthesized analogues, **29** was found to be the potent multitargeted agent with strong BuChE inhibition (IC_{50} of 11.90 nM), moderate AChE inhibition (IC_{50} of 1.73 μM) and potent MAO-A and MAO-B inhibition (2.78, 21.29 μM, respectively). Also, the analogue **29** was found to have potent radical scavenging properties with a Trolox equivalents (TE) value of 3.04, obtained by ORAC test (**Figure 2.11**).

Chromone – indole Hybrids

27; R^1 = H; R^2 = MeO; R^3 = 5-Me
IC$_{50}$ of 0.15 μM against MAO-B enzyme;
MAO-B Selectivity: > 670

Chromone – Donepezil Hybrids

28; R = 6-OBn
IC$_{50}$ of 0.37 μM against AChE,
5.24 μM against BuChE &
0.272 μM against MAO-B enzymes

29;
IC$_{50}$ of 11.90 nM against hBuChE,
IC$_{50}$ of 1.73 μM against hAChE,
IC$_{50}$ of 2.78 μM against hMAO A,
IC$_{50}$ of 21.29 μM against hMAO B,
Strong antioxidant (3.04 TE, ORAC test)
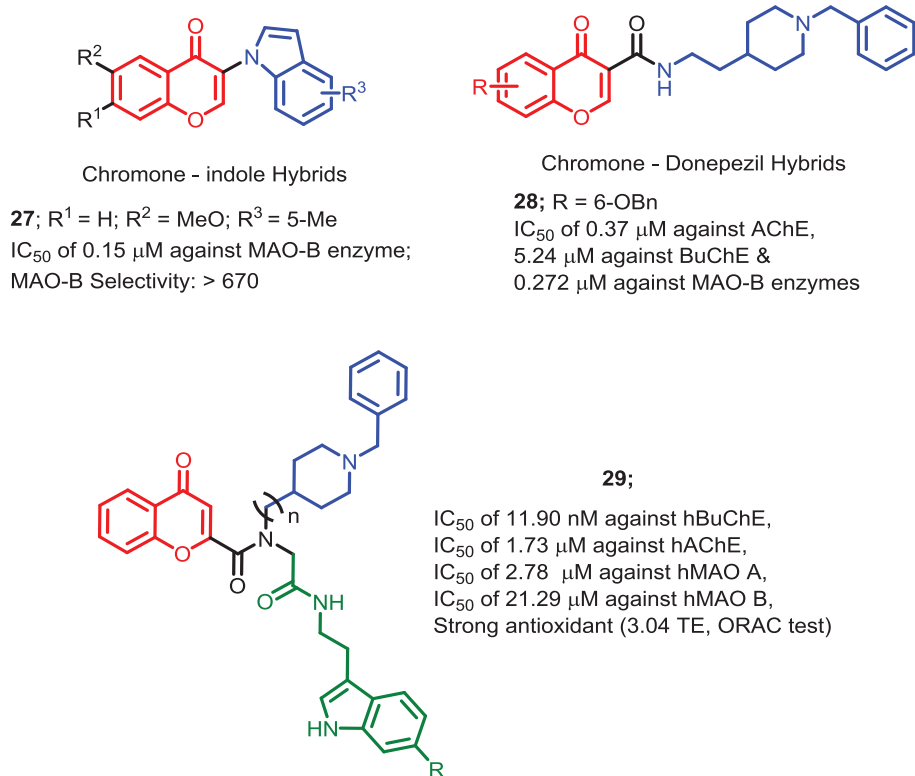
Figure 2.11. Chromone hybrids with indole, donepezil and melatonin as ChE and MAO dual inhibitors

In search of potential MTDL for the effective treatment of AD, the hybrid analogues were designed having chromone functionality (antioxidant and β-secretase 1 (BACE-1) inhibitory potential) and tacrine (ChE inhibition). The synthesized analogues were tested for BACE-1 and ChEs inhibitory potential. For BACE-1 inhibition, **30** was identified as a potent hybrid analogue, with IC$_{50}$ of 2.10 μM (**Figure 2.12**). Many of the synthesized analogues were found to be potent inhibitors of AChE and BuChE, with IC$_{50}$ in the nano and picomolar range. Analogue **31** was found to be the most potent of the series, with IC$_{50}$ of 35 pM against AChE.

30;
n = 8; R^1 = H; R^2 = 5,7 - diOMe
IC$_{50}$ of 2.10 μM against BACE-1

31;
n = 8; R^1 = 6-Br; R^2 = 5-OH, 7-OMe
IC$_{50}$ of 35 pM against AChE &
5.00 nM against BuChE
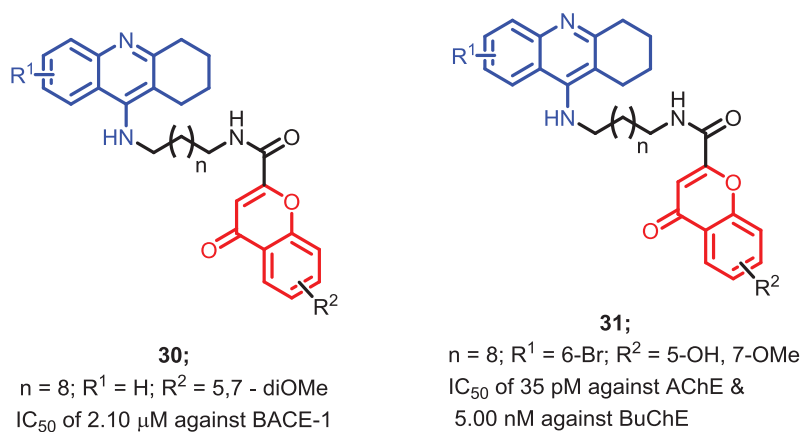
Figure 2.12. Chromone and Tacrine hybrids as MTDL for treatment of Alzheimer's disease

2.3. Chromone Containing Natural PL Inhibitors

Flavones and flavonols are well explored for PL inhibitory effect from the class of polyphenolics. In a study by Lee *et al*., Luteolin-6-C-β-D-boivinopyranoside a novel flavone was isolated from the leaves of *Eremochloa ophiuroides* with 4 known flavones (Luteolin, Orientin, Isoorientin, Derhamnosylmaysin and Isoorientin-2-*O*-α-L-rhamnoside).[71] Luteolin exhibited poor activity ($IC_{50} > 200$ µM), but the enhancement in activity was observed with the substitution of 6-C-β-D-boivinopyranoside ($IC_{50} = 50.5$ µM). Other isolated derivatives also exhibited good to moderate activity with IC_{50} in the range of 18.5 – 44.6 µM (**Figure 2.13**).

Luteolin
$IC_{50} > 200$ µM

Luteolin-6-C-β-D-boivinopyranoside
$IC_{50} = 50.5$ µM

Orientin
$IC_{50} = 31.6$ µM

Isoorientin
$IC_{50} = 44.6$ µM

Derhamnosylmaysin
$IC_{50} = 25.9$ µM

Isoorientin-2-O-α-L-rhamnoside
$IC_{50} = 18.5$ µM
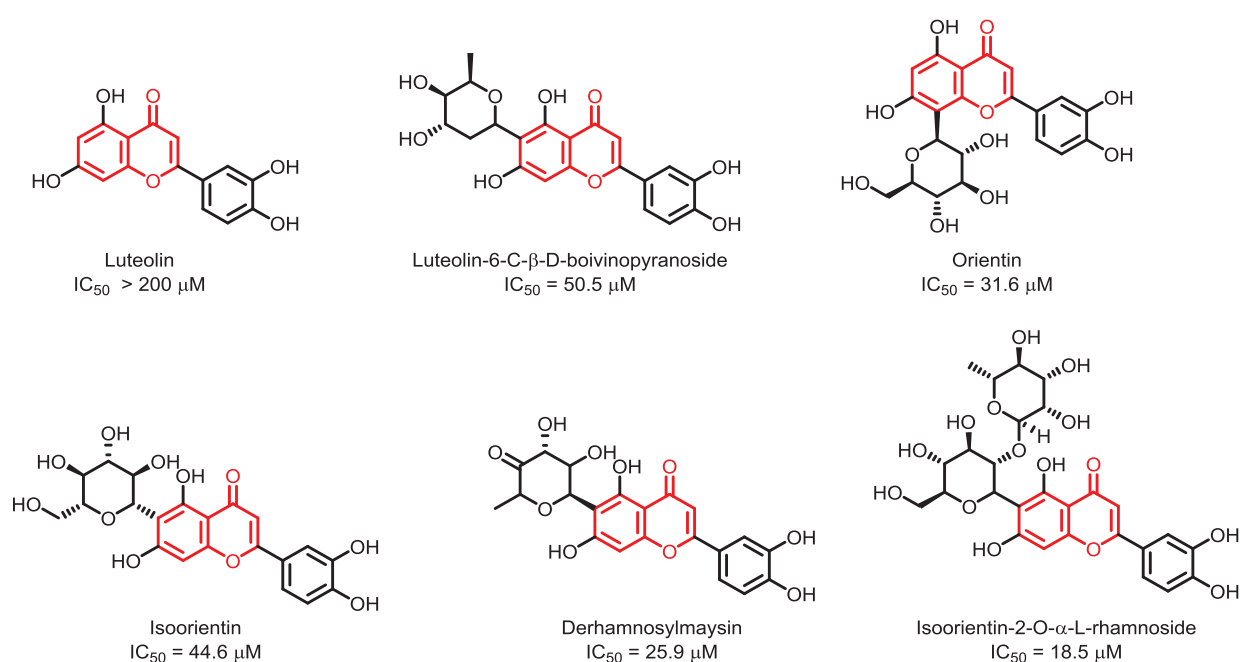
Figure 2.13. Chromone-containing PL inhibitors, isolated from leaves of *Eremochloa ophiuroides*

In another study by Sergent *et al*. various phenolic compounds were screened for PL inhibitory activity, using 4-MUO as a substrate.[72] Among them, quercetin and kaempferol were found to exhibit IC_{50} of 21.5 and 13.4 µM (**Figure 2.14**).

Quercetin
$IC_{50} = 21.5$ µM

Kaempferol
$IC_{50} = 13.4$ µM
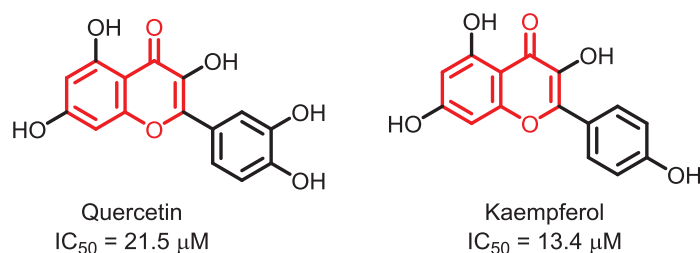
Figure 2.14. PL inhibitory activity of quercetin and kaempferol

Noha *et al*., reported PL inhibitory potential of *Ammannia aegyptiaca* ethanol extract (AEEE). From the extract, Myricetin 3-*O*-β-4C-1-(6"-*O*-galloylglucopyranoside)7-*O*-β-4C-1-glucopyranoside (MGGG), a novel flavone with Kaempferol 3-*O*-rutinoside, Quercetin 3-*O*-rutinoside were isolated for checking their PL inhibitory potential.[73] All the isolated analogues showed poor PL inhibition with IC$_{50}$ values in the range of 66.00 – 92.70 µM (**Figure 2.15**).

Myricetin 3-*O*-β-4C1-(6"-*O*-galloylglucopyranoside) 7-*O*-β-4C1- glucopyranoside (MGGG)
IC$_{50}$ = 92.70 µM

Kaempferol 3-O-rutinoside
IC$_{50}$ = 66.00 µM

Quercetin 3-O-rutinoside
IC$_{50}$ = 68.43 µM
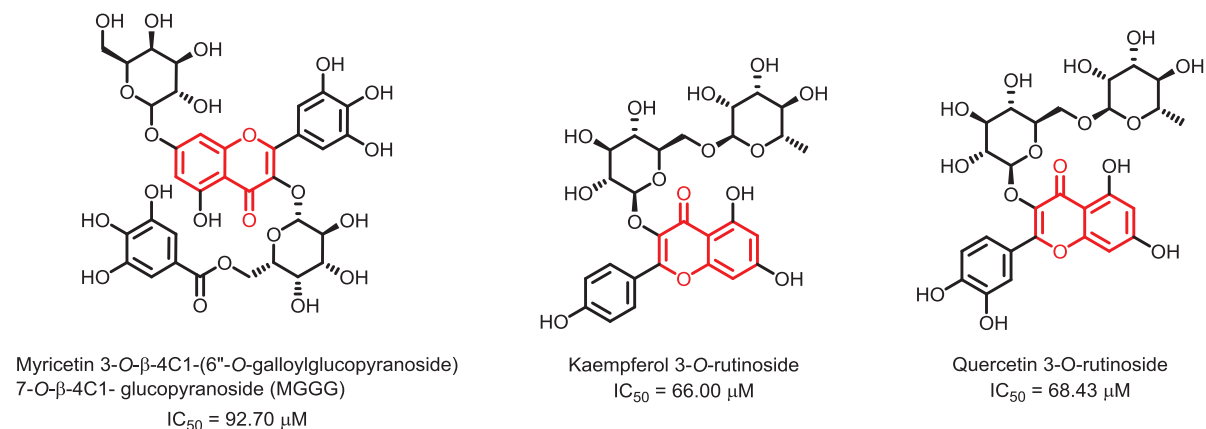
Figure 2.15. Isolated PL inhibitory analogues from AEEE extract

In another report, the activity-guided fractionation of methanolic extract of seeds of *Trigonella foenum-graecum* was performed, followed by the isolation of 3 flavone C-glycosides namely, vicenin-1, isoschaftoside and schaftoside.[74] The PL inhibitory IC$_{50}$ values were found to be 207 µg/mL, 330 µg/mL and 130 µg/mL, respectively (**Figure 2.16**).

Vicenin-1
IC$_{50}$ = 207 µg/mL

Isoschaftoside
IC$_{50}$ = 330 µg/mL

Schaftoside
IC$_{50}$ = 130 µg/mL
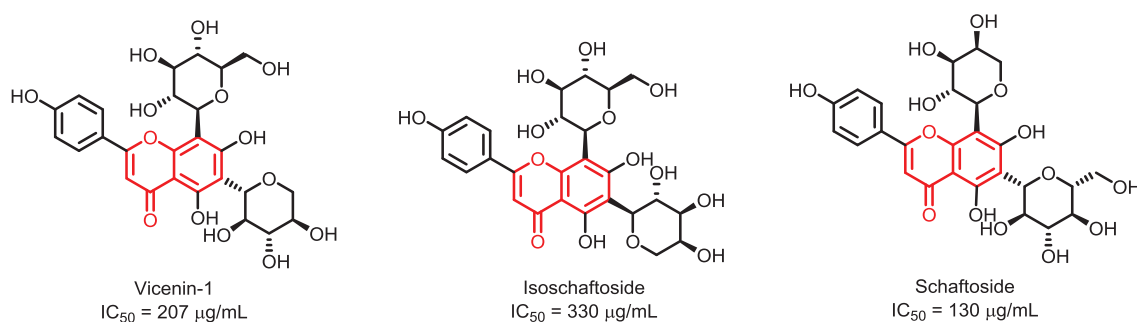
Figure 2.16. Flavone containing PL inhibitory natural products from methanolic extract of seeds of *Trigonella foenum-graecum*

Hou *et al*. identified PL inhibitory constituents from *Mori radicis* that include, kuwanon C (KC), kuwanon G (KG) and morusin [75] with good activities having IC$_{50}$ values of 4.47, 4.85, 9.94 µM, respectively (**Figure 2.17**). The PL inhibitory assay was performed using 4-methylumbelliferyl oleate (4-MU oleate) substrate. The enzyme kinetics study revealed a mixed inhibitory mechanism. Also, in a study by Jeon *et al.* 20 polyphenolic analogues from

the leaves of *Morus alba* with 8 analogues containing flavone nucleus were isolated.[76] These flavone-containing analogues, except one flavone glycoside were poor in PL inhibitory potential (>70 µM). As shown in **Figure 2.17**, the above-mentioned flavone-glycoside exhibited moderate activity with an IC_{50} value of 18.6 µM. The PL inhibition assay was performed with *p*-NPB as a substrate.

Kuwanon C
IC_{50} = 4.47 µM

Kuwanon G
IC_{50} = 4.85 µM

Morusin
IC_{50} = 9.94 µM

Flavone-glycoside
IC_{50} = 18.6 µM
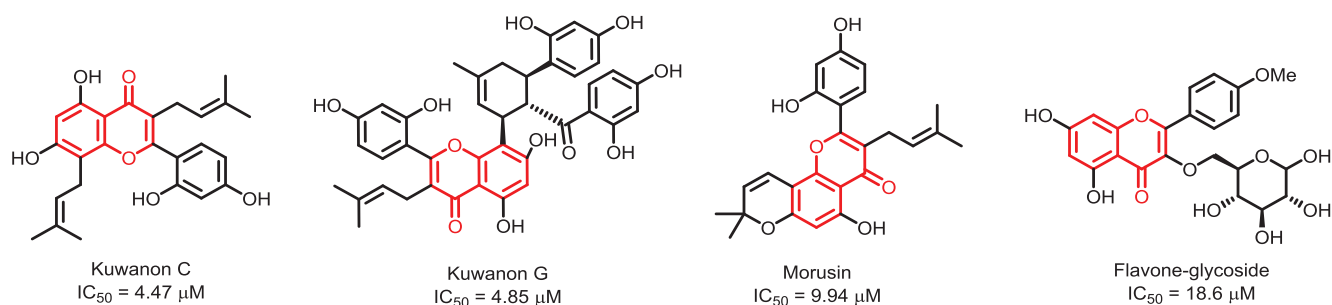
Figure 2.17. PL inhibitory flavones from *Mori radicis* and *Morus alba*

Through bio-guided fractionation of methanolic extract of wood of *Populus alba*, nine bioactive compounds were isolated by Elsbaey *et al*. [77] Among them, two were flavone glycosides, namely, rutin and narcissin. The flavone glycosides exhibited poor activity with IC_{50} of 152.3 and 122.4 µM (**Figure 2.18**). In a study by Huang *et al.*, through spectroscopic and molecular dynamics simulation studies, the interactions and inhibitory mechanisms of tangeretin (TAN), nobiletin (NBT), and their acidic hydroxylated forms, 5-demethyltangeretin (5-DT) and 5-demethylnobiletin (5-DN) on PL were studied.[78] The PL inhibitory IC_{50} values were found to be 14.69, 3.60, 13.18 and 4.18 µM (**Figure 2.18**). The enzyme inhibition kinetic study proved the mixed inhibitory mechanism of all four analogues. It was also confirmed from ultraviolet-visible (UV–Vis) spectroscopy, circular dichroism (CD), fluorescence spectroscopy, molecular docking and MD simulation that the analogues bind at the catalytic as well as non-catalytic site of the PL enzyme.
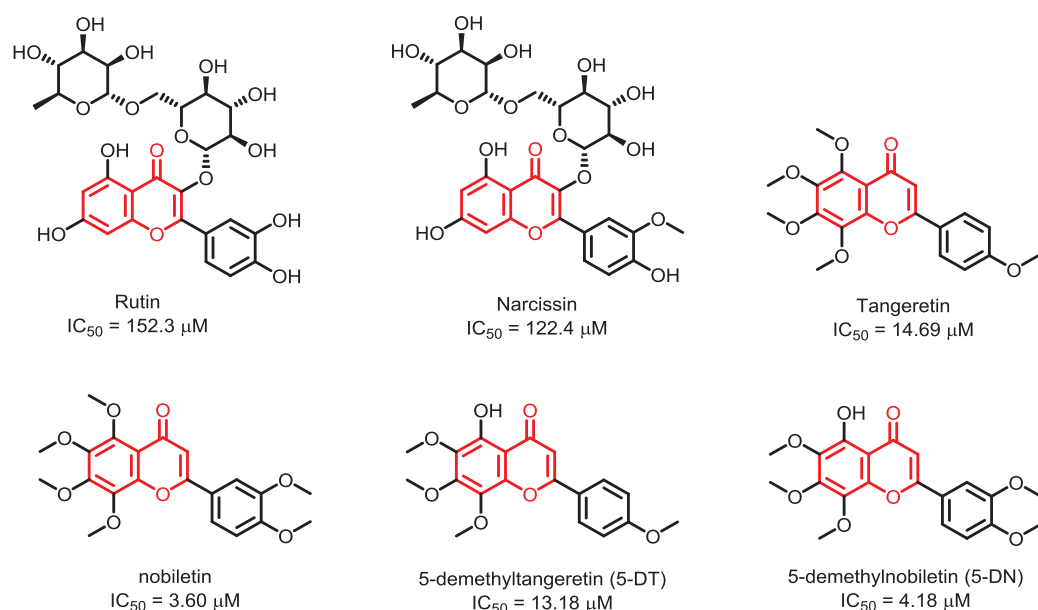
Figure 2.18. PL inhibitory Flavone analogues from wood of *Populus alba*

To understand the anti-hyperlipidemic mechanism of leaf extract of *Ginkgo biloba*, the major bioactives from the leaves of *G. biloba* were extracted.[79] Isoginkgetin, bilobetin, ginkgetin and sciadopitysin exhibited strong to moderate PL inhibitory potential with IC_{50} in the range of 2.90 – 12.78 µM (**Figure 2.19**). For PL inhibitory screening, 4-MU was used as a substrate. From the enzyme kinetics study, the isoginkgetin, bilobetin and ginkgetin showed mixed inhibitory mechanisms with K_i values < 2.5 µM.
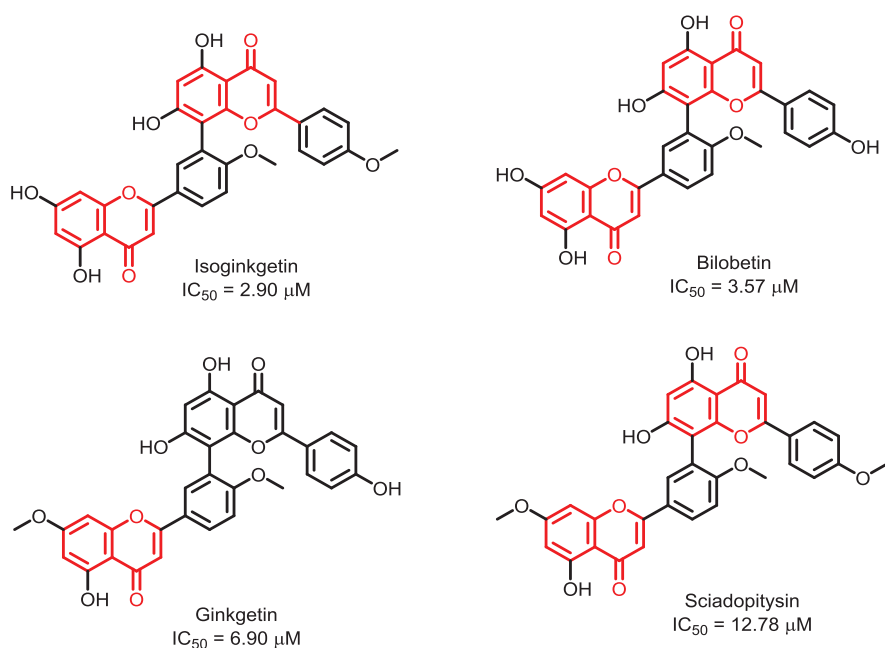
Figure 2.19. PL inhibitory Bis-flavone glycosides from leaf extract of *Ginkgo biloba*

Through the chromatographic study of extracts of flowers of *Cucumis sativa, a* total of 47 flavone glycosides were identified by Olennikov *et al.*[80] Among these flavones, 12 selected ones were screened for PL inhibitory activity using PL of porcine and human origin. Isoorientin-2″-*O*-glucoside and Cucumerin D exhibited good PL inhibitory activity with IC_{50} of 12.68 & 12.53 μM for porcine PL and 10.06 & 10.35 μM for human PL, respectively (**Figure 2.20**).

<table>
<tr><td align="center">Isoorientin-2"-*O*-glucoside
IC_{50} = 12.68 (porcine PL) & 10.06 μM (human PL)</td><td align="center">Cucumerin D
IC_{50} = 12.53 ((porcine PL) & 10.35 μM (human PL).</td></tr>
</table>
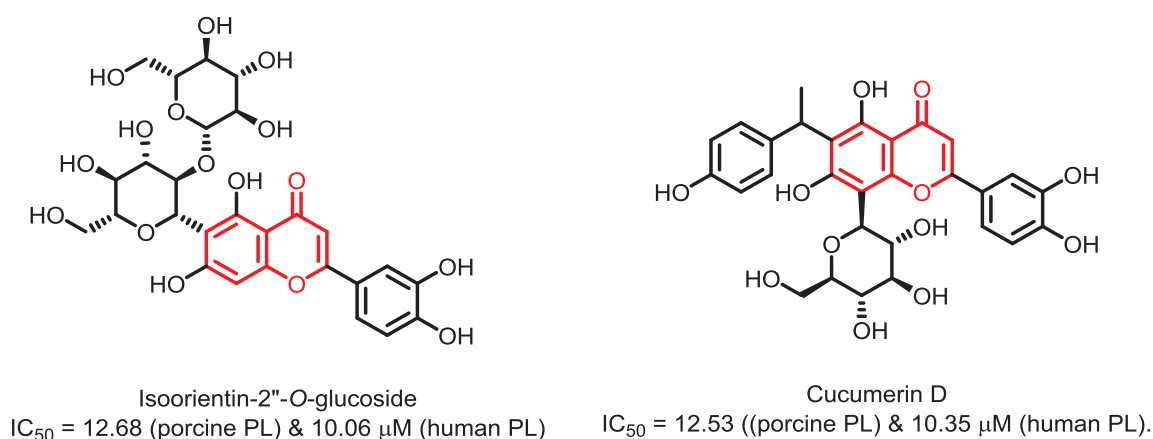
Figure 2.20. Flavone analogues from extracts of flowers of *Cucumis sativa* with PL inhibitory activity

2.4. Synthetic Heterocyclic Analogues as PL Inhibitors

Apart from natural products, there are number of reports on synthetic PL inhibitors. Many of the synthetic analogues with various heterocycles namely, triazole, benzimidazole, quinazolinone, carbazole, indole, isatin, thiazolidinedione, rhodamine, coumarin, chromone, etc. have been designed and reported to have potential PL inhibitory activities.

2.4.1. Azole containing PL inhibitors

In a study by Jalaja *et al.*, an electron rich triazole heterocycle was utilized by for design of PL inhibitors.[81] As shown in **Figure 2.21**, (*E*)-labda-8(17),12-diene-15,16-dial (**32**) natural product (IC_{50} = 14.63 μM) was taken as a hit for semi-synthetic modification. The semi-synthetic labdane appended triazoles were synthesized *via* click chemistry approach. Among these analogues, **33** and **34** exhibited excellent inhibitory activity with IC_{50} of 0.75 and 0.77 μM, respectively (**Figure 2.21**). Also, none of the analogues were cytotoxic on Hep G2 cell lines, in the concentration range of 0.5 to 100 μM.

In a study by Mentese *et al.*, a novel microwave-based synthetic method was optimized for the synthesis of various benzimidazole analogues.[82] The synthesized analogues were screened

for PL inhibitory activity. The analogue **35** exhibited potent inhibitory activity (IC_{50} = 0.40 µM). In another study, a novel series of benzimidazole and bisbenzimidazole analogues were designed and synthesized as PL inhibitors.[83] Among the synthesized analogues, **36** and **37** exhibited potent inhibition with IC_{50} values of 1.72 and 0.98 µM, respectively (**Figure 2.21**).
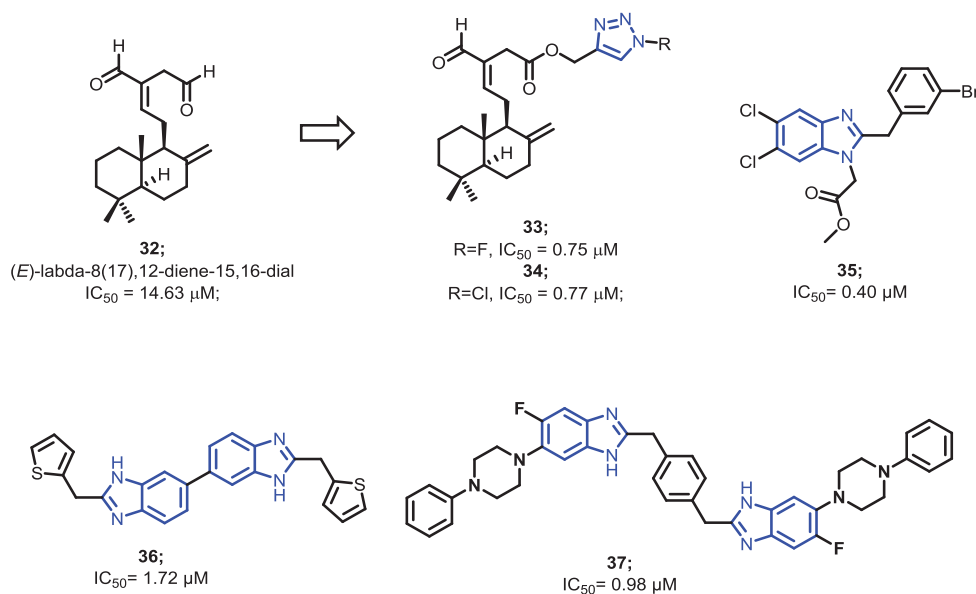
Figure 2.21. PL inhibitory activity of unmodified natural product (**32**) and triazole (**33**, **34**), benzimidazole (**35-37**) containing synthetic analogues

2.4.2. Carbazole and Indole containing PL inhibitors

In many of the reports by Sridhar *et al*., α-ketoamide fragment-based analogues were rationally designed by the incorporation of ketoamide on *N*-containing heterocycles such as carbazole and indole. Carbazole based series of 24 analogues were designed and synthesized followed by *in vitro* PL inhibitory screening.[84] The analogue **38** was found to exhibit potent activity among the series (IC_{50} of 6.31 µM) with competitive inhibitory mechanism. It was then followed by removal of structurally hindered phenyl ring to get indole-based analogues in an attempt of increasing the PL inhibitory potency.[85] The analogue **39** with IC_{50} of 4.92 µM, proved hypothesis right, with competitive nature of inhibition. With the substitution of indole ring *via* 5-methoxy substituent, analogue **40** with IC_{50} of 4.53 µM was identified.[86] Further optimization was performed by the design of bis-indole heterocyclic scaffold with the incorporation of geranyl substituent on one of the indoles.[87] The geranyl substituent was observed to increase the lipophilicity as well as hydrophobic interactions with lid domain amino acids. Among the synthesized analogues, **41** was found to exhibit an IC_{50} of 2.95 µM. Further the lead optimization of **41** led to analogue **42** with additional benzyloxy substituent

on 7th position of indole.[88] The optimized analogue **42** was the best active PL inhibitory analogue among the whole ketoaminde series, with IC_{50} of 1.68 µM. The **Figure 2.22** represents structure of all the above-mentioned carbazole and indole-based PL inhibitory analogues with their IC_{50} values.
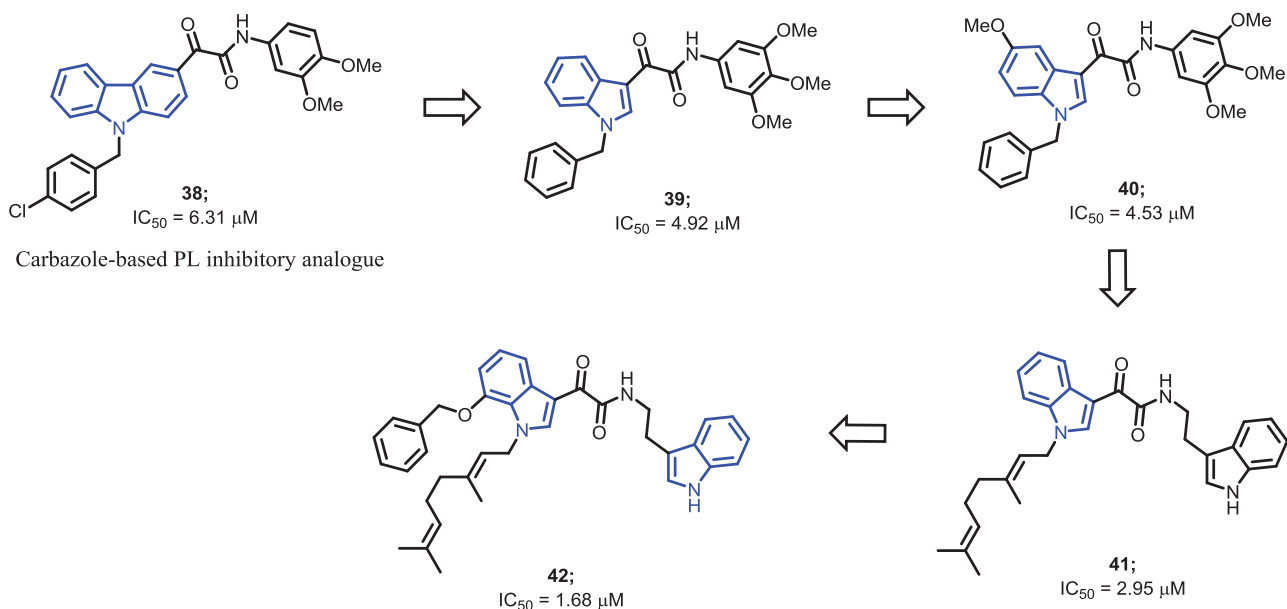
Figure 2.22. Heterocyclic PL inhibitors with carbazole (**38**) and indole nucleus (**39-42**)

2.4.3. Sulphur-containing heterocyclic PL inhibitors

Among various Sulphur-containing heterocycles, Thiazolidinediones (TZDs) represent a renowned class with important contribution towards anti-diabetic medications, in the treatment of type II diabetes mellitus. For the exploration of PL inhibitory potential of the mentioned heterocycle, diaryl substituted pyrazolyl 2,4-thiazolidinediones were synthesized by Sridhar *et al*.[89] From the synthesized analogues, **43** exhibited IC_{50} of 4.81 µM with reversible competitive inhibition (**Figure 2.23**). In a study by Chauhan *et al*., series of rhodanine-3-acetic acid was designed with synthesis and PL inhibitory screening. [90] Among various substituted analogues, the analogue **44** with 2-hydroxynaphthalene substitution exhibited IC_{50} of 5.16 µM (**Figure 2.23**). Further the thiazolidinedione and rhodanine-containing analogues should be optimized to get more potent PL inhibitory leads.

43;
IC$_{50}$ = 4.81 µM

44;
IC$_{50}$ = 5.16 µM
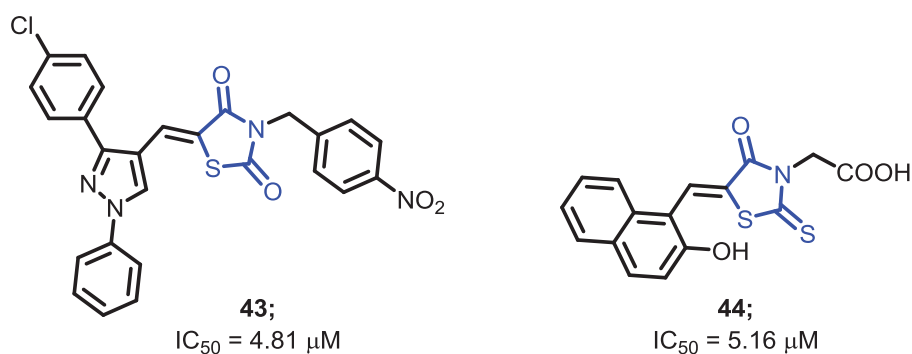
Figure 2.23. PL inhibitory analogues with thiazolidinedione (**43**) and rhodanine (**44**) heterocycles

2.4.4. Oxygen-containing heterocyclic PL inhibitors

There are many *O*-containing heterocycles that plays a major role in the process of drug discovery (including oxirane, oxetane, furan, coumarin, chromone, etc.) Among them, there are reports on coumarin and chromone-containing analogues for PL inhibition. As, in a study by Yadav *et al.*, coumarin-containing analogues were synthesized by *O*-alkylation of umbelliferone.[91] The synthesized analogues were screened for PL inhibitory potential with analogue **45** being potent of the series (IC$_{50}$ = 21.64 µM) (**Figure 2.24**). In another study, a series of coumarin-3-carboxamide analogues were designed, synthesized and evaluated for PL inhibitory activity.[92] Analogue **46** exhibited a moderate inhibitory activity of 19.41 µM with competitive mode of inhibition (**Figure 2.24**). Also, the analogue **46** was found to be non-cytotoxic on 3T3-L1 cell lines till concentration of 20 µM.

In a study by Cardullo *et al.*, a series of semi-synthetic analogues were synthesized by taking naturally isolated compounds (genistein and daidzein) as starting materials. As shown in **Figure 2.24**, the analogue **47** exhibited IC$_{50}$ of 63 µM. The activity was found to be improved as compared with daidzein (IC$_{50}$ of 83 µM)

45;
IC$_{50}$ = 21.64 µM

46;
IC$_{50}$ = 19.41 µM

47;
IC$_{50}$ = 63 µM

Coumarin-containing PL inhibitors

Brominated flavone analogue
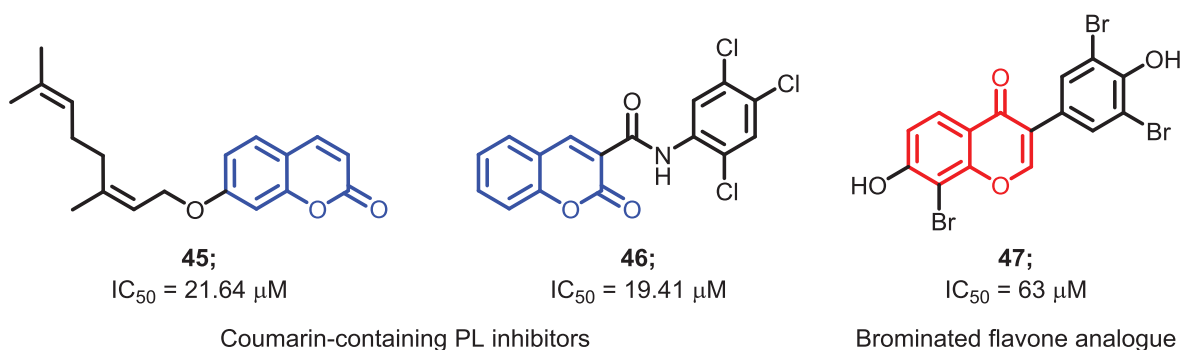
Figure 2.24. PL inhibitory analogues with coumarin (**45**, **46**) and flavone (**47**) scaffolds

2.4.5. Hybrid PL inhibitory analogues

Hybrid analogues are found to be effective in increasing the potency in any of the disease area. Hence, many of the studies are reported for the design and synthesis of hybrid analogues with the help of various heterocycles namely, indole, isatin, thiazolidinedione, coumarin and quinazolinone.

In a study by George *et al.*, thiazolidinedione heterocycle was clubbed with isatin to get a series of thiazolidinedione-containing hybrid analogues. The most potent analogue **48** of the series was exhibited IC_{50} of 7.30 µM.[93] Further to improve the efficacy, a series of indole-thiazolidinedione hybrid analogues were designed and synthesized *via* Knoevenagel condensation of various substituted indole-3-carboxaldehyde with substituted thiazolidinediones.[94] After the PL inhibitory screening of synthesized analogues, **49** was found to be potent of the series, with IC_{50} value of 6.19 µM (**Figure 2.25**). The enzyme kinetics and fluorescence quenching study confirmed the reversible competitive inhibition by analogue **49**.

A novel series of hybrid analogues of 2-substituted quinazolin-4(3*H*)one with coumarin nucleus was designed for PL inhibitory activity by Mentese *et al.*[95] Many of the analogues exhibited moderate to potent PL inhibitory activity with analogue **50** being the potent one with IC_{50} of 2.85 µM (**Figure 2.25**). From the study, it was observed that the conglomeration of coumarin nucleus was found to increase the potential of existing quinazolinone analogues.

The quinazolinone based analogues with amide linkage were designed for the effective interaction with Ser152 amino acid of the active site of PL by George *et al.*[96] The indole heterocycle was clubbed with quinazolinone nucleus with an aim of getting potential PL inhibitors. The best analogue **51** of the series was found to exhibit IC_{50} value of 16.99 µM (**Figure 2.25**). The reversible competitive inhibitory mechanism was confirmed by enzyme kinetics study. Also, the quinazolinone nucleus was hybridized with well-known PL inhibitory indole heterocycle and ketoamide fragment by Auti *et al.*[97] Among the series of 20 analogues, **52** with IC_{50} of 4.86 µM was found to be the best one (**Figure 2.25**).
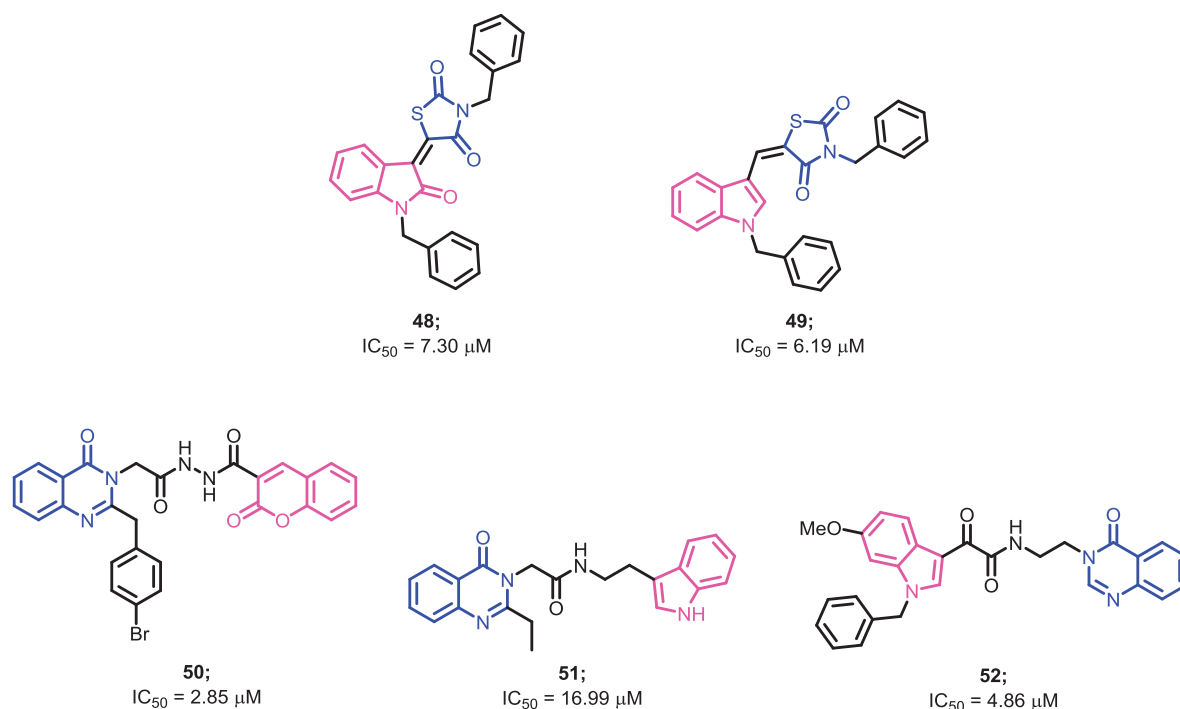
Figure 2.25. PL inhibitory hybrid analogues containing thiazolidinedione, isatin, indole, quinazolinone and coumarin nucleus (**48-52**)

2.5. Gaps in Existing Research

Due to the large imbalance between the energy intake and expenditure associated with a sedentary life, obesity prevalence is increasing in a pandemic proportion. Although diet management and exercise are considered as a key tool for the prevention of obesity, adherence to these strategies seems to be difficult for the obese population. Thus, numerous pharmacotherapies are used for the management of obesity. Based on the exhaustive literature survey, following are the gaps in the existing research in the field of obesity:

- Many of the drugs approved as AOMs are targeting CNS pathways. From the history of AOMs, it is proved that targeting such pathways may lead to serious side effects. In the current scenario, **only a few drugs are available clinically, but their long-term safety is still in question.**

- Among the numerous targets explored for obesity management, inhibition of PL is considered as one of the most promising targets. Orlistat is the only USFDA-approved PL inhibitory drug for the long-term management of obesity. The unavoidable side effects of orlistat include bloating, steatorrhea, fecal incontinence and oily stools.[98] But recently, various reports cite the hepatotoxicity caused by orlistat in long-term treatment regimens. Also, there are 47 cases of acute pancreatitis and 73 cases of kidney stones being filed in FDA adverse reaction files [99]. **These events highlight the**

necessity for the development of effective anti-obesity drugs acting *via* PL inhibition.

- For the development of small molecule inhibitors, natural products have always been an inspiration and numerous phytochemicals have been identified for their PL inhibitory potential. Among these 42% of total natural PL inhibitors are polyphenolics and the major share is of the analogues with bioactive chromone nucleus. Unfortunately, **such analogues are not that potential PL inhibitors as orlistat, which may be due to the absence of structural features that are required for binding the enzyme pocket.**

- In many of the reports, the **isolation of these natural products has not been carried out by focusing on their PL inhibitory activity**.

- Looking at the importance of heterocyclic scaffolds many of the heterocycles, namely indole, carbazole, thiazolidinedione, quinazolinone, coumarin have been utilized for the development of novel PL inhibitors with positive results. **But there is no report on the rational development of chromone-based synthetic PL inhibitory analogues**.

- Being an important PL inhibitory natural product, **the chromone scaffold remained unexplored for rational designing of PL inhibitory analogues**.

2.6. Aim of the Study

Considering the potential gaps in existing research, in this study our aim is, "*to develop chromone-based analogues as potential PL inhibitors for treatment of obesity*".

2.7. Objectives

The objective of the study will be design of chromone-based PL inhibitors using molecular docking studies, followed by synthesis and *in vitro* evaluation to get most potent PL inhibitory lead. Further, the most potent analogue will be tested for *in vivo* anti-obesity activity.

References

(1)   Abdel-Hafez, S. H. Selenium containing heterocycles: Synthesis, anti-inflammatory, analgesic and anti-microbial activities of some new 4-cyanopyridazine-3(2h)selenone derivatives. *Eur. J. Med. Chem.* **2008**, *43* (9), 1971–1977.

(2)   Vasu Govardhana Reddy, P.; Kiran, Y. B. R.; Suresh Reddy, C.; Devendranath Reddy, C. Synthesis and antimicrobial activity of novel phosphorus heterocycles with exocyclic p-c link. *Chem. Pharm. Bull.* **2004**, *52* (3), 307–310.

(3)   Ogawa, Y.; Tokunaga, E.; Kobayashi, O.; Hirai, K.; Shibata, N. Current contributions of organofluorine compounds to the agrochemical industry. *iScience* **2020**, *23* (9), 101467.

(4)   Jampilek, J. Heterocycles in medicinal chemistry. *Molecules* **2019**, *24* (21), 10–13.

(5)   Deiters, A.; Martin, S. F. Synthesis of oxygen- and nitrogen-containing heterocycles by ring-closing metathesis. *Chem. Rev.* **2004**, *104*, 2199–2238.

(6)   Griffith, E. C.; Su, Z.; Turk, B. E.; Chen, S.; Chang, Y. H.; Wu, Z.; Biemann, K.; Liu, J. O. Methionine aminopeptidase (type 2) is the common target for angiogenesis inhibitors agm-1470 and ovalicin. *Chem. Biol.* **1997**, *4* (6), 461–471.

(7)   YANG, Y. H.; MAO, J. W.; TAN, X. L. Research progress on the source, production, and anti-cancer mechanisms of paclitaxel. *Chin. J. Nat. Med.* **2020**, *18* (12), 10–17.

(8)   McMahon, B. A.; Chawla, L. S. The furosemide stress test: current use and future potential. *Ren. Fail.* **2021**, *43* (1), 830–839.

(9)   Keri, R. S.; Budagumpi, S.; Pai, R. K.; Balakrishna, R. G. Chromones as a privileged scaffold in drug discovery: A review. *Eur. J. Med. Chem.* **2014**, *78*, 340–374.

(10)   Ungwitayatorn, J.; Wiwat, C.; Samee, W.; Nunthanavanit, P.; Phosrithong, N. Synthesis, in vitro evaluation, and docking studies of novel chromone derivatives as HIV-1 protease inhibitor. *J. Mol. Struct.* **2011**, *1001* (1–3), 152–161.

(11)   Kuroda, M.; Uchida, S.; Watanabe, K.; Mimaki, Y. Chromones from the tubers of eranthis cilicica and their antioxidant activity. *Phytochemistry* **2009**, *70* (2), 288–293.

(12)   Larget, R.; Lockhart, B.; Renard, P.; Largeron, M. A convenient extension of the wessely-moser rearrangement for the synthesis of substituted alkylaminoflavones as neuroprotective agents in vitro. *Bioorganic Med. Chem. Lett.* **2000**, *10* (8), 835–838.

(13)   Kidwai, M.; Saxena, S.; Khan, M. K. R.; Thukral, S. S. Aqua mediated synthesis of substituted 2-amino-4H-chromenes and in vitro study as antibacterial agents. *Bioorganic Med. Chem. Lett.* **2005**, *15* (19), 4295–4298.

(14)   Al Nakib, T.; Bezjak, V.; Meegan, M.; Chandy, R. Synthesis and antifungal activity of some 3-benzylidenechroman-4-ones, 3-benzylidenethiochroman-4-ones and 2-benzylidene-1-tetralones. *Eur. J. Med. Chem.* **1990**, *25* (5), 455–462.

(15)   Nohara, A.; Umetani, T.; Sanno, Y. A facile synthesis of chromone-3-carboxaldehyde, chromone-3-carboxylic acid and 3-hydroxymethylchromone. *Tetrahedron Lett.* **1973**, *14* (22), 1995–1998.

(16)   Ivasiv, Viktoriya; Albertini, Claudia; Gonçalves, Ana E.; Rossi, Michele; Bolognesi,

M. L. Molecular hybridization as a tool for designing multitarget drug candidates for complex diseases. *Curr. Top. Med. Chem.* **2019**, *19* (19), 1694–1711.

(17) Chooi, Y. C.; Ding, C.; Magkos, F. The epidemiology of obesity. *Metab. Clin. Exp.* **2019**, *92*, 6–10.

(18) Kopelman, P. G. Obesity as a medical problem. *Nature.* **2000**, *404* (6778), 635–643.

(19) Handlon, A. L.; Zhou, H. Melanin-concentrating hormone-1 receptor antagonists for the treatment of obesity. *J. Med. Chem.* **2006**, *49* (14), 4017–4022.

(20) Högberg, T.; Frimurer, T. M.; Sasmal, P. K. Melanin concentrating hormone receptor 1 (MCHR1) antagonists - still a viable approach for obesity treatment? *Bioorganic Med. Chem. Lett.* **2012**, *22* (19), 6039–6047.

(21) Lynch, J. K.; Freeman, J. C.; Judd, A. S.; Iyengar, R.; Mulhern, M.; Zhao, G.; Napier, J. J.; Wodka, D.; Brodjian, S.; Dayton, B. D.; Falls, D.; Ogiela, C.; Reilly, R. M.; Campbell, T. J.; Polakowski, J. S.; Hernandez, L.; Marsh, K. C.; Shapiro, R.; Knourek-Segel, V.; Droz, B.; Bush, E.; Brune, M.; Preusser, L. C.; Fryer, R. M.; Reinhart, G. A.; Houseman, K.; Diaz, G.; Mikhail, A.; Limberis, J. T.; Sham, H. L.; Collins, C. A.; Kym, P. R. Optimization of chromone-2-carboxamide melanin concentrating hormone receptor 1 antagonists: Assessment of potency, efficacy, and cardiovascular safety. *J. Med. Chem.* **2006**, *49* (22), 6569–6584.

(22) Iyengar, R. R.; Lynch, J. K.; Mulhern, M. M.; Judd, A. S.; Freeman, J. C.; Gao, J.; Souers, A. J.; Zhao, G.; Wodka, D.; Doug Falls, H.; Brodjian, S.; Dayton, B. D.; Reilly, R. M.; Swanson, S.; Su, Z.; Martin, R. L.; Leitza, S. T.; Houseman, K. A.; Diaz, G.; Collins, C. A.; Sham, H. L.; Kym, P. R. An evaluation of 3,4-methylenedioxy phenyl replacements in the aminopiperidine chromone class of MCHR1 antagonists. *Bioorganic Med. Chem. Lett.* **2007**, *17* (4), 874–878.

(23) Joshi, S. R.; Standl, E.; Tong, N.; Shah, P.; Kalra, S.; Rathod, R. Therapeutic potential of α-glucosidase inhibitors in type 2 diabetes mellitus: An evidence-based review. *Expert Opin. Pharmacother.* **2015**, *16* (13), 1959–1981.

(24) A. Rane, R.; Karunanidhi, S.; Jain, K.; Shaikh, M.; Hampannavar, G.; Karpoormath, R. A recent perspective on discovery and development of diverse therapeutic agents inspired from isatin alkaloids. *Curr. Top. Med. Chem.* **2016**, *16* (11), 1262–1289.

(25) Khan, F. A.; Maalik, A. Advances in pharmacology of isatin and its derivatives: a review. *Trop. J. Pharm. Res.* **2015**, *14* (10), 1937–1942.

(26) Xie, C.; Tang, L. M.; Li, F. N.; Guan, L. P.; Pan, C. Y.; Wang, S. H. Structure-based design, synthesis, andanticonvulsant activity of isatin-1-N-phenylacetamide derivatives. *Med. Chem. Res.* **2014**, *23* (5), 2161–2168.

(27) Xie, Z.; Wang, G.; Wang, J.; Chen, M.; Peng, Y.; Li, L.; Deng, B.; Chen, S.; Li, W. Synthesis, biological evaluation, and molecular docking studies of novel isatin-thiazole derivatives as α-glucosidase inhibitors. *Molecules* **2017**, *22* (4), 659.

(28) Zhang, X. M.; Guo, H.; Li, Z. S.; Song, F. H.; Wang, W. M.; Dai, H. Q.; Zhang, L. X.; Wang, J. G. Synthesis and evaluation of isatin-β-thiosemicarbazones as novel agents against antibiotic-resistant gram-positive bacterial species. *Eur. J. Med. Chem.* **2015**, *101*, 419–430.

(29) Bal, T. R.; Anand, B.; Yogeeswari, P.; Sriram, D. Synthesis and evaluation of anti-

HIV activity of isatin β-thiosemicarbazone derivatives. *Bioorganic Med. Chem. Lett.* **2005**, *15* (20), 4451–4455.

(30) Rahim, F.; Malik, F.; Ullah, H.; Wadood, A.; Khan, F.; Javid, M. T.; Taha, M.; Rehman, W.; Ur Rehman, A.; Khan, K. M. Isatin based schiff bases as inhibitors of α-glucosidase: Synthesis, characterization, in vitro evaluation and molecular docking studies. *Bioorg. Chem.* **2015**, *60*, 42–48.

(31) Rahim, F.; Taha, M.; Iqbal, N.; Hayat, S.; Qureshi, F.; Uddin, I.; Zaman, K.; Rab, A.; Wadood, A.; Uddin, N.; Nawaz, M.; Shah, S. A. A.; Khan, K. M. Isatin based thiosemicarbazide derivatives as potential inhibitor of α-glucosidase, synthesis and their molecular docking study. *J. Mol. Struct.* **2020**, *1222*, 128922.

(32) Wang, G.; Wang, J.; He, D.; Li, X.; Li, J.; Peng, Z. Synthesis, in vitro evaluation and molecular docking studies of novel coumarin-isatin derivatives as α-glucosidase inhibitors. *Chem. Biol. Drug Des.* **2017**, *89* (3), 456–463.

(33) Wang, G.; Chen, M.; Qiu, J.; Xie, Z.; Cao, A. Synthesis, in vitro α-glucosidase inhibitory activity and docking studies of novel chromone-isatin derivatives. *Bioorganic Med. Chem. Lett.* **2018**, *28* (2), 113–116.

(34) Wang, G.; Chen, M.; Wang, J.; Peng, Y.; Li, L.; Xie, Z. Z.; Deng, B.; Chen, S.; Li, W. Synthesis, biological evaluation and molecular docking studies of chromone hydrazone derivatives as α-glucosidase inhibitors. *Bioorganic Med. Chem. Lett.* **2017**, *27* (13), 2957–2961.

(35) Kantankar, A.; Jayaprakash Rao, Y.; Mallikarjun, G.; Hemasri, Y.; Kethiri, R. R. Rational design, synthesis, biological evaluation and molecular docking studies of chromone-pyrimidine derivatives as potent anti-cancer agents. *J. Mol. Struct.* **2021**, *1239*, 130502.

(36) Yavuz, S. Ç.; Akkoç, S.; Tüzün, B.; Şahin, O.; Saripinar, E. Efficient synthesis and molecular docking studies of new pyrimidine-chromeno hybrid derivatives as potential antiproliferative agents. *Synth. Commun.* **2021**, *51* (14), 2135–2159.

(37) Shaw, A. Y.; Chang, C. Y.; Liau, H. H.; Lu, P. J.; Chen, H. L.; Yang, C. N.; Li, H. Y. Synthesis of 2-styrylchromones as a novel class of antiproliferative agents targeting carcinoma cells. *Eur. J. Med. Chem.* **2009**, *44* (6), 2552–2562.

(38) Kaplánek, R.; Jakubek, M.; Rak, J.; Kejík, Z.; Havlík, M.; Dolenský, B.; Frydrych, I.; Hajdúch, M.; Kolář, M.; Bogdanová, K.; Králová, J.; Džubák, P.; Král, V. Caffeine-hydrazones as anticancer agents with pronounced selectivity toward T-lymphoblastic leukaemia cells. *Bioorg. Chem.* **2015**, *60*, 19–29.

(39) Reddy, O. S.; Suryanarayana, C. V.; Narayana, K. J. P.; Anuradha, V.; Babu, B. H. Synthesis and cytotoxic evaluation for some new 2,5-disubstituted pyrimidine derivatives for anticancer activity. *Med. Chem. Res.* **2015**, *24* (5), 1777–1788.

(40) China Raju, B.; Nageswara Rao, R.; Suman, P.; Yogeeswari, P.; Sriram, D.; Shaik, T. B.; Kalivendi, S. V. Synthesis, structure-activity relationship of novel substituted 4h-chromen-1,2,3,4-tetrahydropyrimidine-5-carboxylates as potential anti-mycobacterial and anticancer agents. *Bioorganic Med. Chem. Lett.* **2011**, *21* (10), 2855–2859.

(41) Chen, Q. H.; Yu, K.; Zhang, X.; Chen, G.; Hoover, A.; Leon, F.; Wang, R.; Subrahmanyam, N.; Addo Mekuria, E.; Harinantenaina Rakotondraibe, L. A new class

of hybrid anticancer agents inspired by the synergistic effects of curcumin and genistein: Design, synthesis, and anti-proliferative evaluation. *Bioorganic Med. Chem. Lett.* **2015**, *25* (20), 4553–4556.

(42)   Shatokhin, S. S.; Tuskaev, V. A.; Gagieva, S. C.; Markova, A. A.; Pozdnyakov, D. I.; Melnikova, E. K.; Bulychev, B. M.; Oganesyan, E. T. Synthesis, cytotoxic and antioxidant activities of new N-substituted 3-(benzimidazol-2-yl)-chromones containing 2,6-di-tert-butylphenol fragment. *J. Mol. Struct.* **2022**, *1249*, 131683.

(43)   Moellering, R. C. Discovering new antimicrobial agents. *Int. J. Antimicrob. Agents* **2011**, *37* (1), 2–9.

(44)   Cano, P. A.; Islas-Jácome, A.; Rangel-Serrano, Á.; Anaya-Velázquez, F.; Padilla-Vaca, F.; Trujillo-Esquivel, E.; Ponce-Noyola, P.; Martínez-Richa, A.; Gámez-Montaño, R. In vitro studies of chromone-tetrazoles against pathogenic protozoa, bacteria, and fungi. *Molecules* **2015**, *20* (7), 12436–12449.

(45)   Pathan, N.; Ali, P.; Rahatgaonkar, A.; Al-Mousa, K. An efficient one pot I_2/DMSO mediated synthesis and molecular modeling of novel fused pyrimidine-chromone hybrids bearing potential antibacterial and antifungal pharmacophores sites. *J. Heterocycl. Chem.* **2021**, *58* (8), 1675–1689.

(46)   Arango, V.; Domínguez, J. J.; Cardona, W.; Robledo, S. M.; Muñoz, D. L.; Figadere, B.; Sáez, J. Synthesis and leishmanicidal activity of quinoline-triclosan and quinoline-eugenol hybrids. *Med. Chem. Res.* **2012**, *21* (11), 3445–3454.

(47)   Otero, E.; Vergara, S.; Robledo, S. M.; Cardona, W.; Carda, M.; Vélez, I. D.; Rojas, C.; Otálvaro, F. Synthesis, leishmanicidal and cytotoxic activity of triclosan-chalcone, triclosan-chromone and triclosan-coumarin hybrids. *Molecules* **2014**, *19* (9), 13251–13266.

(48)   Nalla, V.; Shaikh, A.; Bapat, S.; Vyas, R.; Karthikeyan, M.; Yogeeswari, P.; Sriram, D.; Muthukrishnan, M. Identification of potent chromone embedded [1,2,3]-triazoles as novel anti-tubercular agents. *R. Soc. Open Sci.* **2018**, *5* (4), 171750.

(49)   Coa, J. C.; García, E.; Carda, M.; Agut, R.; Vélez, I. D.; Muñoz, J. A.; Yepes, L. M.; Robledo, S. M.; Cardona, W. I. Synthesis, leishmanicidal, trypanocidal and cytotoxic activities of quinoline-chalcone and quinoline-chromone hybrids. *Med. Chem. Res.* **2017**, *26* (7), 1405–1414.

(50)   García, E.; Coa, J. C.; Otero, E.; Carda, M.; Vélez, I. D.; Robledo, S. M.; Cardona, W. I. Synthesis and antiprotozoal activity of furanchalcone–quinoline, furanchalcone–chromone and furanchalcone–imidazole hybrids. *Med. Chem. Res.* **2018**, *27* (2), 497–511.

(51)   Mhyre, T. R.; Nw, R.; Boyd, J. T.; Hall, G.; Room, C. Protein aggregation and fibrillogenesis in cerebral and systemic amyloid disease. In *Subcellular Biochemistry*; 2012; Vol. 65, pp 389–455.

(52)   Husain, A.; Balushi K, A.; Akhtar, M. J.; Khan, S. A. Coumarin linked heterocyclic hybrids: A promising approach to develop multi target drugs for alzheimer's disease. *J. Mol. Struct.* **2021**, *1241*, 130618.

(53)   Holmquist, L.; Stuchbury, G.; Berbaum, K.; Muscat, S.; Young, S.; Hager, K.; Engel, J.; Münch, G. Lipoic acid as a novel treatment for alzheimer's disease and related

dementias. *Pharmacol. Ther.* **2007**, *113* (1), 154–164.

(54)   Jalili-Baleh, L.; Nadri, H.; Forootanfar, H.; Küçükkılınç, T. T.; Ayazgök, B.; Sharifzadeh, M.; Rahimifard, M.; Baeeri, M.; Abdollahi, M.; Foroumadi, A.; Khoobi, M. Chromone–lipoic acid conjugate: Neuroprotective agent having acceptable butyrylcholinesterase inhibition, antioxidant and copper-chelation activities. *DARU J. Pharm. Sci.* **2021**, *29* (1), 23–38.

(55)   Bhagat, S.; Shah, P.; Garg, S. K.; Mishra, S.; Kamal Kaur, P.; Singh, S.; Chakraborti, A. K. Aminophosphonates as novel anti-leishmanial chemotypes: Synthesis, biological evaluation, and comfa studies. *MedChemComm.* **2014**, *5* (5), 665–670.

(56)   Valasani, K. R.; Hu, G.; Chaney, M. O.; Yan, S. S. Structure-based design and synthesis of benzothiazole phosphonate analogues with inhibitors of human ABAD-Aβ for treatment of alzheimer's disease. *Chem. Biol. Drug Des.* **2013**, *81* (2), 238–249.

(57)   Atherton, F. R.; Hassall, C. H.; Lambert, R. W. Synthesis and structure-activity relationships of antibacterial phosphonopeptides incorporating (1-aminoethyl)phosphonic acid and (aminomethyl)phosphonic acid. *J. Med. Chem.* **1986**, *29* (1), 29–40.

(58)   Thaslim Basha, S.; Sudhamani, H.; Rasheed, S.; Venkateswarlu, N.; Vijaya, T.; Naga Raju, C. Microwave-assisted neat synthesis of α-aminophosphonate/phosphinate derivatives of 2-(2-aminophenyl)benzothiazole as potent antimicrobial and antioxidant agents. *Phosphorus, Sulfur Silicon Relat. Elem.* **2016**, *191* (10), 1339–1343.

(59)   Shaikh, S.; Dhavan, P.; Ramana, M. M. V.; Jadhav, B. L. Design, synthesis and evaluation of new chromone-derived aminophosphonates as potential acetylcholinesterase inhibitor. *Mol. Divers.* **2021**, *25* (2), 811–825.

(60)   Kapková, P.; Alptüzün, V.; Frey, P.; Erciyas, E.; Holzgrabe, U. Search for dual function inhibitors for alzheimer's disease: synthesis and biological activity of acetylcholinesterase inhibitors of pyridinium-type and their Aβ fibril formation inhibition capacity. *Bioorganic Med. Chem.* **2006**, *14* (2), 472–478.

(61)   Sharma, P.; Tripathi, A.; Tripathi, P. N.; Prajapati, S. K.; Seth, A.; Tripathi, M. K.; Srivastava, P.; Tiwari, V.; Krishnamurthy, S.; Shrivastava, S. K. Design and development of multitarget-directed N-benzylpiperidine analogs as potential candidates for the treatment of alzheimer's disease. *Eur. J. Med. Chem.* **2019**, *167*, 510–524.

(62)   Abdpour, S.; Jalili-Baleh, L.; Nadri, H.; Forootanfar, H.; Bukhari, S. N. A.; Ramazani, A.; Ebrahimi, S. E. S.; Foroumadi, A.; Khoobi, M. Chromone derivatives bearing pyridinium moiety as multi-target-directed ligands against alzheimer's disease. *Bioorg. Chem.* **2021**, *110*, 104750.

(63)   Shih, J. C.; Chen, K.; Ridd, M. J. Monoamine oxidase: from genes to behavior. *Annu. Rev. Neurosci.* **1999**, *22*, 197–217.

(64)   Mellick, G. D.; Buchanan, D. D.; McCann, S. J.; James, K. M.; Johnson, A. G.; Davis, D. R.; Liyou, N.; Chan, D.; Le Couteur, D. G. Variations in the monoamine oxidase B LPAR;MAOB) gene are associated with parkinson's disease. *Mov. Disord.* **1999**, *14* (2), 219–224.

(65)   Bar-Am, O.; Amit, T.; Weinreb, O.; Youdim, M. B. H.; Mandel, S. Propargylamine

containing compounds as modulators of proteolytic cleavage of amyloid protein precursor: involvement of MAPK and PKC activation. *J. Alzheimer's Dis.* **2010**, *21* (2), 361–371.

(66) Yogev-Falach, M.; Bar-Am, O.; Amit, T.; Weinreb, O.; Youdim, M. B. H.; Yogev-Falach, M.; Bar-Am, O.; Amit, T.; Weinreb, O.; Youdim, 2, M. B. H. A multifunctional, neuroprotective drug, ladostigil (TV-3,326), regulates holo-app translation and processing. *FASEB J.* **2006**, *20* (12), 2177–2179.

(67) Legoabe, L. J.; Petzer, A.; Petzer, J. P. Inhibition of monoamine oxidase by selected c6-substituted chromone derivatives. *Eur. J. Med. Chem.* **2012**, *49*, 343–353.

(68) Gaspar, A.; Teixeira, F.; Uriarte, E.; Milhazes, N.; Melo, A.; Cordeiro, M. N. D. S.; Ortuso, F.; Alcaro, S.; Borges, F. Towards the discovery of a novel class of monoamine oxidase inhibitors: Structure-property-activity and docking studies on chromone amides. *ChemMedChem* **2011**, *6* (4), 628–632.

(69) Wang, X. B.; Yin, F. C.; Huang, M.; Jiang, N.; Lan, J. S.; Kong, L. Y. Chromone and donepezil hybrids as new multipotent cholinesterase and monoamine oxidase inhibitors for the potential treatment of alzheimer's disease. *RSC Med. Chem.* **2020**, *11* (2), 225–233.

(70) Pachón-Angona, I.; Refouvelet, B.; Andrýs, R.; Martin, H.; Luzet, V.; Iriepa, I.; Moraleda, I.; Diez-Iriepa, D.; Oset-Gasque, M. J.; Marco-Contelles, J.; Musilek, K.; Ismaili, L. Donepezil + chromone + melatonin hybrids as promising agents for alzheimer's disease therapy. *J. Enzyme Inhib. Med. Chem.* **2019**, *34* (1), 479–489.

(71) Lee, E. M.; Lee, S. S.; Chung, B. Y.; Cho, J. Y.; Lee, I. C.; Ahn, S. R.; Jang, S. J.; Kim, T. H. Pancreatic lipase inhibition by c-glycosidic flavones isolated from Eremochloa ophiuroides. *Molecules* **2010**, *15* (11), 8251–8259.

(72) Sergent, T.; Vanderstraeten, J.; Winand, J.; Beguin, P.; Schneider, Y. J. Phenolic compounds and plant extracts as potential natural anti-obesity substances. *Food Chem.* **2012**, *135* (1), 68–73.

(73) Swilam, N.; Nawwar, M. Antidiabetic and anti-obesity acylated avonol diglucoside from Ammannia baccifera l . subsp . aegyptiaca (willd .) koehne waste (Preprint) **2020**, 1–32.

(74) Fernando, W. I. T.; Attanayake, A. M. K. C.; Perera, H. K. I.; Sivakanesan, R.; Jayasinghe, L.; Araya, H.; Fujimoto, Y. Isolation, identification and characterization of pancreatic lipase inhibitors from Trigonella foenum-graecum seeds. *South African J. Bot.* **2019**, *121*, 418–421.

(75) Hou, X. D.; Ge, G. B.; Weng, Z. M.; Dai, Z. R.; Leng, Y. H.; Ding, L. Le; Jin, L. L.; Yu, Y.; Cao, Y. F.; Hou, J. Natural constituents from cortex Mori radicis as new pancreatic lipase inhibitors. *Bioorg. Chem.* **2018**, *80*, 577–584.

(76) Jeong, J. Y.; Jo, Y. H.; Kim, S. B.; Liu, Q.; Lee, J. W.; Mo, E. J.; Lee, K. Y.; Hwang, B. Y.; Lee, M. K. Pancreatic lipase inhibitory constituents from Morus alba leaves and optimization for extraction conditions. *Bioorganic Med. Chem. Lett.* **2015**, *25* (11), 2269–2274.

(77) Elsbaey, M.; Amen, Y.; Nakagawa, T.; Shimizu, K. White poplar: Targeted isolation of pancreatic lipase inhibitors. *Ind. Crops Prod.* **2019**, *141*, 111778.

(78) Huang, X.; Zhu, J.; Wang, L.; Jing, H.; Ma, C.; Kou, X.; Wang, H. Inhibitory mechanisms and interaction of tangeretin, 5-demethyltangeretin, nobiletin, and 5-demethylnobiletin from citrus peels on pancreatic lipase: Kinetics, spectroscopies, and molecular dynamics simulation. *Int. J. Biol. Macromol.* **2020**, *164*, 1927–1938.

(79) Liu, P. K.; Weng, Z. M.; Ge, G. B.; Li, H. L.; Ding, L. Le; Dai, Z. R.; Hou, X. D.; Leng, Y. H.; Yu, Y.; Hou, J. Biflavones from Ginkgo biloba as novel pancreatic lipase inhibitors: inhibition potentials and mechanism. *Int. J. Biol. Macromol.* **2018**, *118*, 2216–2223.

(80) Olennikov, D. N. Separation, characterization and mammal pancreatic lipase inhibitory potential of cucumber flower flavonoids. *Separations* **2023**, *10* (4), 255–275.

(81) Jalaja, R.; Leela, S. G.; Valmiki, P. K.; Salfeena, C. T. F.; Ashitha, K. T.; Krishna Rao, V. R. D.; Nair, M. S.; Gopalan, R. K.; Somappa, S. B. Discovery of natural product derived labdane appended triazoles as potent pancreatic lipase inhibitors. *ACS Med. Chem. Lett.* **2018**, *9* (7), 662–666.

(82) Menteşe, E.; Bektaş, H.; Ülker, S.; Bekircan, O.; Kahveci, B. Microwave-assisted synthesis of new benzimidazole derivatives with lipase inhibition activity. *J. Enzyme Inhib. Med. Chem.* **2014**, *29* (1), 64–68.

(83) Menteşe, E.; Yılmaz, F.; Emirik, M.; Ülker, S.; Kahveci, B. Synthesis, molecular docking and biological evaluation of some benzimidazole derivatives as potent pancreatic lipase inhibitors. *Bioorg. Chem.* **2018**, *76*, 478–486.

(84) Sridhar, S. N. C.; Ginson, G.; Venkataramana Reddy, P. O.; Tantak, M. P.; Kumar, D.; Paul, A. T. Synthesis, evaluation and molecular modelling studies of 2-(carbazol-3-yl)-2-oxoacetamide analogues as a new class of potential pancreatic lipase inhibitors. *Bioorganic Med. Chem.* **2017**, *25* (2), 609–620.

(85) Sridhar, S. N. C.; Palawat, S.; Paul, A. T. Design, synthesis, biological evaluation and molecular modelling studies of indole glyoxylamides as a new class of potential pancreatic lipase inhibitors. *Bioorg. Chem.* **2019**, *85*, 373–381.

(86) Sridhar, S. N. C.; Palawat, S.; Paul, A. T. Design, synthesis, biological evaluation and molecular modelling studies of conophylline inspired novel indolyl oxoacetamides as potent pancreatic lipase inhibitors. *New J. Chem.* **2020**, *44* (28), 12355–12369.

(87) Sridhar, S. N. C.; Palawat, S.; Paul, A. T. Design, synthesis, evaluation, and molecular modeling studies of indolyl oxoacetamides as potential pancreatic lipase inhibitors. *Arch. Pharm.* **2020**, *353* (8), 1–11.

(88) Sridhar, S. N. C.; Sengupta, P.; Palawat, S.; Dileep, P. S.; George, G.; Paul, A. T. Synthesis, molecular modelling, in vitro and in vivo evaluation of conophylline inspired novel benzyloxy substituted indole glyoxylamides as potent pancreatic lipase inhibitors. *J. Biomol. Struct. Dyn.* **2022**, *40* (19), 9530–9542.

(89) Sridhar, S. N. C.; Bhurta, D.; Kantiwal, D.; George, G.; Monga, V.; Paul, A. T. Design, synthesis, biological evaluation and molecular modelling studies of novel diaryl substituted pyrazolyl thiazolidinediones as potent pancreatic lipase inhibitors. *Bioorganic Med. Chem. Lett.* **2017**, *27* (16), 3749–3754.

(90) Chauhan, D.; George, G.; Sridhar, S. N. C.; Bhatia, R.; Paul, A. T.; Monga, V. Design, synthesis, biological evaluation, and molecular modeling studies of rhodanine

derivatives as pancreatic lipase inhibitors. *Arch. Pharm.* **2019**, *352* (10).

(91)   Yadav, N.; Auti, P.; George, G.; Paul, A. T. Design, synthesis and biological evaluation of o-alkyl umbelliferone derivatives as pancreatic lipase inhibitors. *J. Indian Chem. Soc.* **2020**, *97* (8), 1265–1271.

(92)   Yadav, N.; Paul, A. T. Synthesis of amide warhead containing coumarin derivatives as potential pancreatic lipase inhibitors: in silico and in vitro evaluation for obesity treatment. *Med. Chem. Res.* **2023**, *32* (10), 2219–2233.

(93)   George, G.; Auti, P. S.; Paul, A. T. Design, synthesis,: in silico molecular modelling studies and biological evaluation of novel indole-thiazolidinedione hybrid analogues as potential pancreatic lipase inhibitors. *New J. Chem.* **2021**, *45* (3), 1381–1394.

(94)   George, G.; Auti, P. S.; Paul, A. T. Design, synthesis and biological evaluation of n-substituted indole-thiazolidinedione analogues as potential pancreatic lipase inhibitors. *Chem. Biol. Drug Des.* **2021**, *98* (1), 49–59.

(95)   Menteşe, E.; Karaali, N.; Akyüz, G.; Yılmaz, F.; Ülker, S.; Kahveci, B. Synthesis and evaluation of α-glucosidase and pancreatic lipase inhibition by quinazolinone-coumarin hybrids. *Chem. Heterocycl. Compd.* **2016**, *52* (12), 1017–1024.

(96)   George, G.; Yadav, N.; Auti, P. S.; Paul, A. T. Molecular modelling, synthesis and in vitro evaluation of quinazolinone hybrid analogues as potential pancreatic lipase inhibitors. *J. Biomol. Struct. Dyn.* **2022**, *41* (19), 9583–9601.

(97)   Auti, P. S.; Nandi, A.; Kumari, V.; Paul, A. T. Design, synthesis, biological evaluation and molecular modelling studies of oxoacetamide warhead containing indole-quinazolinone based novel hybrid analogues as potential pancreatic lipase inhibitors. *New J. Chem.* **2022**, *46* (24), 11648–11661.

(98)   Garza, A. L. de la; Milagro Yoldi, F. I.; Boque, N.; Campión Zabalza, J.; Martinez, J. A. Natural inhibitors of pancreatic lipase as new players in obesity treatment. *Planta Med.* **2011**, *77* (8), 773–785.

(99)   Elizebeth, B.; Rebecca, K.; Micheal, C.; Wolfe, S. M. *Petition to FDA to Ban Orlistat (Alli, Xenical)*; 2013. https://www.citizen.org/wp-content/uploads/migration/1942.pdf.

CHAPTER 3
MATERIALS AND METHODS

CHAPTER 3

3. Materials and Methods

3.1. Synthesis and Characterization

The synthesis of all the analogues was performed according to the schemes reported in each section. The chemicals required for synthetic work were purchased from Sigma Aldrich, Tokyo Chemical Industry (TCI), Spectrochem, etc. Thin Layer Chromatography (TLC) plates (silica gel G60, F_{254}, make: Merck) were used for reaction monitoring. The melting point of synthesized analogues were determined using electrothermal capillary melting point apparatus. The IR spectra were recorded on Shimadzu IR Spirit Fourier Transform Infrared (FTIR) Spectrophotometer. Bruker Avance II 400 spectrometer (400 MHz) was used for recording NMR spectra. $CDCl_3$ solvent used for NMR was procured from Sigma Aldrich. Bruker Compass Data Analysis 4.1 mass spectrometer was utilized for obtaining HR-MS spectra of all the analogues.

Peak purity analysis was performed using DIONEX ULTIMATE 3000 UHPLC system with Diode Array Detector (Make: Thermo SCIENTIFIC). The X-Bridge column (Column dimension: 4.6 mm * 250 mm, 5.0 µm) was procured from Waters. The solvent system used was ACN: Water with a flow rate of 1.00 mL/min, with a run time of 15 min.

3.2. PL Inhibition Assay and Enzyme Kinetics

Orlistat, porcine PL (Type II) and 4-nitrophenyl butyrate were procured from Sigma-Aldrich (MO, USA). Tris buffer and sodium chloride (molecular biology grade) were procured from Sisco Research Laboratories (MH, India). DMSO (molecular biology grade) was procured from Hi Media.

3.2.1. PL Inhibition Assay

The procedure used for *in vitro* screening was previously optimized in our laboratory.[1,2] For the assay, Tris-HCl buffer was prepared by dissolving 3g of Tris and 1.5 g of NaCl in Milli-Q water and the pH was adjusted to 7.4 using HCl and the volume was made to 100 mL using Milli-Q water. The enzyme solution was prepared by suspending crude porcine PL in Tris buffer (5 mg/mL), followed by vigorous shaking and centrifugation to get the supernatant as PL enzyme solution. The inhibitor solution was prepared in the concentration range of 2000-15.625 µg/mL using DMSO as a solvent. 4-Nitrophenyl butyrate solution (10 mM concentration) was prepared in Acetonitrile and used as a substrate. For PL inhibition assay, the mixture of 220 µL of buffer, 25 µL of enzyme and 5 µL of inhibitor (orlistat, analogues)

was preincubated at 37 ˚C for 5 minutes. It was then followed by the addition of 1.25 µL of substrate and was checked for the absorbance at 405 nm (absorbance maxima of 4-nitrophenol) using BioTek SYNERGY microplate reader (VT, USA). The complete assay was performed in triplicate and the %inhibition was calculated using the formula:

$$\%\text{Inhibition} = [(A_E - A_T) / A_E] * 100 \ldots\ldots\ldots\ldots\ldots \textbf{Formula 3.1}$$

Where, A_E is the absorbance of enzyme control (without inhibitor), A_T is the difference in absorbance of test sample with and without inhibitor. The linear regression graph was then plotted for the calculation of IC_{50} values.

3.2.2. Enzyme Kinetics

Enzyme kinetics study was performed using the protocol established in our laboratory.[3] For the study, PL inhibition assay procedure was performed for different concentrations of substrate (25, 50, 100, 200 µM). The double reciprocal Lineweaver-Burk plot was plotted to understand the nature of inhibition. Also, the inhibition constant (K_i) was calculated using Cheng-Prusoff equation.

3.3. Fluorescence Quenching Study

Fluorescence quenching experiment was performed for the identification of active site binding of analogues as PL active site contains fluorescence emitting amino acids (Thr, Tyr). For the study, previously reported methods were used with some modifications.[4,5] Briefly, buffer (2.64 mL), PL (300 µL), inhibitor (60 µL) were mixed and transferred to a cuvette of 3 cm path length. The fluorescence spectra were recorded using Fluorolog-3 fluorescence spectrophotometer (Horiba Jobin Yvon Inc., France). The excitation wavelength was set as 290 nm and the emission was recorded at the wavelength range of 305 to 500 nm by keeping the slit width of 1.5 nm. For the identification of quenching mechanism, Stern-Volmer equation was utilized as follows:

$$\frac{F_0}{F} = 1 + k_q \tau_0 [Q] = 1 + K_{SV}[Q] \quad \ldots\ldots\ldots\ldots\ldots \textbf{Formula 3.2}$$

In above equation, F_0 and F are the fluorescence intensities before and after the addition of quencher. k_q is the quenching rate constant, K_{SV} is the Stern-Volmer dynamic quenching constant, [Q] is the concentration of quencher and τ_0 is the average lifetime of bimolecular fluorescence which is 1.59 ns for human PL.

The binding constant (K_b) and number of binding sites (n) were calculated using following equation (modified Stern-Volmer equation) :

$$log\left[\frac{F_0-F}{F}\right] = logK_b + nlog[Q] \ldots\ldots\ldots\ldots\ldots \textbf{Formula 3.3}$$

Where, K_b is the binding constant and n is the number of binding sites.

3.4. Molecular Modelling Studies

3.4.1. Molecular Docking Study

The molecular docking study of the synthesized analogues was performed using Molegro Virtual Docker 6.0.33 software. All the designed analogues and orlistat were drawn using ChemBio Office Ultra 14.0 Suite and the energy minimization was performed *via* Chem3D module, with the utilization of Molecular Mechanics 2 (MM2) force field. The PL protein (PDB ID: 1LPB) was extracted from RCSB PDB site and was prepared using MVD software. The grid was prepared by taking the centre of cocrystal ligand (MUP). The obtained grid parameters (8.36, 23.16, 53.61 (x, y, z), radius 7 Å) were validated by checking the RMSD value after the superimposition of native pose and docked pose of MUP. The energy minimized analogues were then docked at the validated grid using docking wizard panel.[6]

3.4.2. Molecular Dynamics Study

For molecular dynamics simulation study, the Desmond module of Schrodinger software was utilized. The docked pose of ligand-protein complex was imported into the workspace. The model system was then prepared using "system builder panel" by the incorporation of the orthorhombic box surrounding the complex, that was solvated using SPC water model. The molecular dynamics simulation was then performed for 100 ns at 310 K temperature and 1.013 bar pressure. The NPT ensemble class was selected for the complete simulation. The results were then analysed using "simulation interaction diagram" panel.[7]

CHAPTER 3

References

(1) George, G.; Auti, P. S.; Paul, A. T. Design, synthesis and biological evaluation of N-substituted indole-thiazolidinedione analogues as potential pancreatic lipase inhibitors. *Chem. Biol. Drug Des.* **2021**, *98* (1), 49–59.

(2) George, G.; Yadav, N.; Auti, P. S.; Paul, A. T. Molecular modelling, synthesis and in vitro evaluation of quinazolinone hybrid analogues as potential pancreatic lipase inhibitors. *J. Biomol. Struct. Dyn.* **2022**, *41* (19), 9583–9601.

(3) Jagetiya, S.; Auti, P. S.; Paul, A. T. Design, synthesis, molecular modelling and in vitro evaluation of indolyl ketohydrazide-hydrazone analogs as potential pancreatic lipase inhibitors. *Chem. Biodivers.* **2023**, *20*, 1–16.

(4) Ramos, P.; Coste, T.; Piémont, E.; Lessinger, J. M.; Bousquet, J. A.; Chapus, C.; Kerfelec, B.; Férard, G.; Mély, Y. Time-resolved fluorescence allows selective monitoring of TRP30 environmental changes in the seven-TRP-containing human pancreatic lipase. *Biochemistry* **2003**, *42* (43), 12488–12496.

(5) Zhang, J.; Xiao, L.; Yang, Y.; Wang, Z.; Li, G. Lignin binding to pancreatic lipase and its influence on enzymatic activity. *Food Chem.* **2014**, *149*, 99–106.

(6) George, G.; Auti, P. S.; Sengupta, P.; Paul, A. T. Design and synthesis of echitamine-inspired hybrid analogues containing thiazolidinediones as potential pancreatic lipase inhibitors. *Lett. Drug Des. Discov.* **2022**, *19* (11), 956–968.

(7) Auti, P. S.; Nandi, A.; Kumari, V.; Paul, A. T. Design, synthesis, biological evaluation and molecular modelling studies of oxoacetamide warhead containing indole-quinazolinone based novel hybrid analogues as potential pancreatic lipase inhibitors. *New J. Chem.* **2022**, *46* (24), 11648–11661.

CHAPTER 4

SERIES-I: DESIGN, SYNTHESIS & BIOLOGICAL EVALUATION

4. Series I: Design, Synthesis and PL Inhibitory Evaluation of Acrylate Linked Chromone Analogues

4.1. Rationale

As mentioned in chapter 2, many of the heterocyclic scaffolds, e.g. indole, quinazolinone, triazole, coumarin, and thiazolidinedione, have been identified as potential leads for PL inhibition[1–3]. In addition to the synthetic analogues, various phytochemicals have also been identified for their PL inhibitory potential. These phytochemicals can be divided into various classes, like polyphenols, saponins, alkaloids, benzofurans, etc. Among these chemical classes, the majority of the PL inhibitors have been found to be of polyphenolic origin (42% of total natural PL inhibitors)[4], that mainly possess a chromone scaffold as a bioactive heterocycle. For e.g. Quercetin (IC_{50} of 21.5 ± 9.4 µM), Kaempferol (IC_{50} of 13.4 ± 4.1 µM), Derhamnosylmaysin (IC_{50} of 25.9 ± 3.7 µM), Orientin (IC_{50} of 31.6 ± 2.7 µM), etc. have been reported for their PL inhibitory potential (**Figure 4.1**).[5,6]
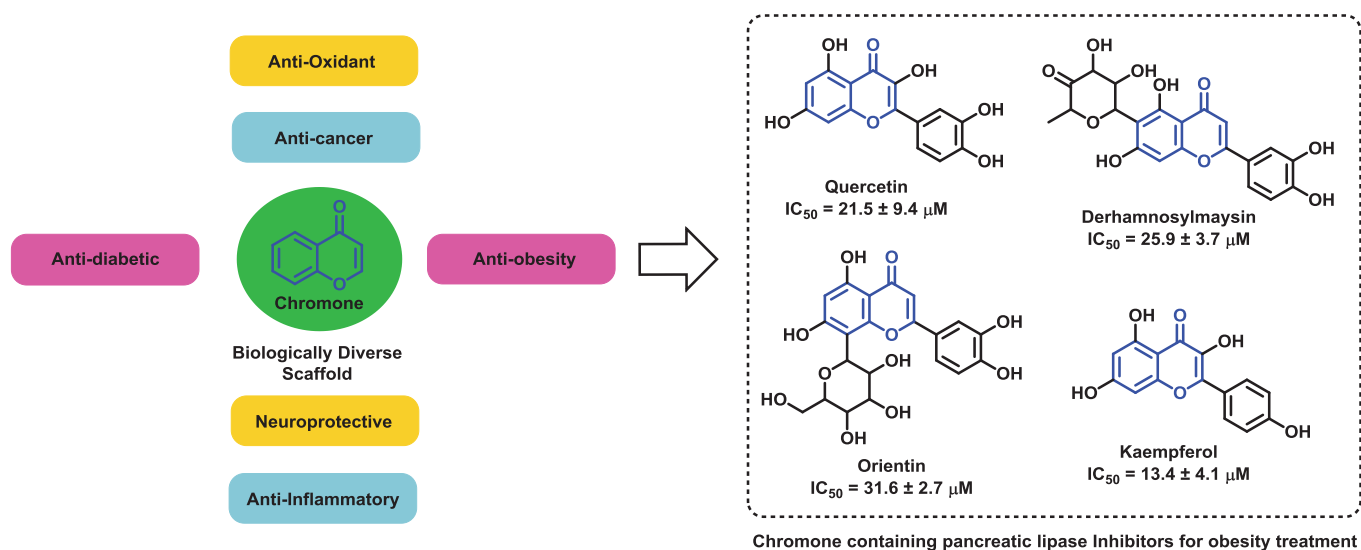
Figure 4.1. Medicinal importance of chromone scaffold, emphasizing on PL inhibitory analogues as anti-obesity agents

These naturally isolated analogues showed poor to moderate PL inhibitory potential that may be due to a lack of structural requirement for binding with the key active site amino acids. From the literature, it is confirmed that the active site of PL enzyme consists of a hydrophobic lid domain (Gly76-Lys80, Tyr114 and Leu213-Met217) enclosing the highly restricted catalytic triad that is made up of Ser152-Asp176-His263 amino acids.[7] For any molecule to reach the catalytic triad, it needs to be interact with the hydrophobic lid domain (with alkyl or aromatic interactions) for its opening. From above observation, it was

confirmed that there is pharmacophoric requirement for binding at the active site of PL. As shown in **Figure 4.2**, following pharmacophoric features are required for potential binding of an inhibitor at the active site of PL:

a)   Aromatic/long chain alkyl groups for interaction with Phe77, Tyr114, Phe215 amino acids.

b)   Fragment with hydrogen/covalent bond forming ability.

c)   Electron rich aromatic moiety for interaction with Arg256 amino acid.

d)   Spacer for alignment of both the aromatic moieties for the interaction with respective amino acids.
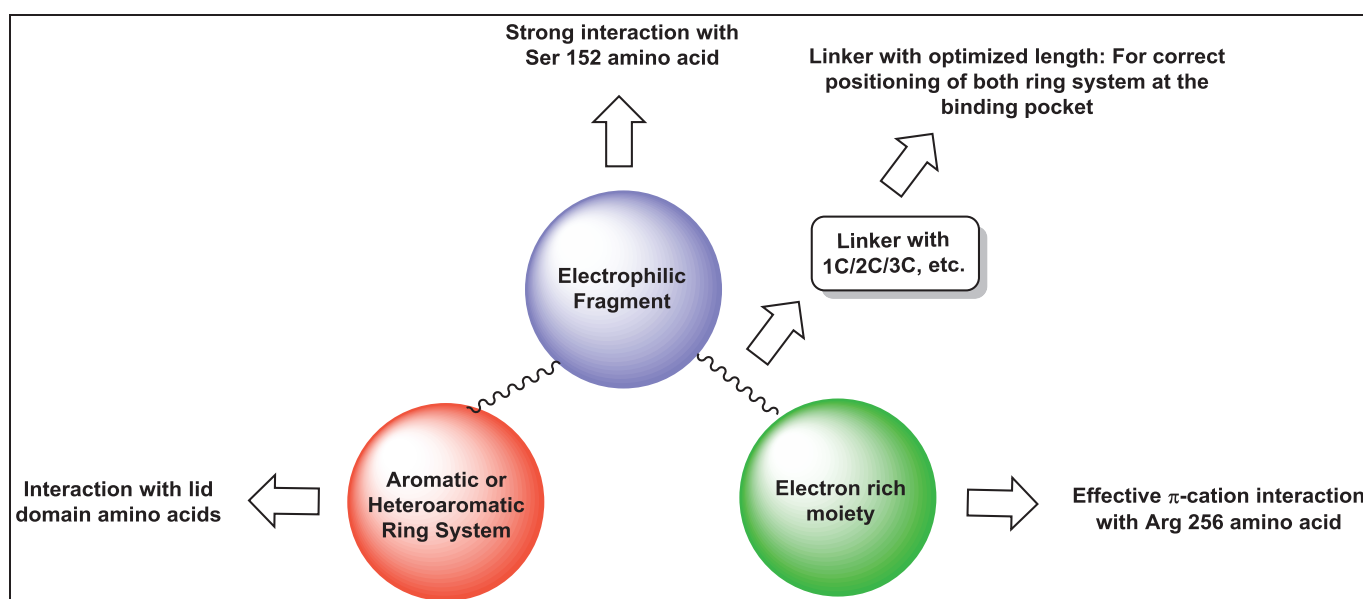
Figure 4.2. Pharmacophoric features for pancreatic lipase inhibition

Also, the active site of PL contains nucleophilic Ser152 amino acid residue and many of the fragments have been utilized to interact with Ser 152. As shown in **Figure 4.3**, various fragments such as acrylate[8,9], α,β-unsaturated ketone[10], α-ketoamide[2,11], β-lactone[12], etc. have been reported to be present in many of the synthetic and natural product-based PL inhibitors. Many of the acrylate-based natural product analogues have been reported to have good to poor PL inhibitory potential. Such analogues have potential for enhancement in activity through synthetic modification.

Among the fragments targeting Ser152 amino acid, acrylate has advantages in terms of rigidity and weak nucleophilicity (less adverse effects). Being a weak nucleophile, it will not

be affecting other biological targets. Also, numerous natural product-containing PL inhibitors have been reported with acrylate fragment for targeting Ser152 amino acid.
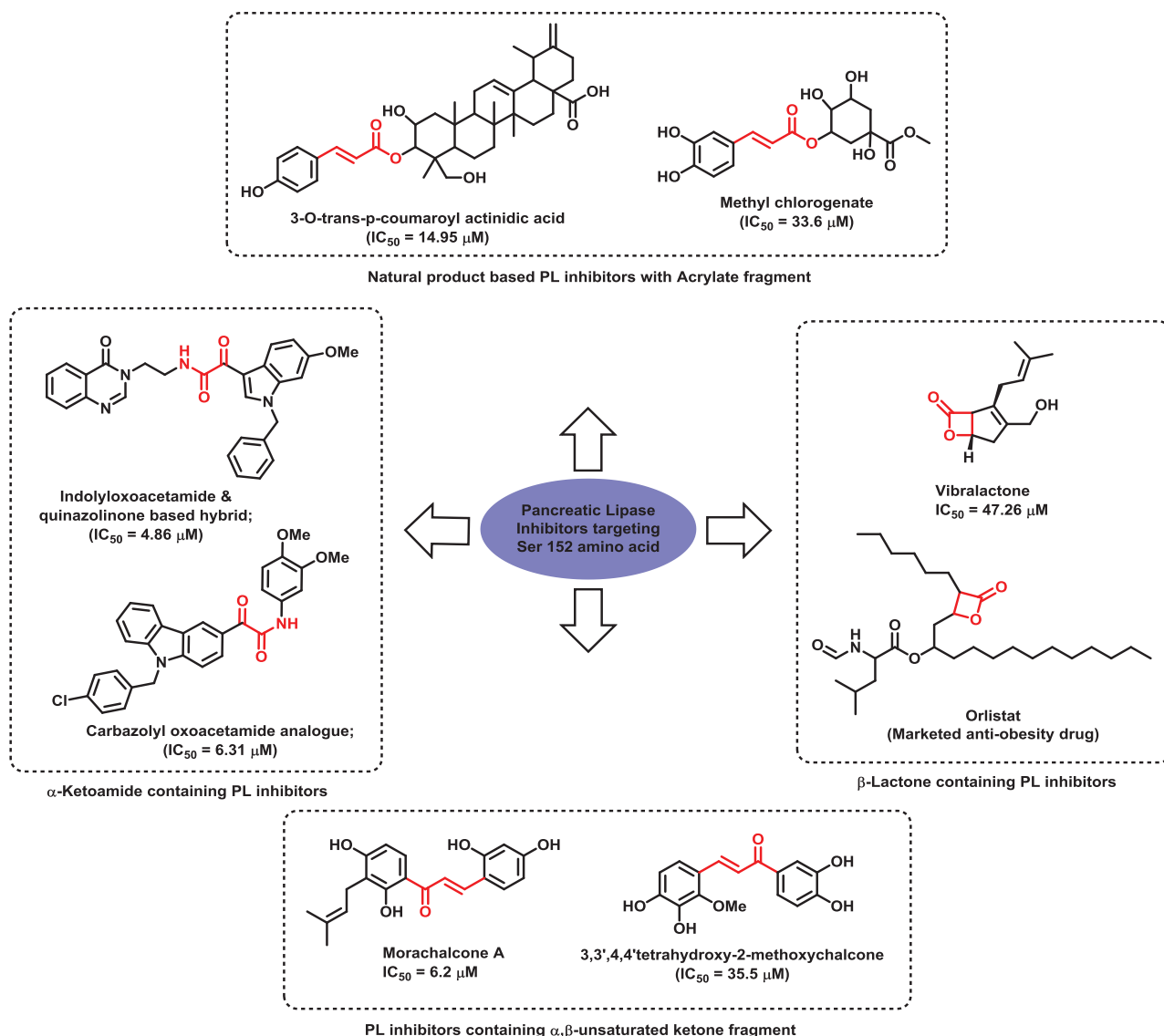
Figure 4.3. Examples of PL inhibitors with various fragments, targeting Ser 152 amino acid

As per the above observations, it was concluded that many of the natural product containing PL inhibitors contains acrylate fragment but there is no single report on rational drug design approach taking acrylate fragment in consideration. Also, being a privileged heterocycle, synthetic chromone-based PL inhibitors are least. Taking such gaps in consideration, in this study we have designed acrylate linked chromone analogues for PL inhibition. As shown in **Figure 4.4**, the analogues were designed with the hypothesis that the chromone ring will interact with Phe77, Tyr114 and Phe215 amino acids *via* π-π stacking, the acrylate fragment will interact with Ser152 and aryl/heteroaryl moiety will interact with Arg256 *via* π-cation interaction. Also, the linker was placed in between chromone acrylate and aryl/heteroaryl

moiety with the aim of better positioning of chromone, acrylate and aromatic/heteroaromatic moiety for respective interactions with the active site amino acids.
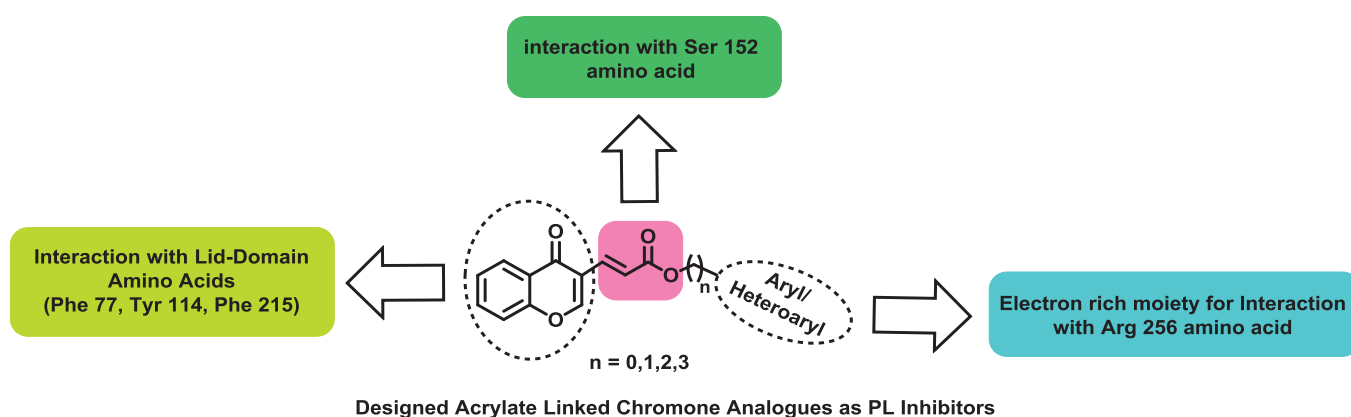
Figure 4.4. Rationale for the design of acrylate linked chromone analogues as PL inhibitors

The effect of length of linker (n = 0,1,2,3) on binding at PL active site was checked using molecular docking study. As shown in **Figure 4.5** the analogue with no carbon linker (n=0) exhibited low docking score as compared with the one carbon (n = 1) linker analogue. Also, there was a lack of interactions with important amino acids such as, Phe77, Tyr114, Phe215, Arg256, etc. As the molecular docking study proved poor binding of analogue with no carbon linker, the synthesis of analogues with one carbon (n=1) linker was carried out for the investigation of their PL inhibitory potential.
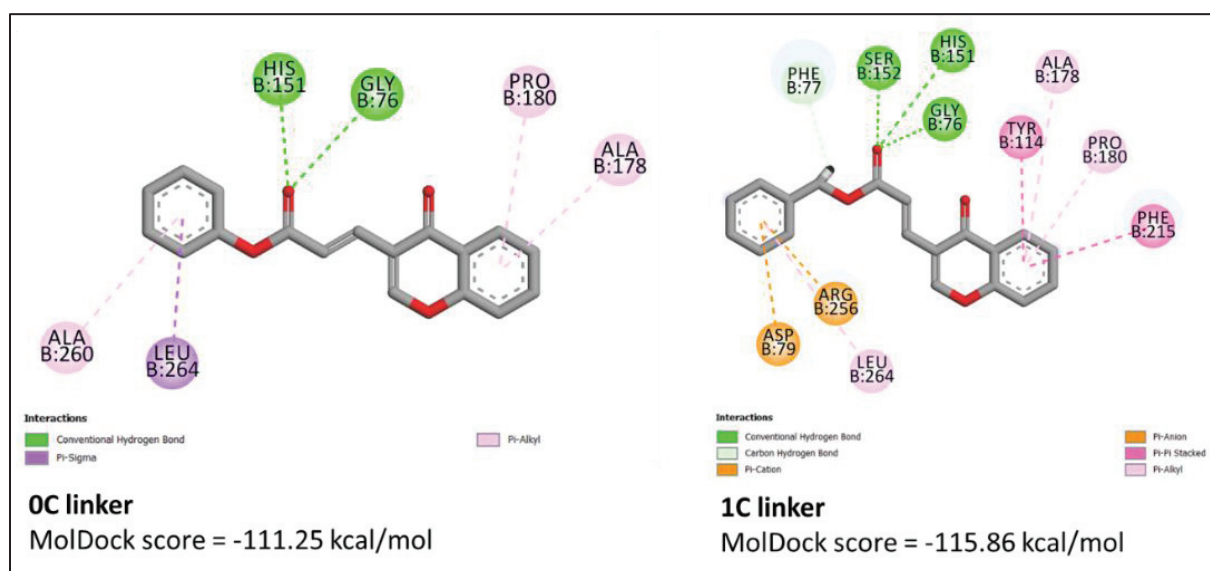
Figure 4.5. Molecular docking analysis of acrylate linked chromone analogues with various carbon linkers (n = 0, 1) at PL active site

4.2. Synthesis and Characterization

The designed acrylate linked chromone analogues were prepared by using the optimized reaction (**Scheme 4.1**). Briefly, the substituted 3-Formylchromones (**2a-f**) were prepared by the reaction of substituted 2'-Hydroxyacetophenones (**1a-f**) and *N,N*-Dimethylformamide (DMF) in the presence of catalytic amount of POCl$_3$ (Vilsmeier haack reaction). It was further reacted with malonic acid in the presence of pyridine and ethanol at reflux temperature to get Chromone-3-acrylic acid (**3a-f**). The final analogues were prepared by the reaction of various benzyl alcohols (**4a-p**) with Chromone-3-acrylic acid (**3a-f**), using EDC.HCl coupling agent and DMAP as a base in DMF. Further, the structure of synthesized analogues were elucidated using various spectroscopic techniques such as IR, NMR and HR-MS. Through ^{1}H NMR, a singlet of 1H at δ value in the range of 8.08-8.14 ppm confirmed the presence of a proton at 2nd position of chromone ring. One aliphatic proton (CH$_2$) of benzyl moiety resonated in the δ range of 5.14-5.67 ppm as a singlet, confirming the attachment of benzyl ring. Further the peaks of additional substituents such as, methyl, methoxy, benzyloxy, etc. were in their standard range. The presence of carbonyl carbons of chromone and ester were further confirmed *via* ^{13}C NMR spectrum. For all the analogues, the carbonyl carbon of ketone of chromone were found to resonate at δ value in the range of 174.66-176.08 ppm, whereas the ester carbonyl peak was found in δ range of 166.50-167.37 ppm. The structures were further confirmed via HR-MS analysis by the presence of [M+H]$^+$ peaks in the spectrum, with the values, coinciding with the calculated m/z values. In the case of all the analogues, the % Purity was found to be in the range of 92.94-99.91%, with the retention time (t_R) in the range of 4.16 – 9.38 min.
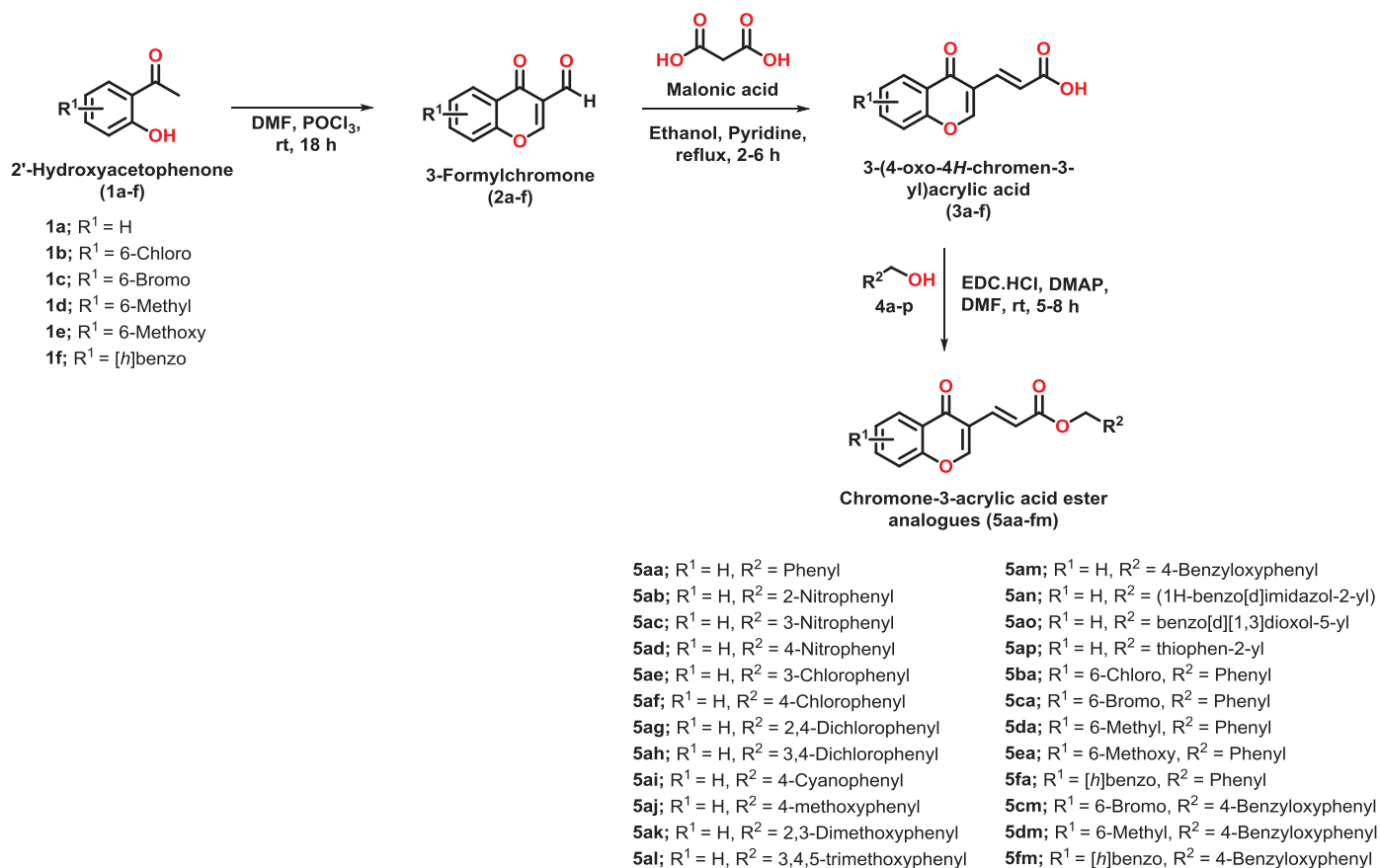
Scheme 4.1. Synthesis of designed acrylate linked chromone analogues (**5aa-5fm**)

4.2.1. General Procedure for the synthesis of 3-Formylchromone (2a-f).

The mixture of 2'-Hydroxyacetophenone (**1a-f**) (7.34 mmol) and *N,N*-Dimethylformamide (DMF) (7 mL) was stirred for 15 min in ice bath. To the above mixture, Phosphorous oxychloride (POCl$_3$) (44.06 mmol) was added dropwise. The reaction mixture was then stirred at room temperature for 18 h. After the completion of reaction (confirmed by TLC), the mixture was added in ice cold water and the resultant precipitate was filtered to get the 3-Formylchromone (**2a-f**).[13]

4.2.2. General Procedure for the synthesis of Chromone-3-acrylic acid (3a-f).

A mixture of substituted 3-Formylchromone (7.98 mmol), malonic acid (9.97 mmol) and pyridine (0.5 mL) was refluxed in 8 mL of ethanol for 2-6 hours. The resultant mixture was cooled and the precipitated product was filtered and washed with ethanol to get the pure product (**3a-f**).[14]

4.2.3. General Procedure for the synthesis of chromone-3-acrylic acid ester analogues (5aa-fm).

The mixture of substituted Chromone-3-acrylic acid (**3a-f**) (0.462 mmol), 3-Dimethylamino-propyl)-ethyl-carbodiimide Hydrochloride (EDC.HCl) (0.924 mmol), 4-(Dimethylamino)pyridine (DMAP) (0.924 mmol) were stirred in DMF in ice cold condition for 15 min. It was then followed by the addition of substituted Benzyl alcohol (**4a-p**) (0.924 mmol) followed by stirring at room temperature for 5-8 hours. After the confirmation by TLC, the reaction mixture was quenched by the addition of cold water, followed by extraction with ethyl acetate. The ethyl acetate layer was then evaporated, followed by column chromatography to get the final analogues (**5aa-fm**).

4.2.4. Analytical Data for the final compounds:

Benzyl (*E*)-3-(4-oxo-4H-chromen-3-yl)acrylate (5aa). Yield: 91%; buff white crystalline solid; MP = 130–132 ˚C; ^{1}H NMR (400 MHz, CDCl$_3$) δ (ppm) = 8.27 (dd, J = 1.2 Hz, 8 Hz, 1H), 8.11 (s, 1H), 7.71-7.67 (m, 1H), 7.49-7.33 (m, 9H), 5.25 (s, 2H); ^{13}C NMR (100 MHz, CDCl$_3$) δ (ppm) = 175.89, 167.19, 157.54, 155.51, 136.07, 135.97, 134.04, 128.54, 128.16, 126.35, 125.88, 124.20, 121.86, 119.27, 118.11, 66.31; IR (ATR): υ (cm^{-1}) = 3852.38, 3741.63, 3673.36, 3613.43, 2924.46, 2310.45, 1745.01, 1696.06, 1647.92, 1540.40, 1458.20, 1405.42, 1358.88, 1236.27, 1154.46, 982.59, 856.21, 795.72, 751.74, 685.00; HRMS (ESI$^+$) calculated for C$_{19}$H$_{15}$O$_4$ [M + H$^+$], 307.0970; found 307.0960; HPLC purity: 99.91%, t_R = 4.160 min.

2-Nitrobenzyl (*E*)-3-(4-oxo-4H-chromen-3-yl)acrylate (5ab). Yield: 88%; white amorphous solid; MP = 168-170 ˚C; ^{1}H NMR (400 MHz, CDCl$_3$) δ (ppm) = 8.29 (dd, J = 1.6 Hz, 8 Hz, 1H), 8.16-8.13 (m, 2H), 7.74-7.67 (m, 3H), 7.51-7.45 (m, 5H), 5.67 (s, 2H); ^{13}C NMR (100 MHz, CDCl$_3$) δ (ppm) = 175.97, 166.75, 158.07, 155.50, 147.33, 136.85, 134.16, 133.87, 132.60, 128.70, 128.58, 126.33, 126.00, 125.03, 124.20, 121.23, 119.10, 118.17, 62.91; IR (ATR): υ (cm^{-1}) = 3851.81, 3741.41, 3673.29, 3613.90, 1742.27, 1690.37, 1636.24, 1526.08, 1462.58, 1411.02, 1352.36, 1244.42, 1153.90, 1093.71, 1036.16, 974.39, 856.63, 775.35, 722.34, 684.27; HRMS (ESI$^+$) calculated for C$_{19}$H$_{14}$NO$_6$ [M + H$^+$], 352.0821; found 352.0855; HPLC purity: 97.24%, t_R = 5.127 min.

3-Nitrobenzyl (*E*)-3-(4-oxo-4H-chromen-3-yl)acrylate (5ac). Yield: 85%; white amorphous solid; MP = 194-196 ˚C; ^{1}H NMR (400 MHz, DMSO-d$_6$) δ (ppm) = 8.95 (s, 1H), 8.30-8.14 (m, 3H), 7.90-7.56 (m, 6H), 7.32 (s, 1H), 5.37 (s, 2H); ^{13}C NMR (100 MHz,

DMSO-d$_6$) δ (ppm) = 175.80, 166.67, 161.13, 155.54, 148.27, 139.00, 137.87, 135.17, 135.01, 130.63, 126.70, 125.92, 123.94, 123.44, 122.97, 119.88, 119.05, 118.33, 64.94; IR (ATR): υ (cm^{-1}) = 3851.94, 3741.56, 3673.35, 3613.70, 2382.24, 2309.15, 1916.75, 1700.26, 1521.42, 1461.83, 1408.99, 1343.47, 1293.91, 1158.31, 982.35, 795.08, 734.27, 677.96; HRMS (ESI$^+$) calculated for C$_{19}$H$_{14}$NO$_6$ [M + H$^+$], 352.0821; found 352.0861; HPLC purity: 99.32%, t_R = 5.110 min.

4-Nitrobenzyl (*E*)-3-(4-oxo-4H-chromen-3-yl)acrylate (5ad). Yield: 80%; white amorphous solid; MP = 182-185 °C; ^{1}H NMR (400 MHz, CDCl$_3$) δ (ppm) = 8.30-8.27 (m, 1H), 8.25-8.22 (m, 2H), 8.14 (s, 1H), 7.78-7.69 (m, 1H), 7.57 (d, *J* = 8.8 Hz, 2H), 7.51-7.45 (m, 4H), 5.34 (s, 2H); ^{13}C NMR (100 MHz, CDCl$_3$) δ (ppm) = 176.07, 167.07, 158.13, 155.63, 143.58, 137.00, 134.32, 128.38, 126.49, 126.16, 124.33, 123.99, 123.94, 121.29, 119.21, 118.29, 64.91; IR (ATR): υ (cm^{-1}) = 3852.89, 3741.10, 3672.55, 3613.86, 2929.16, 2857.17, 2382.56, 2308.62, 1702.76, 1653.16, 1514.61, 1459.12, 1401.48, 1339.88, 1280.67, 1209.94, 1146.63, 971.31, 845.52, 747.51 cm^{-1}; HRMS (ESI$^+$) calculated for C$_{19}$H$_{14}$NO$_6$ [M + H$^+$], 352.0821; found 352.0878; HPLC purity: 92.94%, t_R = 5.123 min.

3-Chlorobenzyl (*E*)-3-(4-oxo-4H-chromen-3-yl)acrylate (5ae). Yield: 82%; white amorphous solid; MP = 154-156 °C; ^{1}H NMR (400 MHz, CDCl$_3$) δ (ppm) = 8.27 (dd, *J* = 1.2 Hz, 8 Hz, 1H), 8.12 (s, 1H), 7.72-7.68 (m, 1H), 7.49-7.37 (m, 6H), 7.30-7.27 (m, 3H), 5.21 (s, 2H); ^{13}C NMR (100 MHz, CDCl$_3$) δ = 175.89, 167.03, 157.74, 155.51, 138.11, 136.35, 134.43, 134.09, 129.84, 128.29, 128.06, 126.36, 126.06, 125.93, 124.21, 121.56, 119.19, 118.14, 65.35; IR (ATR): υ (cm^{-1}) = 3852.47, 3741.40, 3673.34, 3614.23, 2309.34, 1746.76, 1701.83, 1656.16, 1618.09, 1551.89, 1460.29, 1409.20, 1355.73, 1279.78, 1210.19, 1145.92, 974.69, 858.28, 755.56, 685.03; HRMS (ESI$^+$) calculated for C$_{19}$H$_{14}$ClO$_4$ [M + H$^+$], 341.0581; found 341.0560; HPLC purity: 98.61%, t_R = 7.450 min.

4-Chlorobenzyl (*E*)-3-(4-oxo-4H-chromen-3-yl)acrylate (5af). Yield: 86%; white amorphous solid; MP = 140-142 °C; ^{1}H NMR (400 MHz, CDCl$_3$) δ (ppm) = 8.28-8.26 (m, 1H), 8.11 (s, 1H), 7.72-7.68 (m, 1H), 7.49-7.39 (m, 4H), 7.35-7.34 (m, 4H), 5.20 (s, 2H); ^{13}C NMR (100 MHz, CDCl$_3$) δ (ppm) = 176.02, 167.22, 157.80, 155.63, 136.36, 134.73, 134.21, 134.16, 129.65, 128.85, 126.49, 126.06, 124.33, 121.77, 119.33, 118.26, 65.59; IR (ATR): υ (cm^{-1}) = 3852.84, 3742.00, 3673.47, 3613.82, 2309.65, 1745.84, 1699.30, 1649.62, 1541.37, 1459.51, 1410.06, 1358.89, 1270.79, 1144.51, 1084.92, 973.72, 854.40, 804.57, 759.97,

682.36; HRMS (ESI⁺) calculated for $C_{19}H_{14}ClO_4$ [M + H⁺], 341.0581; found 341.0630; HPLC purity: 97.17%, t_R = 7.420 min.

2,4-Dichlorobenzyl (*E*)-3-(4-oxo-4H-chromen-3-yl)acrylate (5ag). Yield: 80%; white amorphous solid; MP = 150-152 ˚C; ¹H NMR (400 MHz, CDCl₃) δ (ppm) = 8.28 (dd, *J* = 1.6 Hz, 8 Hz, 1H), 8.14 (s, 1H), 7.73-7.69 (m, 1H), 7.50-7.39 (m, 6H), 7.28-7.26 (m, 1H), 5.31 (s, 2H); ¹³C NMR (100 MHz, CDCl₃) δ (ppm) = 175.91, 166.91, 157.84, 155.50, 136.52, 134.52, 134.11, 132.47, 130.42, 129.35, 127.20, 126.35, 125.96, 124.20, 121.39, 119.15, 118.13, 62.95; IR (ATR): υ (cm⁻¹) = 3852.19, 3741.66, 3673.34, 1711.39, 1650.44, 1614.75, 1542.41, 1460.92, 1410.42, 1283.94, 1205.22, 1138.54, 1101.91, 1057.01, 999.42, 853.94, 815.89, 753.22, 688.28; HRMS (ESI⁺) calculated for $C_{19}H_{13}Cl_2O_4$ [M + H⁺], 375.0191; found 375.0218; HPLC purity: 96.59%, t_R = 6.603 min.

3,4-Dichlorobenzyl (*E*)-3-(4-oxo-4H-chromen-3-yl)acrylate (5ah). Yield: 92%; white amorphous solid; MP = 161-163 ˚C; ¹H NMR (400 MHz, CDCl₃) δ (ppm) = 8.27 (dd, *J* = 1.6 Hz, 8 Hz, 1H), 8.12 (s. 1H), 7.72-7.68 (m, 1H), 7.50- 7.41 (m, 6H), 7.23 (dd, *J* = 2 Hz, 8.4 Hz, 1H), 5.18 (s, 2H); ¹³C NMR (100 MHz, CDCl₃) δ (ppm) = 176.02, 167.09, 157.98, 155.61, 133.69, 136.46, 134.24, 132.78, 132.33, 130.66, 130.06, 127.41, 126.47, 126.09, 124.31, 121.48, 119.24, 118.26, 64.83; IR (ATR): υ (cm⁻¹) = 3852.64, 3741.97, 3673.29, 3613.68, 1746.76, 1701.46, 1658.62, 1617.21, 1521.03, 1460.88, 1401.52, 1354.91, 1281.26, 1210.40, 1147.72, 977.62, 866.14, 824.54, 756.87, 684.87; HRMS (ESI⁺) calculated for $C_{19}H_{13}Cl_2O_4$ [M + H⁺], 375.0191; found 375.0175; HPLC purity: 99.71%, t_R = 6.053 min.

4-Cyanobenzyl (*E*)-3-(4-oxo-4H-chromen-3-yl)acrylate (5ai). Yield: 82%; white amorphous solid; MP = 166-169 ˚C; ¹H NMR (400 MHz, CDCl₃) δ (ppm) = 8.27 (dd, *J* = 1.2 Hz, 8 Hz, 1H), 8.13 (s, 1H), 7.73-7.65 (m, 3H), 7.51-7.43 (m, 6H), 5.28 (s, 2H); ¹³C NMR (100 MHz, CDCl₃) δ (ppm) = 176.02, 167.05, 158.08, 155.59, 141.57, 136.87, 134.28, 132.48, 128.28, 126.44, 126.11, 124.27, 121.29, 119.16, 118.74, 118.26, 111.99, 65.15; IR (ATR): υ (cm⁻¹) = 3852.25, 3741.79, 3673.38, 3613.28, 2379.66, 2309.95, 1917.21, 1704.42, 1659.15, 1520.19, 1461.52, 1410.64, 1361.15, 1286.60, 1212.87, 1155.74, 983.21, 858.62, 761.80, 689.82; HRMS (ESI⁺) calculated for $C_{20}H_{14}NO_4$ [M + H⁺], 332.0923; found 332.0906; HPLC purity: 99.12%, t_R = 4.573 min.

4-Methoxybenzyl (*E*)-3-(4-oxo-4H-chromen-3-yl)acrylate (5aj). Yield: 85%; white amorphous solid; MP = 124-126 ˚C; 1H NMR (400 MHz, CDCl₃) δ (ppm) = 8.26 (dd, *J* = 1.6 Hz, 8 Hz, 1H), 8.10 (s, 1H), 7.71-7.67 (m, 1H), 7.48-7.31 (m, 6H), 6.90 (d, *J* = 8.4 Hz, 2H),

5.18 (s, 2H), 3.81 (s, 3H); ^{13}C NMR (100 MHz, CDCl$_3$) δ (ppm) = 175.87, 167.24, 159.58, 157.45, 155.50, 135.79, 134.02, 130.05, 128.19, 136.35, 125.85, 124.19, 121.99, 119.28, 118.10, 113.92, 66.15, 55.29; IR (ATR): υ (cm^{-1}) = 3851.22, 3741.55, 3673.20, 3626.04, 1695.41, 1655.98, 1612.31, 1554.40, 1512.47, 1458.15, 1408.56, 1354.60, 1283.49, 1248.96, 1145.89, 1029.95, 953.83, 818.11, 752.40, 684.02; HRMS (ESI$^+$) calculated for C$_{20}$H$_{17}$O$_5$ [M + H$^+$], 337.1076; found 337.1060; HPLC purity: 98.43%, t_R = 5.310 min.

2,3-Dimethoxybenzyl (*E*)-3-(4-oxo-4H-chromen-3-yl)acrylate (5ak). Yield: 95%; white crystalline solid; MP = 120-123 ˚C; ^{1}H NMR (400 MHz, CDCl$_3$) δ (ppm) = 8.27 (dd, *J* = 1.2 Hz, 8 Hz, 1H), 8.11 (s, 1H), 7.72-7.67 (m, 1H), 7.49-7.42 (m, 3H), 7.38-7.34 (m, 1H), 7.09-7.00 (m, 2H), 6.91 (dd, *J* = 1.6 Hz, 8 Hz, 1H), 5.31 (s, 2H), 3.89 (s, 3H), 3.88 (s, 3H); ^{13}C NMR (100 MHz, CDCl$_3$) δ (ppm) = 176.04, 167.36, 157.64, 155.65, 152.84, 147.66, 135.97, 134.16, 130.15, 126.49, 126.00, 124.36, 124.21, 122.15, 121.77, 119.45, 118.25, 112.75, 61.88, 61.28, 55.95 ppm; IR (ATR): υ (cm^{-1}) = 3858.36, 3746.72, 3613.58, 2935.64, 2828.46, 2313.11, 1699.01, 1650.96, 1611.18, 1562.19, 1460.06, 1412.58, 1355.39, 1277.08, 1144.80, 1083.55, 988.38, 858.93, 756.52, 682.63; HRMS (ESI$^+$) calculated for C$_{21}$H$_{19}$O$_6$ [M + H$^+$], 367.1182; found 367.1178; HPLC purity: 99.02%, t_R = 5.417 min.

3,4,5-Trimethoxybenzyl (*E*)-3-(4-oxo-4H-chromen-3-yl)acrylate (5al). Yield: 92%; white amorphous solid; MP = 141-144 ˚C; ^{1}H NMR (400 MHz, CDCl$_3$) δ (ppm) = 8.28 (d, *J* = 8 Hz, 1H), 8.13 (s, 1H), 7.72-7.69 (m, 1H), 7.50-7.38 (m, 4H), 6.64 (s, 2H), 5.18 (s, 2H), 3.89 (s, 6H), 3.85 (s, 3H); ^{13}C NMR (100 MHz, CDCl$_3$) δ (ppm) = 175.93, 167.24, 157.68, 155.51, 153.31, 137.84, 136.13, 134.10, 131.64, 126.33, 125.92, 124.19, 121.78, 119.23, 118.14, 105.34, 66.57, 60.85, 56.15; IR (ATR): υ (cm^{-1}) = 3852.21, 3741.91, 3673.60, 3613.78, 2930.64, 2309.85, 1746.53, 1700.28, 1655.42, 1514.38, 1458.78, 1411.52, 1332.12, 1286.27, 1239.06, 1164.53, 1122.80, 1001.01, 861.08, 773.52; HRMS (ESI$^+$) calculated for C$_{22}$H$_{21}$O$_7$ [M + H$^+$], 397.1287; found 397.1309; HPLC purity: 99.49%, t_R = 4.523 min.

4-(Benzyloxy)benzyl (*E*)-3-(4-oxo-4H-chromen-3-yl)acrylate (5am). Yield: 80%; white amorphous solid; MP = 140-142 ˚C; ^{1}H NMR (400 MHz, CDCl$_3$) δ (ppm) = 8.26 (dd, *J* = 1.2 Hz, 8Hz, 1H), 8.09 (s, 1H), 7.71-7.66 (m, 1H), 7.48-7.46 (m, 1H), 7.44-7.38 (m, 5H), 7.36-7.31 (m, 5H), 6.97 (d, *J* = 8.8 Hz, 2H), 5.18 (s, 2H), 5.07 (s, 2H); ^{13}C NMR (100 MHz, CDCl$_3$) δ (ppm) = 175.87, 167.23, 158.78, 157.45, 155.50, 136.85, 135.81, 134.01, 130.04, 128.59, 128.47, 127.98, 127.45, 126.35, 125.85, 124.19, 121.97, 119.28, 118.10, 114.86, 66.11; IR (ATR): υ (cm^{-1}) = 3851.94, 3742.03, 3673.10, 3613.77, 1745.82, 1699.29, 1665.04,

1617.92, 1516.76, 1460.94, 1412.09, 1354.80, 1292.39, 1244.51, 1150.98, 996.21, 863.37, 803.99, 744.84, 686.80; HRMS (ESI$^+$) calculated for $C_{26}H_{21}O_5$ [M + H$^+$], 413.1389; found 413.1422; HPLC purity: 97.42%, t_R = 9.173 min.

(1H-Benzo[d]imidazol-2-yl)methyl (*E*)-3-(4-oxo-4H-chromen-3-yl)acrylate (5an). Yield: 80%; buff white crystalline solid; MP = 250-253 ˚C; ^{1}H NMR (400 MHz, DMSO-d$_6$) δ (ppm) = 12.67 (s, 1H), 8.94 (s, 1H), 8.14 (dd, J = 1.6 Hz, 8 Hz, 1H), 7.86-7.82 (m, 1H), 7.71 (d, J = 8.4 Hz, 1H), 7.58-7.52 (m, 4H), 7.34 (d, J = 16 Hz, 1H), 7.20-7.18 (m, 2H), 5.41 (s, 2H); ^{13}C NMR (100 MHz, DMSO-d$_6$) δ (ppm) = 175.77, 166.50, 161.25, 155.52, 138.04, 135.13, 126.66, 125.93, 123.96, 122.43, 119.86, 119.03, 118.34, 66.06; IR (ATR): υ (cm^{-1}) = 3853.63, 3742.84, 3613.88, 2936.87, 2613.82, 2309.93, 1723.55, 1612.98, 1552.34, 1440.39, 1361.08, 1301.34, 1224.89, 1129.59, 1045.43, 991.00, 926.71, 845.06, 736.93, 678.35; HRMS (ESI$^+$) calculated for $C_{20}H_{15}N_2O_4$ [M + H$^+$], 347.1032; found 347.1070; HPLC purity: 99.58%, t_R = 4.590 min.

Benzo[d][1,3]dioxol-5-ylmethyl (*E*)-3-(4-oxo-4H-chromen-3-yl)acrylate (5ao). Yield: 90%; buff white solid; MP = 142-144 ˚C; ^{1}H NMR (400 MHz, CDCl$_3$) δ (ppm) = 8.27 (dd, *J* = 1.2 Hz, 8 Hz, 1H), 8.11 (s, 1H), 7.71-7.67 (m, 1H), 7.49-7.32 (m, 4H), 6.90-6.87 (m, 2H), 6.80 (d, *J* = 8 Hz, 1H), 5.97 (s, 2H), 5.14 (s, 2H); ^{13}C NMR (100 MHz, CDCl$_3$) δ (ppm) = 175.86, 167.16, 157.51, 155.50, 147.77, 147.57, 135.94, 134.03, 129.82, 126.36, 125.87, 124.20, 122.20, 121.87, 119.26, 118.11, 109.04, 108.23, 101.14, 66.30; IR (ATR): υ (cm^{-1}) = 3852.07, 3741.61, 3672.96, 3613.66, 1699.46, 1660.46, 1660.35, 1618.07, 1510.08, 1459.70, 1351.61, 1290.48, 1244.51, 1208.30, 1149.18, 1101.81, 1032.78, 1000.12, 928.53, 802.57, 760.24; HRMS (ESI$^+$) calculated for $C_{20}H_{15}O_6$ [M + H$^+$], 351.0869; found 351.0902; HPLC purity: 97.29%, t_R = 4.967 min.

Thiophen-2-ylmethyl (*E*)-3-(4-oxo-4H-chromen-3-yl)acrylate (5ap). Yield: 88%; white solid; MP = 138-140 ˚C; ^{1}H NMR (400 MHz, CDCl$_3$) δ (ppm) = 8.26 (dd, *J* = 1.2 Hz, 8 Hz, 1H), 8.10 (s, 1H), 7.71-7.67 (m, 1H), 7.48-7.41 (m, 3H), 7.35-7.31 (m, 2H), 7.14 (d, *J* = 3.2 Hz, 1H), 7.00-6.98 (m, 1H), 5.39 (s, 2H); ^{13}C NMR (100 MHz, CDCl$_3$) δ (ppm) = 175.95, 167.08, 157.70, 155.61, 138.16, 136.32, 134.16, 128.88, 126.93, 126.91, 126.47, 126.00, 124.31, 121.75, 119.34, 118.23, 60.71; IR (ATR): υ (cm^{-1}) = 3851.62, 3741.09, 3609.93, 3564.77, 3363.81, 1746.78, 1698.72, 1651.45, 1613.90, 1549.65, 1459.27, 1412.38, 1349.68, 1281.86, 1143.41, 995.30, 950.81, 849.26, 755.21, 686.30; HRMS (ESI$^+$) calculated for $C_{17}H_{13}O_4S$ [M + H$^+$], 313.0535; found 313.0521; HPLC purity: 98.88%, t_R = 5.230 min.

Benzyl (*E*)-3-(6-chloro-4-oxo-4H-chromen-3-yl)acrylate (5ba). Yield: 75%; brown solid; MP = 145-146 ˚C; ^{1}H NMR (400 MHz, CDCl$_3$) δ (ppm) = 8.22 (d, *J* = 2.8 Hz, 1H), 8.10 (s, 1H), 7.63 (dd, *J* = 2.8 Hz, 9.2 Hz, 1H), 7.45-7.32 (m, 8H), 5.25 (s, 2H); ^{13}C NMR (100 MHz, CDCl$_3$) δ (ppm) = 174.82, 167.16, 157.62, 153.95, 136.10, 135.56, 134.40, 132.07, 128.70, 128.35, 125.89, 125.24, 122.51, 119.99, 119.44, 66.54; IR (ATR): υ (cm^{-1}) = 3852.73, 3740.97, 3673.52, 3613.85, 2380.02, 2310.12, 1916.67, 1744.66, 1698.24, 1654.51, 1520.78, 1458.95, 1391.54, 1338.19, 1277.96, 1152.23, 1005.97, 796.51, 734.25, 694.26; HRMS (ESI$^+$) calculated for C$_{19}$H$_{14}$ClO$_4$ [M + H$^+$], 341.0581; found 341.0902; HPLC purity: 95.73%, t_R = 8.420 min.

Benzyl (*E*)-3-(6-bromo-4-oxo-4H-chromen-3-yl)acrylate (5ca). Yield: 85%; brown solid; MP = 170-175 ˚C; ^{1}H NMR (400 MHz, CDCl$_3$) δ (ppm) = 8.38 (d, *J* = 2.4 Hz, 1H), 8.10 (s, 1H), 7.77 (dd, *J* = 2.4 Hz, 8 Hz, 1H), 7.43-7.32 (m, 8H), 5.25 (s, 2H); ^{13}C NMR (100 MHz, CDCl$_3$) δ (ppm) = 174.66, 167.14, 157.60, 154.39, 137.16, 136.09, 135.54, 129.09, 128.70, 128.35, 125.58, 122.52, 120.20, 119.54, 66.54; IR (ATR): υ (cm^{-1}) = 3851.78, 3741.14, 3673.50, 3614.22, 2311.04, 1706.27, 1645.23, 1544.35, 1459.39, 1374.19, 1328.01, 1274.01, 1196.25, 1149.66, 975.72, 901.60, 837.65, 791.55, 752.32, 699.19; HRMS (ESI$^+$) calculated for C$_{19}$H$_{14}$BrO$_4$ [M + H$^+$], 385.0075; found 385.0051; HPLC purity: 99.84%, t_R = 9.133 min.

Benzyl (*E*)-3-(6-methyl-4-oxo-4H-chromen-3-yl)acrylate (5da). Yield 82%; buff white crystalline solid; MP = 130-132 ˚C; ^{1}H NMR (400 MHz, CDCl$_3$) δ (ppm) = 8.08 (s, 1H), 8.04 (d, *J* = 0.8 Hz, 1H), 7.50-7.48 (m, 1H), 7.46-7.31 (m, 8H), 5.25 (s, 2H), 2.46 (s, 3H); ^{13}C NMR (100 MHz, CDCl$_3$) δ (ppm) = 176.08, 167.37, 157.60, 153.92, 136.31, 136.21, 136.10, 135.38, 128.67, 128.30, 125.76, 123.99, 121.70, 119.17, 117.98, 66.41, 21.13; IR (ATR): υ (cm^{-1}) = 3852.66, 3741.58, 3673.44, 3613.33, 2922.38, 2384.10, 2309.60, 1709.42, 1649.90, 1522.64 1481.56, 1349.78, 1282.43, 1152.41, 988.86, 909.90, 862.63, 809.94, 746.39, 690.70; HRMS (ESI$^+$) calculated for C$_{20}$H$_{17}$O$_4$ [M + H$^+$], 321.1127; found 321.1121; HPLC purity: 98.18%, t_R = 7.217 min.

Benzyl (*E*)-3-(6-methoxy-4-oxo-4H-chromen-3-yl)acrylate (5ea). Yield 85%; buff white amorphous solid; MP = 171-173 ˚C; ^{1}H NMR (400 MHz, CDCl$_3$) δ (ppm) = 8.09 (s, 1H), 7.61 (d, *J* = 2.8 Hz, 1H), 7.48, 7.28 (m, 9H), 5.25 (s, 2H), 3.90 (s, 3H); ^{13}C NMR (100 MHz, CDCl$_3$) δ (ppm) = 175.83, 167.36, 157.56, 157.43, 150.47, 136.31, 136.22, 128.67, 128.29, 124.99, 124.15, 121.68, 119.66, 118.53, 105.50, 66.41, 56.10; IR (ATR): υ (cm^{-1}) = 3851.95, 3741.40, 3673.26, 3613.64, 2379.46, 2310.16, 1916.49, 1745.05, 1700.03, 1652.41, 1521.74,

1474.84, 1339.70, 1282.41, 1145.32, 1009.20, 866.07, 803.45, 731.68, 691.08; HRMS (ESI$^+$) calculated for $C_{20}H_{17}O_5$ [M + H$^+$], 337.1076; found 337.1058; HPLC purity: 94.36%, t_R = 6.097 min.

Benzyl (E)-3-(4-oxo-4H-benzo[h]chromen-3-yl)acrylate (5fa). Yield: 84%; brown solid; MP = 145-146 °C; ^{1}H NMR (400 MHz, CDCl$_3$) δ (ppm) = 8.22 (d, J = 2.8 Hz, 1H), 8.10 (s, 1H), 7.63 (dd, J = 2.8 Hz, 9.2 Hz, 1H), 7.45-7.32 (m, 8H), 5.25 (s, 2H); ^{13}C NMR (100 MHz, CDCl$_3$) δ (ppm) = 174.82, 167.16, 157.62, 153.95, 136.10, 135.56, 134.40, 132.07, 128.70, 128.35, 125.89, 125.24, 122.51, 119.99, 119.44, 66.54; IR (ATR): υ (cm^{-1}) = 3852.73, 3740.97, 3673.52, 3613.85, 2380.02, 2310.12, 1916.67, 1744.66, 1698.24, 1654.51, 1520.78, 1458.95, 1391.54, 1338.19, 1277.96, 1152.23, 1005.97, 796.51, 734.25, 694.26; HRMS (ESI$^+$) calculated for $C_{19}H_{14}ClO_4$ [M + H$^+$], 351.0881; found 351.0802; HPLC purity: 95.42%, t_R = 9.383 min.

4-(Benzyloxy)benzyl (*E*)-3-(6-bromo-4-oxo-4H-chromen-3-yl)acrylate (5cm). Yield: 78%; yellow solid; MP = 179-181 °C; ^{1}H NMR (400 MHz, CDCl$_3$) δ (ppm) = 8.38 (d, J = 2.4 Hz, 1H), 8.09 (s, 1H), 7.77 (dd, J = 2.8 Hz, 9.2 Hz, 1H), 7.45-7.32 (m, 10H), 6.98 (d, J = 8.8 Hz, 2H), 5.18 (s, 2H), 5.08 (s, 2H); ^{13}C NMR (100 MHz, CDCl$_3$) δ (ppm) = 174.66, 167.21, 158.96, 157.50, 154.40, 137.15, 136.98, 135.38, 130.25, 129.11, 128.74, 128.50, 128.14, 127.59, 125.59, 122.67, 120.19, 119.59, 119.53, 115.02, 70.16, 66.36; IR (ATR): υ (cm^{-1}) = 3852.41, 3741.48, 3673.52, 3613.83, 3069.41, 2945.92, 2379.21, 2310.37, 1697.62, 1645.59, 1516.85, 1458.48, 1379.07, 1241.07, 1150.01, 1019.69, 979.77, 792.75, 728.32, 691.46; HRMS (ESI$^+$) calculated for $C_{26}H_{20}BrO_5$ [M + H$^+$], 491.0494; found 491.0472; HPLC purity: 95.22%, t_R = 8.060 min.

4-(Benzyloxy)benzyl (E)-3-(6-methyl-4-oxo-4H-chromen-3-yl)acrylate (5dm). Yield: 80%; white amorphous solid; MP = 140-142 °C; ^{1}H NMR (400 MHz, CDCl$_3$) δ (ppm) = 8.26 (dd, J = 1.2 Hz, 8Hz, 1H), 8.09 (s, 1H), 7.71-7.66 (m, 1H), 7.48-7.46 (m, 1H), 7.44-7.38 (m, 5H), 7.36-7.31 (m, 5H), 6.97 (d, J = 8.8 Hz, 2H), 5.18 (s, 2H), 5.07 (s, 2H); ^{13}C NMR (100 MHz, CDCl$_3$) δ (ppm) = 175.87, 167.23, 158.78, 157.45, 155.50, 136.85, 135.81, 134.01, 130.04, 128.59, 128.47, 127.98, 127.45, 126.35, 125.85, 124.19, 121.97, 119.28, 118.10, 114.86, 66.11; IR (ATR): υ (cm^{-1}) = 3851.94, 3742.03, 3673.10, 3613.77, 1745.82, 1699.29, 1665.04, 1617.92, 1516.76, 1460.94, 1412.09, 1354.80, 1292.39, 1244.51, 1150.98, 996.21, 863.37, 803.99, 744.84, 686.80; HRMS (ESI$^+$) calculated for $C_{26}H_{21}O_5$ [M + H$^+$], 493.1629; found 493.1622; HPLC purity: 97.49%, t_R = 6.740 min.

4-(benzyloxy)benzyl (E)-3-(4-oxo-4H-benzo[*h*]chromen-3-yl)acrylate (5fm). Yield: 88%; yellow solid; MP = 179-181 ˚C; ^{1}H NMR (400 MHz, CDCl$_3$) δ (ppm) = 8.38 (d, J = 2.4 Hz, 1H), 8.09 (s, 1H), 7.77 (dd, J = 2.8 Hz, 9.2 Hz, 1H), 7.45-7.32 (m, 10H), 6.98 (d, J = 8.8 Hz, 2H), 5.18 (s, 2H), 5.08 (s, 2H); ^{13}C NMR (100 MHz, CDCl$_3$) δ (ppm) = 174.66, 167.21, 158.96, 157.50, 154.40, 137.15, 136.98, 135.38, 130.25, 129.11, 128.74, 128.50, 128.14, 127.59, 125.59, 122.67, 120.19, 119.59, 119.53, 115.02, 70.16, 66.36; IR (ATR): υ (cm^{-1}) = 3852.41, 3741.48, 3673.52, 3613.83, 3069.41, 2945.92, 2379.21, 2310.37, 1697.62, 1645.59, 1516.85, 1458.48, 1379.07, 1241.07, 1150.01, 1019.69, 979.77, 792.75, 728.32, 691.46; HRMS (ESI$^+$) calculated for C$_{26}$H$_{20}$BrO$_5$ [M + H$^+$], 498.0482; found 498.0472; HPLC purity: 97.16%, t_R = 8.273 min.

4.3. Biological Evaluation

4.3.1. *In vitro* PL inhibition

The synthesized acrylate linked chromone analogues were screened for PL inhibitory activity, using the assay protocol, standardized in our laboratory[2]. The porcine pancreatic lipase (Type II) was utilized, with 4-Nitrophenylbutyrate as a substrate. All the concentrations of inhibitors (**5aa-5fm**) were prepared using dimethyl sulfoxide (DMSO). The absorbance of the resultant solution was recorded at 405 nm on microplate reader, for the calculation of % inhibition followed by IC$_{50}$ values. All the analogues were found to have IC$_{50}$ values in the range of 5.16-48.81 µM (**Table 4.1**). Many of the analogues (**5ad, 5ae, 5ah, 5ak-am, 5ao, 5ca, 5ea, 5fa, 5cm, 5dm, 5fm**), were found to exhibit good activity (5.16-15.29 µM), whereas some analogues (**5aa, 5ab, 5af, 5aj, 5an, 5ba, 5da**) had shown moderate activity (15.69-25.27 µM). Few of the analogues (**5ac, 5ag, 5ai, 5ap**) showed poor inhibitory activity (33.48-48.81 µM). Among all the analogues, **5am** and **5ad** were found to be the most potent PL inhibitory analogues (IC$_{50}$ = 5.16, 5.82 µM, respectively). The standard drug orlistat exhibited potent PL inhibition with IC$_{50}$ value of 0.86 µM.

Table 4.1. *In vitro* PL inhibitory activity of synthesized acrylate linked chromone analogues (**5aa-5fm**) and orlistat

Code	R^1	R^2	IC$_{50}$ (µM ± SEM)*
5aa	H	Phenyl	25.27 ± 0.550
5ab	H	2-Nitrophenyl	17.37 ± 0.383
5ac	H	3-Nitrophenyl	42.73 ± 1.803
5ad	**H**	**4-Nitrophenyl**	**5.82 ± 0.933**

5ae	H	3-Chlorophenyl	15.29 ± 1.065
5af	H	4-Chlorophenyl	18.01 ± 1.715
5ag	H	2,4-Dichlorophenyl	33.48 ± 1.857
5ah	H	3,4-Dichlorophenyl	11.01 ± 0.168
5ai	H	4-Cyanophenyl	40.54 ± 1.280
5aj	H	4-Methoxyphenyl	17.15 ± 1.749
5ak	H	2,3-Dimethoxyphenyl	9.44 ± 1.472
5al	H	3,4,5-Trimethoxyphenyl	7.85 ± 0.099
5am	**H**	**4-Benzyloxyphenyl**	**5.16 ± 0.287**
5an	H	(1*H*-benzo[d]imidazol-2-yl)	16.74 ± 0.005
5ao	H	benzo[d][1,3]dioxol-5-yl	14.51 ± 0.564
5ap	H	thiophen-2-yl	48.81 ± 3.112
5ba	6-Chloro	Phenyl	15.69 ± 1.006
5ca	6-Bromo	Phenyl	10.29 ± 0.426
5da	6Methyl	Phenyl	18.58 ± 1.288
5ea	6-Methoxy	Phenyl	14.26 ± 0.940
5fa	[*h*]benzo	Phenyl	10.53 ± 1.365
5cm	6-Bromo	4-Benzyloxyphenyl	8.94 ± 0.754
5dm	6-Methyl	4-Benzyloxyphenyl	11.97 ± 1.947
5fm	[*h*]benzo	4-Benzyloxyphenyl	8.72 ± 0.441
Orlistat	-	-	0.86 ± 0.09

*The experiment is performed in triplicate (n=3)

4.3.2. Structure Activity Relationship (SAR)

The preliminary SAR was generated, by analysing PL inhibitory activities of the synthesized acrylate linked chromone analogues (**5aa-fm**). As shown in **Figure 4.6**, the SAR part has been divided into 2 categories; 1) Effect of Substituted chromone ring (R^1 substitution), 2) Effect of Substituted aromatic ring (R^2 substitution). On chromone ring, the effect of various substituents (electron donating & electron withdrawing) on 6th position were analysed. The analogue with bromo substitution showed better potency (**5ca**; IC_{50} = 10.29 ± 0.426 µM) as compared with unsubstituted analogue (**5aa**; IC_{50} = 25.27 ± 0.550 µM). In case of R^2

substitution, the effect of various substituted aromatic and heteroaromatic rings was analysed. For aromatic substitution, the electron donating groups (EDG) were found to be effective compared to electron withdrawing groups (EWG). Among various EDG (Benzyloxy, Trimethoxy, Dimethoxy, Methoxy), the analogue with 4-Benzyloxy substitution showed potent activity (**5am**; $IC_{50} = 5.16 \pm 0.287$ µM) and was found to be the most potent analogue of the series. In case of analogues with EWG (Nitro, Chloro, Dichloro, Cyano), the Nitro substitution on 4th position of phenyl ring (analogue **5ad**) showed potent activity with IC_{50} of 5.82 ± 0.933 µM. Analogue with 4-Cyano substitution showed poor PL inhibitory potential (**5ai**; $IC_{50} = 40.54 \pm 1.280$ µM). The effect of various heterocycles on PL inhibition have also been checked and the analogue with benzo[d][1,3]dioxol-5-yl and (1*H*-benzo[d]imidazol-2-yl) substitutions (**5ao, 5an**) showed good inhibition with IC_{50} of 14.51 ± 0.564 and 16.74 ± 0.005 µM, respectively. The analogue **5ap** with thiophen-2-yl substitution showed very poor PL inhibitory potential ($IC_{50} = 48.81 \pm 3.112$ µM). After analyzing the effect of R^1 and R^2 groups, the analogue having R^1 as 6-Bromo and R^2 as 4-Benzyloxy was synthesized, and PL inhibitory activity was analysed. It showed potent activity (**5cm**; $IC_{50} = 8.94 \pm 0.754$ µM) but was not found as potent as analogue **5am** ($IC_{50} = 5.16 \pm 0.287$ µM).
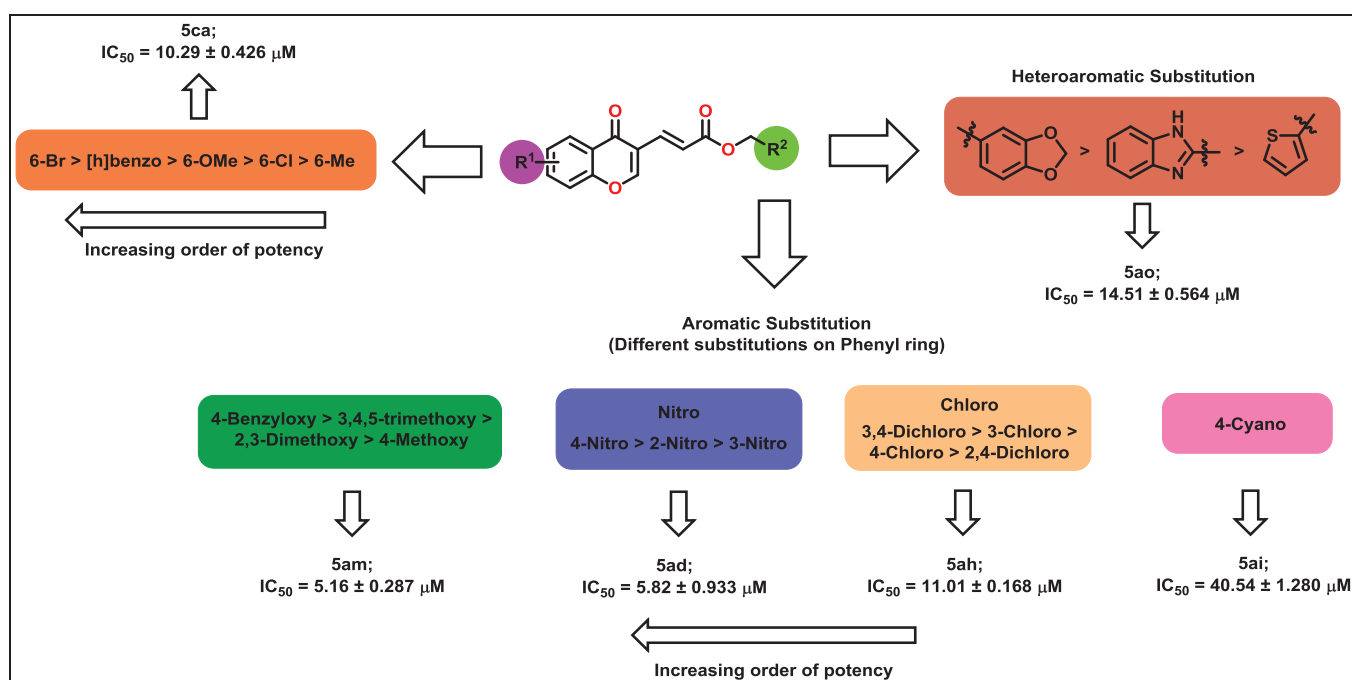
Figure 4.6. Structure Activity Relationship (SAR) study of acrylate linked chromone analogues (**5aa-5fm**)

4.3.3. Enzyme Kinetics

After the *in vitro* screening of synthesized acrylate linked chromone analogues for PL inhibitory activity, the enzyme kinetics of most potent analogue **5am** was performed to

understand the nature of inhibition (competitive, non-competitive, uncompetitive). For performing the same, PL inhibition assay protocol was performed by taking 4 different substrate concentrations (25, 50, 100, 200 μM). The assay was performed in triplicate using 3 different inhibitor concentrations (0, 0.625, 5 μM). As, shown in **Figure 4.7**, the plots were found to converge at y-axis with concentration dependent increase in K_m value and no change in V_{max}. Such results clearly indicate competitive nature of inhibition of analogue **5am**.
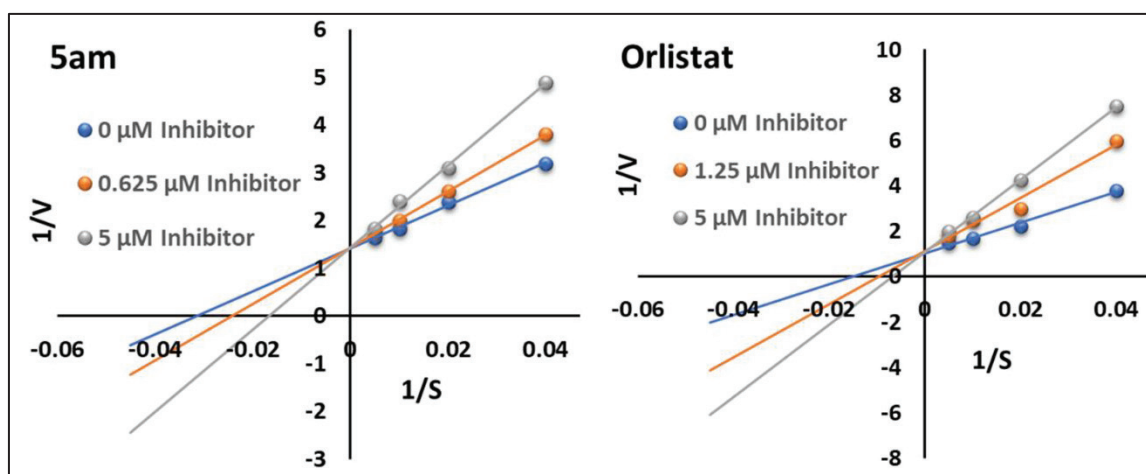
Figure 4.7. Double reciprocal Lineweaver–Burk plot of analogue **5am** and **orlistat**

The K_i value of analogue **5am** was calculated by Cheng–Prusoff equation and was found to be 2.003 μM. As reported, orlistat was also observed to have competitive inhibition having K_i value of 0.488 μM (**Table 4.2**).

Table 4.2. Enzyme kinetics study of analogue **5am** and **orlistat**

Code	K_m (apparent)			V_{max}			V_{max} (Average) (μM/min)	K_i (μM)	Nature of inhibition
	0 μM	0.625 μM	5 μM	0 μM	0.625 μM	5 μM			
5am	31.717	41.224	59.950	0.704	0.698	0.695	0.699	2.003	Competitive
Orlistat	65.740	102.970[a]	144.750	0.974	0.884	0.909	0.922	0.488	Competitive

[a] Calculated for 1.25 μM concentration

4.3.4. Fluorescence Quenching Study

The human PL is made up of 449 amino acids, among which seven are Tryptophan (Trp) residues. These seven Trp residues are mainly responsible for fluorescence emission of protein in association with 25 Phenylalanine (Phe) and 16 Tyrosine (Tyr) residues.[15] If any of the ligand binds at the active site and interacts with above mentioned aromatic amino acids,

then the fluorescence intensity of PL decreases leading to the phenomenon known as fluorescence quenching. Based on this hypothesis, the fluorescence quenching effect of most potent analogue **5am** on PL fluorescence was tested. As explained in detailed in Chapter 3, 6 concentrations of analogue **5am** in serial dilutions (0.3125 - 20 µg/mL) were tested to observe the concentration-dependent fluorescence quenching of PL enzyme.

The effect of quenching was performed at 298 K and the graph of Fluorescence Intensity *Vs* Wavelength was plotted. As shown in **Figure 4.8**, the PL enzyme without any inhibitor presented highest fluorescence intensity of 32,230 cps. In the presence of analogue **5am**, there was a decrease in fluorescence intensity, up to 19,410 cps. Also, such decrease in fluorescence intensity was found to have concentration-dependent effect.
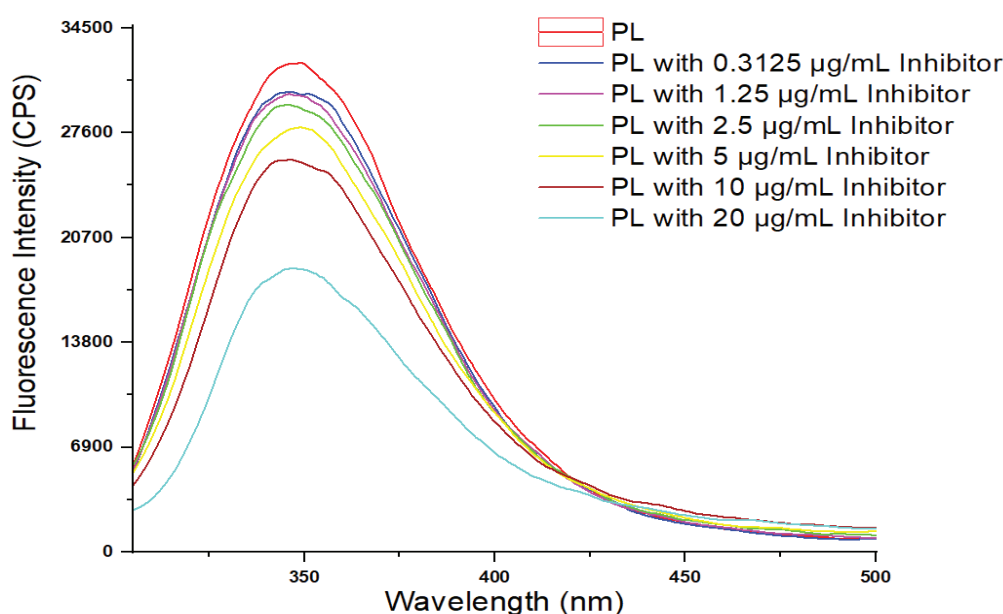
Figure 4.8. Fluorescence quenching of porcine PL by analogue **5am**

The analogue **5am** can quench the fluorescence intensity of PL either by collision or complex formation or by both the mechanisms. To identify the underlying mechanism of quenching by **5am**, Stern-Volmer equation was utilized (chapter 3, **Formula 3.2**).[15–17]

The graph of F_0/F Vs [Q] was plotted by keeping the y-intercept as 1. As shown in **Figure *4.9***, there is a linear relationship between F_0/F and [Q], that eliminates the possibility of dynamic quenching. For mixed quenching, the points should incline towards the y-axis, but the graph shows no inclination of data towards y-axis. Such results provided the proof that the quenching caused by analogue **5am** is due to the complex formation between PL and the inhibitor **5am.**
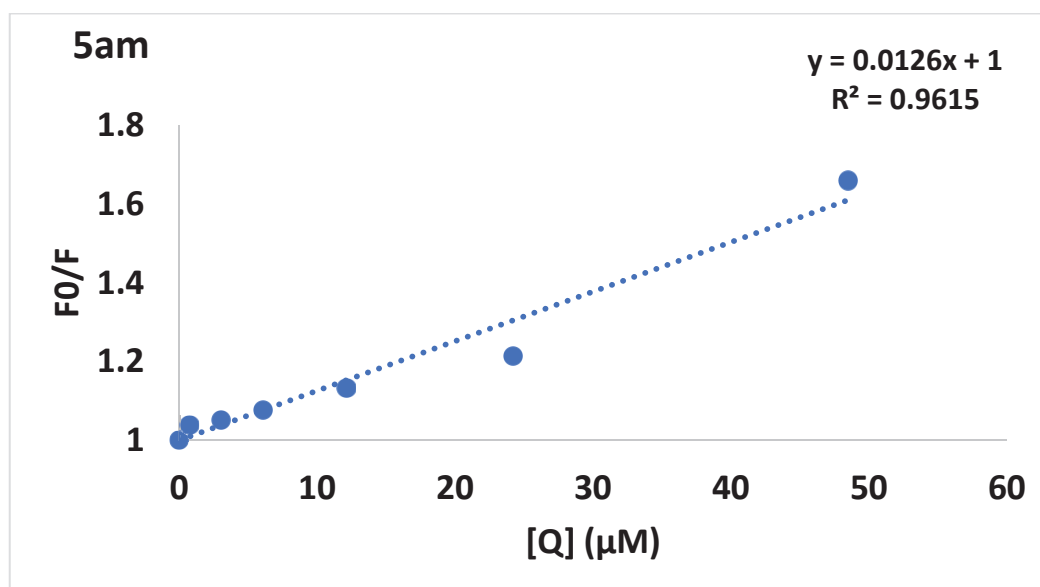
Figure 4.9. Stern-Volmer plot of PL with analogue **5am**

The values of k_q and K_{SV} were calculated from the graph of F_0/F Vs [Q]. As shown in **Table 4.3**, the k_q value was found to be 7.92×10^{12} L mol^{-1}sec^{-1}. As the k_q values are much higher than the maximal dynamic quenching constant (2.0×10^{10} L mol^{-1}sec^{-1}), it further confirms that the quenching caused by **5am** is not due to dynamic quenching.[17]

Table 4.3. The values of kq, K_{SV} and n, K_b obtained from Stern-Volmer and double logarithmic plot

Analogue	$K_{SV}/10^4$ (L mol^{-1})	$k_q/10^{12}$ (L mol^{-1}sec^{-1})	n	$K_b/10^5$
5am	1.26	7.92	0.64	2.06

After the confirmation of static quenching mechanism, the binding constant (K_b) and number of binding sites (n) were calculated using following **Formula 3.3** of chapter3.

From the plot of log[(F_0-F)/F] Vs log [Q], the value of number of binding sites (n) was found to be 0.76 with high binding constant value of 1.93×10^5 L mol^{-1} at 298 K temperature (**Figure 4.10**). As the value of n is closer to 1, it means the analogue **5am** binds at one binding site of PL enzyme.
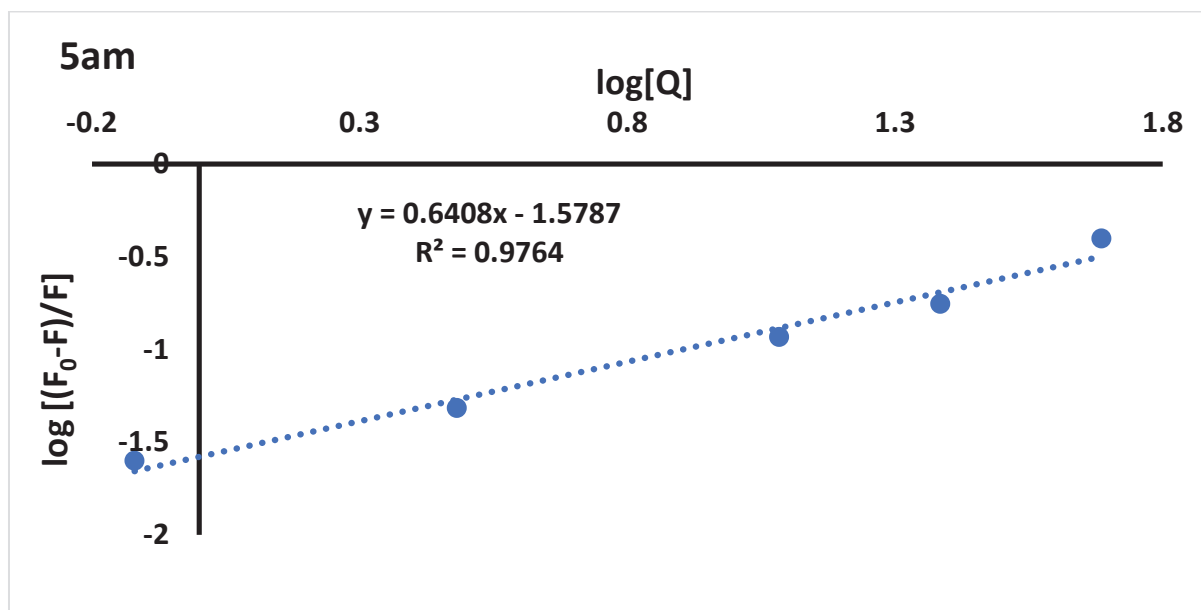
Figure 4.10. Double logarithmic plot for the calculation of binding constant (K_b) and number of binding sites (n)

4.4. Molecular Modelling Studies

4.4.1. Molecular Docking Study

As mentioned before, the preliminary design of the acrylate linked chromone analogues was performed by keeping the pharmacophoric features required for binding of analogues at the PL active site. The designed analogues were validated by molecular docking analysis. For docking study, the structure of the PL protein (PDB ID: 1LPB) was retrieved from RCSB PDB and the docking was performed using MVD software. The grid coordinates were generated as 8.36, 23.16, 53.61 (x, y, z), keeping the radius 7 Å. The grid parameters were validated by the superimposition of docked pose over a co-crystalized ligand (Methoxyundecylphosphinic acid i.e., MUP). The conformers were superimposed, with an RMSD value of 0.83 (**Figure 4.11**).
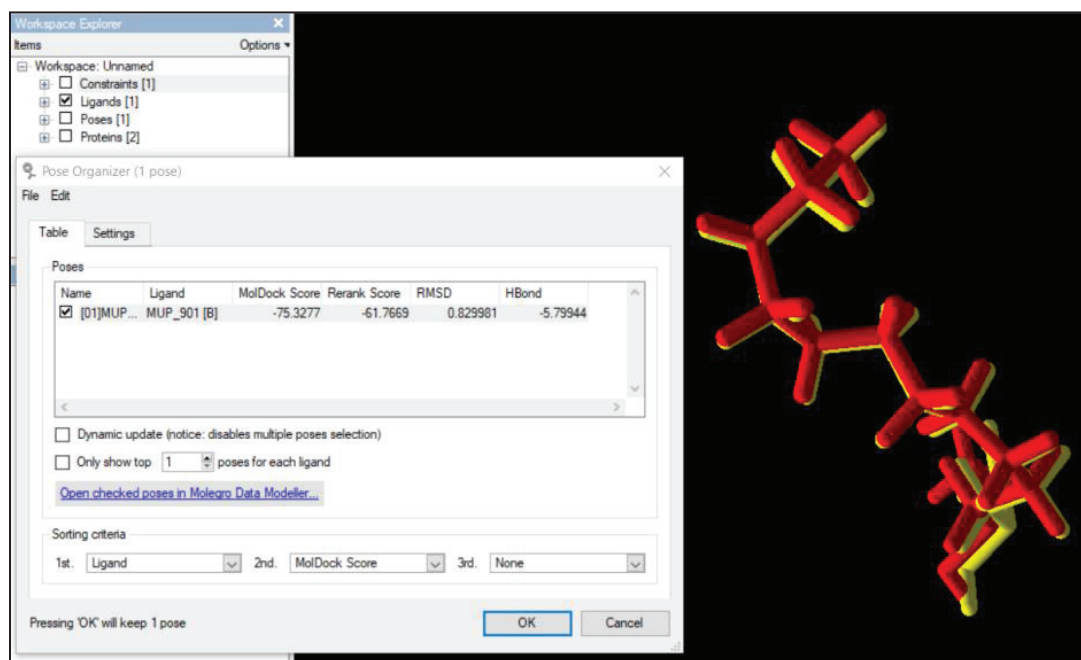
Figure 4.11. Results of grid validation, showing overlapping of docked pose (yellow) on native pose (red) of MUP

The synthesized analogues **5aa-fm** were docked and analyzed for docking score and various interactions at the binding site of PL. As shown in **Table 4.4**, the prototype analogue **5aa** was found to interact with lid domain amino acids (Tyr114. Gly76, Phe77). Also, the Ser152 shown hydrogen bonding with the keto group of acrylate fragment. Further, various substituted chromone analogues, depending upon synthetic feasibility were docked and the docking results were analysed. All the analogues were found to have MolDock score in the range of -115.86 to -160.07 kcal/mol. The prototype analogue **5aa** had shown moderate MolDock score of -115.86 kcal/mol. The analogue **5am** with benzyloxy substituent on phenyl ring was found to have highest MolDock score of -160.07 kcal/mol. Further the docking pose of analogue **5am** was analysed for various docking interactions.

Table 4.4. Molecular docking results of acrylate linked chromone analogues (**5aa-5fm**) and orlistat

Code	MolDock Score (kcal/mol)	Amino acid Interactions				
		H-Bond/ C-H Bond	**π–π stack**	**π-Alkyl/ Alkyl**	**π -Sigma/ π-Sulfur**	**π-cation/ π-anion**
5aa	-115.86	Gly76, Phe77, His151, Ser152, Leu153	Tyr114	Ala178, Pro180, Ala260, Leu264	-	-
5ab	-129.38	Gly76, Phe77, His151, Phe215, His263	Tyr114, Phe215	Ala178, Pro180, Arg256, Ala259, Ala260	Leu264	-
5ac	-126.92	Phe77, His151, Ser152, Arg256	Tyr114, Phe215	Ala178, Pro180, Leu264	-	Arg256
5ad	-125.98	Phe77, Asp79, His151, Ser152, His263	Tyr114, Phe215	Leu78, Ala178, Pro180	-	Arg256
5ae	-123.24	Gly76, Phe77, His151, Ser152, Phe215, His263	Tyr114, Phe215	Ala178, Pro180, Trp252, Arg256, Ala259, Ala260, Leu264	-	Arg256
5af	125.51	Gly76, Phe77, His151, Ser152, Leu153	Tyr114	Ile78, Ala178, Pro180, Trp252, Arg256	-	Arg256
5ag	-134.71	Gly76, Phe77, His151,		Ile78, Ala178, Pro180, Trp252, Arg256, Ala260, His263, Leu264	-	Arg256
5ah	-130.02	His151, Ser152, Arg256	Tyr114, Phe215	Ile78, Trp252, Arg256, Ala259, Ala260, Leu264	-	-
5ai	-131.24	Gly76, Phe77, His151, Ser152	Tyr114	Ala178, Pro180, Ala259, Leu264	-	Arg256
5aj	-125.77	Gly76, His151, Ser152	Tyr114, Phe215	Ala178, Pro180, Leu264	-	Asp79, Arg256
5ak	-126.24	Asp79, His151, Ser152, Arg256	Tyr114, Phe215	Ala178, Pro180, Arg256, Ala259, Ala260	Leu264	-
5al	-125.18	Gly76, Phe77, Asp79, His151, Ser152	Tyr114, Phe215	Ala178, Pro180, Leu264	-	Arg256
5am	-160.07	Gly76, Phe77, Asp79, His151, Ser152, Arg256, His263	Tyr114	Leu153, Ala178, Pro180, Ala259	-	Arg256
5an	-123.59	Gly76, Phe77, Asp79, His151, Ser152, His263	Tyr114	Ile78, Ala178, Pro180, Leu264	-	Asp79, Arg256
5ao	-133.73	Gly76, His151, Ser152, Arg256	Tyr114, Phe215	Ala178, Pro180, Ala259, Ala260, Leu264	-	Arg256
5ap	-124.81	Gly76, Phe77, His151, Ser152, His263	Tyr114, Phe215	Ala178, Pro180, Arg256, Ala259, Ala260	His263, Leu264	-
5ba	-120.34	Gly76, Phe77, His151, Ser152	Tyr114, Phe215	Ala178, Pro180, Ala259, Ala260, Leu264		Arg256
5ca	-125.19	Gly76, Asp79, His151, Phe215, Arg256		Ala178, Pro180, Ile20, Phe215, Ala259, Ala260, Leu264		Arg256
5da	-125.39	Gly76, His151, Ser152	Tyr114, Phe215	Ala178, Pro180, Arg256, Ala259, Ala260	Leu264	-
5ea	-127.66	Gly76, His151	Tyr114	Ala178, Pro180, Arg256,	Leu264	-

				Ala259, Ala260		
5fa	-138.52	Gly76, His151, Ser152	Phe215	Ile78, Ala178, Pro180, Leu264	His263	-
5cm	-153.02	Gly 76, Phe 77, His 151, Ser 152, His 263		Ala178, Pro180, Trp252, Ala259		Arg256, His263
5dm	-128.52	Gly76, His151, Ser152		Ala178, Pro180, Ala259, Ala260	-	-
5fm	-148.52	Gly76, His151, Ser152	Phe215	Ile78, Ala178, Pro180, Leu264	His263	-
Orlistat	-139.49	Gly76, Phe77, Asp79, His151, Ser152, Arg256	-	Ile78, Ile209, Ile213, Arg256, Leu264	Phe215	-

As shown in **Figure 4.12**, the analogue **5am** showed many of the requisite interactions with the active site amino acids. The phenyl ring also exhibited π–Alkyl interaction with Leu153 and Ala178. The benzyloxy substituent was found to interact with Tyr114 and Pro180 *via* π–π stacking and π–Alkyl interactions. The chromone part formed hydrogen bonding and π–cation interactions with Arg256 and π–Alkyl interaction with Ala259. The carbonyl oxygen of acrylate linkage played major role in the formation of hydrogen bonding interaction with Gly76, His151 and Ser152. The His263 showed hydrogen bonding with oxygen of the acrylate ester. The standard drug Orlistat was also found to have similar interactions with MolDock score of -139.49 kcal/mol.
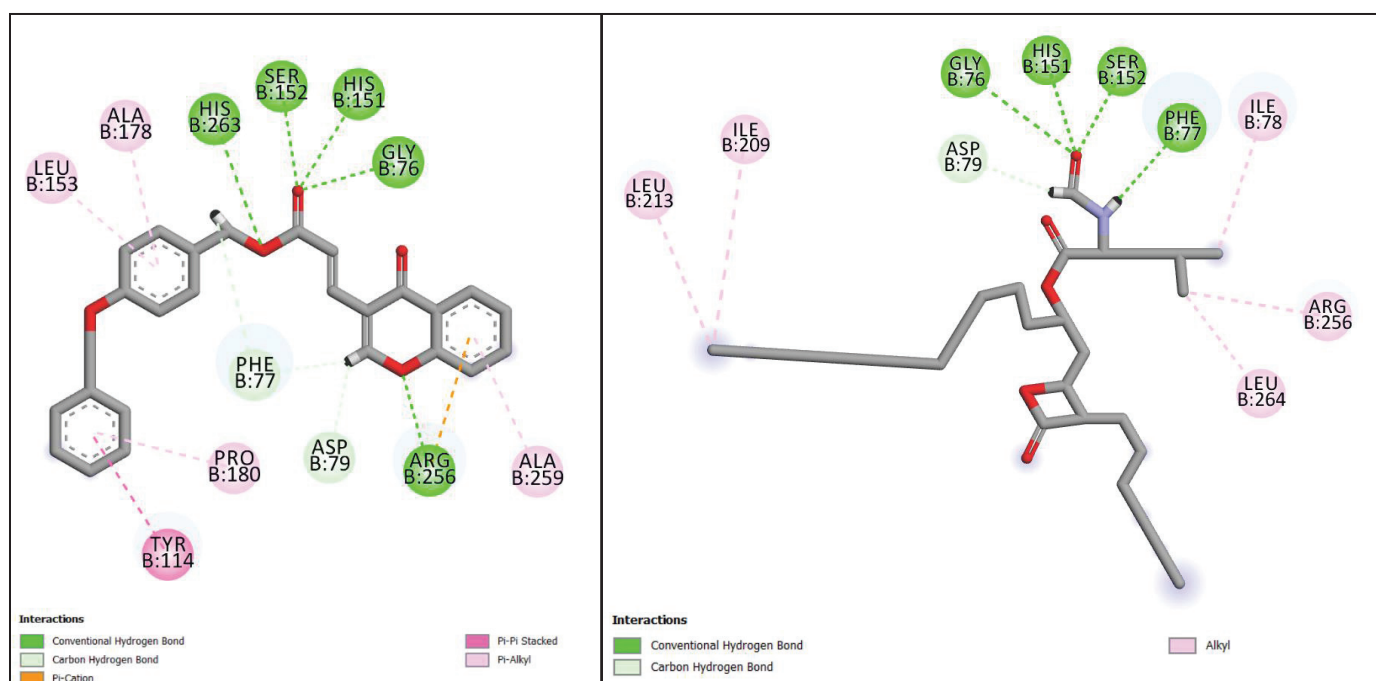
Figure 4.12. 2D interaction diagram of analogue **5am** and **orlistat**, bound at the active site of PL enzyme (PDB ID: 1LPB)

4.4.2. Molecular Dynamics Analysis

The molecular docking analysis provides preliminary information about the docking interactions but fails to predict the extent of docking interactions in dynamic condition. As the enzymes present in our body are continuously in dynamic condition, it is necessary to predict the behaviour of the ligand in dynamic physiological conditions of our body. Hence, the ligand-protein complex of most potent analogue **5am** was subjected to molecular dynamics simulation for 100 ns. After molecular dynamics simulation, the results were analysed by taking protein-ligand RMSD, protein-ligand contacts and ligand-protein contacts in consideration. As shown in **Figure 4.13** the protein was found to be stable throughout the simulation with RMSD value less than 4.0 Å. The ligand RMSD value was up to 3.0 Å till 60 ns of time and found to deviate up to 6.4 Å from 60-100 ns.
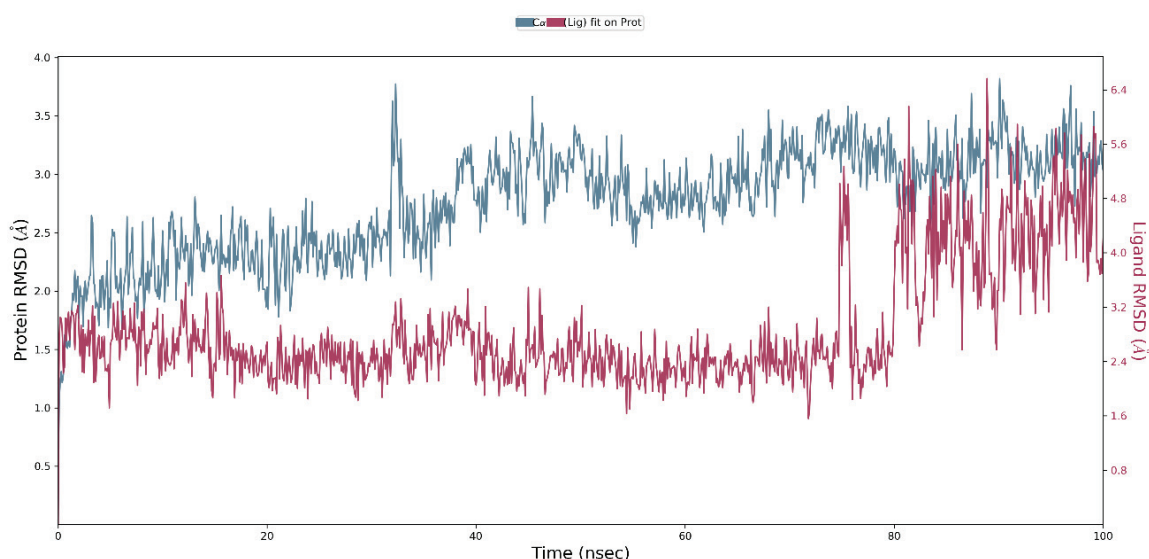
Figure 4.13. RMSD plot for protein-ligand complex of analogue **5am**, bound at PL active site (PDB ID: 1LPB) for 100 ns of simulation time

Further, the ligand-protein interactions formed throughout the simulation time of 100 ns were analysed to get the clear idea about the stability of the complex. As shown in **Figure 4.14**, Phe 77 was found to interact for 0.85 fraction of time *via* various interactions (H-bonding, hydrophobic interactions and water bridges). Tyr114 and Phe215 were also found to interact for 1.1 and 0.9 fraction of time respectively, *via* hydrophobic interaction and formation of water bridges.
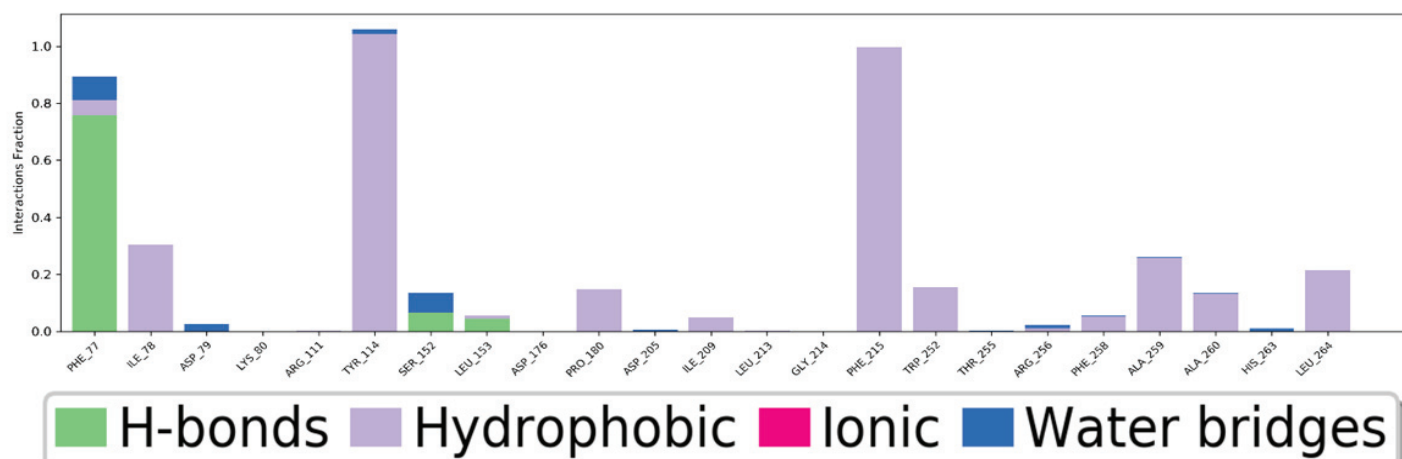
Figure 4.14. Stacked bar plot of the fraction of time of the interactions of analogue **5am** for 100 ns of simulation time

Figure 4.15 depicts the long duration of interactions with Phe77, Ile78, Tyr114 and Phe215 amino acids. Such an extent of interactions with Phe77, Tyr114 and Phe215 (Lid domain amino acids) proves the effectivity of designed analogues in opening of the lid domain of PL.
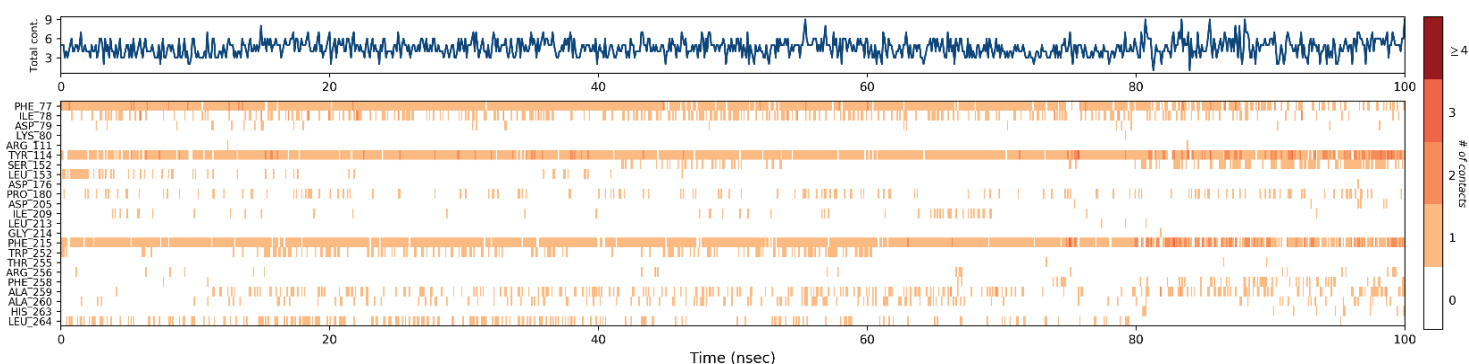
Figure 4.15. A timeline representation of protein and ligand contacts

The chromone ring was involved in interaction with the lid domain amino acids, namely Tyr114 and Phe215 via π-π interaction for 49% and 65% of simulation time. Another amino acid, Phe77 had shown H-bonding interaction with the carbonyl oxygen of the acrylate linkage for 75% of the simulation time (**Figure 4.16**). For analysing the extent of binding interactions throughout the simulation time, the time frame analysis was performed.
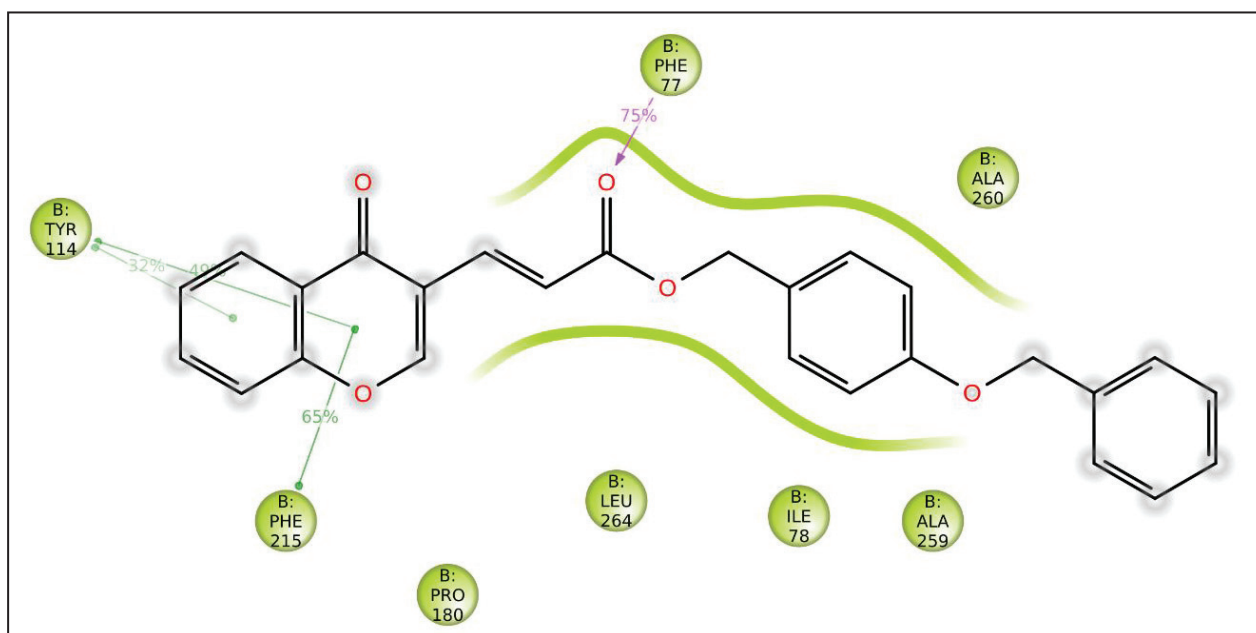
Figure 4.16. Ligand-protein interactions for 100 ns of the simulation time

As shown in **Table 4.5**, Phe77, Tyr114 and Phe215 were found to interact significantly for 75-98%, 31-49%, 65-77% of simulation time, respectively. It shows the role of lid domain amino acids in the stability of ligand-protein complex in dynamic simulated physiological environment.

Table 4.5. Time frame analysis of protein-ligand interactions

Time Frame (ns)	Duration of Amino acid Interactions (%)				
	H-Bonding			**π–π stacking**	
	Phe77	**Leu153**	**Tyr114**[a]	**Phe215**	**Trp252**
0-20	98	19	31 & 41	74	0
0-40	98	10	30 & 48	77	12
0-60	96	0	37 & 42	75	13
0-80	94	0	38 & 42	76	10
0-100	75	0	32 & 49	65	0

[a] Duration of Interaction (%) of Tyr 114 with phenyl and pyran-4-one of chromone ring, respectively.

4.5. Conclusion

In conclusion, a series of 24 acrylate linked chromone analogues were designed and synthesized followed by PL inhibitory screening. The analogues were designed by the attachment of acrylate fragment on chromone heterocycle, with the aim of targeting Ser152 amino acid. The analogues were designed by looking into various aspects such as docking score and amino acid interactions. The analogues were synthesized and screened for *in vitro*

PL inhibition activity. The analogues **5am** (IC$_{50}$ = 5.16 ± 0.287 μM) and **5ad** (IC$_{50}$ = 5.82 ± 0.933 μM) were found to be the most potent analogues of the series, as compared with the standard drug orlistat ((IC$_{50}$ = 0.86 ± 0.09 μM). The analogue **5am** was found to inhibit PL enzyme *via* competitive inhibition, which was proved through enzyme kinetics and fluorescence quenching study. The analogue **5am** was further subjected to molecular dynamics simulation for 100 ns. It was found to be stable with RMSD value in the range of 2.4-6.4 Å. However, the analogue **5am** and **5ad** is required to be optimized further in terms of potency as well as pharmacokinetic properties, to get the analogue with greater potential as an anti-obesity agent as compared with orlistat.

References

(1)   George, G.; Auti, P. S.; Paul, A. T. Design, synthesis and biological evaluation of N-substituted indole-thiazolidinedione analogues as potential pancreatic lipase inhibitors. *Chem. Biol. Drug Des.* **2021**, *98* (1), 49–59.

(2)   Auti, P. S.; Nandi, A.; Kumari, V.; Paul, A. T. Design, synthesis, biological evaluation and molecular modelling studies of oxoacetamide warhead containing indole-quinazolinone based novel hybrid analogues as potential pancreatic lipase inhibitors. *New J. Chem.* **2022**, *46* (24), 11648–11661.

(3)   Kahveci, B.; Yılmaz, F.; Menteşe, E.; Ülker, S. Design, synthesis, and biological evaluation of coumarin–triazole hybrid molecules as potential antitumor and pancreatic lipase agents. *Arch. Pharm. (Weinheim).* **2017**, *350* (8), 1–9.

(4)   Sayeed, M.; Mallappa, A.; Swamy, K.; Rani, U. Natural bio-active compounds. In *Natural Bio-active Compounds: Volume 1: Production and Applications*; Akhtar, M. S., I., Eds.; Springer US: 2019; Vol. 1, pp 149–191.

(5)   Sergent, T.; Vanderstraeten, J.; Winand, J.; Beguin, P.; Schneider, Y. J. Phenolic compounds and plant extracts as potential natural anti-obesity substances. *Food Chem.* **2012**, *135* (1), 68–73.

(6)   Lee, E. M.; Lee, S. S.; Chung, B. Y.; Cho, J. Y.; Lee, I. C.; Ahn, S. R.; Jang, S. J.; Kim, T. H. Pancreatic lipase inhibition by C-glycosidic flavones isolated from Eremochloa ophiuroides. *Molecules* **2010**, *15* (11), 8251–8259.

(7)   Thomas, A.; Allouche, M.; Basyn, F.; Brasseur, R.; Kerfelec, B. Role of the lid hydrophobicity pattern in pancreatic lipase activity. *J. Biol. Chem.* **2005**, *280* (48), 40074–40083.

(8)   Jang, D. S.; Lee, G. Y.; Kim, J.; Lee, Y. M.; Kim, J. M.; Kim, Y. S.; Kim, J. S. A new pancreatic lipase inhibitor isolated from the roots of Actinidia arguta. *Arch. Pharm. Res.* **2008**, *31* (5), 666–670.

(9)   Nakai, M.; Fukui, Y.; Asami, S.; Toyoda-Ono, Y.; Iwashita, T.; Shibata, H.; Mitsunaga, T.; Hashimoto, F.; Kiso, Y. Inhibitory effects of Oolong tea polyphenols on pancreatic lipase in vitro. *J. Agric. Food Chem.* **2005**, *53* (11), 4593–4598.

(10)   Rajan, L.; Palaniswamy, D.; Mohankumar, S. K. Targeting obesity with plant-derived pancreatic lipase inhibitors: A comprehensive review. *Pharmacol. Res.* **2020**, *155*, 104681–104714.

(11)   Sridhar, S. N. C.; Ginson, G.; Venkataramana Reddy, P. O.; Tantak, M. P.; Kumar, D.; Paul, A. T. Synthesis, evaluation and molecular modelling studies of 2-(carbazol-3-yl)-2-oxoacetamide analogues as a new class of potential pancreatic lipase inhibitors. *Bioorganic Med. Chem.* **2017**, *25* (2), 609–620.

(12)   Liu, D. Z.; Wang, F.; Liao, T. G.; Tang, J. G.; Steglich, W.; Zhu, H. J.; Liu, J. K. Vibralactone: A lipase inhibitor with an unusual fused β-lactone produced by cultures of the basidiomycete Boreostereum vibrans. *Org. Lett.* **2006**, *8* (25), 5749–5752.

(13)   Pervaram, S.; Ashok, D.; Reddy, C. V. R.; Sarasija, M.; Rao, B. A. Synthesis and antimicrobial activity of (*Z*)-3-{[3-oxobenzofuran-2(3H)-ylidene]methyl}-4H-chromen-4-one derivatives. *Russ. J. Gen. Chem.* **2018**, *88* (3), 566–572.

(14)   Chernov, N. M.; Shutov, R. V.; Barygin, O. I.; Dron, M. Y.; Starova, G. L.; Kuz'mich, N. N.; Yakovlev, I. P. Synthesis of chromone-containing allylmorpholines through a morita–baylis–hillman-type reaction. *European J. Org. Chem.* **2018**, 6304–6313.

(15)   Zhang, J.; Xiao, L.; Yang, Y.; Wang, Z.; Li, G. Lignin binding to pancreatic lipase and its influence on enzymatic activity. *Food Chem.* **2014**, *149*, 99–106.

(16)   Ramos, P.; Coste, T.; Piémont, E.; Lessinger, J. M.; Bousquet, J. A.; Chapus, C.; Kerfelec, B.; Férard, G.; Mély, Y. Time-resolved fluorescence allows selective monitoring of TRP30 environmental changes in the seven-TRP-containing human

pancreatic lipase. *Biochemistry* **2003**, *42* (43), 12488–12496.

(17)   Martinez-Gonzalez, A. I.; Alvarez-Parrilla, E.; Díaz-Sánchez, Á. G.; de la Rosa, L. A.; Núñez-Gastélum, J. A.; Vazquez-Flores, A. A.; Gonzalez-Aguilar, G. A. In vitro inhibition of pancreatic lipase by polyphenols: A kinetic, fluorescence spectroscopy and molecular docking study. *Food Technol. Biotechnol.* **2017**, *55* (4), 519–530.

CHAPTER 5

SERIES-II: DESIGN, SYNTHESIS & BIOLOGICAL EVALUATION

CHAPTER 5

5. Series-II: Design, Synthesis and PL Inhibitory Evaluation of Acrylate Linked Chromone Analogues

5.1. Rationale:

In chapter 4, a series of 23 acrylate linked chromone analogues with the linker length of 1 carbon atom (n=1) were developed. The analogue **5am** with IC_{50} of 5.16 ± 0.287 μM was the most potent of the series. Further, through a molecular docking study, the effect of linker length (n=2,3,4) on the binding of analogues at the active site pocket was analyzed. **Figure 5.1** depicts that the prototype analogue with a linker length of 1 carbon atom exhibited a docking score of -116.77 kcal/mol, but all the requisite interactions were present. When compared with the analogue having 2 carbon atom linker, there was an increase in docking score of -121.31 kcal/mol with necessary interactions. As the linker length increased to 3 carbon atoms, the docking score improved to -128.20 kcal/mol, but the important amino acid interactions vanished.
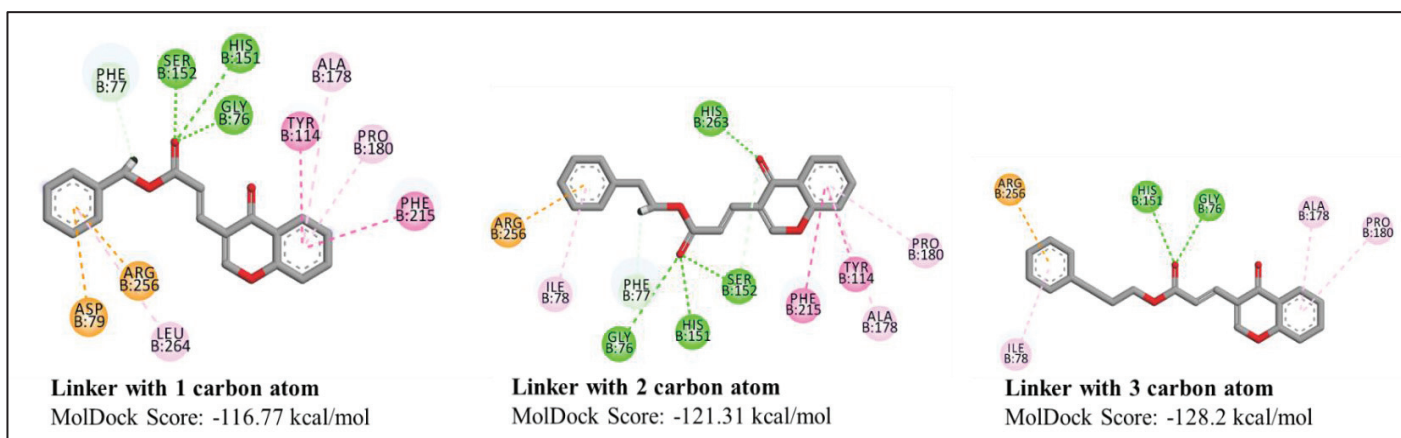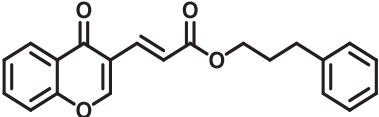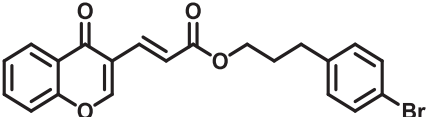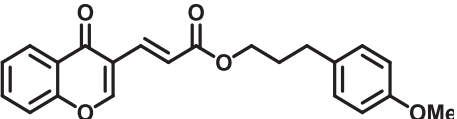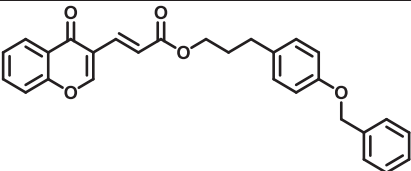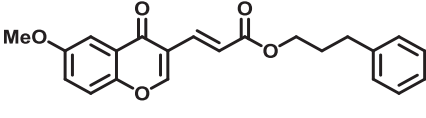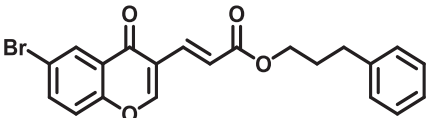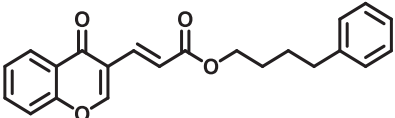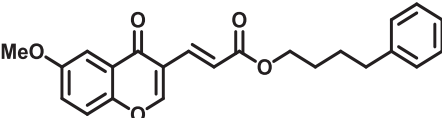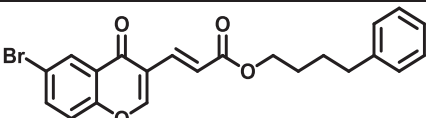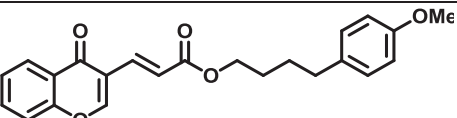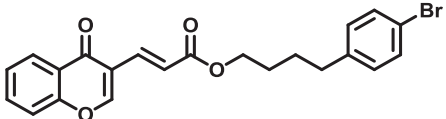
Figure 5.1. 2D interaction diagram of analogues with linker length of 1, 2, 3 carbon atoms

Further detailed analysis was performed through docking study by keeping different substituents on aromatic moieties with linker lengths of three and four carbon atoms, respectively. **Table 5.1** represents the docking analysis of analogues with selective substitutions on aromatic and heteroaromatic ring systems. The analogues with the linker length of 3 and 4 carbon atoms were found to be devoid of many of the interactions, i.e. lid domain, catalytic triad or interaction with Arg256. The trend was common for the analogues with varying substitutions.

Table 5.1. Docking analysis of analogues with the linker length of 3 and 4 carbon atoms

Sr. No.	Structure	MolDock Score	Lid Domain Interactions	Interactions with Catalytic Triad	Interactions with Arg256
Linker length of Three carbon atoms (n = 3)					
1		-128.20	Gly76	His151	
2		-130.54	Gly76, Phe77, Phe215	Ser152, His263	π-cation interaction
3		-132.60	Gly76, Tyr114, Phe215,	Ser152, His263	-
4		-155.65	Ile78	His263	-
5		-137.22	Gly76, Tyr114, Phe215,	Ser152	-
6		-126.77	Phe77, Tyr114	Ser152	-
Linker length of four carbon atoms (n = 4)					
7		-131.17	Gly76	His263	π-cation interaction
8		-134.48	Gly76	His263	π-cation interaction
9		-127.06	Phe77, Phe215	-	-
10		-131.52	-	His263	π-cation interaction

11		-136.13	Tyr114, Phe215	His263	π-cation interaction

By taking all such observations in consideration, the series II analogues were designed as shown in **Figure 5.2**. In this series, the linker length of 2 carbon atoms was fixed and the analogues with various substituents were synthesized as per the synthetic feasibility for PL inhibitory screening. Some of the analogues with a linker length of 3 carbon atoms were also synthesized for the confirmation of docking results.
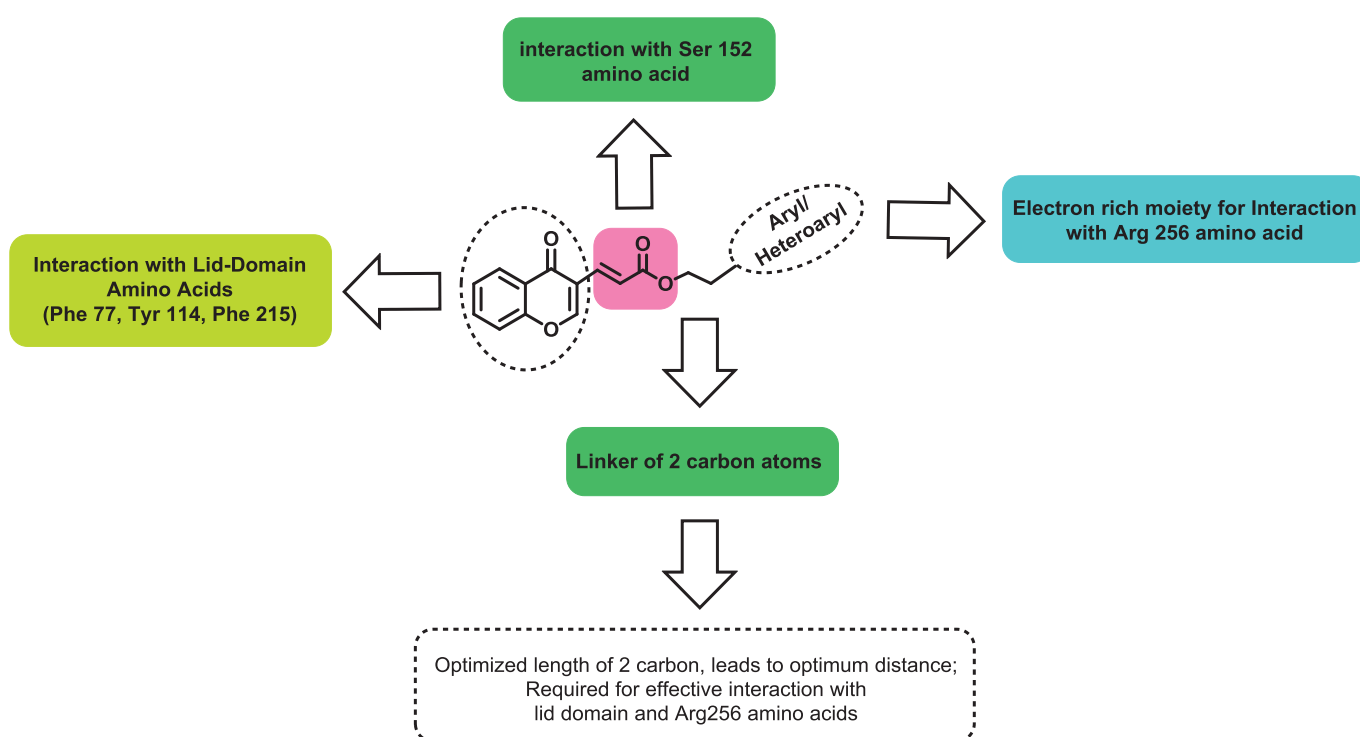
Figure 5.2. Rationale for the design of **Series II** analogues

5.2. Synthesis and Characterization

To check the PL inhibitory effect of designed acrylate linked chromone analogues, the analogues with different substituents, including EWGs, EDGs, heterocycles were synthesized using optimized reaction conditions (**Scheme 5.1**). As explained in chapter 4, the various substituted chromone-3-acrylic acids were prepared using a two-step methodology. Finally, the Chromone-3-acrylic acids were coupled with various substituted alcohols (Phenylethyl

alcohols, Phenylpropyl alcohols) to get the substituted Chromone-3-acrylic acid ester analogues (**6aa-gj**, **8aa-ac**).

Further, the structure of synthesized analogues were elucidated using various spectroscopic techniques such as IR, NMR and HR-MS. The purity of the synthesized analogues was determined using HPLC analysis. In the case of all the analogues, the % Purity was found to be above 95%, with the retention time (t_R) in the range of 4.16 – 11.49 min. All the analogues were novel, so the melting points were checked and reported for future reference. Through ^{1}H NMR, a singlet of 1H at δ value in the range of 8.09-8.26 ppm confirmed the presence of a proton at 2nd position of chromone ring. Two aliphatic protons (CH$_2$) of phenethyl moiety resonated in the δ range of 4.20-4.59 and 2.69-4.24 ppm as a triplet, confirming the attachment of phenethyl moiety. Further the peaks of additional substituents such as, methyl, methoxy, benzyloxy, phenoxy, etc. were in their standard range. The presence of carbonyl carbons of chromone and ester were further confirmed *via* ^{13}C NMR spectrum. For all the analogues, the carbonyl carbon of ketone of chromone were found to resonate at δ value in the range of 174.72-177.00 ppm, whereas the ester carbonyl peak was found in δ range of 167.25-167.56 ppm. The structures were further confirmed via HR-MS analysis by the presence of [M+H]$^{+}$ peaks in the spectrum, with the values, coinciding with the calculated m/z values.
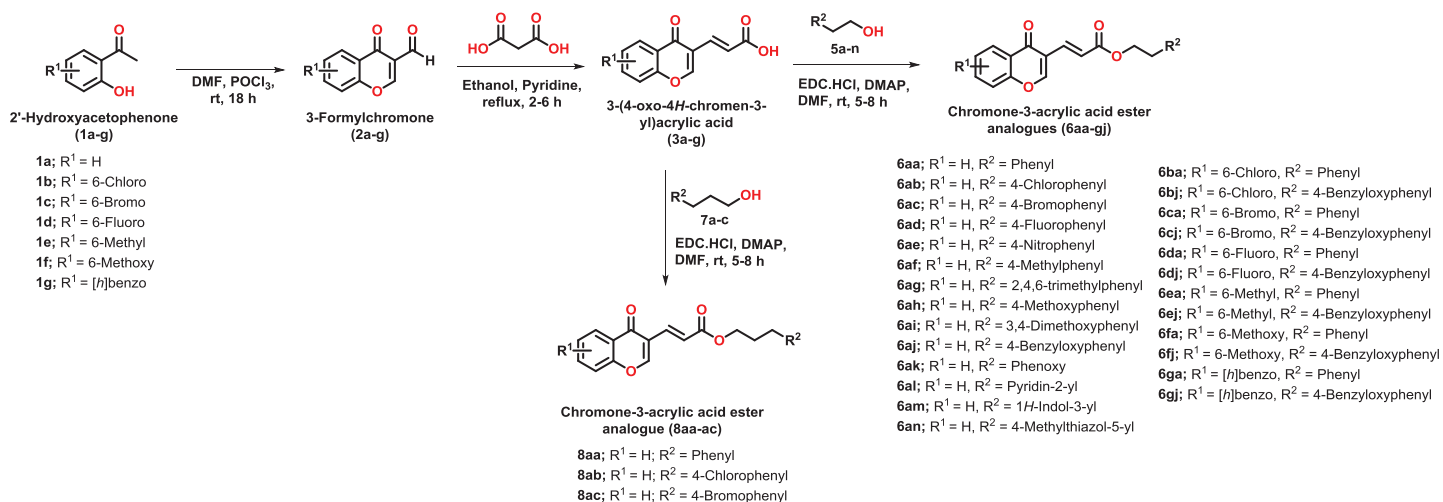
Scheme 5.1. Synthesis of designed Chromone-3-acrylic acid ester analogues (**6aa-gj**, **8aa-ac**)

5.2.1 General procedure for the synthesis of 3-Formylchromone (2a-g)

For the synthesis of 3-Formyl chromone, various substituted 2'-Hydroxyacetophenones (**1a-g**; 7.34 mmol) were dissolved in 7 mL of DMF and stirred at ice-cold condition for 15 minutes. POCl$_3$ (44.06 mmol) was then added to the above solution in dropwise fashion at

ice-cold condition. The reaction mixture was then allowed to stir at room temperature for 18 h. The completion of reaction was checked by TLC. The reaction mixture was then poured into ice-cold water, followed by filtration of formed precipitated products (**2a-g**) that were used further without any purification.[1]

5.2.2 General procedure for the synthesis of Chromone-3-acrylic acid (3a-g)

Substituted 3-Formylchromone (**2a-g**; 7.98 mmol) and Malonic acid (9.97 mmol) were suspended in 8 mL of ethanol, followed by the addition of 0.5 mL of Pyridine. The suspension was then stirred at reflux temperature for 2-6 h. After the completion of reaction (monitored by TLC), the reaction was stopped and cooled, followed by filtration and washing of the precipitate with cold ethanol to get the pure product (**3a-g**).[1]

5.2.3 General procedure for the synthesis of Chromone-3-acrylic acid ester analogues (6aa-gj, 8aa-ac)

For the synthesis of final ester analogues, Chromone-3-acrylic acid (**3a-g**; 0.462 mmol) was dissolved in DMF, followed by the addition of EDC.HCl (0.924 mmol), DMAP (0.924 mmol). The resultant mixture was stirred in ice-cold condition for 15 minutes. It was then followed by the addition of substituted phenylethyl alcohol (**5a-n**), phenylpropyl alcohol (**7a-c**) for the synthesis of **6aa-gj** and **8aa-ac,** respectively. The reaction mixture was then stirred for 5-8 hours at room temperature. After completion of the reaction (confirmed by TLC), reaction mixture was poured in cold water followed by filtration of the precipitate. The filtered product was then recrystallized using hot ethanol to get the purified product.[1]

5.2.4 Analytical data for final analogues (6aa-gj, 8aa-ac)

phenethyl (E)-3-(4-oxo-4H-chromen-3-yl)acrylate (6aa) Yield: 88%; buff white crystalline solid; MP = 121-121.3 ˚C; ^{1}H NMR (400 MHz, CDCl$_3$) δ (ppm) = 8.27 (dd, J = 8, 1.6 Hz, 1H), 8.10 (s, 1H), 7.71-7.67 (m, 1H), 7.49-7.41 (m, 2H), 7.37 (s, 1H), 7.34-7.21 (m, 6H), 4.41 (t, J = 6.8 Hz, 2H), 3.012 (t, J = 7.2 Hz, 2H); ^{13}C NMR (100 MHz, CDCl$_3$) δ (ppm) = 175.92, 167.32, 157.50, 155.51, 137.91, 135.63, 134.03, 128.96, 128.50, 126.53, 126.32, 125.87, 124.20, 122.01, 119.28, 118.11, 65.09, 35.19; IR: υ (cm^{-1}) = 3061.60, 3027.16, 2946.82, 2875.09, 1753.17, 1704.39, 1644.14, 1609.71, 1558.06, 1500.67, 1460.50, 1403.11, 1354.33, 1291.21, 1259.64, 1213.73, 1147.74, 1035.84, 984.19, 918.19, 857.94, 803.42, 757.51, 688.64, 608.30, 539.44, 496.40, 464.83, 407.45; HRMS (ESI$^+$) calculated for C$_{20}$H$_{17}$O$_4$ [M + H$^+$], 321.1127; found 321.1115; HPLC purity: 99.58%, t_R = 4.590 min.

4-chlorophenethyl (E)-3-(4-oxo-4H-chromen-3-yl)acrylate (6ab) Yield: 82%; white crystalline solid; MP = 140.7-141.2 ˚C; ^{1}H NMR (400 MHz, CDCl$_3$) δ (ppm) = 8.27 (dd, J = 1.2, 8 Hz, 1H), 8.10 (s, 1H), 7.72-7.68 (m, 1H), 7.49-7.44 (m, 2H), 7.40-7.32 (m, 2H), 7.29-7.26 (m, 2H), 7.20-7.18 (m, 2H), 4.38 (t, J = 6.8 Hz, 2H), 2.97 (t, J = 6.8 Hz, 2H); ^{13}C NMR (100 MHz, CDCl$_3$) δ (ppm) = 176.07, 167.40, 157.72, 155.64, 136.56, 135.95, 134.20, 132.50, 130.43, 128.75, 126.45, 126.04, 124.32, 121.97, 119.36, 118.26, 64.86, 34.66; IR: υ (cm^{-1}) = 3073.07, 2946.82, 1704.39, 1644.14, 1609.71, 1558.06, 1494.93, 1460.50, 1400.24, 1354.33, 1291.21, 1259.64, 1210.87, 1150.61, 1041.57, 975.58, 918.19, 857.94, 843.59, 803.42, 760.38, 720.21, 688.64, 659.95, 605.43, 545.18, 527.96, 487.79, 410.32; HRMS (ESI$^+$) calculated for C$_{20}$H$_{16}$ClO$_4$ [M + H$^+$], 355.0737; found 355.0722; HPLC purity: 99.79%, t_R = 6.423 min.

4-bromophenethyl (E)-3-(4-oxo-4H-chromen-3-yl)acrylate (6ac) Yield: 80%; buff white crystalline solid; MP = 162-162.4 ˚C; ^{1}H NMR (400 MHz, CDCl$_3$) δ (ppm) = 8.27 (dd, J = 1.6, 8 Hz, 1H), 8.11 (s, 1H), 7.72-7.68 (m, 1H), 7.49-7.40 (m, 4H), 7.36 (s, 1H), 7.32 (s, 1H), 7.14-7.12 (m, 2H), 4.38 (t, J = 6.8 Hz, 2H), 2.95 (t, J = 6.8 Hz, 2H); ^{13}C NMR (100 MHz, CDCl$_3$) δ (ppm) = 176.08, 167.40, 157.74, 155.63, 137.08, 135.96, 134.20, 131.71, 130.83, 126.46, 126.04, 124.32, 121.96, 120.56, 119.35, 118.26, 64.77, 34.72; IR: υ (cm^{-1}) = 3075.94, 2946.82, 2367.21, 1839.25, 1776.13, 1701.52, 1644.14, 1609.71, 1560.93, 1494.93, 1460.50, 1400.24, 1354.33, 1288.34, 1259.64, 1213.73, 1147.74, 1070.27, 1038.70, 975.58, 915.32, 860.80, 843.59, 800.55, 760.38, 720.21, 685.77, 637.00, 602.56, 539.44, 502.14, 484.92, 407.45; HRMS (ESI$^+$) calculated for C$_{20}$H$_{16}$BrO$_4$ [M + H$^+$], 399.0232; found 399.0198; HPLC purity: 99.61%, t_R = 6.867 min.

4-fluorophenethyl (E)-3-(4-oxo-4H-chromen-3-yl)acrylate (6ad) Yield: 82%; white crystalline solid; MP = 133.8-134.2 ˚C; ^{1}H NMR (400 MHz, CDCl$_3$) δ (ppm) = 8.27 (dd, J = 1.6, 8 Hz, 1H), 8.11 (s, 1H), 7.72-7.68 (m, 1H), 7.49-7.41 (m, 2H), 7.37-7.28 (m, 2H), 7.23-7.20 (m, 2H), 7.10-6.97 (m, 2H), 4.38 (t, J = 7.2 Hz, 2H), 2.97 (t, J = 6.8 Hz, 2H); ^{13}C NMR (100 MHz, CDCl$_3$) δ (ppm) = 176.08, 167.43, 161.70 (d, J = 242.8 Hz), 157.70, 155.64, 135.89, 134.19, 133.74, 133.71, 130.54, 130.47, 126.45, 126.03, 124.32, 122.02, 119.37, 118.26, 115.31 (d, J = 21.1 Hz), 65.12, 34.51; IR: υ (cm^{-1}) = 3738.76, 3075.94, 2946.82, 2875.09, 2361.47, 2332.78, 1704.39, 1644.14, 1609.71, 1558.06, 1503.54, 1460.50, 1400.24, 1351.46, 1291.21, 1259.64, 1210.87, 1147.74, 1104.70, 978.45, 921.06, 855.07, 820.63, 791.94, 754.64, 685.77, 605.43, 499.27, 453.36, 421.79; HRMS (ESI$^+$) calculated for C$_{20}$H$_{16}$FO$_4$ [M + H$^+$], 339.1033; found 339.1016; HPLC purity: 99.94%, t_R = 5.190 min.

4-nitrophenethyl (E)-3-(4-oxo-4H-chromen-3-yl)acrylate (6ae) Yield: 75%; buff yellow crystalline solid; MP = 184.1-184.6 ˚C; ^{1}H NMR (400 MHz, CDCl$_3$) δ (ppm) = 8.26 (dd, J = 1.2, 8 Hz, 1H), 8.18-8.16 (m, 2H), 8.11 (s, 1H), 7.73-7.68 (m, 1H), 7.49-7.40 (m, 4H), 7.36 (d, J = 0.4 Hz, 1H), 7.32 (s, 1H), 4.45 (t, J = 6.8 Hz, 2H), 3.11 (t, J = 6.8 Hz, 2H); ^{13}C NMR (100 MHz, CDCl$_3$) δ (ppm) = 176.08, 167.33, 157.92, 155.62, 146.99, 145.96, 136.31, 134.26, 129.94, 126.43, 126.10, 124.29, 123.89, 121.62, 119.24, 118.27, 64.07, 35.15; IR: υ (cm^{-1}) = 3067.33, 2955.43, 1704.39, 1652.75, 1606.84, 1555.19, 1506.41, 1457.63, 1405.98, 1339.99, 1285.47, 1253.91, 1216.60, 1144.87, 1107.57, 995.66, 926.80, 855.07, 800.55, 760.38, 691.51, 642.73, 602.56, 533.70, 473.44, 410.32; HRMS (ESI$^+$) calculated for C$_{20}$H$_{16}$NO$_6$ [M + H$^+$], 366.0978; found 366.0958; HPLC purity: 98.68%, t_R = 4.503 min.

4-methylphenethyl (E)-3-(4-oxo-4H-chromen-3-yl)acrylate (6af) Yield: 84%; white amorphous solid; MP = 120.8-121.1 ˚C; ^{1}H NMR (400 MHz, CDCl$_3$) δ (ppm) = 8.28 (dd, J = 1.6, 8 Hz, 1H), 8.10 (s, 1H), 7.72-7.68 (m, 1H), 7.49-7.41 (m, 2H), 7.37-7.28 (m, 2H), 7.17-7.11 (m, 4H), 4.39 (t, J = 7.2 Hz, 2H), 2.97 (t, J = 6.8 Hz, 2H), 2.33 (s, 3H); ^{13}C NMR (100 MHz, CDCl$_3$) δ (ppm) = 176.05, 167.46, 157.58, 155.65, 136.16, 135.69, 134.92, 134.15, 129.32, 128.96, 126.46, 125.99, 124.34, 122.22, 119.44, 118.24, 65.38, 34.88, 21.17; IR: υ (cm^{-1}) = 3061.60, 2949.69, 2860.74, 1707.26, 1649.88, 1615.44, 1560.93, 1515.02, 1463.37, 1405.98, 1354.33, 1288.34, 1213.73, 1153.48, 1104.70, 1041.57, 989.93, 918.19, 863.67, 806.29, 783.33, 760.38, 720.21, 688.64, 608.30, 565.26, 536.57, 493.53, 456.23; HRMS (ESI$^+$) calculated for C$_{21}$H$_{19}$O$_4$ [M + H$^+$], 335.1283; found 335.1273; HPLC purity: 99.60%, t_R = 6.390 min.

2,4,6-trimethylphenethyl (E)-3-(4-oxo-4H-chromen-3-yl)acrylate (6ag) Yield: 88%; white amorphous solid; MP = 165.2-165.6 ˚C; ^{1}H NMR (400 MHz, CDCl$_3$) δ (ppm) = 8.29 (dd, J = 1.6, 8 Hz, 1H), 8.11 (s, 1H), 7.73-7.68 (m, 1H), 7.50-7.30 (m, 4H), 6.86 (s, 2H), 4.27 (t, J = 7.6 Hz, 2H), 3.04 (t, J = 8 Hz, 2H), 2.37 (s, 6H), 2.26 (s, 3H); ^{13}C NMR (100 MHz, CDCl$_3$) δ (ppm) = 176.04, 167.55, 157.59, 155.64, 137.02, 136.05, 135.79, 134.16, 130.99, 129.14, 126.47, 126.00, 124.34, 122.20, 119.43, 118.25, 63.30, 28.86, 20.96, 20.01; IR: υ (cm^{-1}) = 2955.43, 2906.65, 1715.87, 1655.61, 1615.44, 1558.06, 1457.63, 1403.11, 1348.59, 1288.34, 1219.47, 1208.00, 1150.61, 998.53, 918.19, 855.07, 794.81, 757.51, 720.21, 685.77, 608.30, 573.87, 536.57, 487.79, 456.23; HRMS (ESI$^+$) calculated for C$_{23}$H$_{23}$O$_4$ [M + H$^+$], 363.1596; found 363.1578; HPLC purity: 98.32%, t_R = 9.783 min.

4-methoxyphenethyl (E)-3-(4-oxo-4H-chromen-3-yl)acrylate (6ah) Yield: 92%; buff white crystalline solid; MP = 153-153.5 ˚C; ^{1}H NMR (400 MHz, CDCl$_3$) δ (ppm) = 8.27 (dd, J = 1.2, 8 Hz, 1H), 8.10 (s, 1H), 7.72-7.68 (m, 1H), 7.49-7.28 (m, 4H), 7.19-7.17 (m, 2H), 6.86-6.84 (m, 2H), 4.37 (t, J = 7.2 Hz, 2H), 3.79 (s, 3H), 2.95 (t, J = 7.2 Hz, 2H); ^{13}C NMR (100 MHz, CDCl$_3$) δ (ppm) = 176.06, 167.47, 158.39, 157.62, 155.63, 135.72, 134.16, 130.05, 126.45, 126.00, 124.33, 122.19, 119.41, 118.25, 114.04, 65.47, 55.37, 34.42; IR: υ (cm^{-1}) = 3385.83, 3061.60, 2978.38, 2935.34, 2837.79, 1698.66, 1652.75, 1609.71, 1558.06, 1509.28, 1454.76, 1405.98, 1354.33, 1288.34, 1233.82, 1153.48, 1110.44, 1027.23, 995.66, 915.32, 866.54, 826.37, 757.51, 723.08, 682.91, 605.43, 568.13, 530.83, 473.44, 436.14; HRMS (ESI$^+$) calculated for C$_{21}$H$_{19}$O$_5$ [M + H$^+$], 351.1232; found 351.1216; HPLC purity: 99.63%, t_R = 4.940 min.

3,4-dimethoxyphenethyl (E)-3-(4-oxo-4H-chromen-3-yl)acrylate (6ai) Yield: 90%; white crystalline solid; MP = 124.2-124.8 ˚C; ^{1}H NMR (400 MHz, CDCl$_3$) δ (ppm) = 8.26 (dd, J = 1.6, 8 Hz, 1H), 8.10 (s, 1H), 7.71-7.67 (m, 1H), 7.48-7.41 (m, 2H), 7.37-7.28 (m, 2H), 6.80-6.78 (m, 3H), 4.38 (t, J = 7.2 Hz, 2H), 3.86 (d, J = 9.2 Hz, 6H), 2.95 (t, J = 7.2 Hz, 2H); ^{13}C NMR (100 MHz, CDCl$_3$) δ (ppm) = 176.02, 167.43, 157.62, 155.61, 148.96, 147.79, 135.77, 134.15, 130.52, 126.42, 125.98, 124.29, 122.11, 121.00, 119.36, 118.23, 112.27, 111.38, 65.35, 56.00, 55.97, 34.89; IR: υ (cm^{-1}) = 3741.63, 3061.60, 2935.34, 2834.92, 2361.47, 1747.43, 1701.52, 1658.48, 1612.57, 1575.27, 1558.06, 1515.02, 1457.63, 1420.33, 1405.98, 1351.46, 1291.21, 1248.17, 1150.61, 1007.14, 992.79, 863.67, 800.55, 751.77, 682.91, 611.17, 556.65, 456.23, 404.58; HRMS (ESI$^+$) calculated for C$_{22}$H$_{21}$O$_6$ [M + H$^+$], 381.1338; found 381.1322; HPLC purity: 99.81%, t_R = 4.160 min.

4-(benzyloxy)phenethyl (E)-3-(4-oxo-4H-chromen-3-yl)acrylate (6aj) Yield: 83%; white crystalline solid; MP = 154.4-154.8 ˚C; ^{1}H NMR (400 MHz, CDCl$_3$) δ (ppm) = 8.28 (dd, J = 1.6, 8 Hz, 1H), 8.10 (s, 1H), 7.72-7.68 (m, 1H), 7.49-7.29 (m, 9H), 7.19-7.17 (m, 2H), 6.94-6.92 (m, 2H), 5.05 (s, 2H), 4.37 (t, J = 7.2 Hz, 2H), 2.95 (t, J = 7.2 Hz, 2H); ^{13}C NMR (100 MHz, CDCl$_3$) δ (ppm) = 176.06, 167.46, 157.65, 157.62, 155.63, 137.22, 135.72, 134.16, 130.37, 130.08, 128.68, 128.03, 127.60, 126.45, 126.00, 124.33, 122.19, 119.41, 118.24, 115.00, 70.14, 65.43, 34.44; IR: υ (cm^{-1}) = 3741.63, 3681.38, 3621.12, 3096.03, 3058.73, 2935.34, 2866.48, 2364.34, 2332.78, 1698.66, 1649.88, 1612.57, 1558.06, 1509.28, 1457.63, 1408.85, 1354.33, 1325.64, 1288.34, 1236.69, 1153.48, 1113.31, 1001.40, 918.19, 860.80, 826.37, 746.03, 731.68, 688.64, 611.17, 545.18, 513.61, 461.97; HRMS (ESI$^+$) calculated for C$_{27}$H$_{23}$O$_5$ [M + H$^+$], 427.1545; found 427.1541; HPLC purity: 99.83%, t_R = 7.757 min.

2-phenoxyethyl (E)-3-(4-oxo-4H-chromen-3-yl)acrylate (6ak) Yield: 80%; buff white crystalline solid; MP = 171.3-171.8 ˚C; ^{1}H NMR (400 MHz, CDCl$_3$) δ (ppm) = 8.27 (dd, J = 1.2, 7.6 Hz, 1H), 8.10 (s, 1H), 7.71-7.67 (m, 1H), 7.49-7.37 (m, 4H), 7.33-7.27 (m, 2H), 6.99-6.93 (m, 3H), 4.56 (t, J = 4.8 Hz, 2H), 4.24 (t, J = 4.8 Hz, 2H); ^{13}C NMR (100 MHz, CDCl$_3$) δ (ppm) = 176.00, 167.37, 158.64, 157.69, 155.65, 136.27, 134.18, 129.65, 126.52, 126.02, 124.35, 121.78, 121.27, 119.38, 118.25, 114.81, 66.03, 63.07; IR: v (cm^{-1}) = 3058.73, 2923.87, 2875.09, 2163.49, 1701.52, 1658.48, 1606.84, 1558.06, 1492.06, 1457.63, 1405.98, 1348.59, 1294.08, 1245.30, 1159.22, 1078.88, 1038.70, 998.53, 961.23, 921.06, 878.02, 789.07, 748.90, 682.91, 599.69, 539.44, 502.14, 476.31, 436.14; HRMS (ESI$^+$) calculated for C$_{20}$H$_{17}$O$_5$ [M + H$^+$], 337.1076; found 337.1068; HPLC purity: 99.76%, t_R = 4.713 min.

2-(pyridin-2-yl)ethyl (E)-3-(4-oxo-4H-chromen-3-yl)acrylate (6al) Yield: 78%; white crystalline solid; MP = 126.2-126.8 ˚C; ^{1}H NMR (400 MHz, CDCl$_3$) δ (ppm) = 8.55 (d, J = 4.4 Hz, 1H), 8.26 (dd, J = 1.6, 8 Hz, 1H), 8.10 (s, 1H), 7.711-7.67 (m, 1H), 764-7.60 (m, 1H), 7.48-7.43 (m, 2H), 7.39-7.30 (m, 2H), 7.23 (d, J = 7.6 Hz, 1H), 7.17-7.14 (m, 1H), 4.59 (t, J = 6.8 Hz, 2H), 3.18 (t, J = 6.4 Hz, 2H); ^{13}C NMR (100 MHz, CDCl$_3$) δ (ppm) = 176.08, 167.44, 158.24, 157.66, 155.63, 149.60, 136.57, 135.78, 134.17, 126.45, 126.01, 124.32, 123.70, 122.11, 121.77, 119.40, 118.25, 63.87, 37.62; IR: v (cm^{-1}) = 3055.86, 2995.60, 2961.17, 1695.79, 1655.61, 1615.44, 1558.06, 1463.37, 1405.98, 1354.33, 1291.21, 1259.64, 1213.73, 1150.61, 1110.44, 1050.18, 987.06, 863.67, 800.55, 763.25, 728.81, 682.91, 599.69, 539.44, 487.79, 407.45; HRMS (ESI$^+$) calculated for C$_{19}$H$_{16}$NO$_4$ [M + H$^+$], 322.1079; found 322.1072; HPLC purity: 96.23%, t_R = 4.433 min.

2-(1H-indol-3-yl)ethyl (E)-3-(4-oxo-4H-chromen-3-yl)acrylate (6am) Yield: 82%; brown crystalline solid; MP = 149.5-149.8 ˚C; ^{1}H NMR (400 MHz, CDCl$_3$) δ (ppm) = 8.28 (dd, J = 1.6, 8 Hz, 1H), 8.15 (s, 1H), 8.05 (s, 1H), 7.72-7.67 (m, 2H), 7.49-7.30 (m, 5H), 7.22-7.13 (m, 3H), 4.49 (t, J = 7.2 Hz, 2H), 3.18 (t, J = 7.2 Hz, 2H); ^{13}C NMR (100 MHz, CDCl$_3$) δ (ppm) = 176.10, 167.56, 157.62, 155.63, 136.29, 135.72, 134.16, 127.59, 126.43, 125.99, 124.31, 122.37, 122.26, 122.15, 119.52, 119.40, 118.92, 118.25, 112.19, 111.31, 64.82, 24.92; IR: v (cm^{-1}) = 3738.76, 3345.66, 3273.93, 3061.60, 2978.38, 2361.47, 2332.78, 1692.92, 1624.05, 1558.06, 1517.89, 1457.63, 1397.37, 1354.33, 1305.55, 1225.21, 1182.17, 1096.09, 969.84, 840.72, 728.81, 685.77, 614.04, 545.18, 467.70, 413.19; HRMS (ESI$^+$) calculated for C$_{22}$H$_{18}$NO$_4$ [M + H$^+$], 360.1236; found 360.1223; HPLC purity: 99.39%, t_R = 4.353 min.

2-(4-methylthiazol-5-yl)ethyl (E)-3-(4-oxo-4H-chromen-3-yl)acrylate (6an) Yield: 84%; buff white amorphous solid; MP = 123.4-124.0 ˚C; ^{1}H NMR (400 MHz, CDCl$_3$) δ (ppm) = 8.59 (s, 1H), 8.28 (dd, J = 1.6, 8 Hz, 1H), 8.12 (s, 1H), 7.73-7.68 (m, 1H), 7.50-7.43 (m, 2H), 7.39-7.30 (m, 2H), 4.36 (t, J = 6.8 Hz, 2H), 3.17 (t, J = 6.8 Hz, 2H), 2.44 (s, 3H); ^{13}C NMR (100 MHz, CDCl$_3$) δ (ppm) = 176.06, 167.25, 157.81, 155.64, 150.08, 150.03, 136.28, 134.23, 126.89, 126.47, 126.07, 124.33, 121.73, 119.32, 118.27, 64.24, 26.03, 15.11; IR: υ (cm^{-1}) = 3064.47, 2370.08, 2034.37, 1692.92, 1649.88, 1612.57, 1555.19, 1466.24, 1411.72, 1357.20, 1314.16, 1248.17, 1162.09, 1104.70, 1053.05, 992.79, 961.23, 912.45, 852.20, 791.94, 768.99, 725.95, 685.77, 657.08, 605.43, 573.87, 545.18, 513.61, 464.83, 410.32; HRMS (ESI$^+$) calculated for C$_{18}$H$_{16}$NO$_4$S [M + H$^+$], 342.0800; found 342.0793; HPLC purity: 100.00%, t_R = 4.760 min.

phenethyl (E)-3-(6-chloro-4-oxo-4H-chromen-3-yl)acrylate (6ba) Yield: 85%; brick red amorphous solid; MP = 160.3-160.7 ˚C; ^{1}H NMR (400 MHz, CDCl$_3$) δ (ppm) = 8.25 (d, J = 2.4 Hz, 1H), 8.11 (s, 1H), 7.66 (dd, J = 2.4, 8.8 Hz, 1H), 7.47 (d, J = 8.8 Hz, 1H), 7.37-7.24 (m, 7H), 4.43 (t, J = 7.2 Hz, 2H), 3.04 (t, J = 7.2 Hz, 2H); ^{13}C NMR (100 MHz, CDCl$_3$) δ (ppm) = 174.86, 167.29, 157.56, 153.97, 137.98, 135.22, 134.40, 132.06, 129.08, 128.65, 126.69, 125.87, 125.24, 122.65, 120.00, 119.46, 65.29, 35.30; IR: υ (cm^{-1}) = 3078.81, 3027.16, 2943.95, 2361.47, 2169.23, 1710.13, 1644.14, 1612.57, 1555.19, 1497.80, 1463.37, 1437.54, 1385.90, 1348.59, 1276.86, 1193.65, 1150.61, 1038.70, 987.06, 898.11, 866.54, 837.85, 806.29, 780.46, 748.90, 694.38, 634.13, 545.18, 499.27, 464.83, 416.06; HRMS (ESI$^+$) calculated for C$_{20}$H$_{16}$ClO$_4$ [M + H$^+$], 355.0737; found 355.0726; HPLC purity: 97.82%, t_R = 7.440 min.

4-(benzyloxy)phenethyl (E)-3-(6-chloro-4-oxo-4H-chromen-3-yl)acrylate (6bj) Yield: 90%; brown amorphous solid; MP = 177.5-177.8 ˚C; ^{1}H NMR (400 MHz, CDCl$_3$) δ (ppm) = 8.23 (d, J = 2.4 Hz, 1H), 8.09 (s, 1H), 7.64 (dd, J = 2.4, 8.8 Hz, 1H), 7.46-7.42 (m, 3H), 7.40-7.30 (m, 5H), 7.19-7.17 (m, 2H), 6.94-6.92 (m, 2H), 5.05 (s, 2H), 4.38 (t, J = 6.8 Hz, 2H), 2.95 (t, J = 6.8 Hz, 2H); ^{13}C NMR (100 MHz, CDCl$_3$) δ (ppm) = 174.88, 167.31, 157.68, 157.55, 153.98, 137.22, 135.19, 134.41, 132.07, 130.32, 130.08, 128.70, 128.05, 127.61, 125.88, 125.25, 122.71, 120.00, 119.49, 115.04, 70.17, 65.52, 34.44; IR: υ (cm^{-1}) = 3727.29, 3058.73, 2941.08, 2361.47, 2329.91, 1750.30, 1698.66, 1649.88, 1612.57, 1555.19, 1512.15, 1457.63, 1385.90, 1345.73, 1317.03, 1279.73, 1239.56, 1150.61, 1116.18, 1073.14, 1012.88, 989.93, 918.19, 866.54, 820.63, 734.55, 694.38, 634.13, 608.30, 550.92, 516.48, 467.70,

427.53; HRMS (ESI$^+$) calculated for C$_{27}$H$_{22}$ClO$_5$ [M + H$^+$], 461.1156; found 461.1175; HPLC purity: 98.94%, t_R = 11.490 min.

phenethyl (E)-3-(6-bromo-4-oxo-4H-chromen-3-yl)acrylate (6ca) Yield: 74%; brick red amorphous solid; MP = 167.2-167.6 ˚C; ^{1}H NMR (400 MHz, CDCl$_3$) δ (ppm) = 8.41 (d, J = 2.4 Hz, 1H), 8.12 (s, 1H), 7.80 (dd, J = 2.4, 8.8 Hz, 1H), 7.42-7.31 (m, 5H), 7.29-7.26 (m, 3H), 4.44 (t, J = 7.2 Hz, 2H), 3.04 (t, J = 6.8 Hz, 2H); ^{13}C NMR (100 MHz, CDCl$_3$) δ (ppm) = 174.72, 167.27, 157.53, 154.41, 137.98, 137.16, 135.20, 129.09, 128.65, 126.70, 125.59, 122.68, 120.20, 119.58, 119.55, 65.30, 35.30; IR: υ (cm^{-1}) = 3738.76, 3681.38, 3075.94, 3027.16, 2946.82, 2361.47, 2329.91, 1744.56, 1713.00, 1647.01, 1612.57, 1552.32, 1500.67, 1463.37, 1434.67, 1385.90, 1345.73, 1279.73, 1193.65, 1150.61, 1050.18, 987.06, 863.67, 834.98, 783.33, 746.03, 694.38, 602.56, 542.31, 496.40, 464.83, 416.06; HRMS (ESI$^+$) calculated for C$_{20}$H$_{16}$BrO$_4$ [M + H$^+$], 399.0232; found 399.0221; HPLC purity: 90.90%, t_R = 7.970 min.

4-(benzyloxy)phenethyl (E)-3-(6-bromo-4-oxo-4H-chromen-3-yl)acrylate (6cj) Yield: 81%; yellow amorphous solid; MP = 174.9-175.4 ˚C; ^{1}H NMR (400 MHz, CDCl$_3$) δ (ppm) = 8.39 (d, J = 2.4 Hz, 1H), 8.09 (s, 1H), 7.78 (dd, J = 8.8, 2.4 Hz, 1H), 7.45-7.29 (m, 8H), 7.19-7.17 (m, 2H), 6.94-6.92 (m, 2H), 5.05 (s, 2H), 4.37 (t, J = 6.8 Hz, 2H), 2.95 (t, J = 7.2 Hz, 2H); ^{13}C NMR (100 MHz, CDCl$_3$) δ (ppm) = 174.72, 167.29, 157.68, 157.52, 154.41, 137.22, 137.16, 135.17, 130.31, 130.08, 129.09, 128.70, 128.05, 127.61, 125.59, 122.72, 120.20, 119.59, 119.54, 115.03, 70.16, 65.52, 34.44; IR: υ (cm^{-1}) = 3067.33, 2938.21, 2869.35, 2361.47, 1735.96, 1704.39, 1655.61, 1615.44, 1552.32, 1512.15, 1460.50, 1385.90, 1285.47, 1239.56, 1190.78, 1159.22, 1119.05, 1053.05, 1001.40, 866.54, 817.76, 777.59, 734.55, 694.38, 608.30, 548.05, 525.09, 467.70, 418.93 ; HRMS (ESI$^+$) calculated for C$_{27}$H$_{22}$BrO$_5$ [M + H$^+$], 505.0651; found 505.067; HPLC purity: 93.78%, t_R = 6.430 min.

phenethyl (E)-3-(6-fluoro-4-oxo-4H-chromen-3-yl)acrylate (6da) Yield: 86%; buff yellow crystalline solid; MP = 144.2-145.0 ˚C; ^{1}H NMR (400 MHz, CDCl$_3$) δ (ppm) = 8.13 (s, 1H), 7.93 (dd, J = 2.8, 8 Hz, 1H), 7.54-7.51 (m, 1H), 7.47-7.42 (m, 1H), 7.38-7.32 (m, 3H), 7.29-7.24 (m, 4H), 4.44 (t, J = 6.8 Hz, 2H), 3.04 (t, J = 6.8 Hz, 2H); ^{13}C NMR (100 MHz, CDCl$_3$) δ (ppm) = 175.28, 175.25, 167.33, 157.67, 138.00, 135.33, 129.10, 128.64, 126.68, 122.52, 122.31, 120.48, 120.40, 118.78, 111.49, 111.25, 65.28, 35.30; IR: υ (cm^{-1}) = 3744.50, 3678.51, 3621.12, 3075.94, 2946.82, 2361.47, 1744.56, 1710.13, 1644.14, 1563.80, 1480.58, 1451.89, 1394.50, 1357.20, 1279.73, 1242.43, 1159.22, 1098.96, 1047.31, 984.19, 923.93,

895.24, 872.28, 826.37, 786.20, 737.42, 694.38, 605.43, 562.39, 527.96, 499.27, 467.70, 430.40; HRMS (ESI$^+$) calculated for $C_{20}H_{16}FO_4$ [M + H$^+$], 339.1033; found 339.1026; HPLC purity: 98.44%, t_R = 5.657 min.

4-(benzyloxy)phenethyl (E)-3-(6-fluoro-4-oxo-4H-chromen-3-yl)acrylate (6dj) Yield: 89%; buff white amorphous solid; MP = 177.2-177.6 ˚C; ^{1}H NMR (400 MHz, CDCl$_3$) δ (ppm) = 8.10 (s, 1H), 7.91 (dd, J = 3.2, 8.4 Hz, 1H), 7.50 (dd, J = 4, 8.8 Hz, 1H), 7.44-7.36 (m, 6H), 7.34-7.27 (m, 2H), 7.19-7.14 (m, 2H), 6.95-6.91 (m, 2H), 5.05 (s, 2H), 4.38 (t, J = 6.8 Hz, 2H), 2.95 (t, J = 7.2 Hz, 2H); ^{13}C NMR (100 MHz, CDCl$_3$) δ (ppm) = 175.29, 167.36, 161.28, 158.82, 157.67, 151.89, 137.22, 135.30, 130.33, 130.13, 130.08, 128.70, 128.05, 127.61, 127.58, 125.60, 125.53, 122.57, 122.32, 120.48, 120.40, 118.80, 115.13, 115.03, 11.51, 111.27, 70.17, 65.50, 34.44; IR: υ (cm^{-1}) = 3061.60, 2941.08, 2863.61, 2378.69, 1698.66, 1647.01, 1618.31, 1569.53, 1515.02, 1480.58, 1451.89, 1388.77, 1279.73, 1236.69, 1162.09, 1130.52, 1107.57, 1076.01, 1012.88, 987.06, 918.19, 866.54, 823.50, 780.46, 731.68, 694.38, 665.69, 608.30, 553.78, 513.61, 470.57, 433.27; HRMS (ESI$^+$) calculated for $C_{27}H_{22}FO_5$ [M + H$^+$], 445.1451; found 445.1427; HPLC purity: 95.56%, t_R = 8.387 min.

phenethyl (E)-3-(6-methyl-4-oxo-4H-chromen-3-yl)acrylate (6ea) Yield: 85%; yellow crystalline solid; MP = 129.7-130.3 ˚C; ^{1}H NMR (400 MHz, CDCl$_3$) δ (ppm) = 8.10 (s, 1H), 8.07 (d, J = 0.8 Hz 1H), 7.52 (dd, J = 1.6, 8.4 Hz, 1H), 7.44-7.39 (m, 2H), 7.36-7.24 (m, 6H), 4.44 (t, J = 7.2 Hz, 2H), 3.04 (t, J = 6.8 Hz, 2H), 2.49 (s, 3H); ^{13}C NMR (100 MHz, CDCl$_3$) δ (ppm) = 176.13, 167.51, 157.54, 153.94, 138.05, 136.10, 135.97, 135.38, 129.09, 128.63, 126.66, 125.75, 123.99, 121.86, 119.20, 117.98, 65.19, 35.32, 21.14; IR: υ (cm^{-1}) = 3064.47, 3024.29, 2958.30, 2932.48, 2863.61, 2172.10, 1807.69, 1750.30, 1713.00, 1629.79, 1609.71, 1483.45, 1446.15, 1385.90, 1311.29, 1285.47, 1242.43, 1190.78, 1150.61, 1035.84, 995.66, 938.28, 900.98, 875.15, 823.50, 783.33, 746.03, 691.51, 616.91, 545.18, 490.66, 421.79; HRMS (ESI$^+$) calculated for $C_{21}H_{19}O_4$ [M + H$^+$], 335.1283; found 335.1277; HPLC purity: 99.19%, t_R = 6.517 min.

4-(benzyloxy)phenethyl (E)-3-(6-methyl-4-oxo-4H-chromen-3-yl)acrylate (6ej) Yield: 87%; buff white crystalline solid; MP = 171.2-171.5 ˚C; ^{1}H NMR (400 MHz, CDCl$_3$) δ (ppm) = 8.06-8.05 (m, 2H), 7.49 (dd, J = 2, 8.4 Hz, 1H), 7.44-7.41 (m, 2H), 7.40-7.36 (m, 4H), 7.33-7.27 (m, 2H), 7.19-7.17 (m, 2H), 6.95-6.92 (m, 2H), 5.05 (s, 2H), 4.37 (t, J = 7.2 Hz, 2H), 2.95 (t, J = 7.2 Hz, 2H); ^{13}C NMR (100 MHz, CDCl$_3$) δ (ppm) = 177.00, 167.49,

157.64, 157.52, 153.92, 137.21, 136.07, 135.92, 135.35, 130.37, 130.06, 128.66, 128.01, 127.58, 125.72, 123.97, 121.88, 119.18, 117.97, 115.00, 70.13, 65.39, 34.44; IR: υ (cm^{-1}) = 3744.50, 3621.12, 3385.83, 3064.47, 2866.48, 2361.47, 2332.78, 2094.63, 1744.56, 1695.79, 1652.75, 1612.57, 1509.28, 1466.24, 1428.94, 1385.90, 1337.12, 1285.47, 1225.21, 1159.22, 1116.18, 1050.18, 998.53, 923.93, 866.54, 812.03, 731.68, 688.64, 614.04, 550.92, 516.48, 461.97, 421.79; HRMS (ESI$^+$) calculated for C$_{28}$H$_{25}$O$_5$ [M + H$^+$], 441.1702; found 441.1736; HPLC purity: 99.14%, t_R = 9.910 min.

phenethyl (E)-3-(6-methoxy-4-oxo-4H-chromen-3-yl)acrylate (6fa) Yield: 92%; buff yellow crystalline solid; MP = 155.6-156.0 ˚C; ^{1}H NMR (400 MHz, CDCl$_3$) δ (ppm) = 8.10 (s, 1H), 7.64 (d, J = 3.2 Hz, 1H), 7.44-7.40 (m, 2H), 7.36-7.24 (m, 7H), 4.43 (t, J = 6.8 Hz, 2H), 3.93 (s, 3H), 3.03 (t, J = 7.2 Hz, 2H); ^{13}C NMR (100 MHz, CDCl$_3$) δ (ppm) = 175.88, 167.49, 157.56, 157.39, 150.48, 138.06, 135.96, 129.09, 128.62, 126.66, 124.99, 124.16, 121.86, 119.66, 118.55, 105.47, 65.20, 56.09, 35.32; IR: υ (cm^{-1}) = 3730.15, 3064.47, 3007.08, 2961.17, 2895.17, 2840.66, 2361.47, 2332.78, 1919.59, 1882.29, 1741.70, 1701.52, 1644.14, 1609.71, 1572.40, 1480.58, 1443.28, 1405.98, 1342.86, 1199.39, 1150.61, 1018.62, 992.79, 860.80, 820.63, 751.77, 694.38, 602.56, 565.26, 487.79, 464.83, 424.66; HRMS (ESI$^+$) calculated for C$_{21}$H$_{19}$O$_4$ [M + H$^+$], 351.1232; found 351.1222; HPLC purity: 94.41%, t_R = 5.547 min.

4-(benzyloxy)phenethyl (E)-3-(6-methoxy-4-oxo-4H-chromen-3-yl)acrylate (6fj) Yield: 87%; buff yellow crystalline solid; MP = 162.6-162.9 ˚C; ^{1}H NMR (400 MHz, CDCl$_3$) δ (ppm) = 8.09 (s, 1H), 7.63 (d, J = 4.4 Hz, 1H), 7.44-7.27 (m, 9H), 7.19-7.17 (m, 2H), 6.94-6.92 (m, 2H), 5.05 (s, 2H), 4.37 (t, J = 6.8 Hz, 2H), 3.91 (s, 3H), 2.95 (t, J = 6.8 Hz, 2H); ^{13}C NMR (100 MHz, CDCl$_3$) δ (ppm) = 175.92, 167.54, 157.67, 157.59, 157.39, 150.52, 137.24, 135.94, 130.41, 130.10, 128.70, 128.05, 127.62, 125.01, 124.19, 121.93, 119.68, 118.59, 115.03, 105.50, 70.17, 65.44, 56.12, 34.48; IR: υ (cm^{-1}) = 3061.60, 3001.34, 2938.21, 2869.35, 2613.98, 2364.34, 1888.03, 1698.66, 1649.88, 1609.71, 1569.53, 1512.15, 1471.98, 1428.94, 1337.12, 1285.47, 1230.95, 1205.13, 1164.96, 1055.92, 998.53, 926.80, 863.67, 820.63, 783.33, 731.68, 691.51, 611.17, 559.52, 516.48, 464.83, 427.53; HRMS (ESI$^+$) calculated for C$_{28}$H$_{25}$O$_6$ [M + H$^+$], 457.1651; found 457.1642; HPLC purity: 99.19%, t_R = 8.190 min.

phenethyl (E)-3-(4-oxo-4H-benzo[h]chromen-3-yl)acrylate (6ga) Yield: 78%; yellow crystalline solid; MP = 180.5-181.2 ˚C; ^{1}H NMR (400 MHz, CDCl$_3$) δ (ppm) = 8.47-8.44 (m,

1H), 8.26 (s, 1H), 8.18 (d, $J = 8.4$ Hz, 1H), 7.94-7.92 (m, 1H), 7.80 (d, $J = 8.4$ Hz, 1H), 7.74-7.66 (m, 2H), 7.47-7.40 (m, 2H), 7.36-7.28 (m, 3H), 7.26-7.22 (m, 2H), 4.43 (t, $J = 7.2$ Hz, 2H), 3.02 (t, $J = 7.2$ Hz, 2H); ^{13}C NMR (100 MHz, CDCl$_3$) δ (ppm) = 175.87, 167.45, 156.64, 153.10, 138.04, 136.02, 135.62, 129.74, 129.10, 128.64, 128.29, 127.59, 126.67, 126.12, 123.82, 122.65, 122.27, 120.98, 120.71, 120.57, 65.26, 35.32; IR: υ (cm^{-1}) = 3081.68, 2946.82, 1707.26, 1647.01, 1609.71, 1558.06, 1503.54, 1449.02, 1411.72, 1377.29, 1339.99, 1276.86, 1144.87, 1067.40, 1035.84, 989.93, 866.54, 834.98, 800.55, 760.38, 691.51, 648.47, 608.30, 576.74, 496.40, 470.57, 441.88, 410.32; HRMS (ESI$^+$) calculated for C$_{24}$H$_{19}$O$_4$ [M + H$^+$], 371.1283; found 371.1277; HPLC purity: 98.14%, t_R = 8.213 min.

4-(benzyloxy)phenethyl (E)-3-(4-oxo-4H-benzo[h]chromen-3-yl)acrylate (6gj) Yield: 80%; yellow crystalline solid; MP = 170.1-170.8 °C; ^{1}H NMR (400 MHz, CDCl$_3$) δ (ppm) = 8.47 (d, $J = 8$ Hz, 1H), 8.26 (s, 1H), 8.20 (d, $J = 8.8$ Hz 1H), 7.94 (d, $J = 7.6$ Hz, 1H), 7.80 (d, $J = 8.8$ Hz, 1H), 7.74-7.67 (m, 2H), 7.48-7.30 (m, 7H), 7.19 (d, $J = 8.8$ Hz, 2H), 6.94 (d, $J = 8.8$ Hz, 2H), 5.05 (s, 2H), 4.39 (t, $J = 7.2$ Hz, 2H), 2.97 (t, $J = 8$ Hz, 2H); ^{13}C NMR (100 MHz, CDCl$_3$) δ (ppm) = 175.89, 167.47, 157.67, 156.64, 153.12, 137.23, 136.04, 135.59, 130.38, 130.09, 129.75, 128.69, 128.30, 128.03, 127.61, 126.13, 123.84, 122.70, 122.28, 120.99, 120.73, 120.59, 115.03, 70.16, 65.49, 34.46; IR: υ (cm^{-1}) = 3896.58, 3738.76, 3681.38, 3644.07, 3621.12, 3078.81, 2941.08, 2860.74, 2361.47, 2160.62, 1836.38, 1744.56, 1707.26, 1647.01, 1609.71, 1555.19, 1512.15, 1449.02, 1411.72, 1380.16, 1279.73, 1239.56, 1150.61, 1038.70, 992.79, 912.45, 866.54, 832.11, 800.55, 766.12, 725.95, 688.64, 645.60, 576.74, 516.48, 453.36, 410.32; HRMS (ESI$^+$) calculated for C$_{31}$H$_{25}$O$_5$ [M + H$^+$], 477.1702; found 477.1694; HPLC purity: 97.17%, t_R = 6.307 min.

3-phenylpropyl (E)-3-(4-oxo-4H-chromen-3-yl)acrylate (8aa) Yield: 94%; buff white amorphous solid; MP = 162.3-164.2 °C; ^{1}H NMR (400 MHz, CDCl$_3$) δ (ppm) = 8.29 (dd, $J = 1.6, 8$ Hz, 1H), 8.12 (s, 1H), 7.73-7.68 (m, 1H), 7.50-7.42 (m, 2H), 7.37 (d, $J = 8.4$ Hz, 2H), 7.32-7.27 (m, 2H), 7.22-7.18 (m, 3H), 4.22 (t, $J = 6.4$ Hz, 2H), 2.75 (t, $J = 7.2$ Hz, 2H), 2.06-1.99 (m, 2H); ^{13}C NMR (100 MHz, CDCl$_3$) δ (ppm) = 176.00, 167.48, 157.51, 155.54, 141.28, 135.52, 134.05, 128.47, 128.44, 126.37, 125.97, 125.89, 124.23, 122.17, 119.32, 118.13, 63.88, 32.22, 30.33; IR: υ (cm^{-1}) = 3050.12, 2952.56, 2886.57, 2350.00, 1704.39, 1661.35, 1612.57, 1500.67, 1463.37, 1405.98, 1339.99, 1213.73, 1156.35, 1098.96, 1001.40, 958.36, 852.20, 797.68, 771.86, 748.90, 685.77, 619.78, 545.18, 482.05, 418.93; HRMS (ESI$^+$) calculated for C$_{21}$H$_{19}$O$_4$ [M + H$^+$], 335.1283; found 335.1274; HPLC purity: 98.84%, t_R = 6.187 min.

3-(4-chlorophenyl)propyl (E)-3-(4-oxo-4H-chromen-3-yl)acrylate (8ab) Yield: 95%; buff white amorphous solid; MP = 155.0-156.4 ˚C; ^{1}H NMR (400 MHz, CDCl$_3$) δ (ppm) = 8.28 (dd, J = 1.6, 8 Hz, 1H), 8.12 (s, 1H), 7.72-7.68 (m, 1H), 7.49-7.43 (m, 2H), 7.42-7.31 (m, 4H), 7.08 (d, J = 8.4 Hz, 1H), 4.20 (t, J = 6.4 Hz, 2H), 2.69 (t, J = 7.6 Hz, 2H), 2.04-1.96 (m, 2H); ^{13}C NMR (100 MHz, CDCl$_3$) δ (ppm) = 176.10, 167.53, 157.71, 155.65140.37, 135.76, 134.18, 131.61, 130.36, 126.47, 126.02, 124.34, 122.13, 119.95, 119.38, 118.26, 63.73, 31.80, 30.27; IR: υ (cm^{-1}) = 3050.15, 2854.52, 2886.57, 2385.05, 1702.59, 1665.58, 1612.57, 1500.67, 1468.33, 1505.26, 1339.99, 1210.55, 1186.35, 1098.96, 958.36, 852.20, 797.68, 748.90, 685.77, 620.85, 545.18, 482.05, 418.93; HRMS (ESI$^+$) calculated for C$_{21}$H$_{18}$ClO$_4$ [M + H$^+$], 369.0894; found 369.0899; HPLC purity: 97.26%, t_R = 6.220 min.

3-(4-bromophenyl)propyl (E)-3-(4-oxo-4H-chromen-3-yl)acrylate (8ac) Yield: 95%; white amorphous solid; MP = 156.3-158.6 ˚C; ^{1}H NMR (400 MHz, CDCl$_3$) δ (ppm) = 8.29 (dd, J = 1.6, 6.4 Hz, 1H), 8.12 (s, 1H), 7.73-7.69 (m, 1H), 7.50-7.41 (m, 2H), 7.37 (d, J = 6.0 Hz, 2H), 7.27-7.25 (m, 2H), 7.15-7.13 (m, 2H), 4.21 (t, J = 6.4 Hz, 2H), 2.72 (d, J = 7.2 Hz, 2H), 2.05-1.97 (m, 2H); ^{13}C NMR (100 MHz, CDCl$_3$) δ (ppm) = 175.98, 167.41, 157.57, 155.53, 139.72, 135.63, 134.06, 131.70, 129.81, 128.53, 126.34, 125.90, 124.22, 122.02, 119.27, 118.13, 63.62, 31.61, 30.21; IR: υ (cm^{-1}) = 3050.12, 2952.56, 2886.57, 2350.00, 1704.39, 1661.35, 1612.57, 1500.67, 1463.37, 1405.98, 1339.99, 1213.73, 1156.35, 1098.96, 1001.40, 958.36, 852.20, 797.68, 771.86, 748.90, 685.77, 619.78, 545.18, 482.05, 418.93; HRMS (ESI$^+$) calculated for C$_{21}$H$_{18}$BrO$_4$ [M + H$^+$], 412.0310; found 412.0315; HPLC purity: 99.80%, t_R = 5.880 min.

5.3. Biological Evaluation

5.3.1. *In vitro* PL Inhibition

After the synthesis of acrylate linked Chromone analogues, they were tested for PL inhibitory activity using porcine PL enzyme and 4-Nitrophenyl butyrate as a substrate, utilizing the established protocol.[2–4] The PL inhibitory activity of all the analogues is depicted in **Table 5.2**. Firstly, the effect of length of linker was evaluated by the PL inhibitory screening of analogues **6aa** and **8aa-ac**. The analogue **6aa** with Ethyl linker (IC$_{50}$ = 16.01 µM) was found to be effective in PL inhibition, as compared with Propyl linker (Analogue **8aa-ac**; IC$_{50}$ = 30.01 - 38.84 µM). Further, the ethyl linker was kept constant and the effect of various R^2 substituents were checked for the activity. The analogues **6ag**, and **6aj** (IC$_{50}$ = 11.01 and 5.64 µM) exhibited potent activity as compared with the prototype analogue **6aa**. The effect of R^1

substituents was also identified and the analogues **6fa** and **6ga** with 6-Methoxy and fused [*h*]Benzo substituents were found to exhibit potent activity than analogue **6aa**. Hence, by the combination of substituents of analogues **6fa** and **6ga** with analogue **6aj**, the highly potent analogues **6fj** and **6gj** were obtained with IC_{50} values of 4.92 and 4.23 µM, respectively. All the obtained IC_{50} values were compared to orlistat (IC_{50} = 0.86 µM).

Table 5.2. *In vitro* PL inhibitory activity of acrylate linked chromone analogues (**6aa-gj**, **8aa-ac**) and orlistat

Code	R^1	R^2	IC_{50} (µM ± SEM)*
6aa	H	Phenyl	16.01 ± 0.274
6ab	H	4-Chlorophenyl	49.07 ± 0.274
6ac	H	4-Bromophenyl	19.16 ± 0.652
6ad	H	4-Fluorophenyl	41.62 ± 1.269
6ae	H	4-Nitrophenyl	51.57 ± 0.139
6af	H	4-Methylphenyl	17.09 ± 0.403
6ag	H	2,4,6-Trimethylphenyl	11.01 ± 0.956
6ah	H	4-Methoxyphenyl	14.66 ± 1.204
6ai	H	3,4-Dimethoxyphenyl	20.29 ± 0.978
6aj	H	4-Benzyloxyphenyl	5.64 ± 0.811
6ak	H	Phenoxy	15.19 ± 1.162
6al	H	Pyridin-2-yl	13.20 ± 2.297
6am	H	1*H*-Indol-3-yl	12.61 ± 0.330
6an	H	4-Methylthiazol-5-yl	19.21 ± 0.351
6ba	6-Chloro	Phenyl	42.21 ± 2.265
6bj	6-Chloro	4-Benzyloxyphenyl	19.46 ± 0.480
6ca	6-Bromo	Phenyl	12.30 ± 1.665
6cj	6-Bromo	4-Benzyloxyphenyl	8.49 ± 1.879
6da	6-Fluoro	Phenyl	32.53 ± 1.725
6dj	6-Fluoro	4-Benzyloxyphenyl	14.12 ± 1.095
6ea	6-Methyl	Phenyl	19.10 ± 0.295
6ej	6-Methyl	4-Benzyloxyphenyl	29.54 ± 4.117
6fa	6-Methoxy	Phenyl	11.32 ± 2.449

6fj	6-Methoxy	4-Benzyloxyphenyl	4.92 ± 1.398
6ga	[*h*]benzo	Phenyl	11.87 ± 1.796
6gj	[*h*]benzo	4-Benzyloxyphenyl	4.23 ± 0.747
8aa	H	Phenyl	31.49 ± 1.363
8ab	H	4-Chlorophenyl	30.01 ± 0.434
8ac	H	4-Bromophenyl	38.84 ± 0.954
Orlistat	-	-	0.86 ± 0.09

*The experiment is performed in triplicate (n=3)

5.3.2. Structure-Activity Relationship (SAR)

The results obtained from the *in vitro* PL inhibition study were analysed to summarize the effect of various substituents on PL inhibitory activity. As shown in **Figure 5.3**, the ethyl linker (**6aa**; IC_{50} = 16.01 µM) was found to be optimal for PL inhibitory activity, as increasing the length of linker led to decreased activity (**8aa-ac** with propyl linker; IC_{50} = 30.01 - 38.84 µM). The R^2 substitution could be aromatic or heteroaromatic. In the case of aromatic substitutions, electron-withdrawing groups (EWG) such as chloro, bromo, fluoro and nitro at the 4th position of aromatic ring led to a decrease in activity (IC_{50} in the range of 19.16 - 51.57 µM). There was a slight increase in activity with the substitution by electron donating groups (EDG) such as methyl and methoxy, among which 2,4,6-Trimethylphenyl substituted analogue (**6ag**) exhibited IC_{50} value of 11.01 ± 0.956 µM. Further, the substitution by a bulkier substituent such as benzyloxy group at the 4th position led to potent inhibition (**6aj**; IC_{50} = 5.64 ± 0.811 µM). The replacement of the phenyl ring with a heterocyclic ring system such as Pyridin-2-yl, 1*H*-Indol-3-yl exhibited slightly increased activity (**6al**, **6am**; IC_{50} = 13.20 ± 2.297, 12.61 ± 0.330 µM) as compared with **6aa**. However, the 4-Methylthiazol-5-yl substituted analogue (**6an**; IC_{50} = 19.21 ± 0.351 µM) showed a deterioration in the activity than **6aa**.

Replacement of Ethyl with Propyl linker, lead to decreased activity ⟹ **8aa;** $IC_{50} = 31.49 \pm 1.363\ \mu M$

Ethyl linker was found to increase the PL inhibitory potential ⟹ **6aa;** $IC_{50} = 16.01 \pm 0.274\ \mu M$

Linker

6ca; $IC_{50} = 12.30 \pm 1.665\ \mu M$ & 6cj; $IC_{50} = 8.49 \pm 1.879\ \mu M$

6-Bromo > 6-Fluoro > 6-Chloro

6-Methoxy ≅ [*h*]Benzo > 6-Methyl

6fa; $IC_{50} = 11.32 \pm 2.449\ \mu M$

6fj; $IC_{50} = 4.92 \pm 1.398\ \mu M$

6gj; $IC_{50} = 4.23 \pm 0.747\ \mu M$

Substitution on Phenyl ring

Electron donating groups slightly increases the activity (**6ag;** $IC_{50} = 11.01 \pm 0.956\ \mu M$)

Electron withdrawing groups lead to decreased activity (**6ab-6ae;** $IC_{50} = 19.16\text{-}51.57\ \mu M$)

Replacement with bulkier substituent (Benzyloxy), lead to 3-fold increase in activity

6aj; $IC_{50} = 5.64 \pm 0.811\ \mu M$

Heterocyclic ring system

6am; $IC_{50} = 12.61 \pm 0.330\ \mu M$

Figure 5.3. Structure-activity relationship (SAR) of screened analogues (**6aa-gj**, **8aa-ac**)

Further, by keeping R^1 as Phenyl and 4-Benzyloxyphenyl, the effect of various substituents on 6th position of chromone were checked. Substitution by EWG (Chloro, Bromo, Fluoro) showed less potent activity when compared to EDG (Methoxy, Methyl, fused [*h*]Benzo) on PL inhibition. Among EDG, 6-Methoxy and fused [*h*]Benzo showed the highest inhibition in the series, with analogues **6fj** and **6gj** having IC_{50} values of 4.92 ± 1.398 & 4.23 ± 0.747 μM, respectively.

5.3.3. Enzyme Kinetics Study

From the *in vitro* PL inhibitory screening, the analogue **6gj** was identified to exhibit potent IC_{50} value of 4.23 ± 0.747 μM. Further, an enzyme kinetics study was performed to identify the type of inhibition of **6gj**.[1,5] The study was performed by taking 3 different concentrations of inhibitor (**6gj**) and 4 concentrations of substrate. The time-dependent inhibition was

105

determined and various parameters such as V_{max}, K_m and K_i were estimated using a double reciprocal Lineweaver-Burk plot. As shown in **Figure 5.4**, all three plots converged at y-axis suggesting the phenomenon of competitive inhibition.
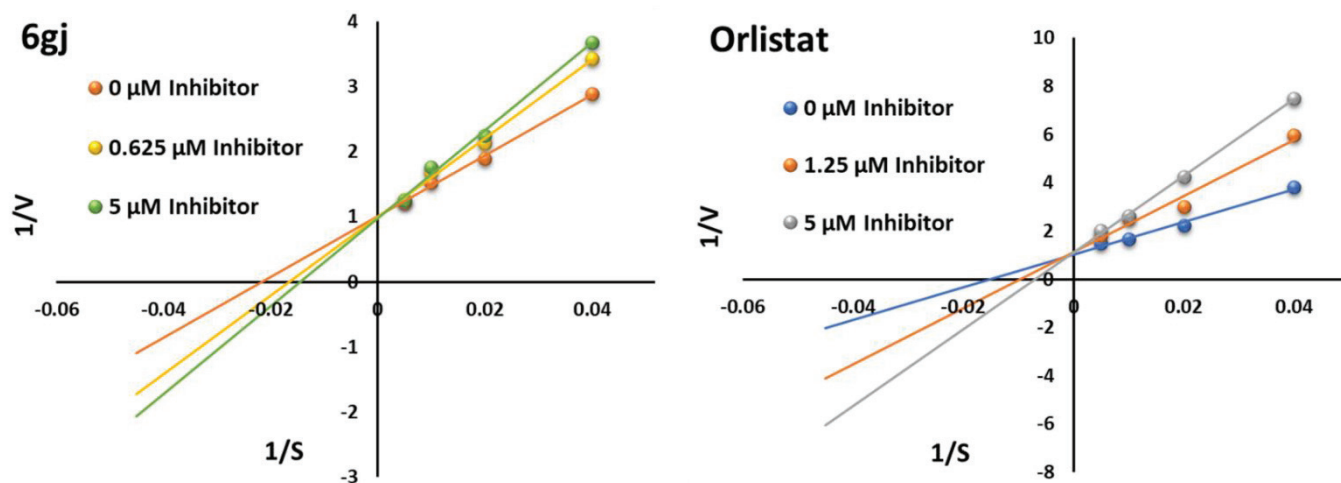
Figure 5.4. Double reciprocal Lineweaver-Burk plot of analogue **6gj** and orlistat

Further, as shown in **Table 5.3**, there is a concentration-dependent increase in K_m values with constant V_{max} value throughout the concentration range. The inhibition constant (K_i) was found to be 1.601 μM and the results were similar to that of orlistat (K_i of 0.488). Such results confirmed that the analogue **6gj** inhibited PL enzyme *via* competitive inhibitory mechanism.

Table 5.3. Enzyme kinetics study of analogue **6gj** and **orlistat**

Code	K_m (apparent)			V_{max}			V_{max} (Average) (μM/min)	K_i (μM)	Nature of inhibition
	0 μM	0.625 μM	5 μM	0 μM	0.625 μM	5 μM			
6gj	46.587	60.846	69.479	0.997	1.009	1.031	1.012	1.601	Competitive
Orlistat	65.74	102.97	144.75	0.974	0.884	0.909	0.922	0.488	Competitive

5.3.4. Fluorescence quenching study

As explained in chapter 4, the human Plis responsible for fluorescence emission due to the presence of seven Tryptophan (Trp), 25 Phenylalanine (Phe) and 16 Tyrosine (Tyr) residues.[6] Therefore, the fluorescence quenching effect of most potent PL inhibitory analogue **6gj** on PL fluorescence was tested to confirm its active site binding. As explained in the detailed experimental section (chapter 3), 6 concentrations of analogue **6gj** in serial dilutions (0.3125 -

20 µg/mL) were tested to observe the concentration-dependent effect of analogue **6gj** on the fluorescence intensity of PL enzyme.

The effect of quenching was performed at 298 K and the graph of Fluorescence Intensity *Vs* Wavelength was plotted. As shown in **Figure 5.5**, PL enzyme without any inhibitor presented highest fluorescence intensity of 33720 cps. In the presence of analogue **6gj**, a decrease in fluorescence intensity in concentration-dependent manner was observed.
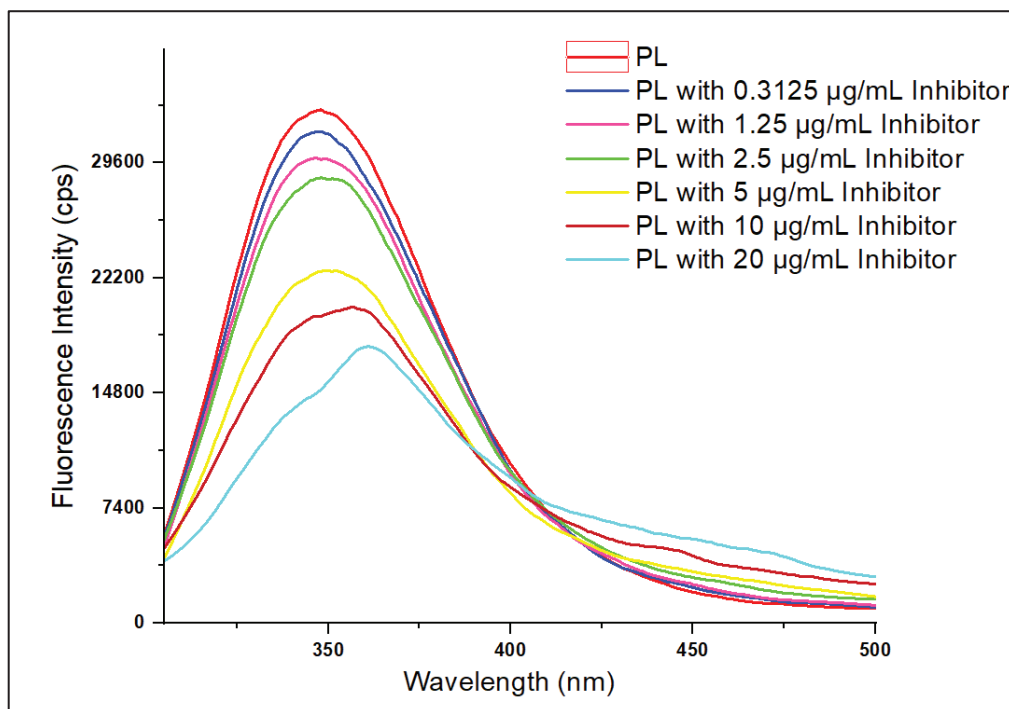
Figure 5.5. Fluorescence quenching of porcine PL by analogue **6gj**

To identify the underlying mechanism of quenching by **6gj** and hence to depict its binding site, Stern-Volmer equation was utilized (chapter 3, **Formula 3.2**).[6–8]

The graph of F_0/F Vs [Q] was plotted at the temperatures of 298, 304, 310 K by keeping the y-intercept as 1. As shown in **Figure 5.6**, there is a linear relationship between F_0/F and [Q], that eliminates the possibility of dynamic quenching. For mixed quenching, the points should incline towards the y-axis, but the graph shows no inclination of data towards y-axis.[7] Such results provided the proof that the quenching caused by analogue **6gj** is due to the complex formation between PL and the inhibitor.
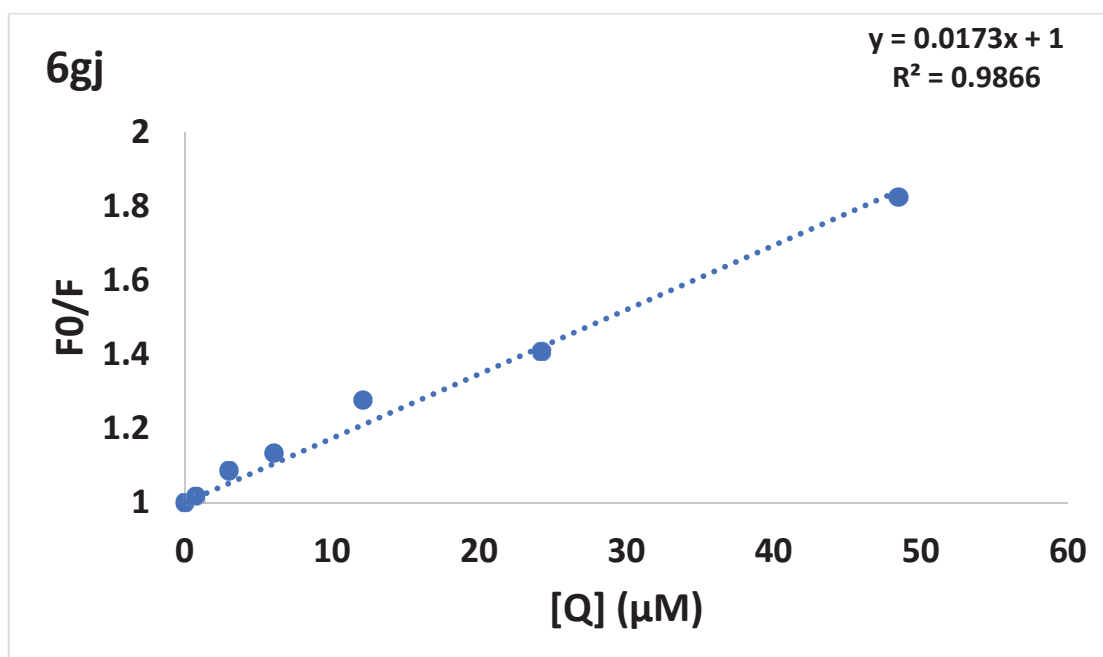
Figure 5.6. Stern-Volmer plot of PL with analogue **6gj**

The values of k_q and K_{SV} were calculated from the graph of F_0/F Vs [Q]. As shown in **Table 5.4**, the k_q value was found to be 1.08×10^{13} L mol^{-1}sec^{-1}. As the k_q values are much higher than the maximal dynamic quenching constant (2.0×10^{10} L mol^{-1}sec^{-1}), it further confirms that the quenching caused by **6gj** is not due to dynamic quenching.[8] The k_q value was also found to be greater than the best analogue of previous series (**5am;** $k_q = 7.92 \times 10^{12}$ L mol^{-1}sec^{-1}). It also confirms the better binding of **6gj** as compared with **5am**. Further, the binding constant (K_b) and number of binding sites (n) were calculated using double logarithmic Stern-Volmer equation (chapter 3, **Formula 3.3**). From the plot of log[(F$_0$-F)/F] Vs log [Q], the value of number of binding sites (n) was found to be 0.77 with the binding constant value of 2.08×10^5 L mol^{-1} (**Figure 5.7**).
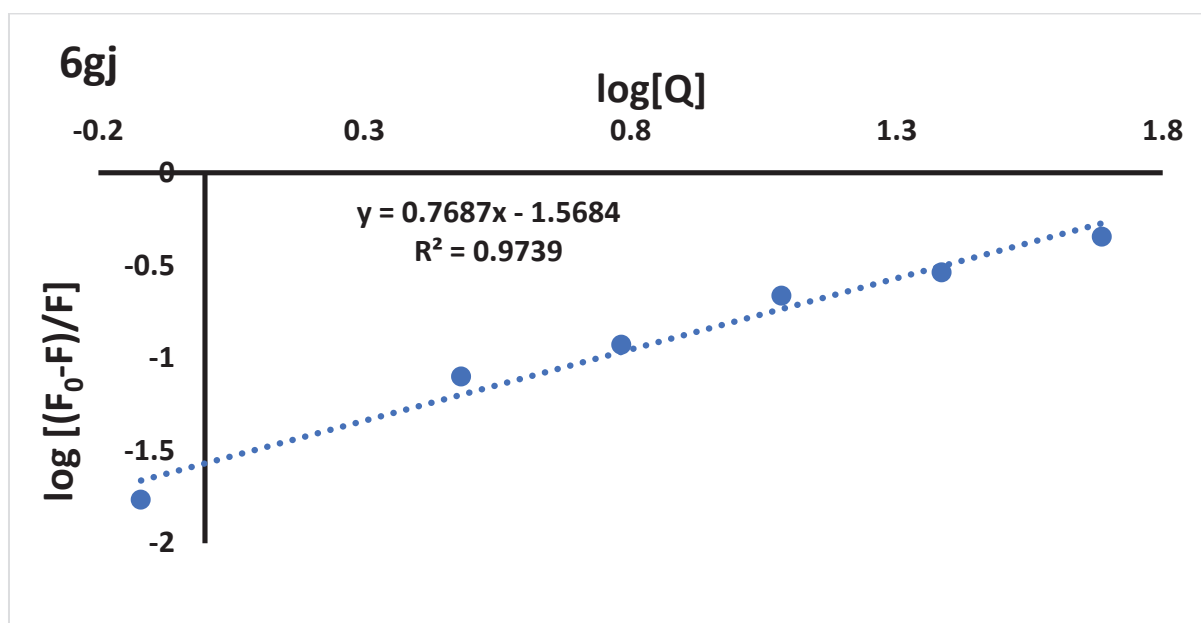
Figure 5.7. Double logarithmic plot for the calculation of binding constant (K_b) and number of binding sites (n)

As compared with analogue **5am** (K_b = 2.06 × 10^5 L mol^{-1}), there was a slight increase in K_b value by **6gj**. As the value of n is closer to 1, it means the analogue **6gj** binds at one binding site of PL enzyme.

Table 5.4. The values of k_q, K_{SV} and n, K_b obtained from Stern-Volmer and double logarithmic plot

Analogue	$K_{SV}/10^4$ (L mol^{-1})	$k_q/10^{13}$ (L $mol^{-1}sec^{-1}$)	n	$K_b/10^5$
6gj	1.73	1.08	0.77	2.08

5.4. Molecular Modelling Studies
5.4.1. Molecular Docking Study

The molecular docking study was performed for evaluating the binding poses of various synthesized analogues at PL active site. As previously explained in chapter 4, the active site of PL enzyme consists of highly restricted catalytic triad consists of Ser152, Asp176 and His263 amino acids, protected by hydrophobic lid domain consists of Gly76-Lys80, Tyr114 and Leu213- Met217 amino acids. Interaction with such amino acids including Arg256 is important for better binding of an inhibitor at PL active site.[9,10]

All the analogues were docked using previously validated grid parameters, i.e. 8.36, 23.16, 53.61 (x, y, z), keeping the radius 7 Å.[1] The structure of PL was obtained from RCSB PDB,

with PDB ID of 1LPB.[11] The docking was performed using MVD software, as per the procedure detailed in experimental section.[12] The docking score of all the analogues was in the range of -121.31 to -158.81 kcal/mol. The chromone ring was found to interact with lid domain amino acids with π-π stacking interaction (**Table 5.5**). In case of many of the synthesized analogues, the Ser152 amino acid was found to interact *via* H-bonding interactions with acrylate fragment.

Table 5.5. Molecular docking result of acrylate linked chromone analogues (**6aa-gj**, **8aa-ac**) and orlistat

Code	MolDock score (kcal/mol)	Amino acid interactions					
		H-Bond/ C-H Bond	π–π stack/ π– π T shape	π-Alkyl/ Alkyl	π -Sigma	Halogen	π-cation/ π-anion
6aa	-121.31	Gly76, Phe77, His151	Tyr114, Phe215	Ala178, Ala259	-	-	Arg256
6ab	-129.59	Gly76, His151, Ser152, His263	Phe215	Ala259, Ala260	-	-	Arg256
6ac	-127.96	Gly76, Phe77, His151, Ser152, His263	Tyr114	Ala178, Pro180, Ala259	-	-	Arg256
6ad	-128.38	Gly76, His151, Ser152, His263	Tyr114	Ala178, Pro180, Ala259	-	-	Arg256
6ae	-134.28	Gly76, Phe77, His151, Ser152, His263	Tyr114, Phe215	Ala178, Pro180, Ala259	-	-	Arg256
6af	-131.91	Gly76, Phe77, His151	Tyr114, Phe215	Ala178, Pro180, Ile209, Ala259	-	-	Arg256
6ag	-138.89	Gly76, Phe77, His151	-	Tyr114, Leu153, Ala178, Pro180, Ile209, Phe215, Ala259	-	-	Arg256, His263
6ah	-130.64	Gly76, Asp79, His151, Ser152	-	Leu153, Ala178, Ala259	-	-	Arg256
6ai	-136.12	Gly76, Asp79, Phe77, His151	-	Ala178, Arg256, Ala259	-	-	His263
6aj	-144.12	Phe77, Tyr114, Ser152, Pro180, His263	-	Ile78, Ala259, Ala260	-	-	His151
6ak	-130.26	Gly76, Phe77, His151, Ser152, His263	Ty114, Phe215, His263	Ala178, Pro180, Ala259	-	-	Arg256
6al	-122.44	Gly76, Phe77, His151, Ser152, Arg256, His263	Tyr114, Phe215	Ala178, Pro180, Ala259	-	-	-
6am	-148.82	Phe77, Asp79, His151, Ser152, Phe215, Arg256, His263	Tyr114, Phe215	Ala178, Pro180, Ala259	Ala178, Phe215	-	Arg256
6an	-131.81	Phe77, Asp79, His151, Ser152	Tyr114	Ala178, Pro180, Phe215, Ala259,	Ala260	-	-

							His263, Leu264
6ba	-129.14	Gly76, Phe77, His151	Tyr114, Phe215	Ala178, Trp252, Ala259	-	-	Arg256
6bj	-141.80	Phe77, Ser152, Leu153	Phe215	Trp252, Arg256, Ala259, Ala260, Leu264	-	-	-
6ca	-129.33	Gly76, Phe77, His151	Tyr114, Phe215	Trp252, Ala259	Ala178	-	Arg256
6cj	-136.53	Tyr114, His151, Phe215	-	Arg256	Leu264	-	-
6da	-128.95	Gly76, Asp79, His151, Ser152	Tyr114	Ala178, Pro180, Arg256, Ala259, Ala260	Leu264	-	-
6dj	-140.25	Phe77, Gly76, His151, Ser152	Phe77,	Ala178, Ala259	-	Thr255	Arg256
6ea	-127.33	Gly76, Phe77, His151	Tyr114	Ala178, Pro180, Ile209, Phe215, Arg256, Ala259, Ala260, Leu264	-	-	-
6ej	-142.88	Gly76, Phe77, His151, Ala259	-	Ile78, Ala178, Pro180, Ile209, Phe215, Ala259, Ala260	-	-	-
6fa	-126.99	His151, Phe215	Tyr114, Phe215	Ala260	Leu264	-	-
6fj	-150.31	Gly76, Phe77, His151, Ser152, His263	Tyr114	Ala178, Pro180, Ala259	-	-	Arg256
6ga	-133.08	Gly76, Phe77, His151, Ser152, His263	Tyr114, Phe215	Ala178, Pro180, Arg256, Ala259, Ala260, Leu264	-	-	-
6gj	-158.81	Gly76, Phe77, Asp79, His151, Ser152	Trp252	Ile78, Ala178, Pro180, Ala259	Ile209	-	Arg256
8aa	-128.20	Gly76, His151	-	Ile78, Ala178, Pro180	-	-	Arg256
8ab	-132.25	Gly76, Phe77, His151, Ser152, Leu153	-	Ala178, Pro180, Trp252, Arg256, Ala259	-	-	-
8ac	-130.54	Gly76, His151, His263	Phe215	Ala178, Pro180, Trp252, Ala259, Arg256	-	-	Arg256
Orlistat	-139.49	Asp79, Arg111, Arg256	-	Ile78, Arg111, Tyr114, Leu153, Ala178, Phe215, Ala259, Ala260	Phe215	-	-

As shown in **Figure 5.8**, the most potent PL inhibitory analogue **6gj** was found to interact with Phe77, Ala178, Trp252 amino acids. It also interacted with catalytic Ser152 amino acid *via* H-bonding interaction. Also, the Arg256 amino acid was involved in π-cation interaction

with the chromone ring. Further the molecular dynamics analysis is required for better understanding of the docking results.
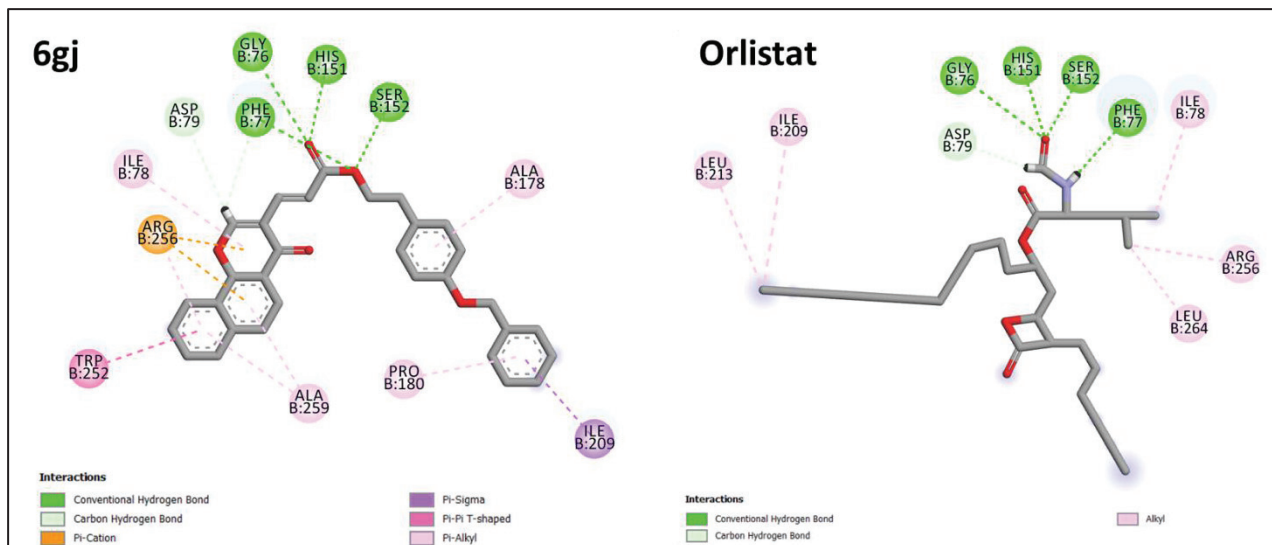
Figure 5.8. 2D interaction diagram of **6gj** and orlistat, with the active site of PL enzyme

5.4.2. Molecular Dynamics Simulation

The molecular dynamics simulation of analogue **6gj** at the PL active site was performed for 100 ns using the established protocol (chapter 3).[2] Firstly, the protein-ligand RMSD plot was analyzed. As shown in **Figure 5.9**, the ligand RMSD was found to deviate up to 14 Å. Till 60 ns of time, the ligand RMSD was low (up to 6 Å), that was found to elevate from 60-100 ns. Interestingly, the protein RMSD was within the range (up to 4.2 Å) upto 80 ns and then found to increase till 5 Å. This results explained the moderate stability of the complex.
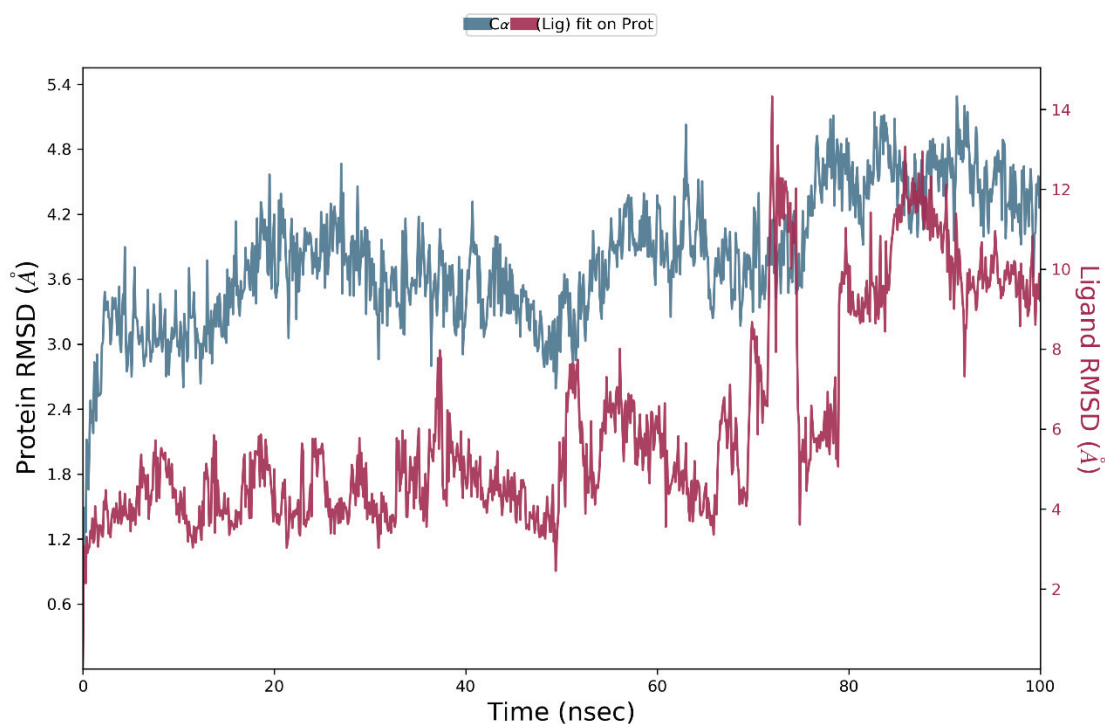
Figure 5.9. RMSD plot of analogue **6gj**, obtained after molecular dynamics simulation of 100 ns

Through PL contacts histogram it was observed that the analogue **6gj** interacted with essential amino acids such as, Phe77, Ile78, Tyr114, Phe215 with more than 0.5 fraction of time (**Figure 5.10**). Such amino acids are lid domain amino acids; hence, the lid domain opening is ensured. Further, the amino acids such as, Leu153, Ala259, Ala260, His263 were interacted with **6gj** with more than 0.2 fraction of simulation time.
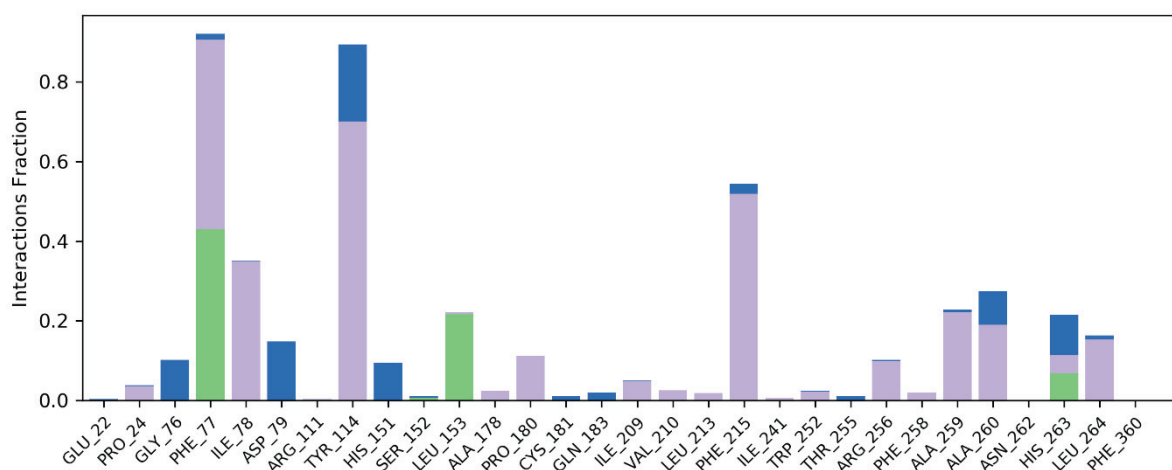
Figure 5.10. Stacked bar plot of protein-ligand (**6gj**) contacts

Also, from the PL contacts timeline graph (**Figure 5.11**) it was observed that the above-mentioned lid domain amino acids were interacted for most of the simulation time (brown

color throughout the simulation time). Still there is a need of optimization of existing inhibitor (**6gj**) for better stability during the dynamics simulation.
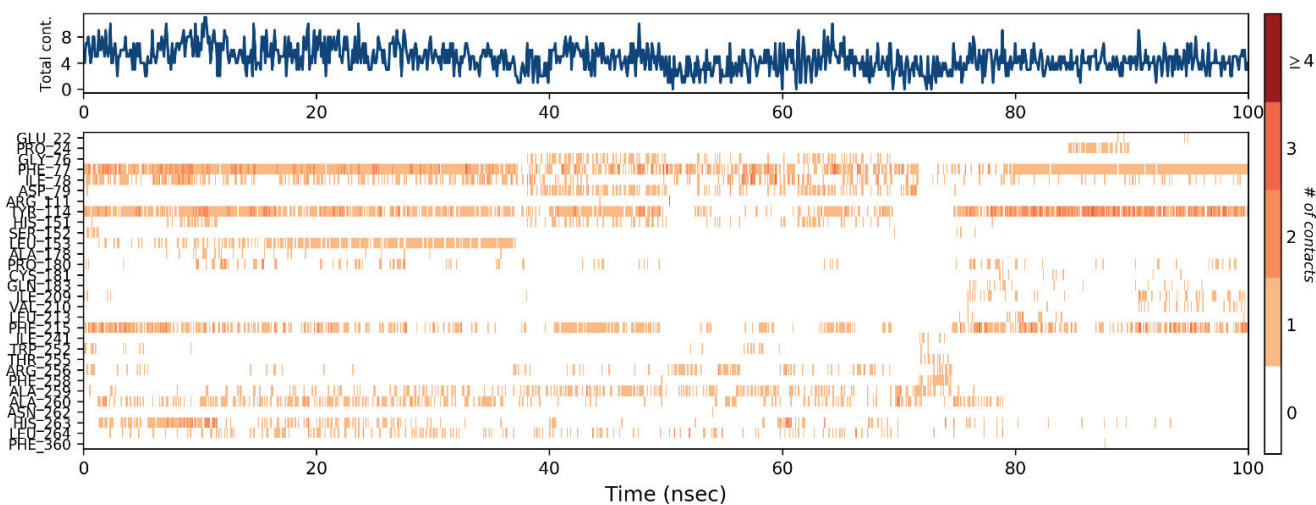
Figure 5.11. A timeline representation of protein-ligand (**6gj**) contacts

5.5. Conclusion

In conclusion, a series of 29 acrylate linked chromone analogues with two carbon linker (n = 2) were designed and synthesized for PL inhibitory screening. The analogues were docked at PL active site and were found to bind effectively with MolDock score in the range of -121.31 to -158.81 kcal/mol. These analogues exhibited effective interaction with the amino acids of lid domain and catalytic triad. Further, Vilsmeier Haack cyclization was utilized for synthesis of 3-Formyl chromone, that acted as a starting point for the synthesis of Chromone-3-acrylic acid *via* Doebner modification to Knoevenagel condensation. The analogues exhibited potential *in vitro* PL inhibitory activities, with analogues **6fj**, **6gj** representing potent activity with IC$_{50}$ of 4.92 and 4.23 μM, respectively. The fluorescence quenching study confirmed the binding of analogue **6gj** at the binding site with binding constant (K$_b$) of 2.08 × 10^5 L mol^{-1}. Also, the enzyme kinetics study revealed its competitive nature of inhibition with K_i value of 1.601 μM. The molecular dynamics simulation of analogue **6gj** at the PL active site for 100 ns indicated moderate stability of the complex. Further lead optimization followed by *in vivo* anti-obesity screening may lead to development of better anti-obesity candidate.

CHAPTER 5

References:

(1)   Auti, P. S.; Jagetiya, S.; Paul, A. T. Chromone-3-acrylic acid ester analogues : Design , synthesis and biological evaluation as potential pancreatic lipase inhibitors. *J. Mol. Struct.* **2023**, *1293*, 136257.

(2)   Auti, P. S.; Nandi, A.; Kumari, V.; Paul, A. T. Design, synthesis, biological evaluation and molecular modelling studies of oxoacetamide warhead containing indole-quinazolinone based novel hybrid analogues as potential pancreatic lipase inhibitors. *New J. Chem.* **2022**, *46* (24), 11648–11661.

(3)   George, G.; Auti, P. S.; Paul, A. T. Design, synthesis, in silico molecular modelling studies and biological evaluation of novel indole-thiazolidinedione hybrid analogues as potential pancreatic lipase inhibitors. *New J. Chem.* **2021**, *45* (3), 1381–1394.

(4)   Sridhar, S. N. C.; Palawat, S.; Paul, A. T. Design , synthesis , biological evaluation and molecular modelling studies of indole glyoxylamides as a new class of potential pancreatic lipase inhibitors. *Bioorg. Chem.* **2019**, *85*, 373–381.

(5)   Jagetiya, S.; Auti, P. S.; Paul, A. T. Design, synthesis, molecular modelling and in vitro evaluation of indolyl ketohydrazide-hydrazone analogs as potential pancreatic lipase inhibitors. *Chem. Biodivers.* **2023**, *20*, 1–16.

(6)   Zhang, J.; Xiao, L.; Yang, Y.; Wang, Z.; Li, G. Lignin binding to pancreatic lipase and its influence on enzymatic activity. *Food Chem.* **2014**, *149*, 99–106.

(7)   Ramos, P.; Coste, T.; Piémont, E.; Lessinger, J. M.; Bousquet, J. A.; Chapus, C.; Kerfelec, B.; Férard, G.; Mély, Y. Time-resolved fluorescence allows selective monitoring of TRP30 environmental changes in the seven-TRP-containing human pancreatic lipase. *Biochemistry* **2003**, *42* (43), 12488–12496.

(8)   Martinez-Gonzalez, A. I.; Alvarez-Parrilla, E.; Díaz-Sánchez, Á. G.; de la Rosa, L. A.; Núñez-Gastélum, J. A.; Vazquez-Flores, A. A.; Gonzalez-Aguilar, G. A. In vitro inhibition of pancreatic lipase by polyphenols: A kinetic, fluorescence spectroscopy and molecular docking study. *Food Technol. Biotechnol.* **2017**, *55* (4), 519–530.

(9)   George, G.; Yadav, N.; Auti, P. S.; Paul, A. T. Molecular modelling, synthesis and in vitro evaluation of quinazolinone hybrid analogues as potential pancreatic lipase inhibitors. *J. Biomol. Struct. Dyn*. **2023**, *41* (19), 9583–9601.

(10) Sridhar, S. N. C.; Sengupta, P.; Palawat, S.; Dileep, P. S.; George, G.; Paul, A. T. Synthesis, molecular modelling, in vitro and in vivo evaluation of conophylline inspired novel benzyloxy substituted indole glyoxylamides as potent pancreatic lipase inhibitors. *J. Biomol. Struct. Dyn.* **2022**, *40* (19), 9530–9542.

(11) Egloff, M.-P.; Marguet, F.; Buono, G.; Verger, R.; Cambillau, C.; Van Tilbeurgh, H. A 2.46 Å resolution structure of the pancreatic lipase-colipase complex inhibited by a c11 alkyl phosphonate. *Biochemistry* **1995**, *34* (9), 2751–2762.

(12) George, G.; Auti, P. S.; Sengupta, P.; Paul, A. T. Design and synthesis of echitamine-inspired hybrid analogues containing thiazolidinediones as potential pancreatic lipase inhibitors. *Lett. Drug Des. Discov.* **2022**, *19* (11), 956–968.

CHAPTER 6

SERIES-III: DESIGN, SYNTHESIS & BIOLOGICAL EVALUATION

6. Series III: Design, Synthesis and PL Inhibitory Evaluation of Acrylate Linked Chromone Analogues

6.1. Rationale

In the chapter 5, a series of acrylate linked chromone analogues with the linker length of 2 carbon atoms (n =2) were synthesized and evaluated for their PL inhibitory potential. From the series, analogue **6gj** was found to exhibit the most potential with an IC_{50} value of 4.23 ± 0.747 μM. Further, to optimize the series with the aim of improving PL inhibition, molecular docking analysis was performed and it was inferred that there was a scope of substitution of linker carbon atoms for additional interactions at the active site of PL. Hence, series II analogues were modified by the substitution of aromatic and keto functionality, with the aim of having additional π-π and H-bonding interactions. As shown in **Figure 6.1**, the chromone ring was found to interact with Arg256 and Ala259 with π-cation and π-Alkyl interactions. The two phenyl rings attached to linker carbon atoms acted as flanking groups for extensive interaction with lid domain amino acids (Tyr114, Ala178, Phe215). Also, the additional oxo group on linker carbon was found to interact with Phe77, Ser152 and Leu153 amino acids *via* H-bonding interactions. The docking score of the modified prototype analogue was improved to **-168.33** kcal/mol compared to the previous series analogues (**6aa-gj**). A docking study of various substituted analogues has been performed and the representative data is shown in molecular docking section.
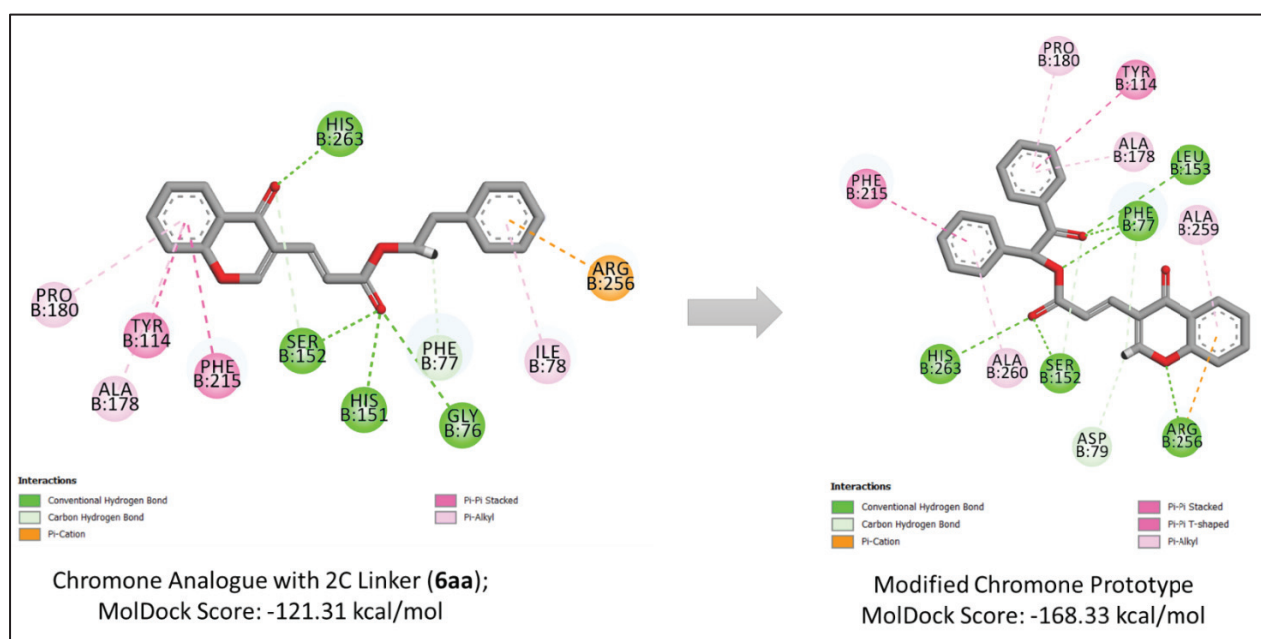
Figure 6.1. Docking comparison of **6aa** with its modified prototype analogue

As per the docking results, in this series, we modified the analogues of series II by substituting linker carbon atoms. In chapter 5, for all the analogues, the chromone ring was found to interact with lid domain amino acids, whereas the remaining aromatic ring was involved in π-cation interaction with Arg256. In this series, the two phenyl rings, attached to linker atoms were observed to interact with lid domain amino acids, while the chromone ring interacted with Arg256 (**Figure 6.2**). The docking score was improved to -168.33 kcal/mol which depicted better analogue binding at the active site pocket when compared to series II analogues. Also, the additional oxo group on linker carbon was involved in effective H-bonding interactions with Phe77 and Leu153 amino acids. As proposed earlier, the acrylate fragment was found to interact with Ser152 amino acid (H-bonding interaction). Looking at such positive observations, the series of analogues (series III) were synthesized followed by their *in vitro* evaluation.
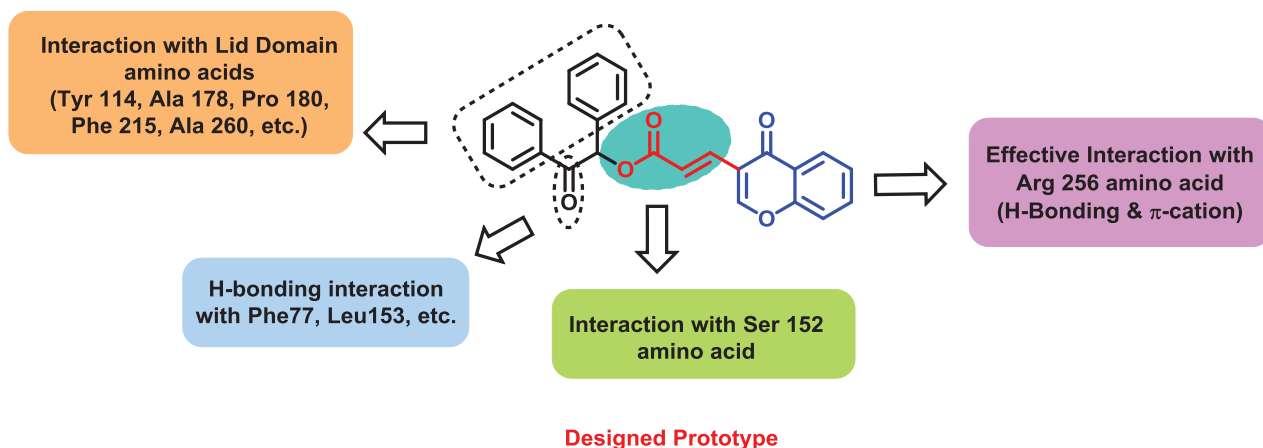
Figure 6.2. Design of chromone and acrylate-based analogue, showing important pharmacophoric features

6.2. Synthesis and Characterization

The synthesis of final analogues (**10aa-ka**, **10ab-gb**) was performed as per **Scheme 6.1**. Various substituted chromone-3-acrylic acids were synthesized as described previously. Further, substituted benzoin were coupled with chromone-3-acrylic acid using EDC.HCl coupling agent, in the presence of DMAP as a base and DMF as a solvent to get final analogues (**10aa-10gb**). All the synthesized analogues were characterized using IR, NMR (^{1}H & ^{13}C) and HR-MS techniques. Prior to *in vitro* analysis, the final analogues were evaluated for peak purity using HPLC. All the analogues had shown % Peak purity in the range of 96.68 - 99.37, with the retention time (t_R) in the range of 4.463 – 10.62 min.

Through ^{1}H NMR, a singlet of 1H at δ value in the range of 8.03-8.31 ppm confirmed the presence of a proton at 2nd position of chromone ring. The aliphatic proton of benzoin resonated in the δ range of 6.91-6.99 ppm as a singlet, confirming the presence of neighbouring electron withdrawing groups. It confirms the presence of benzoin in the structure of all the analogues. Further the peaks of additional substituents such as, methyl, methoxy, benzyloxy, prenyloxy, geranyloxy, etc. were in their standard range. The presence of carbonyl carbons of chromone, ester and benzoin were further confirmed *via* ^{13}C NMR spectrum. For all the analogues, the carbonyl carbon of ketone of chromone and benzoin were found to resonate at δ value in the range of 192.21-174.56 ppm, whereas the ester carbonyl peak was found in δ range of 166.59-166.85 ppm. The structures were further confirmed via HR-MS analysis by the presence of [M+H]$^+$ or [M+Cl]$^-$ peaks in the spectrum, with the values, coinciding with the calculated m/z values.

1a; R^1 = H
1b; R^1 = 6-Chloro
1c; R^1 = 6-Bromo
1d; R^1 = 6-Fluoro
1e; R^1 = 6-Methyl
1f; R^1 = 6-Methoxy
1g; R^1 = [*h*]benzo
1h; R^1 = 6-Benzyloxy
1i; R^1 = 6-Prenyloxy
1j; R^1 = 6-Geranyloxy
1k; R^1 = 7-Geranyloxy

Chromone-3-acrylic acid ester analogues (10aa-ka, 10ab-gb)

10aa; R^1 = H, R^2 = H   **10ab;** R^1 = H, R^2 = OMe
10ba; R^1 = 6-Chloro, R^2 = H   **10bb;** R^1 = 6-Chloro, R^2 = OMe
10ca; R^1 = 6-Bromo, R^2 = H   **10cb;** R^1 = 6-Bromo, R^2 = OMe
10da; R^1 = 6-Fluoro, R^2 = H   **10db;** R^1 = 6-Fluoro, R^2 = OMe
10ea; R^1 = 6-Methyl, R^2 = H   **10eb;** R^1 = 6-Methyl, R^2 = OMe
10fa; R^1 = 6-Methoxy, R^2 = H   **10fb;** R^1 = 6-Methoxy, R^2 = OMe
10ga; R^1 = [*h*]benzo, R^2 = H   **10gb;** R^1 = [*h*]benzo, R^2 = OMe
10ha; R^1 = 6-Benzyloxy, R^2 = H
10ia; R^1 = 6-Prenyloxy, R^2 = H
10ja; R^1 = 6-Geranyloxy, R^2 = H
10ka; R^1 = 7-Geranyloxy, R^2 = H

Scheme 6.1. Synthetic scheme for acrylate linked chromone analogues (**10aa-ka**, **10ab-gb**)

6.2.1 General Procedure for the synthesis of 3-Formylchromone (2a-k).

The mixture of 2'-Hydroxyacetophenone (**1a-k**) (7.34 mmol) and *N,N*-Dimethylformamide (DMF) (7 mL) was stirred for 15 min in ice bath. To the above mixture, Phosphorous oxychloride (POCl$_3$) (44.06 mmol) was added dropwise. The reaction mixture was then stirred at room temperature for 18 h. After the completion of reaction (confirmed by TLC), the mixture was added in ice cold water and the resultant precipitate was filtered to get the 3-Formylchromone (**2a-k**)[1].

6.2.2 General Procedure for the synthesis of Chromone-3-acrylic acid (3a-k).

A mixture of substituted 3-Formylchromone (7.98 mmol), malonic acid (9.97 mmol) and pyridine (0.5 mL) was refluxed in 8 mL of ethanol for 2-6 h. The resultant mixture was cooled and the precipitated product was filtered and washed with ethanol to get the pure product (**3a-k**)[2]

6.2.3 General Procedure for the synthesis of chromone-3-acrylic acid ester analogues (10aa-ka, 10ab-gb).

The mixture of substituted Chromone-3-acrylic acid (**3a-k**) (0.462 mmol), 3-Dimethylamino-propyl)-ethyl-carbodiimide Hydrochloride (EDC.HCl) (0.924 mmol), 4-(Dimethylamino)pyridine (DMAP) (0.924 mmol) were stirred in DMF in ice cold condition for 15 min. It was then followed by the addition of substituted benzoins (**9a, 9b**) (0.924 mmol) followed by stirring at room temperature for 5-8 hours. After the confirmation by TLC, the reaction mixture was quenched by the addition of cold water, followed by extraction with ethyl acetate. The ethyl acetate layer was then evaporated, followed by column chromatography to get the final analogues (**10aa-ka, 10ab-gb**).

6.2.4 Analytical Data for the final compounds:

2-oxo-1,2-diphenylethyl (E)-3-(4-oxo-4H-chromen-3-yl)acrylate (10aa) Yield: 91%; buff white crystalline solid; MP = 207.3-207.6 °C; ^{1}H NMR (400 MHz, CDCl$_3$) δ (ppm) = 8.26 (d, J = 7.6 Hz, 1H), 8.10 (s, 1H), 7.98 (d, J = 7.6 Hz, 2H), 7.69 (t, J = 7.6 Hz, 1H), 7.54-7.36 (m, 12H), 6.97 (s, 1H); ^{13}C NMR (100 MHz, CDCl$_3$) δ (ppm) = 193.98, 175.94, 166.76, 157.85, 155.66, 137.03, 134.85, 134.19, 133.87, 133.58, 129.40, 129.24, 129.03, 128.78, 126.55, 126.05, 124.38, 121.24, 119.38, 118.27, 77.91; IR: υ (cm^{-1}) = 3061.60, 2378.69, 1718.74, 1692.92, 1655.61, 1615.44, 1558.06, 1497.80, 1457.63, 1408.85, 1354.33, 1291.21, 1253.91, 1222.34, 1147.74, 1098.96, 1053.05, 998.53, 941.15, 866.54, 797.68, 763.25,

731.68, 691.51, 608.30, 579.61, 539.44, 490.66, 410.32; HRMS (ESI$^+$) calculated for C$_{26}$H$_{19}$O$_5$ [M + H]$^+$, 411.1232; found 411.1229; HPLC purity: 99.26%, t_R = 4.463 min.

2-oxo-1,2-diphenylethyl(E)-3-(6-chloro-4-oxo-4H-chromen-3-yl)acrylate (10ba) Yield: 82%; buff white amorphous solid; MP = 222.7-223.1 ˚C; ^{1}H NMR (400 MHz, CDCl$_3$) δ (ppm) = 8.21 (d, J = 2.4 Hz, 1H), 8.10 (s, 1H), 7.98-7.96 (m, 2H), 7.63 (dd, J = 2.8, 8.8 Hz, 1H), 7.54-7.50 (m, 3H), 7.45 (s, 2H), 7.43-7.35 (m, 6H), 6.97 (s, 1H); ^{13}C NMR (100 MHz, CDCl$_3$) δ (ppm) = 193.89, 174.72, 166.60, 157.81, 153.95, 136.47, 134.79, 134.41, 133.78, 133.61, 132.09, 129.44, 129.25, 129.00, 128.81, 128.78, 125.91, 125.25, 121.72, 120.01, 119.38, 77.95; IR: υ (cm^{-1}) = 3058.73, 1713.00, 1687.18, 1652.75, 1618.31, 1555.19, 1494.93, 1451.89, 1434.67, 1337.12, 1282.60, 1253.91, 1190.78, 1153.48, 992.79, 944.02, 869.41, 817.76, 763.25, 728.81, 691.51, 634.13, 576.74, 542.31, 490.66, 461.97, 418.93; HRMS (ESI$^+$) calculated for C$_{26}$H$_{18}$ClO$_5$ [M + H]$^+$, 445.0843; found 445.0870; HPLC purity: 97.26%, t_R = 7.320 min.

2-oxo-1,2-diphenylethyl(E)-3-(6-bromo-4-oxo-4H-chromen-3-yl)acrylate (10ca) Yield: 82%; buff white crystalline solid; MP = 218.5-218.7 ˚C; ^{1}H NMR (400 MHz, CDCl$_3$) δ (ppm) = 8.38 (d, J = 2.4 Hz, 1H), 8.10 (s, 1H), 7.98-7.96 (m, 2H), 7.77 (dd, J = 2.4, 8.8 Hz, 1H), 7.54-7.50 (m, 3H), 7.44 (s, 2H), 7.43-7.35 (m, 6H), 6.97 (s,1H); ^{13}C NMR (100 MHz, CDCl$_3$) δ (ppm) = 193.87, 174.56, 166.59, 157.79, 154.39, 137.17, 136.45, 134.79, 133.78, 133.60, 129.44, 129.26, 129.11, 129.00, 128.81, 128.78, 125.59, 121.74, 120.21, 119.57, 119.49, 77.95; IR: υ (cm^{-1}) = 3767.46, 3055.86, 1713.00, 1687.18, 1649.88, 1612.57, 1552.32, 1492.06, 1446.15, 1368.68, 1334.25, 1282.60, 1187.91, 1147.74, 1050.18, 992.79, 944.02, 869.41, 814.90, 760.38, 728.81, 691.51, 605.43, 573.87, 539.44, 490.66, 459.10, 407.45; HRMS (ESI$^+$) calculated for C$_{26}$H$_{18}$BrO$_5$ [M + H]$^+$, 489.0338; found 489.0324; HPLC purity: 98.42%, t_R = 7.907 min.

2-oxo-1,2-diphenylethyl(E)-3-(6-fluoro-4-oxo-4H-chromen-3-yl)acrylate (10da) Yield: 80%; buff white amorphous solid; MP = 210.2-210.5 ˚C; ^{1}H NMR (400 MHz, CDCl$_3$) δ (ppm) = 8.11 (s, 1H), 7.99-7.96 (m, 2H), 7.90 (dd, J = 3.2, 8.0 Hz, 1H), 7.54-7.50 (m, 3H), 7.47 (d, J = 4.4 Hz, 1H), 7.46 (s, 1H), 7.44-7.35 (m, 6H), 6.97 (s, 1H); ^{13}C NMR (100 MHz, CDCl$_3$) δ (ppm) = 193.90, 175.10, 166.63, 160.06 (d, J = 246.5 Hz), 157.90, 151.87, 136.58, 134.81, 133.80, 133.60, 129.43, 129.25, 129.01, 128.79, 125.61, 125.54, 122.44 (d, J = 25.2 Hz), 121.61, 120.49, 120.41, 118.71, 111.45 (d, J = 23.7 Hz), 77.94; IR: υ (cm^{-1}) = 3058.73, 1713.00, 1687.18, 1652.75, 1618.31, 1555.19, 1494.93, 1451.89, 1434.67, 1337.12, 1282.60,

1253.91, 1190.78, 1153.48, 992.79, 944.02, 869.41, 817.76, 763.25, 728.81, 691.51, 634.13, 576.74, 542.31, 490.66, 461.97, 418.93; HRMS (ESI$^+$) calculated for $C_{26}H_{18}FO_5$ [M + H]$^+$, 429.1138; found 429.1130; HPLC purity: 97.53%, t_R = 5.697 min.

2-oxo-1,2-diphenylethyl (E)-3-(6-methyl-4-oxo-4H-chromen-3-yl)acrylate (10ea) Yield: 80%; white amorphous solid; MP = 207.8-208.4 ˚C; ^{1}H NMR (400 MHz, CDCl$_3$) δ (ppm) = 8.08 (s, 1H), 8.04 (d, J = 0.8 Hz, 1H), 7.99-7.97 (m, 2H), 7.54-7.46 (m, 6H), 7.43-7.35 (m, 6H), 6.97 (s, 1H), 2.46 (s, 3H); ^{13}C NMR (100 MHz, CDCl$_3$) δ (ppm) = 194.00, 175.98, 166.81, 157.80, 153.93, 137.26, 136.14, 135.39, 134.84, 133.88, 133.56, 129.37, 129.22, 129.01, 128.76, 125.81, 124.01, 120.91, 119.14, 117.99, 77.86, 21.14 ppm; IR: υ (cm^{-1}) = 3738.76, 3623.99, 3064.47, 2975.52, 2361.47, 2332.78, 1799.08, 1747.43, 1715.87, 1692.92, 1658.48, 1621.18, 1515.02, 1483.45, 1431.81, 1342.86, 1288.34, 1253.91, 1164.96, 1047.31, 992.79, 952.62, 869.41, 817.76, 763.25, 728.81, 691.51, 611.17, 579.61, 542.31, 496.40, 456.23, 424.66; HRMS (ESI$^+$) calculated for $C_{27}H_{21}O_5$ [M + H]$^+$, 425.1389; found 425.1421; HPLC purity: 99.37%, t_R = 6.517 min.

2-oxo-1,2-diphenylethyl(E)-3-(6-methoxy-4-oxo-4H-chromen-3-yl)acrylate (10fa) Yield: 78%; white crystalline solid; MP = 218.3-218.7 ˚C; ^{1}H NMR (400 MHz, CDCl$_3$) δ (ppm) = 8.10 (s, 1H), 7.99-7.97 (m, 2H), 7.61 (d, J = 3.2 Hz, 1H), 7.54-7.50 (m, 3H), 7.49 (s, 1H), 7.46 (s, 1H), 7.43-7.35 (m, 6H), 7.29-7.26 (m, 1H), 6.97 (s, 1H), 3.90 (s, 3H); ^{13}C NMR (100 MHz, CDCl$_3$) δ (ppm) = 194.01, 175.73, 166.80, 157.60, 150.49, 137.25, 134.86, 133.89, 133.57, 129.38, 129.22, 129.01, 128.77, 125.03, 124.16, 120.90, 119.67, 118.50, 105.58, 77.86 , 56.12; IR: υ (cm^{-1}) = 3735.89, 3058.73, 3004.21, 2958.30, 2361.47, 2332.78, 1715.87, 1690.05, 1644.14, 1606.84, 1517.89, 1471.98, 1426.07, 1391.63, 1337.12, 1282.60, 1239.56, 1196.52, 1133.39, 1093.22, 1032.97, 995.66, 944.02, 866.54, 823.50, 763.25, 725.95, 691.51, 605.43, 571.00, 539.44, 493.53, 461.97; HRMS (ESI$^+$) calculated for $C_{27}H_{21}O_6$ [M + H]$^+$, 441.1338; found 441.1327; HPLC purity: 98.96%, t_R = 5.573 min.

2-oxo-1,2-diphenylethyl(E)-3-(4-oxo-4H-benzo[h]chromen-3-yl)acrylate (10ga) Yield: 86%; buff yellow amorphous solid; MP = 208.8-209.3 ˚C; ^{1}H NMR (400 MHz, CDCl$_3$) δ (ppm) = 8.47-8.44 (m, 1H) 8.27 (s, 1H), 8.18 (d, J = 8.8 Hz, 1H), 8.00-7.98 (m, 2H), 7.94-7.92 (m, 1H), 7.79 (d, J = 8.8 Hz, 1H), 7.74-7.66 (m, 2H), 7.56-7.50 (m, 5H), 7.44-7.36 (m, 5H), 6.99 (s, 1H); ^{13}C NMR (100 MHz, CDCl$_3$) δ (ppm) = 193.99, 175.77, 166.75, 156.87, 153.15, 136.89, 136.08, 134.85, 133.86, 133.59, 129.77, 129.40, 129.24, 129.03, 128.78, 128.32, 127.61, 126.18, 123.86, 122.32, 121.74, 121.07, 120.78, 120.55, 77.95; IR: υ (cm^{-1}) =

3070.20, 1698.66, 1649.88, 1615.44, 1558.06, 1506.41, 1443.28, 1411.72, 1380.16, 1342.86, 1279.73, 1253.91, 1193.65, 1153.48, 1070.27, 1035.84, 989.93, 949.75, 915.32, 869.41, 800.55, 763.25, 691.51, 576.74, 536.57, 502.14, 441.88; HRMS (ESI$^+$) calculated for C$_{30}$H$_{21}$O$_5$ [M + H]$^+$, 461.1389; found 461.1388; HPLC purity: 98.02%, t_R = 8.100 min.

2-oxo-1,2-diphenylethyl(E)-3-(6-(benzyloxy)-4-oxo-4H-chromen-3-yl)acrylate **(10ha)** Yield: 88%; white amorphous solid; MP = 200.5-200.9 ˚C; ^{1}H NMR (400 MHz, CDCl$_3$) δ (ppm) = 8.08 (s, 1H), 7.99-7.97 (m, 2H), 7.71 (d, J = 2.8 Hz, 1H), 7.55-7.52 (m, 3H), 7.48-7.47 (m, 4H), 7.43-7.42 (m, 2H), 7.41-7.39 (m, 5H), 7.37-7.35 (m, 3H), 6.98 (s, 1H), 5.16 (s, 1H); ^{13}C NMR (100 MHz, CDCl$_3$) δ (ppm) = 193.99, 175.67, 166.78, 157.63, 156.66, 150.55, 137.21, 136.19, 134.85, 133.88, 133.56, 129.37, 129.22, 129.01, 128.82, 128.76, 128.42, 127.83, 125.01, 124.61, 120.94, 119.76, 118.51, 106.85, 77.86, 70.80; IR: υ (cm^{-1}) = 3735.89, 3058.73, 3004.21, 2958.30, 2361.47, 2332.78, 1715.87, 1690.05, 1644.14, 1606.84, 1517.89, 1471.98, 1426.07, 1391.63, 1337.12, 1282.60, 1239.56, 1196.52, 1133.39, 1093.22, 1032.97, 995.66, 944.02, 866.54, 823.50, 763.25, 725.95, 691.51, 605.43, 571.00, 539.44, 493.53, 461.97; HRMS (ESI$^+$) calculated for C$_{33}$H$_{25}$O$_6$ [M + H]$^+$, 517.1651; found 517.1650; HPLC purity: 97.39%, t_R = 9.213 min.

2-oxo-1,2-diphenylethyl(E)-3-(6-((3-methylbut-2-en-1-yl)oxy)-4-oxo-4H-chromen-3-yl)acrylate (10ia) Yield: 80%; white crystalline solid; MP = 220.2-220.4 ˚C; ^{1}H NMR (400 MHz, CDCl$_3$) δ (ppm) = 8.09 (s, 1H), 7.99-7.97 (m, 2H), 7.62 (d, J = 3.2 Hz, 1H), 7.54-7.50 (m, 3H), 7.48 (d, J = 8.4 Hz, 2H), 7.43-7.35 (m, 6H), 7.29-7.26 (m, 1H), 6.97 (s, 1H), 5.50 (tt, J = 1.2, 6.4 Hz, 1H), 4.61 (d, J = 6.8 Hz, 1H), 1.81 (s, 1H), 1.78 (s, 1H); ^{13}C NMR (100 MHz, CDCl$_3$) δ (ppm) = 194.00, 175.77, 166.80, 157.59, 156.82, 150.40, 139.28, 137.29, 134.85, 133.89, 133.56, 129.36, 129.21, 129.01, 128.76, 124.96, 124.65, 120.85, 119.62, 118.96, 118.48, 106.39, 77.85, 65.69, 25.99, 18.42; IR: υ (cm^{-1}) = 3070.20, 1698.66, 1649.88, 1615.44, 1558.06, 1506.41, 1443.28, 1411.72, 1380.16, 1342.86, 1279.73, 1253.91, 1193.65, 1153.48, 1070.27, 1035.84, 989.93, 949.75, 915.32, 869.41, 800.55, 763.25, 691.51, 576.74, 536.57, 502.14, 441.88; HRMS (ESI$^+$) calculated for C$_{31}$H$_{27}$O$_6$ [M + H]$^+$, 495.1808; found 495.1805; HPLC purity: 97.12%, t_R = 6.150 min.

2-oxo-1,2-diphenylethyl(E)-3-(6-(((E)-3,7-dimethylocta-2,6-dien-1-yl)oxy)-4-oxo-4H-chromen-3-yl)acrylate (10ja) Yield: 82%; white crystalline solid; MP = 210.8-211.2 ˚C; ^{1}H NMR (400 MHz, CDCl$_3$) δ (ppm) = 8.09 (s, 1H), 7.99-7.97 (m, 2H), 7.63 (d, J = 2.8 Hz, 1H), 7.54-7.52 (m, 3H), 7.48 (d, J = 7.6 Hz, 2H), 7.43-4.41 (m, 2H), 7.39-7.35 (m, 4H), 7.30-7.27

(m, 1H), 6.97 (s, 1H), 5.51-5.48 (m, 1H), 5.09-5.07 (m, 1H), 4.64 (d, J = 6.4 Hz, 1H), 2.14-2.08 (m, 4H), 1.77 (s, 3H), 1.67 (s, 3H), 1.60 (s, 3H); ^{13}C NMR (100 MHz, CDCl$_3$) δ (ppm) = 194.00, 175.76, 166.81, 157.59, 156.83, 150.39, 142.35, 137.30, 134.85, 133.89, 133.56, 132.01, 129.37, 129.22, 129.01, 128.76, 124.97, 124.64, 123.84, 120.85, 119.60, 118.72, 118.47, 106.48, 77.85, 65.76, 39.69, 26.42, 25.81, 17.85, 16.91; IR: υ (cm^{-1}) = 3738.76, 3623.99, 3064.47, 2975.52, 2361.47, 2332.78, 1799.08, 1747.43, 1715.87, 1692.92, 1658.48, 1621.18, 1515.02, 1483.45, 1431.81, 1342.86, 1288.34, 1253.91, 1164.96, 1047.31, 992.79, 952.62, 869.41, 817.76, 763.25, 728.81, 691.51, 611.17, 579.61, 542.31, 496.40, 456.23, 424.66; HRMS (ESI$^+$) calculated for C$_{36}$H$_{35}$O$_6$ [M + H]$^+$, 563.2434; found 563.2436; HPLC purity: 98.98%, t_R = 7.343 min.

2-oxo-1,2-diphenylethyl(E)-3-(7-(((E)-3,7-dimethylocta-2,6-dien-1-yl)oxy)-4-oxo-4H-chromen-3-yl)acrylate (10ka) Yield: 80%; buff white crystalline solid; MP = 218.5-218.9 ˚C; ^{1}H NMR (400 MHz, CDCl$_3$) δ (ppm) = 8.16 (d, J = 9.2 Hz, 1H), 8.03 (s, 1H), 7.99-7.97 (m, 2H), 7.54-7.50 (m, 3H), 7.46 (d, J = 1.2 Hz, 2H), 7.43-7.35 (m, 5H), 7.26 (s, 1H), 7.00 (dd, J = 2.4, 6.4 Hz, 1H), 6.96 (s, 1H), 6.85 (d, J = 2.0 Hz, 1H), 5.49-5.46 (m, 1H), 5.09-5.06 (m, 1H), 4.63 (d, J = 6.4 Hz, 2H), 2.14-2.11 (m, 4H), 1.76 (s, 3H), 1.66 (s, 3H), 1.60 (s, 3H); ^{13}C NMR (100 MHz, CDCl$_3$) δ (ppm) = 194.03, 175.31, 166.81, 163.76, 157.40, 157.34, 142.74, 137.26, 134.87, 133.91, 133.55, 132.15, 129.35, 129.21, 129.03, 128.76, 128.73, 127.81, 123.69, 120.99, 119.28, 118.34, 118.06, 115.73, 101.26, 77.87, 65.79, 39.64, 26.35, 25.81, 17.86, 16.92; IR: υ (cm^{-1}) = 3738.76, 3623.99, 3064.47, 2975.52, 2361.47, 2332.78, 1799.08, 1747.43, 1715.87, 1692.92, 1658.48, 1621.18, 1515.02, 1483.45, 1431.81, 1342.86, 1288.34, 1253.91, 1164.96, 1047.31, 992.79, 952.62, 869.41, 817.76, 763.25, 728.81, 691.51, 611.17, 579.61, 542.31, 496.40, 456.23, 424.66; HRMS (ESI$^+$) calculated for C$_{36}$H$_{35}$O$_6$ [M + H]$^+$, 563.2434; found 563.2442; HPLC purity: 96.68%, t_R = 10.620 min.

1,2-bis(4-methoxyphenyl)-2-oxoethyl(E)-3-(4-oxo-4H-chromen-3-yl)acrylate **(10ab)** Yield: 80%; buff white crystalline solid; MP = 235.5-235.7 ˚C; ^{1}H NMR (400 MHz, CDCl$_3$) δ (ppm) = 8.27 (dd, J = 1.2, 6.8 Hz, 1H), 8.11 (s, 1H), 7.98-7.95 (m, 2H), 7.71-7.67 (m, 1H), 7.51-7.40 (m, 6H), 6.92-6.86 (m, 5H), 3.82 (s, 3H), 3.78 (s, 3H); ^{13}C NMR (100 MHz, CDCl$_3$) δ (ppm) = 192.21, 175.76, 166.67, 163.64, 160.22, 157.57, 155.51, 136.63, 134.01, 131.20, 130.10, 127.57, 126.38, 126.20, 125.86, 124.22, 121.28, 119.28, 118.11, 114.50, 113.84, 77.13, 55.45, 55.29; IR: υ (cm^{-1}) = 3061.60, 2378.69, 1718.74, 1692.92, 1655.61, 1615.44, 1558.06, 1497.80, 1457.63, 1408.85, 1354.33, 1291.21, 1253.91, 1222.34, 1147.74, 1098.96, 1053.05, 998.53, 941.15, 866.54, 797.68, 763.25, 731.68, 691.51, 608.30, 579.61,

539.44, 490.66, 410.32; HRMS (ESI⁻) calculated for $C_{28}H_{22}ClO_7$ [M + Cl]⁻, 505.1054; found 505.1058; HPLC purity: 98.94%, t_R = 4.833 min.

1,2-bis(4-methoxyphenyl)-2-oxoethyl(E)-3-(6-chloro-4-oxo-4H-chromen-3-yl)acrylate
(10bb) Yield: 80%; white amorphous solid; MP = 228.2-228.8 ˚C; ¹H NMR (400 MHz, CDCl₃) δ (ppm) = 8.21 (d, *J* = 2.4 Hz, 1H), 8.09 (s, 1H), 7.95 (d, *J* = 9.2 Hz, 2H), 7.62 (dd, *J* = 2.8, 6.0 Hz, 1H), 7.44-7.42 (m, 5H), 6.91-6.86 (m, 5H), 3.82 (s, 3H), 3.78 (s, 3H); ¹³C NMR (100 MHz, CDCl₃) δ (ppm) = 192.23, 174.69, 166.65, 163.79, 160.38, 157.67, 153.94, 136.20, 134.35, 132.03, 131.32, 130.27, 127.64, 126.24, 125.89, 125.24, 121.92, 120.00, 119.43, 114.64, 113.98, 77.31, 55.58, 55.42; IR: υ (cm⁻¹) = 3058.73, 1713.00, 1687.18, 1652.75, 1618.31, 1555.19, 1494.93, 1451.89, 1434.67, 1337.12, 1282.60, 1253.91, 1190.78, 1153.48, 992.79, 944.02, 869.41, 817.76, 763.25, 728.81, 691.51, 634.13, 576.74, 542.31, 490.66, 461.97, 418.93; HRMS (ESI⁻) calculated for $C_{28}H_{21}Cl_2O_7$ [M + Cl]⁻, 539.0664; found 539.0670; HPLC purity: 96.28%, t_R = 4.562 min.

1,2-bis(4-methoxyphenyl)-2-oxoethyl(E)-3-(6-bromo-4-oxo-4H-chromen-3-yl)acrylate
(10cb) Yield: 80%; white crystalline solid; MP = 228.2-228.8 ˚C; ¹H NMR (400 MHz, CDCl₃) δ (ppm) = 8.38 (d, *J* = 2.4 Hz, 1H), 8.10 (s, 1H), 7.95 (d, *J* = 9.2 Hz, 2H), 7.76 (dd, *J* = 2.4, 6.4 Hz, 1H), 7.47-7.36 (m, 5H), 6.91-6.86 (m, 5H), 3.82 (s, 3H), 3.78 (s, 3H); ¹³C NMR (100 MHz, CDCl₃) δ (ppm) = 192.26, 174.56, 166.66, 163.81, 160.40, 157.63, 154.42, 137.14, 136.19, 131.34, 130.29, 129.13, 127.66, 126.26, 125.61, 121.97, 120.20, 119.58, 119.53, 114.67, 113.99, 77.33, 55.59, 55.43; IR: υ (cm⁻¹) = 3061.60, 2378.69, 1718.74, 1692.92, 1655.61, 1615.44, 1558.06, 1497.80, 1457.63, 1408.85, 1354.33, 1291.21, 1253.91, 1222.34, 1147.74, 1098.96, 1053.05, 998.53, 941.15, 866.54, 797.68, 763.25, 731.68, 691.51, 608.30, 579.61, 539.44, 490.66, 410.32; HRMS (ESI⁻) calculated for $C_{28}H_{21}BrClO_7$ [M + Cl]⁻, 583.0159; found 583.0158; HPLC purity: 98.13%, t_R = 6.863 min.

1,2-bis(4-methoxyphenyl)-2-oxoethyl(E)-3-(6-fluoro-4-oxo-4H-chromen-3-yl)acrylate
(10db) Yield: 82%; white crystalline solid; MP = 240.0-240.6 ˚C; ¹H NMR (400 MHz, CDCl₃) δ (ppm) = 8.10 (s, 1H), 7.96 (d, *J* = 8.8 Hz, 2H), 7.89 (dd, *J* = 2.8, 5.2 Hz, 1H), 7.51-7.47 (m, 1H), 7.45-7.42 (m, 4H), 7.42-7.38 (m, 1H), 6.91-6.86 (m, 5H), 3.82 (s, 3H), 3.78 (s, 3H); ¹³C NMR (100 MHz, CDCl₃) δ (ppm) = 192.25, 175.10, 166.69, 163.78, 160.03 (d, *J* = 246.4 Hz), 160.38, 157.75, 151.86, 136.30, 131.33, 130.25, 127.66, 126.26, 125.61, 125.53, 122.52, 122.26, 121.80, 120.47, 120.39, 118.76, 114.64, 113.97, 111.42 (d, *J* = 23.7 Hz), 55.58, 55.42; IR: υ (cm⁻¹) = 3058.73, 1713.00, 1687.18, 1652.75, 1618.31, 1555.19, 1494.93,

1451.89, 1434.67, 1337.12, 1282.60, 1253.91, 1190.78, 1153.48, 992.79, 944.02, 869.41, 817.76, 763.25, 728.81, 691.51, 634.13, 576.74, 542.31, 490.66, 461.97, 418.93; HRMS (ESI-) calculated for $C_{28}H_{21}ClFO_7$ [M + Cl]$^-$, 523.0960; found 523.0962; HPLC purity: 98.23%, t_R = 6.485 min.

1,2-bis(4-methoxyphenyl)-2-oxoethyl(E)-3-(6-methyl-4-oxo-4H-chromen-3-yl)acrylate (10eb) Yield: 85%; white crystalline solid; MP = 220.6-220.8 ˚C; ^{1}H NMR (400 MHz, CDCl$_3$) δ (ppm) = 8.07 (s, 1H), 8.03 (d, J = 1.2 Hz, 1H), 7.96 (d, J = 9.2 Hz, 2H), 7.50-7.43 (m, 5H), 7.39-7.34 (m, 1H), 6.91-6.86 (m, 5H), 3.81 (s, 3H), 3.78 (s, 3H), 2.45 (s, 3H); ^{13}C NMR (100 MHz, CDCl$_3$) δ (ppm) = 192.34, 175.94, 166.85, 163.75, 160.33, 157.64, 153.92, 136.97, 136.07, 135.33, 131.32, 130.23, 127.70, 126.34, 125.79, 124.00, 121.11, 119.18, 117.97, 114.61, 113.95, 77.22, 55.57, 55.41, 21.11; IR: υ (cm^{-1}) = 3058.73, 1713.00, 1687.18, 1652.75, 1618.31, 1555.19, 1494.93, 1451.89, 1434.67, 1337.12, 1282.60, 1253.91, 1190.78, 1153.48, 992.79, 944.02, 869.41, 817.76, 763.25, 728.81, 691.51, 634.13, 576.74, 542.31, 490.66, 461.97, 418.93; HRMS (ESI$^-$) calculated for $C_{31}H_{27}O_9$ [M+CH$_3$COO]$^-$, 543.1655; found 543.1464; HPLC purity: 97.32%, t_R = 5.653 min.

1,2-bis(4-methoxyphenyl)-2-oxoethyl(E)-3-(6-methoxy-4-oxo-4H-chromen-3-yl)acrylate (10fb) Yield: 88%; white amorphous solid; MP = 228.6-229.0 ˚C; ^{1}H NMR (400 MHz, CDCl$_3$) δ (ppm) = 8.09 (s, 1H), 7.97 (d, J = 8.8 Hz, 2H), 7.61 (d, J = 2.8 Hz, 1H), 7.52-7.39 (m, 5H), 7.28-7.25 (m, 1H), 6.92-6.87 (m, 5H), 3.09 (s, 3H), 3.82 (s, 3H), 3.78 (s, 3H); ^{13}C NMR (100 MHz, CDCl$_3$) δ (ppm) = 192.37, 175.71, 166.85, 163.78, 160.35, 157.56, 157.46, 150.49, 136.99, 131.33, 130.24, 127.71, 126.35, 125.02, 124.12, 121.09, 119.66, 118.56, 114.63, 113.97, 105.57, 77.23, 56.10, 55.57, 55.41; IR: υ (cm^{-1}) = 3058.73, 1713.00, 1687.18, 1652.75, 1618.31, 1555.19, 1494.93, 1451.89, 1434.67, 1337.12, 1282.60, 1253.91, 1190.78, 1153.48, 992.79, 944.02, 869.41, 817.76, 763.25, 728.81, 691.51, 634.13, 576.74, 542.31, 490.66, 461.97, 418.93; HRMS (ESI-) calculated for $C_{29}H_{24}ClO_8$ [M + Cl]$^-$, 535.1160; found 535.1145; HPLC purity: 99.15%, t_R = 5.007 min.

1,2-bis(4-methoxyphenyl)-2-oxoethyl(E)-3-(4-oxo-4H-benzo[*h*]chromen-3-yl)acrylate (10gb) Yield: 88%; buff white crystalline solid; MP = 215.2-215.6 ˚C; ^{1}H NMR (400 MHz, CDCl$_3$) δ (ppm) = 8.49-8.47 (m, 1H), 8.31 (s, 1H), 8.21 (d, J = 8.8 Hz, 1H), 7.98-7.94 (m, 3H), 7.81 (d, J = 8.8 Hz, 1H), 7.75-7.68 (m, 2H), 7.58-7.53 (m, 2H), 7.49-7.44 (m, 2H), 6.93-6.87 (m, 5H), 3.83 (s, 3H), 3.79 (s, 3H); ^{13}C NMR (100 MHz, CDCl$_3$) δ (ppm) = 192.34, 175.75, 166.81, 163.79, 160.38, 156.71, 153.16, 136.62, 136.07, 131.37, 130.25, 129.74,

128.31, 127.73, 127.59, 126.35, 126.13, 123.88, 122.33, 121.97, 121.11, 120.80, 120.65, 114.65, 113.99, 77.33, 55.60, 55.45; IR: υ (cm^{-1}) = 3058.73, 1713.00, 1687.18, 1652.75, 1618.31, 1555.19, 1494.93, 1451.89, 1434.67, 1337.12, 1282.60, 1253.91, 1190.78, 1153.48, 992.79, 944.02, 869.41, 817.76, 763.25, 728.81, 691.51, 634.13, 576.74, 542.31, 490.66, 461.97, 418.93; HRMS (ESI⁻) calculated for $C_{32}H_{24}ClO_7$ [M + Cl]⁻, 555.1211; found 555.1195; HPLC purity: 96.79%, t_R = 7.073 min.

Single Crystal XRD

After NMR, HR-MS and IR analysis, the single crystal XRD of analogue **10ab** was performed to get the confirmed structure of the representative analogue. For the preparation of single crystal, the slow solvent evaporation technique was utilized. The analogues **10ab, 10cb, 10fb, 10gb** were dissolved in 1:4 ratio of chloroform:ethanol at room temperature. The sample was kept at room temperature in a vial with small passage for the evaporation of solvent. Among all the analogues, **10ab** was found to crystallize after 3 days and the crystals were washed with ethanol. For X-ray diffraction study, **BRUKER APEX II** Diffractometer was utilized. The **Table 6.1** represents the dimension data of obtained crystal.

Table 6.1. Single crystal X-ray Diffraction data of analogue **10ab**

Crystal Data	**Analogue 10ab**
Crystal Color	Clear, Light colorless
Empirical Formula	$C_{28}H_{22}O_7$
Formula Weight	470.46
Crystal System	Triclinic
Temperature	300 K
Resolution	0.41 X
Cell Dimensions	a = 11.9625 Å, b = 12.5228 Å, c = 15.9491 Å α = 86.076º, β = 82.066º, γ = 87.827º
R value	0.07
Θ_{max}	26.022
Θ_{min}	2.006
Radiation	Mo Kα (λ = 0.71073)

The analogue **10ab** consists of a double bond (acrylate) so that it can exist in any of the geometrical isomeric forms (*E* or *Z*). As shown in **Figure 6.3**, it was found to exist in *E* configuration as the same priority groups (Hydrogens) are on opposite sides of double

bonded carbon atoms. Also, **10ab** contains one enantiomeric centre and by looking at the 3D structure of **10ab**, it was found to exist in *R* configuration.
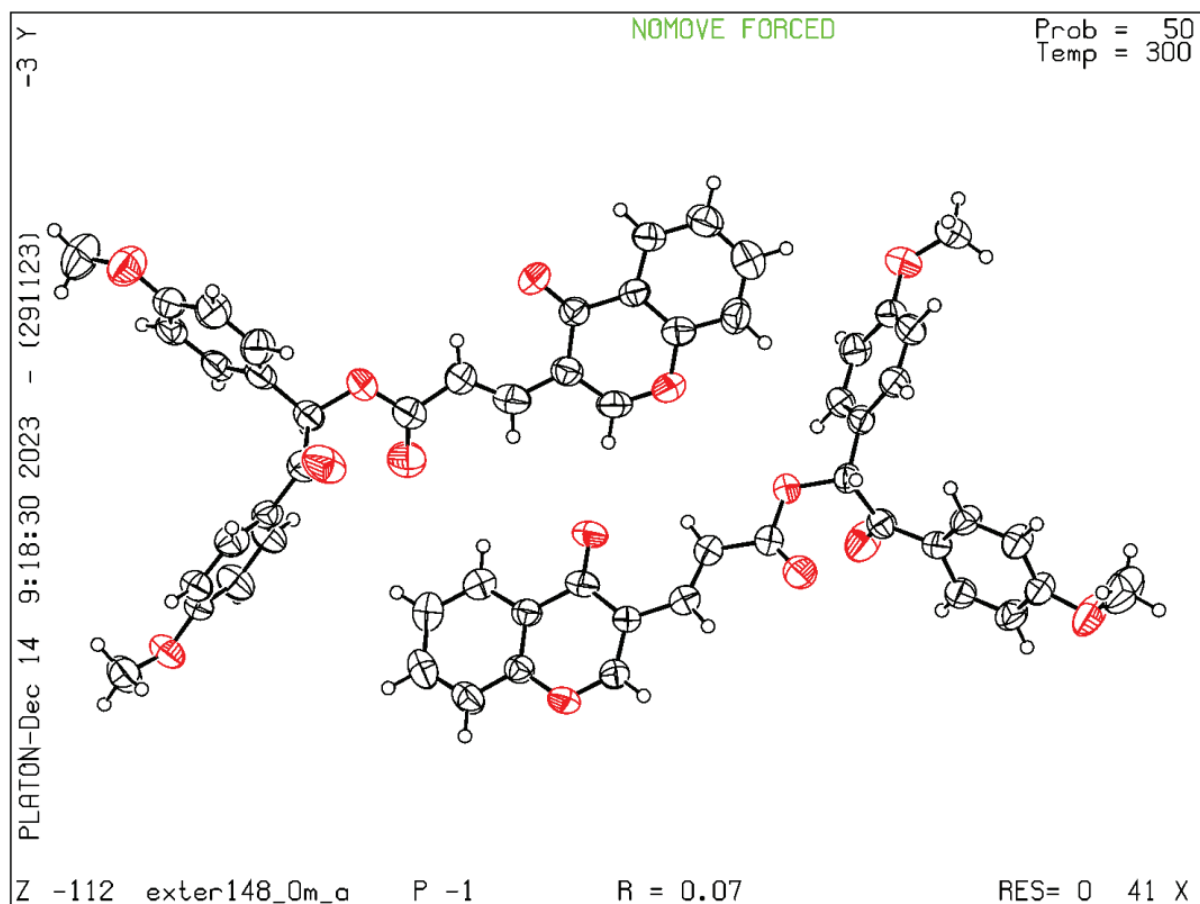
Figure 6.3. ORTEP drawing of analogue **10ab** showing thermal ellipsoid plot

6.3. Biological Evaluation

6.3.1. *In vitro* PL inhibition

All the synthesized analogues (**10aa-ka, 10ab-gb**) were screened for PL inhibitory potential, using the established assay protocol (procedure is explained in chapter 3).[3,4] The PL inhibition activity data of all analogues is represented in **Table 6.2**. As hypothesized above, utilizing the molecular docking study, the prototype analogue **10aa** was found to exhibit the potent activity of 3.32 ± 0.224 µM, as compared with the analogue of previous series (**6gj**; $IC_{50} = 4.23 \pm 0.747$ µM). Further various substituents on chromone ring were evaluated and many of the analogues including, **10ca**, **10fa**, **10ga** were potent in PL inhibition with IC_{50} in the range of 3.62-2.61 µM. Further, the presence of OMe group on two phenyl ring was found to potentiate the activity with analogues **10ab**, **10cb**, **10fb**, **10gb** (IC_{50} in the range of 1.52-1.24 µM). Analogue **10da** and **10db** were found to exhibit poor inhibition with IC_{50}

values in the range of 33.96 - 28.93 µM. Remaining analogues exhibited moderate to good PL inhibitory potential with analogues **10ba**, **10ea** and **10ka** with IC_{50} in the range of 18.53 - 6.71 µM.

Table 6.2. *In vitro* PL inhibitory activity of synthesized acrylate linked chromone analogues (**10aa-ka**, **10ab-gb**) and orlistat

Code	R^1	R^2	IC_{50} (µM ± SEM)*
10aa	**H**	**H**	**3.32 ± 0.224**
10ba	6-Chloro	H	16.21 ± 0.588
10ca	**6-Bromo**	**H**	**3.62 ± 0.284**
10da	6-Fluoro	H	33.96 ± 0.190
10ea	6-Methyl	H	18.53 ± 2.648
10fa	**6-Methoxy**	**H**	**2.61 ± 0.535**
10ga	**[*h*]benzo**	**H**	**2.76 ± 0.445**
10ha	6-Benzyloxy	H	8.41 ± 0.864
10ia	6-Prenyloxy	H	10.60 ± 0.681
10ja	6-Geranyloxy	H	6.71 ± 0.421
10ka	7-Geranyloxy	H	16.98 ± 0.248
10ab	**H**	**Methoxy**	**1.49 ± 0.008**
10bb	6-Chloro	Methoxy	9.32 ± 0.916
10cb	**6-Bromo**	**Methoxy**	**1.52 ± 0.136**
10db	6-Fluoro	Methoxy	28.93 ± 0.865
10eb	6-Methyl	Methoxy	12.25 ± 0.752
10fb	**6-Methoxy**	**Methoxy**	**1.31 ± 0.309**
10gb	**[*h*]benzo**	**Methoxy**	**1.24 ± 0.296**
Orlistat	-	-	0.86 ± 0.09

*The experiment is performed in triplicate (n=3)

6.3.2. Structure Activity Relationship (SAR)

From *in vitro* PL inhibition study of acrylate linked chromone analogues, preliminary SAR was developed to identify the substitution pattern required for potent PL inhibitory activity. As shown in **Table 6.2**, the prototype analogue **10aa** exhibited IC_{50} of 3.32 ± 0.224 µM.

Firstly, various EWGs, EDGs and bulkier groups were substituted on chromone ring to understand the effect on the activity. As shown in **Figure 6.4**, the EWGs (Cl and F) at 6th position of chromone found to deteriorate the activity, when compared with prototype analogue **10aa**. Interestingly, the substitution by Br lead to comparable activity (IC$_{50}$ = 3.62 ± 0.284 µM) as analogue **10aa**. It may be due to the additional interaction of Br with Trp252 amino acid. On the other hand, EDG (OMe) and bulkier group ([*h*]benzo) were found to exhibit much greater activity (**10fa**, **10ga**; IC$_{50}$ = 2.61, 2.76 µM). Unfortunately, in spite of being the EDG, 6-Me substituent was unable to potentiate the activity (**10ea**; 18.53 ± 2.648 µM) as compared with **10aa**. It may be due to the weak electron donating ability of methyl substituent than that of methoxy group. Additionally, the long chain alkyloxy and benzyloxy substituents when placed on 6th and 7th position of chromone were also unable to potentiate the activity (**10ha-ka**; IC$_{50}$ = 6.71-16.98 µM). Further, the effect of OMe group on two phenyl rings attached to linker atoms (R^2) was explored and an increment in the PL inhibitory activity was observed for analogue **10ab** (IC$_{50}$ = 1.49 ± 0.008 µM). Further, the combination of R^1 as 6-OMe, [*h*]-Benzo with R^2 as OMe, gave analogues **10fb** and **10gb** that were the most potent ones with IC$_{50}$ values of 1.31 ± 0.309 and 1.24 ± 0.296 µM, respectively.
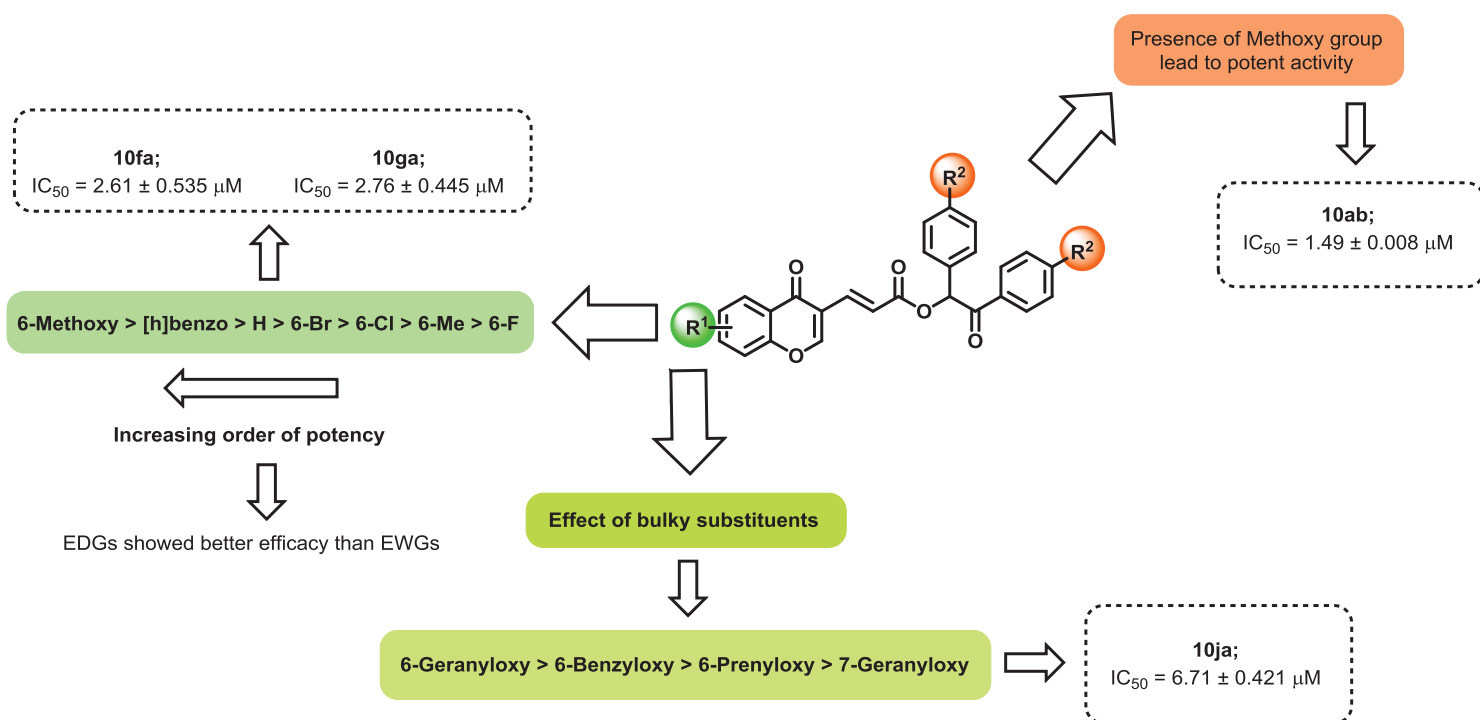
Figure 6.4. Structure Activity Relationship (SAR) study of acrylate linked chromone analogues (**10aa-ka**, **10ab-gb**)

6.3.3. Enzyme Kinetics Study

For determining the mode of PL inhibition of most potent analogue of the series (**10gb**), enzyme kinetics study was performed by utilization of the protocol detailed in chapter 3.[5] The enzyme assay protocol was utilized with 0, 0.625, 5 µM concentration of **10gb**. For comparing the results, orlistat was used as a standard. As shown in **Figure 6.5**, the double reciprocal Lineweaver Burk's plot was analyzed and it was observed that all the lines met Y-axis, showing competitive reversible inhibition of **10gb**. Also, the K_m value was found to increase with increase in concentration of inhibitor (40.33, 72.345, 88.293, respectively). The V_{max} value was found to be constant irrespective of inhibitor concentration.
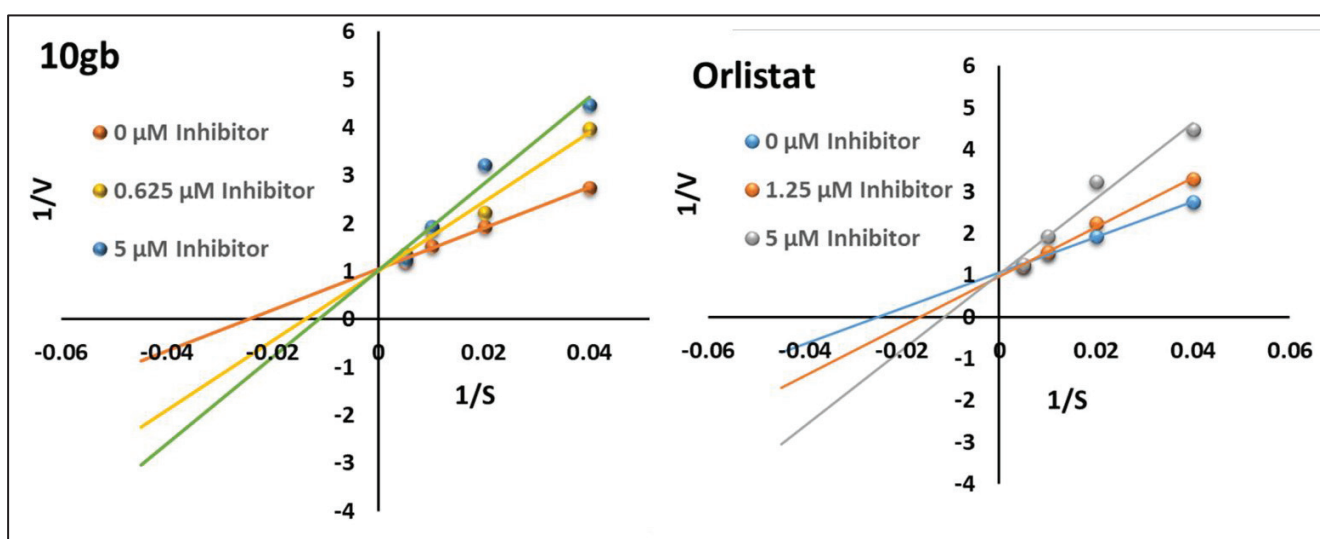
Figure 6.5. Double reciprocal Lineweaver–Burk plot of analogue **10gb** and orlistat

Such results also confirm competitive nature of inhibition. Through Lineweaver burks data, the inhibition constant (K_i) was calculated using Cheng–Prusoff equation and it was found to be 0.554 and 0.488 for **10gb** and orlistat, respectively (**Table 6.3**).

Table 6.3. Enzyme kinetics study of analogue **10gb** and orlistat

Code	K_m (apparent)			V_{max}			V_{max} (Average) (µM/min)	K_i (µM)	Nature of inhibition
	0 µM	0.625 µM	5 µM	0 µM	0.625 µM	5 µM			
10gb	40.383	72.345	88.293	0.948	1.000	0.977	0.975	0.554	Competitive
Orlistat	65.740	102.970[a]	144.75	0.974	0.884	0.909	0.922	0.488	Competitive

[a] Calculated for 1.25 µM concentration

6.3.4. Fluorescence Quenching Study

From the molecular docking study, it was observed that the designed analogue interacts with active site amino acids, including phenylalanine, tyrosine and tryptophan residues.[6,7] Those residues along with other residues are responsible for the intrinsic fluorescence of PL enzyme. Hence, the interaction of such active site residues by a designed inhibitor may lead to fluorescence quenching. To identify such fluorescence quenching and hence, the active site binding ability, the most potent analogue **10gb** was utilized and the study was performed as described in chapter 3. As shown in **Figure 6.6**, the PL exhibited highest fluorescence intensity (32520 cps) and as the concentration of the inhibitor (**10gb**) increased, the proportional decrease in fluorescence intensity was observed.
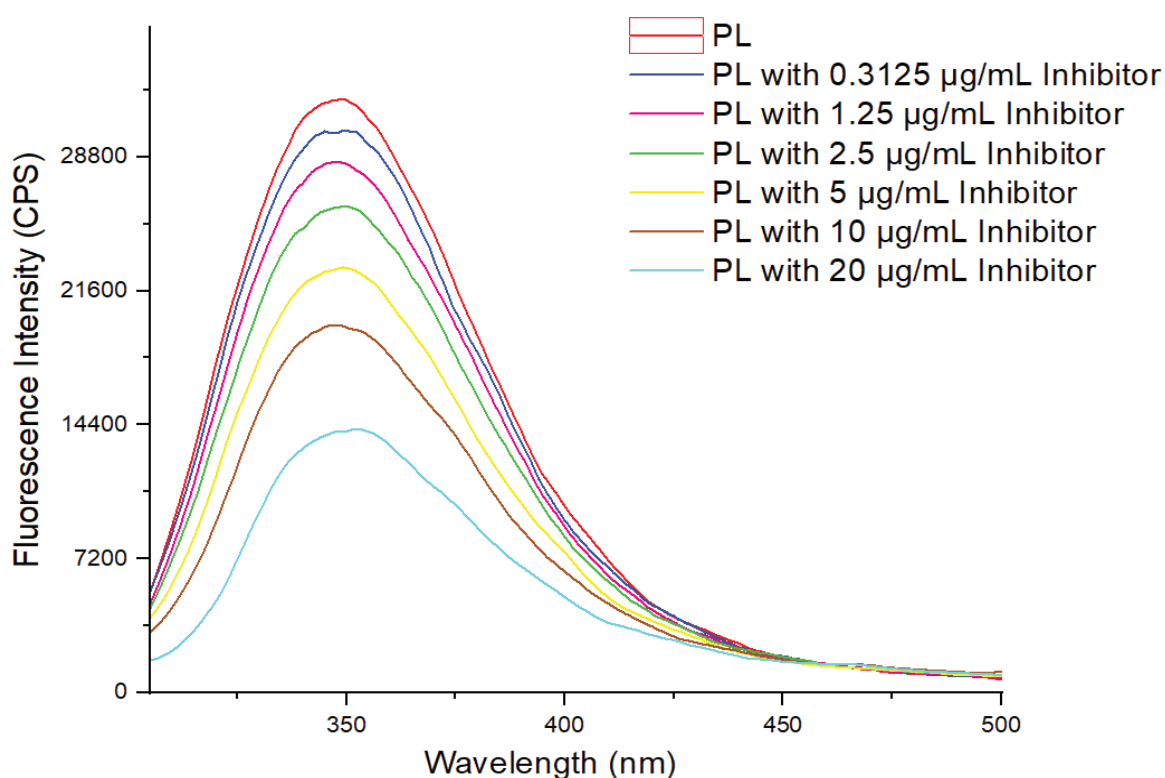
Figure 6.6. Fluorescence quenching of porcine PL by analogue **10gb**

The above fluorescence quenching is mainly due to static or dynamic mechanism. To identify the underlying mechanism of quenching, Stern-Volmer equation was utilized and the values were determined as per **Formula 3.2** (chapter 3).[6,8,9]

The graph of F_0/F Vs [Q] was plotted by keeping the y-intercept as 1. As shown in **Figure 6.7**, a linear relationship between F_0/F and [Q] was observed, that eliminated the possibility of dynamic quenching. In case of mixed quenching, the data points should incline towards the y-

axis, but the graph shows no such inclination of data. Hence, these results concluded that the quenching is due to the complex formation between PL and the inhibitor **10gb.**
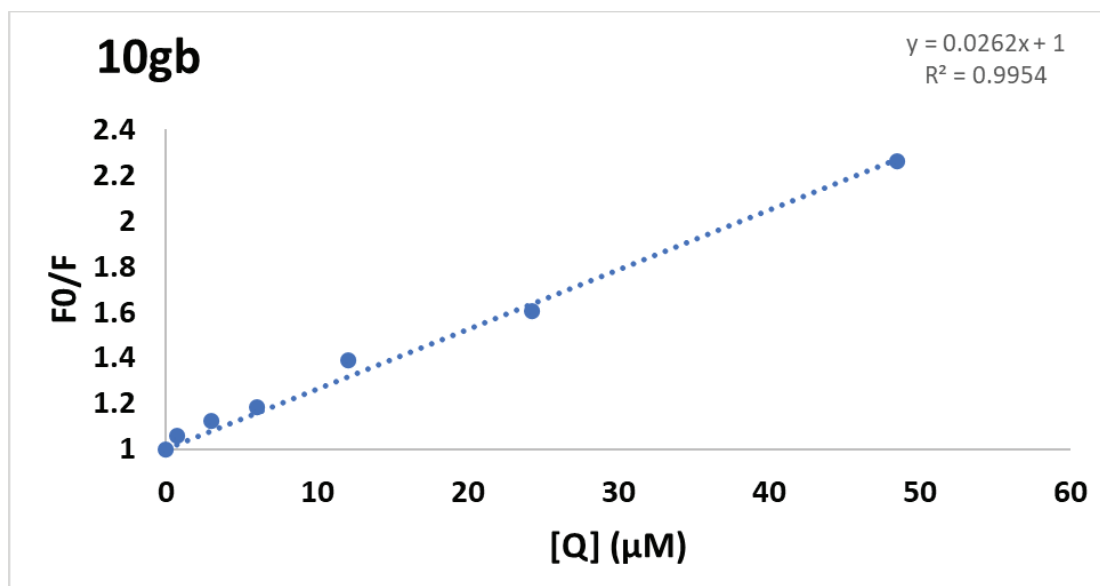
Figure 6.7. Stern-Volmer plot of PL with analogue **10gb**

The values of k_q and K_{SV} were calculated from the graph of F_0/F Vs [Q]. As shown in **Table 6.4**, the k_q value was found to be 1.65×10^{13} L mol^{-1}sec^{-1}. As the k_q values are much higher than the maximal dynamic quenching constant (2.0×10^{10} L mol^{-1}sec^{-1}), it further confirmed that the quenching caused by **10gb** is not due to dynamic quenching.[6]

Table 6.4. Values of k_q, K_{SV} and n, K_b obtained from Stern-Volmer and double logarithmic plot

Analogue	$K_{SV}/10^4$ (L mol^{-1})	$k_q/10^{13}$ (L mol^{-1}sec^{-1})	n	$K_b/10^5$
10gb	2.62	1.65	0.57	2.97

Further, the binding constant (K_b) and number of binding sites (n) were calculated using double logarithmic Stern-Volmer equation, explained in chapter 3 (**Formula 3.3**).

From the plot of log[(F_0-F)/F] *Vs* log [Q], the value of number of binding sites (n) was found to be 0.57 with high binding constant value of 2.97×10^5 L mol^{-1} at 298 K temperature (**Figure 6.8**). As the value of n was closer to 1, it indicated that the analogue **10gb** bind at one binding site of PL enzyme.
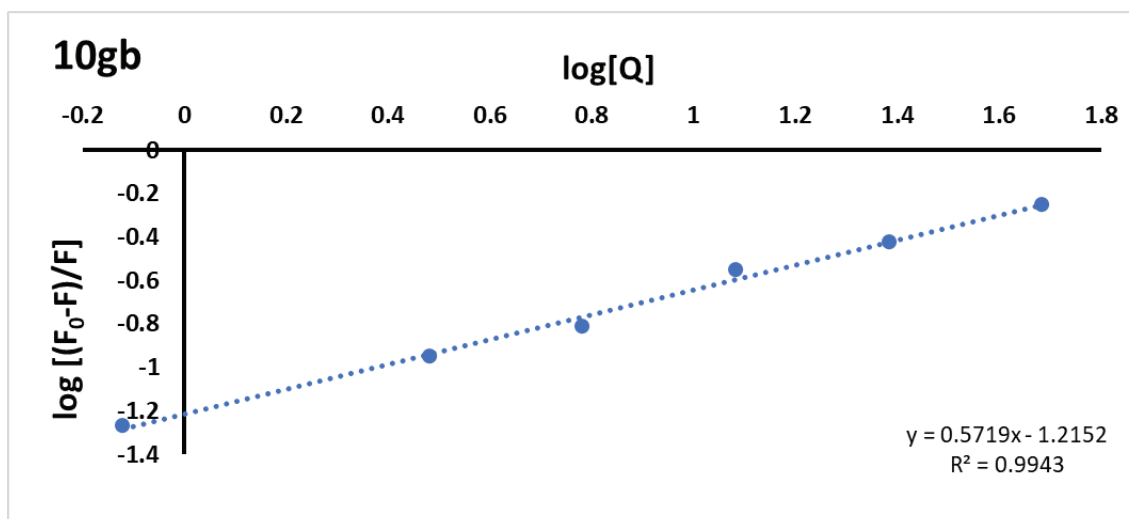
Figure 6.8. Double logarithmic plot for the calculation of binding constant (K_b) and number of binding sites (n)

6.4. Molecular Modelling Studies

6.4.1. Molecular Docking Study

The molecular docking study of the synthesized analogues was performed using the protocol detailed in chapter 3. Briefly, the MVD software was utilized[10] with previously validated grid parameters.[5] The MolDock score and various interactions obtained after docking study were analyzed and are depicted in **Table 6.5**. All the synthesized analogues of the series exhibited higher docking score in the range of -151.81 to -193.09 kcal/mol, than orlistat (MolDock score: -139.49 kcal/mol). Among them, the analogue **10ab** exhibited highest MolDock score of -193.09 kcal/mol, with all the necessary amino acid interactions, including lid domain (Phe77, Asp79, His151, Tyr114, Phe215, etc.), catalytic (Ser152) and the interaction with Arg256 amino acid. Such results also conclude its potential inhibitory activity (IC_{50} of 1.49 ± 0.008 µM).

Table 6.5. Molecular docking results of acrylate linked chromone analogues (**10aa-ka, 10ab-gb**) and orlistat

Code	MolDock Score (kcal/mol)	Amino acid Interactions				
		H-Bond/ C-H Bond	π–π stack	π-Alkyl/ Alkyl	π -Sigma/ π-Sulfur/ Halogen bond	π-cation/ π-anion
10aa	-168.33	Phe77, Asp79, Ser152, Leu153, Arg256, His263	Tyr114, Phe215	Ala178, Pro180, Ala259, Ala260	-	Arg256
10ba	-161.72	Phe77, Ser152, Leu153, Arg256, His263	Tyr114, Phe215	Ala178, Pro180, Arg256, Ala259, Ala260	Thr255	Arg256
10ca	-169.51	Gly76, Phe77, His151, Leu153	Phe215	Ile78, Trp52, Ala259, Ala260	Ala178	Arg256
10da	-164.80	Phe77, Ser152, Leu153, Arg256, His263	Tyr114, Phe215	Ala178, Pro180, Ala259, Ala260	Thr255	Arg256
10ea	-151.81	Phe77, Ser152, Leu153, His263	Tyr114, Phe215	Tyr114, Pro180, Ala260	Leu264	Arg256
10fa	-172.72	Gly76, Phe77, His151, Leu153	Phe215	Ala259, Ala260	Ala178	Arg256
10ga	-159.22	Gly76, His151, Ser152, Arg256, His263	Tyr114, Phe215	Ile78, Ala178, Pro180, Ala260	-	Arg256
10ha	-162.16	Gly76, His151, Ser152, Arg256	Tyr114, Phe215	Ile78, Ala178, Pro180, Ile209, Ala260	-	Arg256
10ia	-162.09	His151, Ser152, His263	Tyr114, Phe215	Ile78, Ala178, Pro180, Ile209, Ala259	Ala260	Asp79, Arg256
10ja	-174.81	Phe77, Ser152, Glu179	Tyr114, His151, Phe215	Ile78, Tyr114, Ala178, Pro180, Ile209, Arg256, Ala259, Leu264	-	-
10ka	-171.91	Tyr114, Arg256	Phe215, Trp252	Phe77, Ala178, Ile209, Phe215, Arg256, Ala259, Ala260	Tyr114, Ala259	-
10ab	-193.09	Phe77, Asp79, His151, Ser152, Leu153, Arg256, His263	Tyr114, Phe215	Ala178, Pro180, Arg256, Ala259, Ala260	-	-
10bb	-170.74	Gly76, Phe77, His151, Ser152, Leu153, His263	Tyr114, Phe215	Pro180, Ile209, Ala260, Ala260, Leu264	-	Asp79, Arg256
10cb	-175.75	Gly76, Phe77, His151, Ser152, Arg256	Tyr114, Phe215	Ile78, Tyr114, Ala178, Pro180, Ala259, Ala260	-	Arg256
10db	-160.48	His151, Ser152, Leu153, His263	Tyr114, Phe215	Pro180, Ile209, Ala260, Leu264		Asp79, Arg256
10eb	-187.25	Gly76, Phe77, His151, Ser152, Leu153	Tyr114, Phe215	Ala178, Pro180, Trp252, Ala259, Ala260	-	Arg256
10fb	-189.81	Gly76, Phe77, His151, Leu153	Tyr114, Phe215	Ile78, Ala178, Ala260	-	Arg256

| **10gb** | -182.86 | Gly76, Phe77, His151, Ser152, Leu153 | Tyr114, Phe215 | Ile78, Ala178, Arg256, Ala259, Ala260 | - | Arg256 |
| **Orlistat** | -139.49 | Gly76, Phe77, Asp79, His151, Ser152, Arg256 | - | Ile78, Ile209, Ile213, Arg256, Leu264 | Phe215 | - |

As shown in **Figure 6.9**, the two phenyl rings were utilized in π-π stacking interactions with Tyr114 and Phe215 amino acids. Additionally, we hypothesize that two methoxy groups with electron donating ability, made these phenyl rings electron rich, leading to stronger π-π stacking and π-Alkyl interactions.
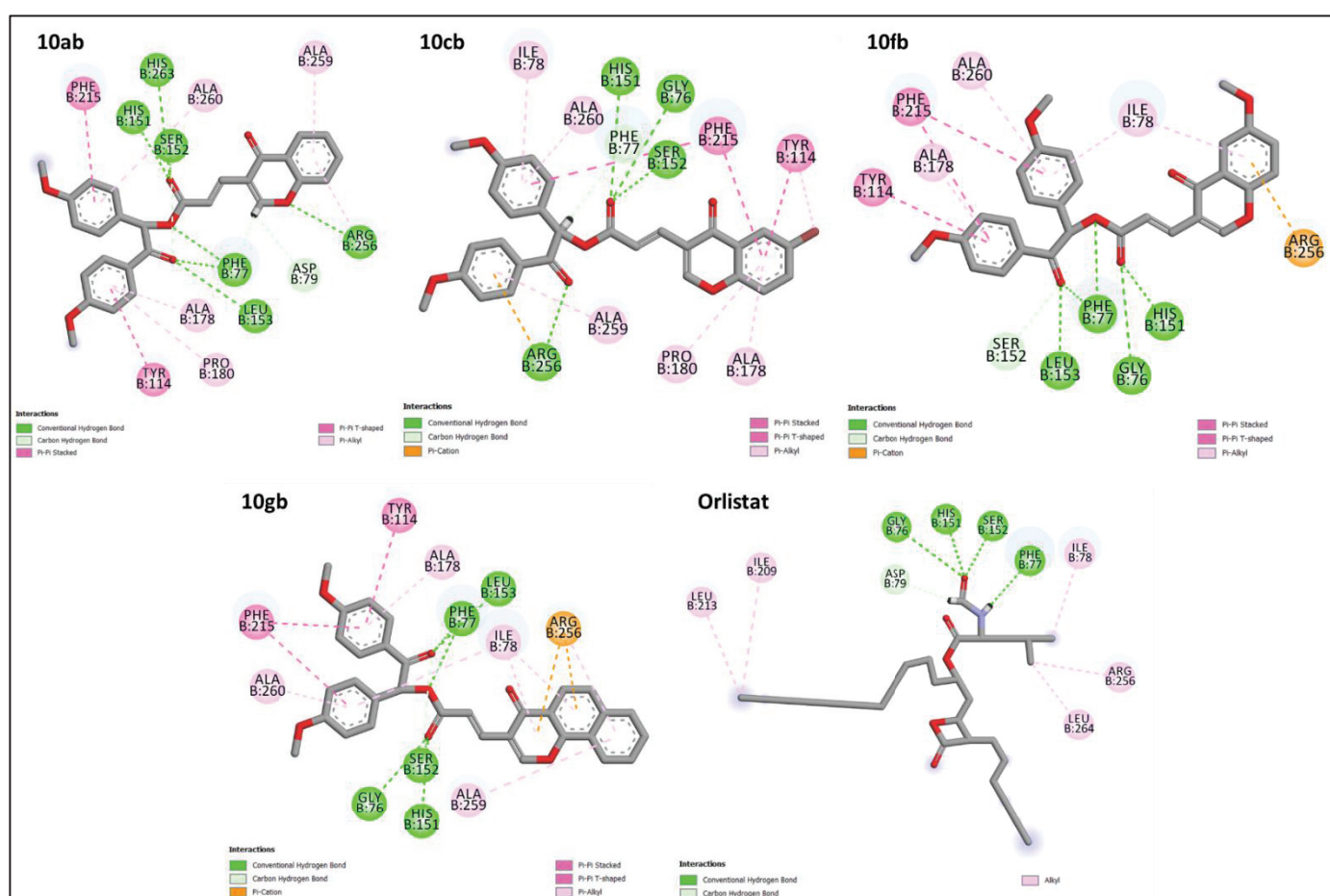
Figure 6.9. 2D interaction diagram of analogue **10ab**, **10cb**, **10fb**, **10gb** and orlistat, bound at the active site of PL enzyme (PDB ID: 1LPB)

137

Such effect gave rise to higher docking score, that finally leads to potent PL inhibition of methoxylated analogues **10ab**, **10cb**, **10fb**, **10gb** (IC_{50} in the range of 1.52-1.24 µM). For the potent analogue **10gb**, there were two π-cation and one π-alkyl interactions of fused [*h*]Benzo Chromone with Arg256, such extended interactions further give *in silico* proof of potent PL inhibitory activity (**10gb**; IC_{50} = 1.24 ± 0.296 µM).

6.4.2. Molecular Dynamics Study

The analogues **10ab**, **10cb**, **10fb**, **10gb** (IC_{50} in the range of 1.52-1.24 µM) were topmost analogues of the series. Further for understanding the stability of protein-ligand complex, the molecular dynamics simulation was performed for 100 ns. Among the above-mentioned analogues, the topmost analogue **10gb** with IC_{50} of 1.24 ± 0.296 µM was chosen for the simulation analysis. The simulation was performed at 100 ns of time interval, using NPT ensemble class, at 37 ºC temperature using detailed protocol, explained in chapter 3.[11,12] After the dynamics study, the trajectories were analyzed using RMSD plot of ligand and protein. As shown in **Figure 6.10**, throughout the simulation, most of the time the ligand RMSD was found to deviate from 5-8 Å. Also, the protein molecule exhibited the RMSD value less than 4.5 Å. Such RMSD values are within the range, that proved the stability of the ligand-protein complex.
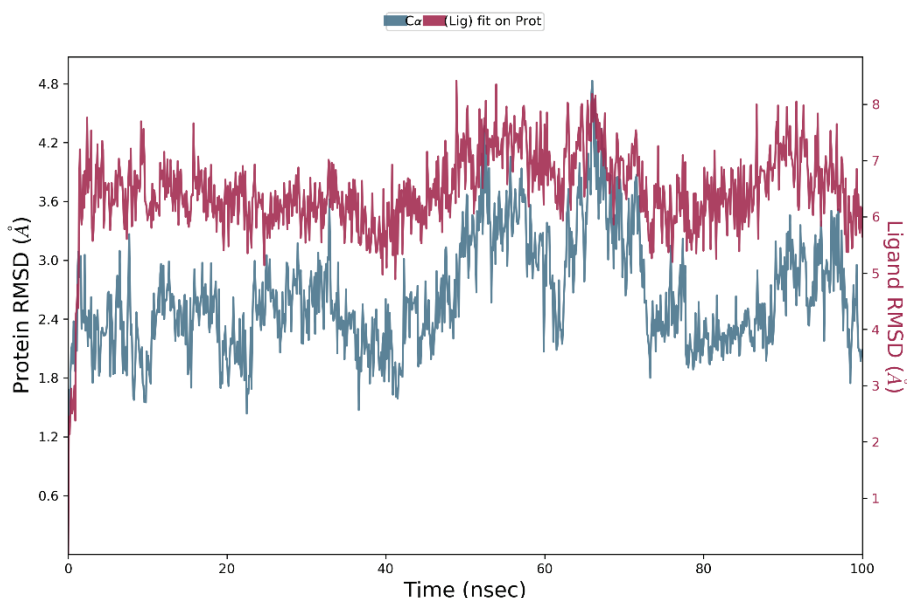
Figure 6.10. RMSD plot for protein-ligand complex of analogue **10 gb** at PL active site for 100 ns of simulation time

The PL contacts histogram and timeline was plotted for the analysis of the extent of interaction, throughout the 100 ns of simulation time. The lid domain amino acids such as,

Tyr114 and Phe215 were found to interact with the ligand for 1.2 and 0.75 fraction of time respectively. Also, there was an interaction of Ser152 and Arg256 for 0.2 and 0.3 fraction of time respectively (**Figure 6.11**).
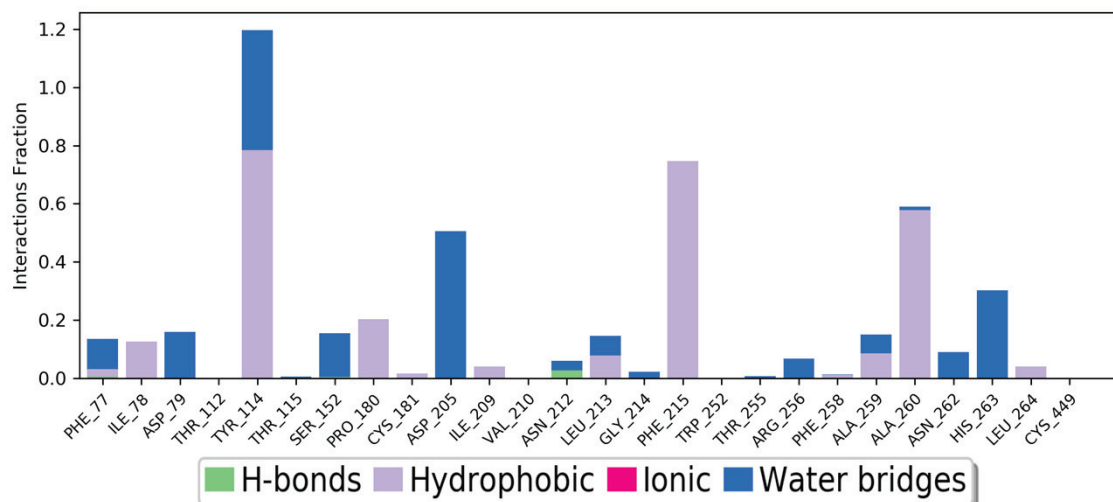
Figure 6.11. Stacked bar plot of the fraction of time of the interactions of analogue **10 gb** for 100 ns of simulation time

The PL contacts timeline also confirms the increased extent of interactions of above-mentioned amino acids (indicated by brown colour) (**Figure 6.12**). Such observations indicate lid domain opening and effective interaction of ligand at PL active site.
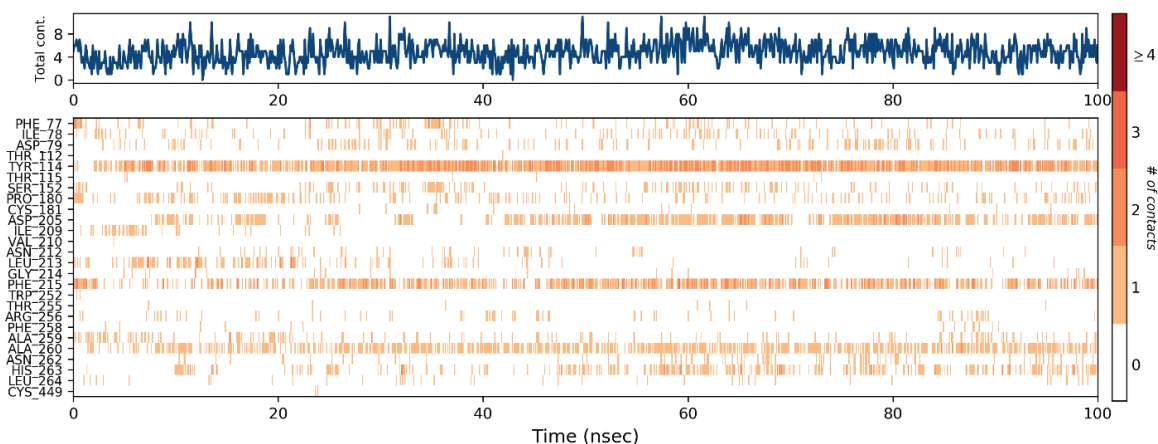
Figure 6.12. A timeline representation of protein and ligand contacts of **10gb**

Further, to analyze the part of ligand involved in interacting with above-mentioned amino acids, Ligand-protein contacts were studied. The Tyr114 amino acid was involved in interaction with chromone ring *via* π-π interaction for 43% of time (**Figure 6.13**). The methoxy group was found interact *via* water-mediated interactions with Asp 205 and His 263 for 40%, 23% of simulation time.
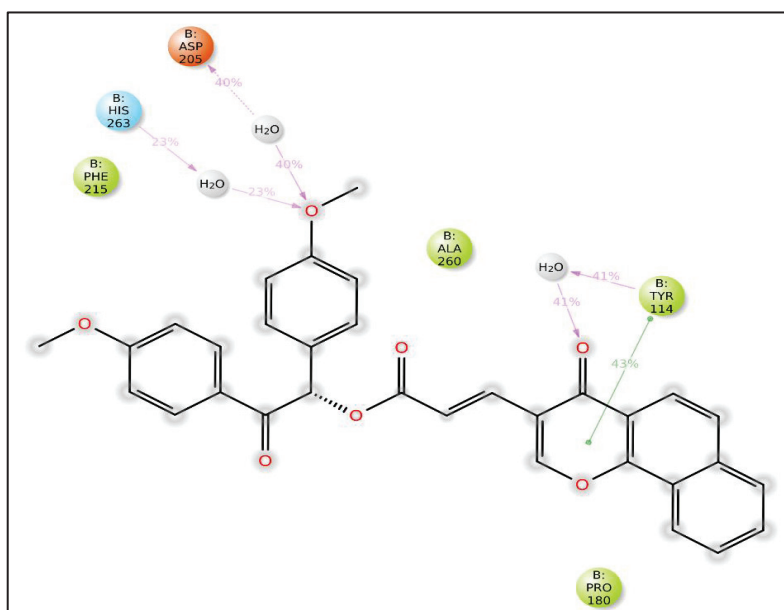
Figure 6.13. Detailed ligand-protein interactions for 100 ns of simulation time

6.5. Conclusion

In conclusion, the previously designed acrylate linked chromone analogues with the linker length of 2 carbon atoms were optimized to get further efficient PL inhibitors. For the optimization, the linker length of 2 carbon atoms was kept constant and the linker atoms were substituted with the additional phenyl ring and the oxo group for better aromatic and H-bonding interactions. Interestingly, the proposed prototype analogue **10aa** was found to bind at the active site more efficiently, as evidenced by the good MolDock score of -168.33 kcal/mol. With such positive results, we have synthesized a series of **18** analogues with EDG, EWG and bulkier substituents. All the analogues were found to bind effectively at the active site of PL with MolDock score in the range of -151.81 to -193.09 kcal/mol. These analogues exhibited effective interaction with the amino acids of lid domain and catalytic triad. A total of 6 analogues were found to exhibit IC_{50} values in the range of 1.24 - 2.76 µM. The analogue **10gb** was the most potent among all the series of analogues with IC_{50} of 1.24 ± 0.296 µM. Fluorescence quenching study confirmed the binding of analogue **10gb** at the binding site with binding constant (K_b) of 2.97×10^5 L mol^{-1}. Also, the enzyme kinetics study revealed its competitive nature of inhibition with K_i value of 0.554 µM. The MD studies of **10gb** for 100 ns proved its stability in the PL complex. Throughout the simulation for most of the time the **10gb** RMSD was found to deviate from 5-8 Å. Also, the protein molecule exhibited the RMSD value less than 4.5 Å. Further, *in vivo* anti-obesity testing may lead to development of better anti-obesity candidate.

CHAPTER 6

References:

(1)   Pervaram, S.; Ashok, D.; Reddy, C. V. R.; Sarasija, M.; Rao, B. A. Synthesis and antimicrobial activity of (*Z*)-3-{[3-oxobenzofuran-2(3H)-ylidene]methyl}-4H-chromen-4-one derivatives. *Russ. J. Gen. Chem.* **2018**, *88* (3), 566–572.

(2)   Chernov, N. M.; Shutov, R. V.; Barygin, O. I.; Dron, M. Y.; Starova, G. L.; Kuz'mich, N. N.; Yakovlev, I. P. Synthesis of chromone-containing allylmorpholines through a morita–baylis–hillman-type reaction. *European J. Org. Chem.* **2018**, 6304–6313.

(3)   George, G.; Yadav, N.; Auti, P. S.; Paul, A. T. Molecular modelling, synthesis and in vitro evaluation of quinazolinone hybrid analogues as potential pancreatic lipase inhibitors. *J. Biomol. Struct. Dyn.* **2022**, *41* (19), 9583–9601.

(4)   Auti, P. S.; Nandi, A.; Kumari, V.; Paul, A. T. Design, synthesis, biological evaluation and molecular modelling studies of oxoacetamide warhead containing indole-quinazolinone based novel hybrid analogues as potential pancreatic lipase inhibitors. *New J. Chem.* **2022**, *46* (24), 11648–11661.

(5)   Auti, P. S.; Jagetiya, S.; Paul, A. T. Chromone-3-acrylic acid ester analogues : design , synthesis and biological evaluation as potential pancreatic lipase inhibitors. *J. Mol. Struct.* **2023**, *1293*, 136257.

(6)   Martinez-Gonzalez, A. I.; Alvarez-Parrilla, E.; Díaz-Sánchez, Á. G.; de la Rosa, L. A.; Núñez-Gastélum, J. A.; Vazquez-Flores, A. A.; Gonzalez-Aguilar, G. A. In vitro inhibition of pancreatic lipase by polyphenols: A kinetic, fluorescence spectroscopy and molecular docking study. *Food Technol. Biotechnol.* **2017**, *55* (4), 519–530.

(7)   Li, Y. Q.; Yang, P.; Gao, F.; Zhang, Z. W.; Wu, B. Probing the interaction between 3 flavonoids and pancreatic lipase by methods of fluorescence spectroscopy and enzymatic kinetics. *Eur. Food Res. Technol.* **2011**, *233* (1), 63–69.

(8)   Ramos, P.; Coste, T.; Piémont, E.; Lessinger, J. M.; Bousquet, J. A.; Chapus, C.; Kerfelec, B.; Férard, G.; Mély, Y. Time-resolved fluorescence allows selective monitoring of TRP30 environmental changes in the seven-TRP-containing human pancreatic lipase. *Biochemistry* **2003**, *42* (43), 12488–12496.

(9)   Zhang, J.; Xiao, L.; Yang, Y.; Wang, Z.; Li, G. Lignin binding to pancreatic lipase and its influence on enzymatic activity. *Food Chem.* **2014**, *149*, 99–106.

(10) George, G.; Auti, P. S.; Sengupta, P.; Paul, A. T. Design and synthesis of echitamine-inspired hybrid analogues containing thiazolidinediones as potential pancreatic lipase inhibitors. *Lett. Drug Des. Discov.* **2022**, *19* (11), 956–968.

(11) Nandi, A.; Auti, P. S.; Jagtap, U. A.; Paul, A. T. Investigating the role of indole and quinazolinone-based hybrid analogues with ketoamide fragment and alkyl extension for potential pancreatic lipase inhibition. *J. Mol. Struct.* **2024**, *1301*, 137337.

(12) Jagetiya, S.; Auti, P. S.; Paul, A. T. Design, synthesis, molecular modelling and in vitro evaluation of indolyl ketohydrazide-hydrazone analogs as potential pancreatic lipase inhibitors. *Chem. Biodivers.* **2023**, *20* (9) 1-16.

CHAPTER 7

ADMET PREDICTION & IN VIVO EXPERIMENTS

CHAPTER 7

7. ADMET Prediction and *In vivo* Experiments

7.1. Rationale

Previous chapters discussed with the design of chromone based analogues as potential PL inhibitors through structure-based drug design and literature survey. It was then followed by various structural optimizations to get the potent lead **10gb** with an IC_{50} value of 1.24 ± 0.296 μM. As we know, *in vitro* activity alone cannot prove the therapeutic effect of any of the drug candidates. Hence, in the drug discovery process, *in vivo* studies are prerequisites for proving the desired effect of any therapeutic candidate. Also, many of the potential lead candidates with good *in vitro* activity may show deterioration in *in vivo* activity because of poor pharmacokinetic parameters.[1–3] These pharmacokinetic parameters are absorption, distribution, metabolism, excretion and toxicity (commonly known as ADMET parameters). Such parameters should be optimum to get the desired pharmacological effect. Therefore, in this study we aimed to predict the ADMET parameters of two topmost leads of each series through *in silico* study. As, ADMET parameters directly affect the *in vivo* performance of drug, such prediction were followed by the *in vivo* anti-obesity testing of the topmost analogue of all the series using a high-fat diet (HFD) induced obesity model.

7.2. Materials and Methods
7.2.1. *In silico* ADMET Prediction

Based on the *in vitro* activities, 6 analogues were selected for ADMET prediction through in silico tools. Free web servers such as Swiss ADME and ProTox-2 were used. Various parameters such as GI absorption, BBB permeation, Pgp substrate ability, metabolism via various CYP enzymes and toxicities were predicted.

7.2.2. *In vivo* Anti-Obesity Study
7.2.2.1. Experimental Protocol

All the experimental procedures on animals were in compliance with the Institutional Animal Ethics Committee of BITS Pilani (Ref No: IAEC/RES/33/07). Briefly, the protocol was divided into three phases.

  i)   Oral Triglyceride Tolerance Test
  ii) Anti-obesity studies (4 weeks treatment)
  iii) Quantification of fecal triglycerides

CHAPTER 7

7.2.2.2. Animals and Diet

For the experiment, Swiss albino mice (Male with the weight of 15–20 g) were purchased from the Central Animal House of Birla Institute of Technology and Science, Pilani (BITS Pilani), Pilani Campus, India (CPCSEA Reg. Number: 417/PO/ReBi/2001/CPCSEA). They were housed in polyacrylic cages and maintained under standard conditions (room temperature $22 \pm 1°C$ and relative humidity of 60%) with a 12 h light/dark cycle.

i) Oral Triglyceride Tolerance Test (OTTT)

To preliminarily examine the *in-vivo* effect of **10gb** on the intestinal absorption of triglycerides and rationalising its dose for anti-obesity effect (4 week treatment regimen), OTTT was performed according to the previously reported protocol [4,5]. The mice were divided into six groups (n=6) and were deprived of food for 12 h before the experiment. The dose of orlistat was considered as 10 mg/kg. Low (5 mg/kg), medium (10 mg/kg) and high dose (20 mg/kg) of test analogue (**10gb**) were evaluated for triglyceride absorption. The mice were orally administered with (1) olive oil as a positive control, (2) filtered water as a negative control, (3) olive oil plus orlistat (10 mg/kg) as reference control (4) olive oil plus **10gb** (Low, medium and high dose). The amount of olive oil administered per animal was fixed to 5 mL/kg. After the administration of olive oil, blood samples were collected at 0, 1.5, 3, 4.5, and 6 h, and the level of triglyceride was determined using commercially available kits (Spinreact S.A.U, Spain).

ii) Anti-Obesity Study

The HFD-induced obesity model was utilized for the development of obesity in the mice. Five groups (**Table 7.1**) were considered, and each group included 7 animals (except for the control group, n=6). The animals were fed with either a normal pellet diet (NPD) or HFD and filtered water *ad libitum*. The anti-obesity effect of **10gb** was determined by the administering it to HFD fed mice over 4 weeks at 2 dose levels (medium & high). [6,7]

Table 7.1 Summary of various groups and drugs administered for the *in-vivo* experiments

#	Animal Group	Drug and Dose
1.	Normal pellet diet / Normal Control (NC)	-
2.	High Fat Diet (HFD) / Disease Control (DC)	-
3.	HFD + Orlistat (10 mg/kg)	Orlistat (10 mg/kg)
4.	HFD + Low dose	10gb (10 mg/kg)
5.	HFD + High dose	10gb (20 mg/kg)

Before the treatment, animals were feeded with HFD, except for NC group for 6 weeks. The HFD used for the study is summarized in **Table 7.2**, and it contained 20% protein, 45% lipids and 35% carbohydrates by weight. [8] It was then followed by the examination of weight and serum triglyceride parameters to determine the induction of obesity.

Table 7.2 Composition of the HFD used in the *in-vivo* experiments.

Ingredients	Qty (g/kg)	Ingredients	Qty (g/kg)
Casein	200	Lard	245
L-Cysteine	3	Soybean oil	25
Starch	125	Vitamin and mineral mix	53
Sucrose	72.8	NaCl	10
Cellulose	50	Cholic acid	2

After the induction of obesity, **10gb/orlistat** was dissolved in 0.3 %v/v CMC and administered to the animals using oral gavage. The body weights of the animals were recorded weekly. At the end of the study, animals were subjected to an overnight fasting, followed by the collection of blood samples using the retro-orbital puncture. The serum was separated by the centrifugation of blood samples (1500 G). Various biochemical parameters including glucose, triglycerides (TG), total cholesterol (TC), and high-density lipoproteins-cholesterol (HDL) were estimated from the serum using commercially available diagnostic kits (Spinreact S.A.U., Spain and Accurex Biomedical Pvt. Ltd., India). The low-density lipoprotein-cholesterol (LDL) was calculated using the following formula. [9]

$$LDL = [(TC - HDL)*0.9] - [TG*0.1]$$……………………. **Formula 7.1**

iii) Quantification of Fecal Triglycerides

The inhibition of PL is characterized by the excretion of feces rich in triglycerides. The feces of the mice were collected during the 4-week treatment period, and triglycerides were quantified. The quantification of fecal triglycerides was performed as per the procedure reported in the literature. [4,10–12] Briefly, 1g of feces were taken in a separatory funnel and was subjected to vigorous shaking with 0.15 M NaCl. To this suspension, chloroform/methanol (4:1, % v/v) was added and the mixture was allowed to separate. The lower organic phase was collected, filtered and dried *in vacuo*. The obtained triglycerides were dissolved in 1 mL

ethanol, and the triglyceride quantification was performed using a commercial kit (Spinreact S.A.U., Spain).

7.2.2.3. Statistical Analysis

The data was represented as mean ± S.E.M, and the differences were analysed using one-way analysis of variance (ANOVA) followed by post-hoc analysis of Tukey's multiple comparison test to determine significant differences between the groups. Statistical calculation was performed using GraphPad Prism (v 5.0). A level of $p < 0.05$ was considered to be statistically significant.

7.3. Results and Discussion

7.3.1. *In silico* ADMET Prediction

The *in silico* ADMET prediction was performed using Swiss ADME and ProTox-2 web servers.[13–15] For the ADMET prediction, top 2 analogues were selected in each series. The results of the ADMET screening were compared with orlistat. As shown in **Table 7.3**, the GI absorption of series-I and II analogues were high, may be due to optimum polarity and low molecular size. Orlistat, being a potent PL inhibitor exhibited low GI absorption. As the PL enzyme is present in periphery, the drug is expected not to enter into the systemic circulation, and even if it enters into the circulation then it should not penetrate the blood brain barrier (BBB) to avoid toxicity issues. It was observed that except **5am**, all the analogues were devoid of BBB penetration. In case of toxicity prediction, except **5ad**, none of the analogue was found to possess any toxicity, namely hepatotoxicity, cytotoxicity and carcinogenicity.

Table 7.3. Summary of *in silico* predicted ADMET parameters for the potential analogues from each series and orlistat

Series	Analogues	GI absorption	Distribution		Metabolism Inhibition					Toxicity		
			BBB Permeation	Pgp Substrate	CYP 1A2	CYP 2C19	CYP 2C9	CYP 2D6	CYP 3A4	Hepato toxic	Cyto toxic	Carcino genic
I	**5ad**	High	No	No	Yes	Yes	Yes	No	No	No	inactive	Yes
	5am	High	Yes	No	Yes	Yes	Yes	No	Yes	No	inactive	No
II	**6fj**	High	No	No	Yes	Yes	Yes	No	Yes	No	inactive	No
	6gj	High	No	No	Yes	Yes	Yes	No	Yes	No	inactive	No
III	**10fb**	High	No	No	Yes	No	Yes	No	Yes	No	inactive	No
	10gb	High	No	No	Yes	No	Yes	No	Yes	No	inactive	No
Ref	**Orlistat**	Low	No	Yes	No	No	Yes	No	No	Yes	Weak	No

Also, for all analogues, the predicted LD_{50} value was found to be 3850 mg/kg, that is very high concentration value, ensuring the safety profile of all the screened analogues. All the predicted results were favourable and there were no predicted toxicity. Finally based on the overall activity and ADMET profile, analogue **10gb** was selected for the *in vivo* anti-obesity testing using HFD induced mice model.

7.3.2. *In vivo* Anti-Obesity Study

7.3.2.1. Oral Triglyceride Tolerance Test (OTTT)

For the selection of the dose of analogue **10gb**, the OTTT study was performed on mice.[4,5] After the ingestion of olive oil, the effect of various doses (5, 10, 20 mg/Kg) of **10gb** on the inhibition of fat absorption was determined. The study was performed as discussed in the methodology section. In case of the oil control group, there was a time-dependent increase in serum triglyceride levels after the ingestion of oil. On the other hand, after the ingestion of orlistat (10 mg/kg), along with oil, triglyceride levels were found to decrease as compared with oil control group. Such observation confirmed the inhibitory activity of orlistat on fat metabolism. All such results are depicted in graphical representation in **Figure 7.1**,
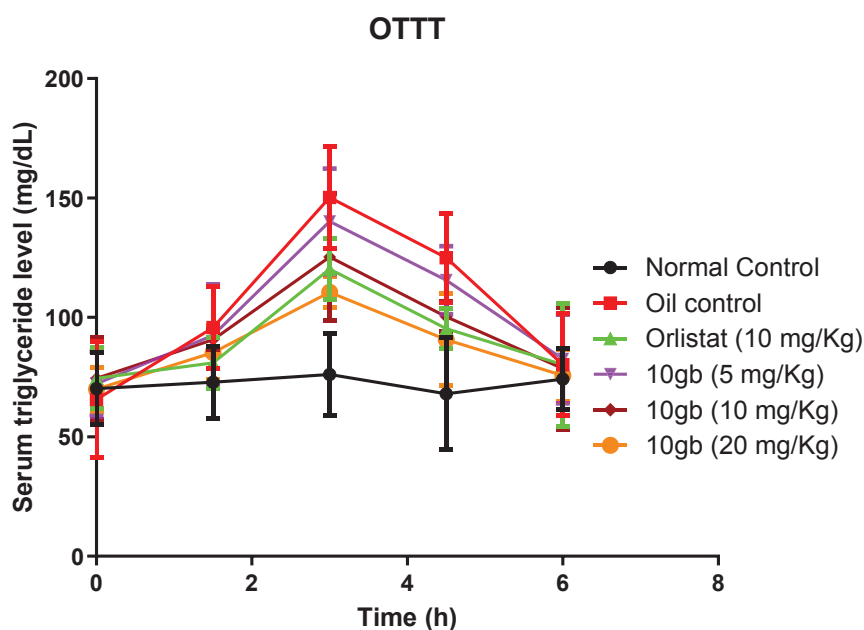
Figure 7.1. Effect of **10gb** and orlistat on OTTT (n = 6)

Interestingly, in case of high (20 mg/kg) and medium dose (10 mg/kg) of analogue **10gb**, the similar results were observed. The high dose analogue was found to decrease triglyceride absorption more efficiently than orlistat. Unfortunately, a lower dose (5 mg/kg) of **10gb** failed to inhibit the triglyceride absorption. Based on the above results, high and medium

doses of analogue **10gb** (20 mg/kg and 10 mg/kg) were selected for the 4-week treatment of HFD-induced obese mice. The reported dose of orlistat (10 mg/kg) was chosen for the comparison.

7.3.2.2. Anti-Obesity Study (4 Week Treatment)

The *in vivo* anti-obesity effect of analogue **10gb** was determined for four weeks on HFD-induced mice.[6,7] Two doses, i.e., 20 mg/kg (High Dose) and 10 mg/kg (Low Dose) were administered through oral route. The reference standard used was orlistat at the dose of 10 mg/kg. After each week the weight of animals were measured to determine the effect of drug. **Figure 7.2** shows the effect of **10gb** and orlistat on weight reduction compared to disease control (DC) and Normal control (NC) groups.
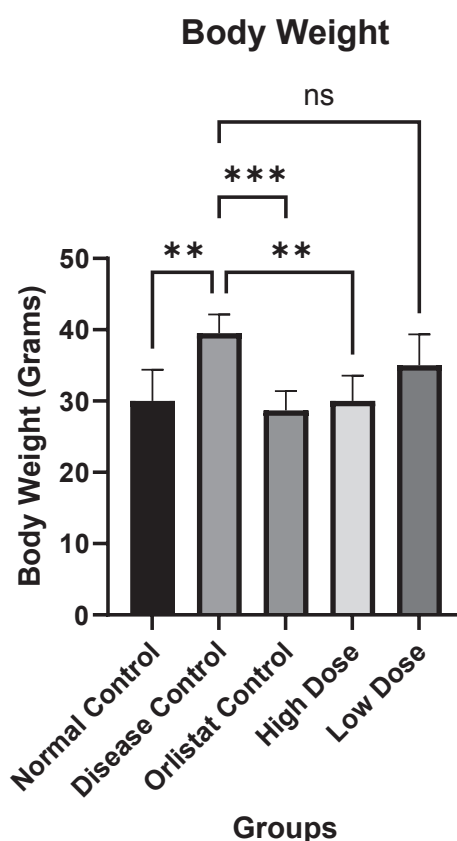
Figure 7.2. Body weight of animals, after 4 weeks of treatment. The values are represented as mean ± SEM. ***p ≤ 0.001, DC *vs* orlistat; **p ≤ 0.01, DC vs **10gb** (20 mg/Kg) and NC *vs* DC, n = 6

There was a significant increase in body weight of DC group as compared with the NC, confirming the effect of HFD. Orlistat was observed to decrease the weight of animals significantly when compared with the DC group. The effect of a high dose (HD) of **10gb** was similar to that of orlistat. The low dose (LD) of **10gb** was also efficient in weight reduction

but not as effective as orlistat and HD of **10gb**. Further, the effect of **10gb** on various serum parameters (triglyceride, total cholesterol, HDL cholesterol, LDL cholesterol and glucose) was tested and the results are summarized in **Figure 7.3**.
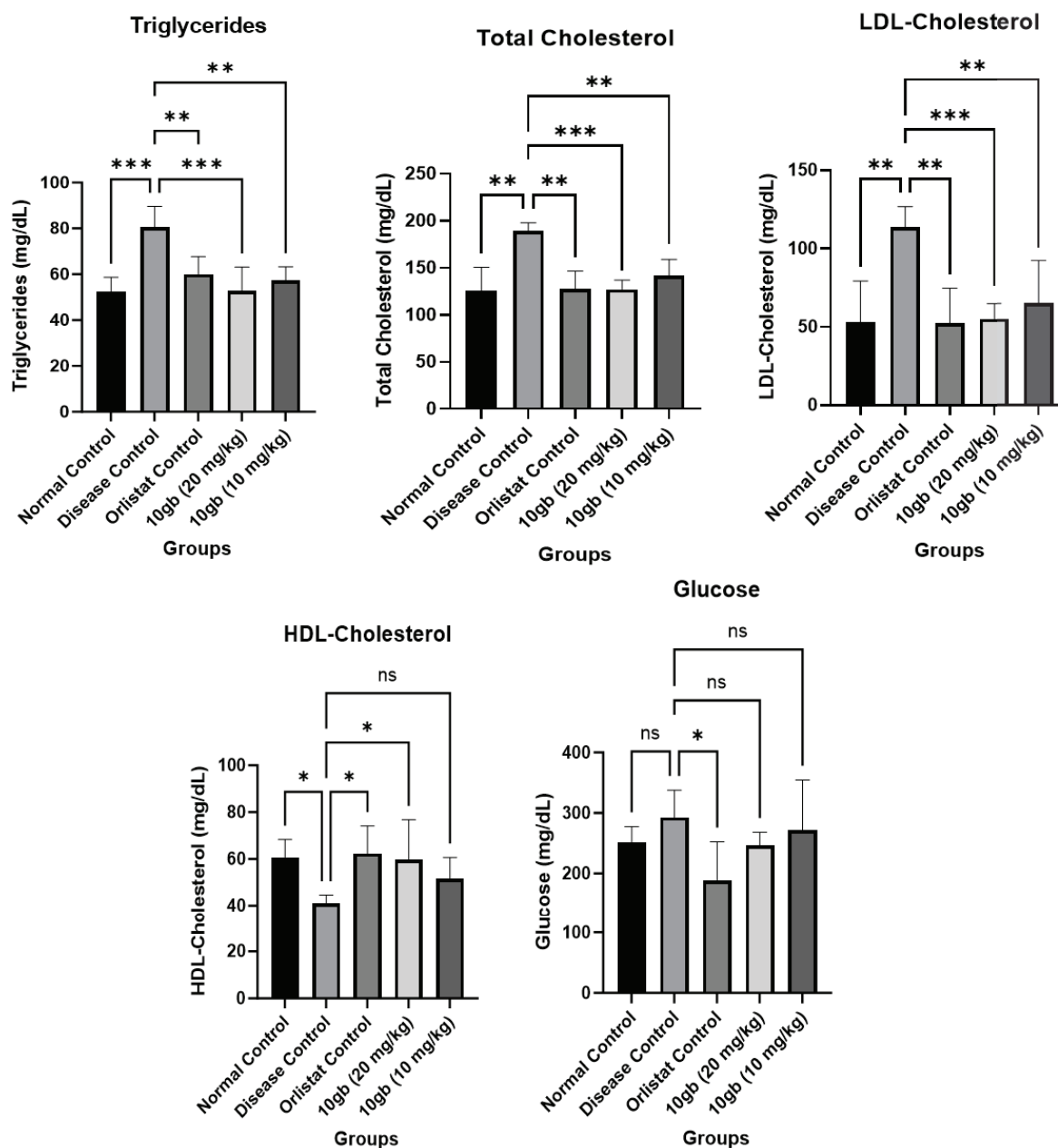
Figure 7.3. The effect of **10gb** and orlistat on various biochemical parameters determined after the treatment period. The values are represented as mean ± SEM. ***$p \leq 0.001$; **$p \leq 0.01$; *$p \leq 0.05$, n = 6

For DC group, there was a significant increase in triglyceride and total cholesterol as compared with the NC group. Orlistat was found to normalize these parameters to the same level as the NC group. Delightedly, we observed that, HD and LD of **10gb** were much

efficacious in decreasing the serum triglyceride levels. The HD analogue also decreased serum total cholesterol levels, more effectively than orlistat and the decrease in total cholesterol levels of LD group was similar as that of orlistat control group.

7.3.2.3. Fecal Triglycerides Quantification

As described before, the PL enzyme is responsible for fat digestion and hence helps in its absorption. The inhibition of fat digestion will lead to unabsorbed triglycerides in the intestine, which will get excreted through the feces, giving rise to steatorrhea as one of the side effects of such medications. Through PL inhibitory screening, the analogue **10gb** was found to exhibit potent IC_{50} value of 1.24 ± 0.296 µM. Further through *in vivo* study, it was observed to normalize the various serum parameters including triglycerides, total cholesterol, HDL and LDL cholesterol, with a reduction in the body weight of animals. Hence, to investigate the PL inhibitory action, after the ingestion of **10gb**, the fecal matter of all the animals were collected at the end of each week during the treatment period, followed by its triglyceride measurement.[4,10–12] As shown in **Figure 7.4**, a high level of triglycerides was observed in HD and LD groups, as compared with the DC group.

Fecal triglycerides
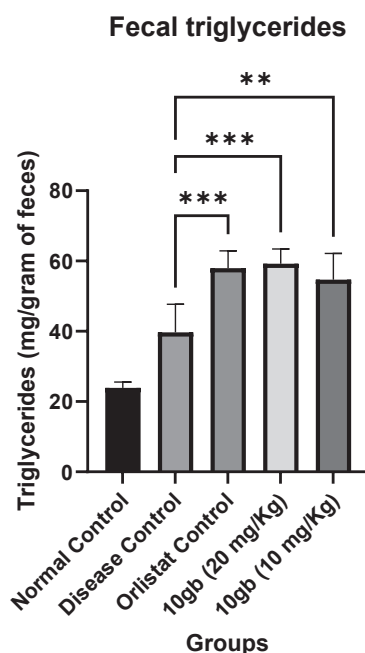
Figure 7.4. Faecal triglyceride levels determined from various groups. The values are represented as mean ± SEM; *** p ≤ 0.001, DC vs orlistat control and DC vs **10gb** (20 mg/kg); ** p ≤ 0.01, DC vs **10gb** (10 mg/Kg), n = 6

7.3.2.4. Histopathological Studies

Further histopathological changes caused by HFD were studied using liver and adipose tissue of the mice. There are several reports of hepatic ballooning and fibrosis in liver and adipose tissue of obese rodents, and it is considered as a characteristic feature of obesity. For the observation of such changes, two stains namely, H&E and picrosirius red were used.

As shown in **Figure 7.5**, the hepatic ballooning was observed due to the lipid accumulation in DC group. There was no such lipid accumulated area in NC group, due to the absence of HFD. In case of OC and **10gb** (HD group), the hepatic ballooning was reduced as compared with **10gb** (LD group).
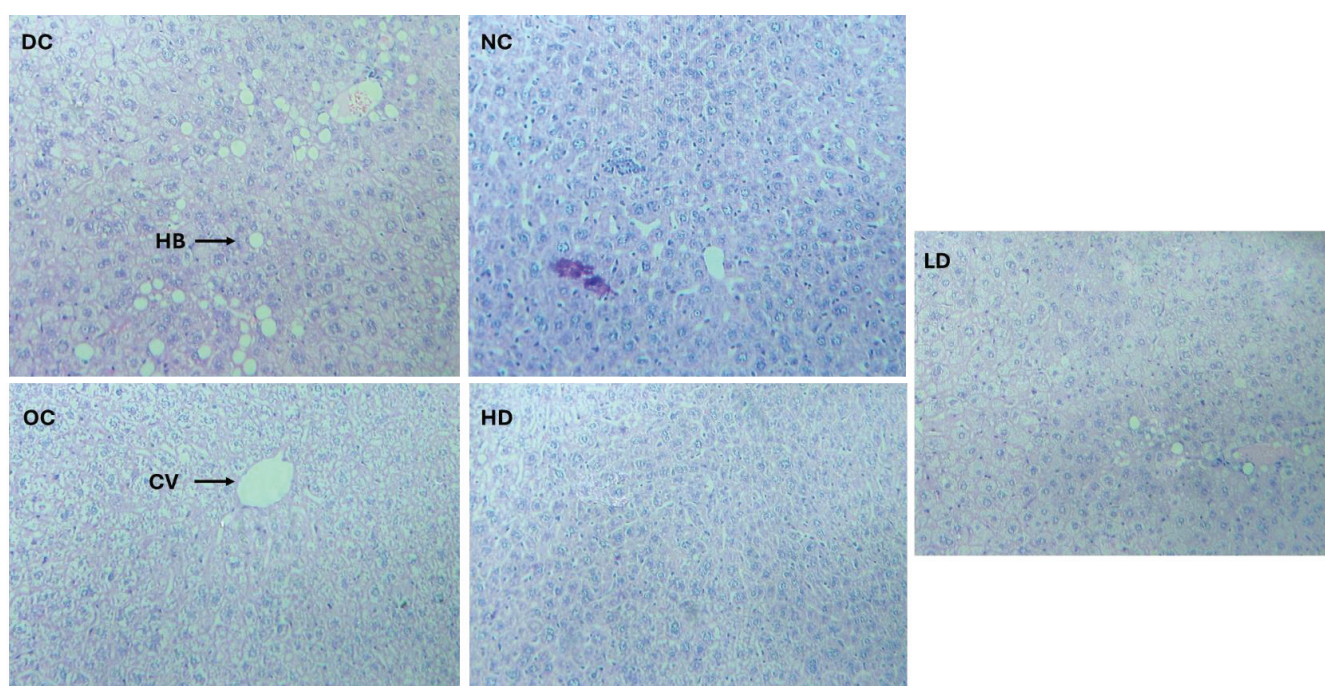
Figure 7.5. H&E staining of liver, after the treatment of **10gb** and orlistat (DC: Disease control; NC: Normal control; OC: Orlistat control; HD: High dose of **10gb**; LD: low dose of **10gb**; HB: Hepatic ballooning, CV: Central vein)

In picrosirius red staining of liver tissue, the fibrosis with collagen deposition was observed for DC group (**Figure 7.6**). Such changes were absent in NC group. After the treatment of HFD induced obese mice with **10gb** (HD) and orlistat, the condition was found to normalized.
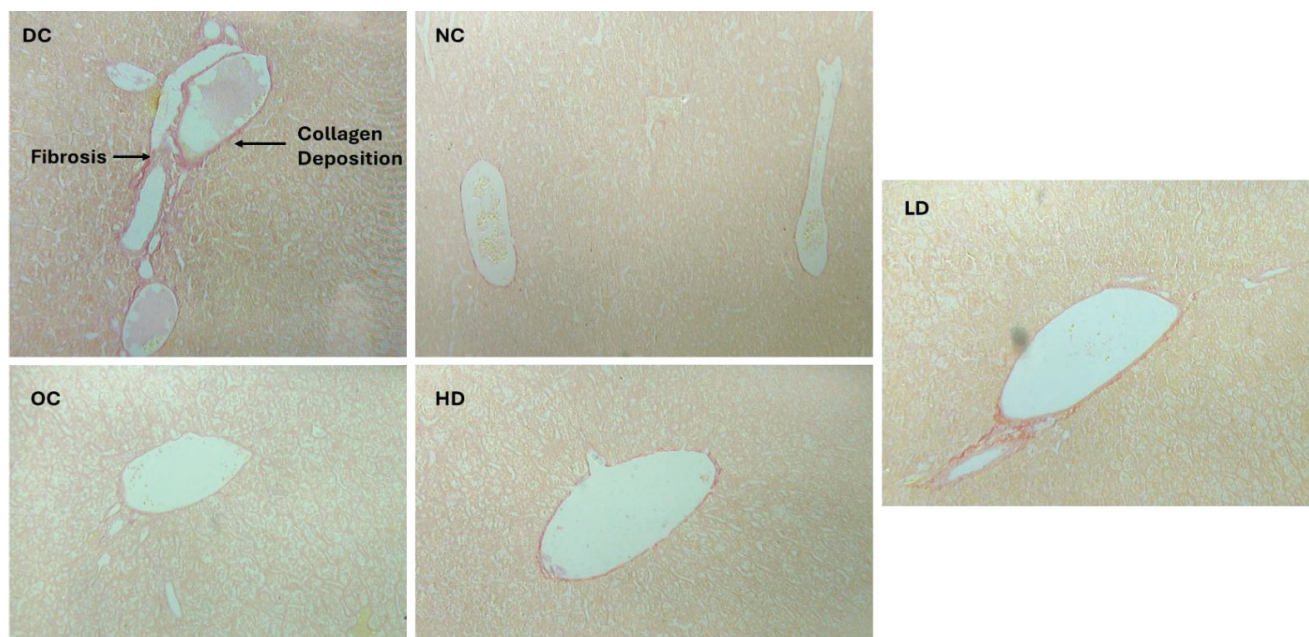
Figure 7.6. Picrosirius red staining of liver, after the treatment of **10gb** and orlistat (DC: Disease control; NC: Normal control; OC: Orlistat control; HD: High dose of **10gb**; LD: low dose of **10gb**)

After the histopathology of adipose tissue (**Figure 7.7**), the size of the adipocytes was found to enlarged in DC group (HFD without treatment) as compared with NC group (with normal pellet diet). Such enlargement may be due to the increased accumulation of triglycerides. For OC and **10gb** (HD) groups such enlargement was reduced to normal, as compared with **10gb** LD group)
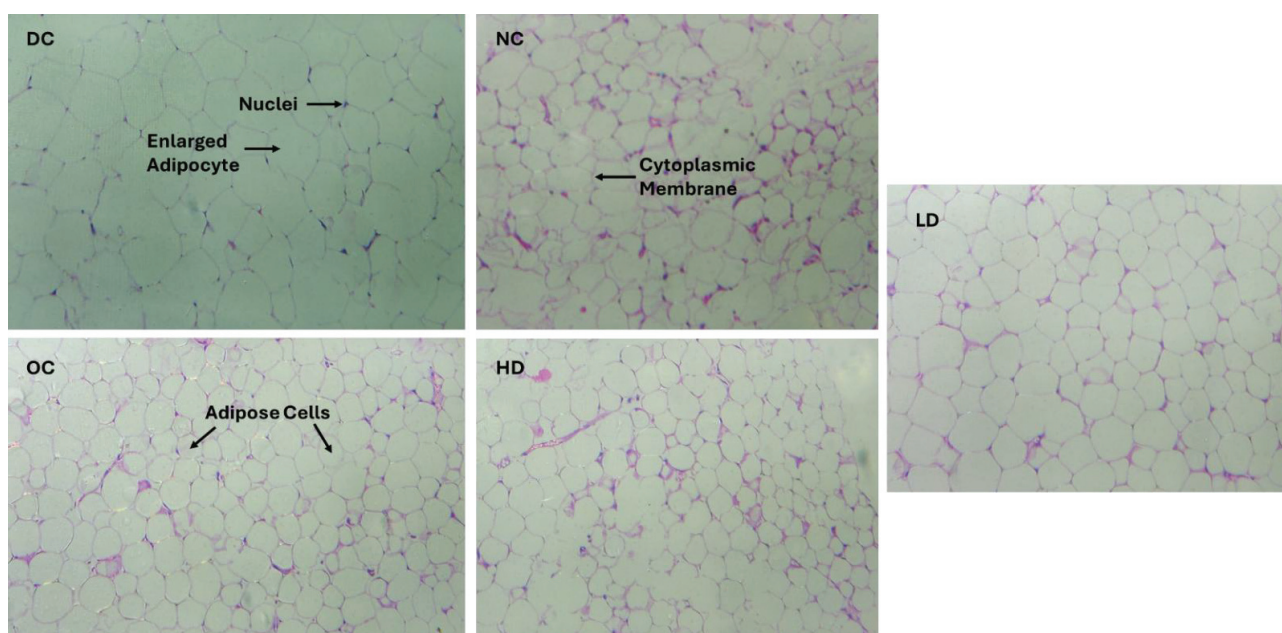
Figure 7.7. H&E staining of adipose tissue, after the treatment of **10gb** and orlistat (DC: Disease control; NC: Normal control; OC: Orlistat control; HD: High dose of **10gb**; LD: low dose of **10gb**)

7.4. Conclusion

In conclusion, the *in silico* ADMET prediction of top analogues of each series (I, II & III) was performed for the visualization of pharmacokinetic parameters. It was then followed by *in vivo* anti-obesity effect of **10gb** (topmost analogue of all the series) using HFD-induced mice model. Through *in silico* ADMET prediction, the analogue **10gb** was found to be devoid of any toxicities and could not penetrate BBB, which depicted its safety. Through *in vivo* screening, **10gb** was found to cause significant weight reduction in obese mice. Further, it also exhibited the normalization of the serum parameters (triglycerides, total cholesterol, HDL and LDL cholesterol) in high dose (20 mg/kg). In addition, the triglyceride excretion caused by **10gb** was also proved through fecal triglyceride measurement. After the histopathological examination of liver and adipose tissue, hepatic fibrosis and lipid accumulation with the increase in size of adipocytes were observed for DC group (HFD without treatment). Such changes were found to be normalized in case of orlistat and **10gb** (HD) treatment groups. There was slight improvement in **10gb** (LD) treatment group. Such effects were comparable to orlistat. Hence, it was concluded that **10gb** exhibited a comparable anti-obesity potential as that of orlistat.

CHAPTER 7

References

(1)   Singh, S. Preclinical pharmacokinetics: An approach towards safer and efficacious drugs. *Curr. Drug Metab.* **2006**, *7* (2), 165–182.

(2)   Cars, O. Efficacy of β-lactam antibiotics : Integration of pharmacokinetics and pharmacodynamics. *Diagn Microbiol Infect Dis.* **1997**, *27*(1-2):29-33

(3)   Dalhoff, A.; Ullmann, U. Correlation between pharmacokinetics, pharmacodynamics and efficacy of antibacterial agents in animal models. *Eur. J. Clin. Microbiol. Infect. Dis.* **1990**, *9* (7), 479–487.

(4)   Chen, T. Y.; Wang, M. M. C.; Hsieh, S. K.; Hsieh, M. H.; Chen, W. Y.; Tzen, J. T. C. Pancreatic lipase inhibition of strictinin isolated from pu'er tea (Cammelia sinensis) and its anti-obesity effects in C57BL6 mice. *J. Funct. Foods* **2018**, *48*, 1–8.

(5)   Pai, S. A.; Martis, E. A. F.; Joshi, S. G.; Munshi, R. P.; Juvekar, A. R. Plumbagin exerts antiobesity effects through inhibition of pancreatic lipase and adipocyte differentiation. *Phyther. Res.* **2018**, *32* (8), 1631–1635.

(6)   Avci, G.; Küçükkurt, I.; Küpeli Akkol, E.; Yeşilada, E. Effects of escin mixture from the seeds of Aesculus hippocastanum on obesity in mice fed a high fat diet. *Pharm. Biol.* **2010**, *48* (3), 247–252.

(7)   Han, L. K.; Kimura, Y.; Kawashima, M.; Takaku, T.; Taniyama, T.; Hayashi, T.; Zheng, Y. N.; Okuda, H. Anti-obesity effects in rodents of dietary teasaponin, a lipase inhibitor. *Int. J. Obes.* **2001**, *25* (10), 1459–1464.

(8)   Pesta, D. H.; Samuel, V. T. A high-protein diet for reducing body fat: Mechanisms and possible caveats. *Nutrition and Metabolism.* **2014,** *11*, 53

(9)   Chen, Y.; Zhang, X.; Pan, B.; Jin, X.; Yao, H.; Chen, B.; Zou, Y.; Ge, J.; Chen, H. A modified formula for calculating low-density lipoprotein cholesterol values. *Lipids Health Dis.* **2010**, *9* (1), 52.

(10)   Grove, K. A.; Sae-Tan, S.; Kennett, M. J.; Lambert, J. D. (-)-Epigallocatechin-3-gallate inhibits pancreatic lipase and reduces body weight gain in high fat-fed obese mice. *Obesity* **2012**, *20* (11), 2311–2313.

(11)   Harach, T.; Aprikian, O.; Monnard, I.; Moulin, J.; Membrez, M.; Béolor, J. C.; Raab,

T.; MacÉ, K.; Darimont, C. Rosemary (Rosmarinus officinalis l.) leaf extract limits weight gain and liver steatosis in mice fed a high-fat diet. *Planta Med.* **2010**, *76* (6), 566–571.

(12)   Uchiyama, S.; Taniguchi, Y.; Saka, A.; Yoshida, A.; Yajima, H. Prevention of diet-induced obesity by dietary black tea polyphenols extract in vitro and in vivo. *Nutrition* **2011**, *27* (3), 287–292.

(13)   Daina, A.; Michielin, O.; Zoete, V. SwissADME: A free web tool to evaluate pharmacokinetics, drug-likeness and medicinal chemistry friendliness of small molecules. *Sci. Rep.* **2017**, *7* (1), 1–13.

(14)   Lagunin, A.; Zakharov, A.; Filimonov, D.; Poroikov, V. QSAR modelling of rat acute toxicity on the basis of pass prediction. *Mol. Inform.* **2011**, *30* (2–3), 241–250.

(15)   Sander, T. *Molecular Properties Prediction - Osiris Property Explorer*. Organic Chemistry Portal.

CHAPTER 8

CONCLUSION AND FUTURE PROSPECTIVES

CHAPTER 8

8. Conclusion and Future Prospectives

8.1. Conclusion

Obesity has grown to epidemic proportions, as over 4 million people die each year because of being obese. There is a high risk of obesity and its associated comorbidities (type 2 diabetes, hypertension, ischemic heart disease, fatty liver disease, cancer, etc). For the management of obesity, proper diet and exercise are the available options. In some situations, obesity complications may go beyond a certain level wherein these options don't work. In such cases, pharmacotherapy will be the preferred choice along with exercise and diet modification. Currently, 6 therapeutic agents are approved for treating obesity. Among these targets PL inhibition being the peripheral target, is regarded as the safest one. Orlistat is the only USFDA-approved PL inhibitory drug for the long-term management of obesity, with unavoidable side effects including bloating, steatorrhea, faecal incontinence and oily stools. Recently, there are reports of some severe side effects such as hepatotoxicity, nephrotoxicity, pancreatitis, etc. on long-term treatment of orlistat. Due to life-threatening side effects of existing medications and scarcity of safe drugs, there is a need to develop newer anti-obesity drugs.

Due to the pharmacological diversity of natural products, it has always been an inspiration for research scientists for the identification of novel drugs. Many of the natural product-based analogues have been identified for PL inhibitory activity with various heterocyclic scaffolds, including indole, benzofuran, chromone/chromanone, etc. Vast literature is available on chromone-based natural PL inhibitors, however, there is no single report on synthetic chromone-based PL inhibitors with a rational design approach. To fill such a gap in PL inhibitory research, in this study, we have designed 3 unique series of chromone-based analogues for the potent inhibition of PL enzyme, with sequential optimization in each series to get chromone-based potent PL inhibitory lead, followed by the *in vivo* anti-obesity testing of the best potent analogue.

The preliminary design was started by the attachment of various pharmacophoric features required for binding at the active site cavity of PL. Mainly 3 fragments, including chromone (electron-rich heterocycle), acrylate fragment (nucleophilic fragment) and aromatic/heteroaromatic moiety were identified for the effective interactions with lid domain, catalytic triad and Arg256 amino acids. The prototype scaffold was designed by looking into the synthetic feasibility, followed by the validation through molecular docking studies. By

keeping the linker length as 1 carbon, various series I analogues were synthesized and screened for PL inhibitory activity. Among these **24** analogues **5ad** and **5am** were the most potent with IC_{50} values of 5.82 ± 0.933 and 5.16 ± 0.287 µM, respectively. Further, the fluorescence quenching and enzyme kinetics study revealed active site binding and competitive inhibition of the topmost analogue (**5am**). The molecular dynamics study also confirmed its stability at the PL active site under physiological dynamics conditions for 100 ns of simulation time.

To optimize series I analogues for better PL inhibitory potential, the linker length was increased to 2 carbon and 3 carbon. Through docking study, the prototype analogue with the linker length of 2 carbon atoms was found to interact efficiently with all the essential amino acids, with the MolDock score of -121.31 kcal/mol. On the other hand, the prototype analogue with 3 carbon linker exhibited good docking score of -128.2 kcal/mol but failed to interact with essential active site amino acids. Also, through *in vitro* results the 2 carbon linker was found to be efficient with analogue **6aa** (IC_{50} of 16.01 ± 0.274 µM) as compared with 3 carbon linker analogue **8aa** ($IC_{50} = 31.49 \pm 1.363$ µM). Hence by keeping 2 carbon linker, various analogues with different substituents on chromone and aromatic moiety were synthesized and screened for PL inhibitory activity. Among the **29** analogues of series II, **6fj** and **6gj** were found to exhibit potential PL inhibitory activities of 4.92 ± 1.398 and 4.23 ± 0.747 µM, respectively. Through molecular dynamics simulation study, the protein was found to deviate with maximum RMSD of 5 Å and ligand RMSD was found to deviate up to 6 Å till 60 ns, that was found to elevate from 60-100 ns. Such results explain moderate stability of the complex and hence further optimization will lead to better stability of the complex.

Finally, the 2 carbon linker was substituted with the additional phenyl ring and the oxo group for better aromatic and H-bonding interactions. Interestingly, the proposed prototype analogue **10aa** was found to bind at the active site more efficiently, as evidenced by the good MolDock score of -168.33 kcal/mol. With such positive results, series III containing **18** analogues with EDG, EWG and bulkier substituents was synthesized. A total of 6 analogues were found to exhibit IC_{50} values in the range of 1.24 - 2.76 µM. The analogue **10gb** was the most potent among all the series of analogues with IC_{50} of 1.24 ± 0.296 µM. **Figure 8.1** summarises the optimization from series I to get the best potent analogue **10gb** of series III. In molecular dynamics simulation of 10gb for 100 ns, the ligand RMSD was found to deviate

from 5-8 Å. Also, the protein molecule exhibited the RMSD value less than 4.5 Å. Such RMSD values are within the range, that proves the stability of the ligand-protein complex.

Further to understand the pharmacokinetics and toxicity pattern, the top analogues in each series, with a total of 6 analogues were subjected to *in silico* ADMET prediction using Swiss ADME and ProTox-2 web servers. Many of the analogues including topmost analogue **10gb** were devoid of any toxicities and also found to be metabolically stable. Analogue **10gb** was then tested for anti-obesity effects through an *in vivo* study utilizing the HFD-induced anti-obesity model on mice. Through OTTT analysis, doses of 10 mg/kg (LD) and 20 mg/kg (HD) of **10gb** were selected for the treatment of HFD-induced obese mice. After the 4-week treatment, the weight of treatment groups (**orlistat** and **10gb**) was lower than the DC group. Also, there was a normalization of spiked levels of triglycerides, total cholesterol and LDL cholesterol in the case of treatment groups. In addition to it, the triglyceride excretion caused by **10gb** was also proved through fecal triglyceride measurement, confirming its PL inhibitory action. After the histopathological examination of liver and adipose tissue, hepatic fibrosis and lipid accumulation with the increase in size of adipocytes were observed for DC group (HFD without treatment). Such changes were found to normalized in case of orlistat and **10gb** (HD) treatment groups. Such results proves equal effectivity of analogue **10gb** (10 mg/kg, 20 mg/kg) as orlistat (10 mg/kg) in the management of the obesity condition.

Overall, we conclude that the designed analogues have anti-obesity potential *via* PL inhibition.

5ad; R = 4-Nitro
IC$_{50}$ = 5.82 ± 0.933 μM

5am; R = 4-Benzyloxy
IC$_{50}$ = 5.16 ± 0.287 μM

6gj; R^1 = [*h*]benzo, R^2 = 4-Benzyloxy
IC$_{50}$ = 4.23 ± 0.747 μM

10ab; R = H
IC$_{50}$ = 1.49 ± 0.008 μM

10cb; R = 6-Bromo
IC$_{50}$ = 1.52 ± 0.136 μM

10fb; R = 6-Methoxy
IC$_{50}$ = 1.31 ± 0.309 μM

10gb; R = [*h*]benzo
IC$_{50}$ = 1.24 ± 0.296 μM
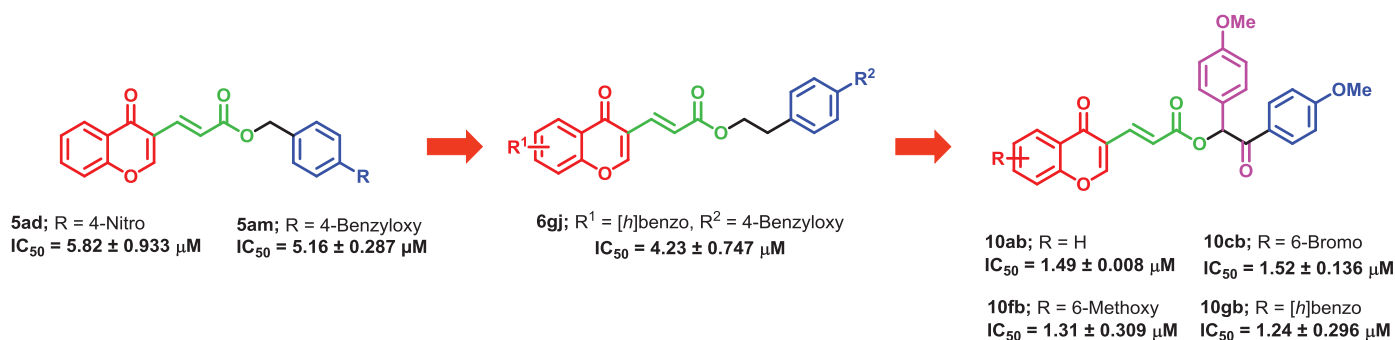
Figure 8.1. Summary of structural optimization to get the best potent PL inhibitors

8.2. Future Prospectives

In this study, chromone based analogues were designed for PL inhibitory potential. A total of 3 series with **71** structurally diverse analogues were synthesized and evaluated for PL inhibitory potential. The analogue **10gb** was found to exhibit potential activity with IC$_{50}$ of

1.24 ± 0.296 µM. **10gb** was also effective as an anti-obesity agent in the *in vivo* study. There are some future studies that can be performed:

- Commercial availability of fewer substituted benzoins has led to less exploration of the diphenyl ring system of the series III. Hence, different substituted benzoins (starting material) can be synthesized and used for synthesis of newer analogues.
- The chromone scaffold can be replaced by different heterocycles, that may lead to more potential PL inhibitors than **10gb**.
- The *in vivo* pharmacokinetic parameters and toxicities can also be determined through animal models.

APPENDICES

Appendix I

List of Publications

From Thesis Work:

- Auti, Prashant S., Sakshi Jagetiya, and Atish T. Paul. "Chromone-3-acrylic acid ester analogues: Design, synthesis and biological evaluation as potential pancreatic lipase inhibitors." *Journal of Molecular Structure* (2023): 136257. {**Journal Publication; Impact Factor: 3.8**}

- Auti, Prashant S. and Atish T. Paul. "Discovery of novel chromone and acrylate-based PL inhibitors: molecular modelling, synthesis, and *in vitro* evaluation for the treatment of obesity." Chemical Biology & Drug Design {**Journal Publication; Impact Factor: 3.0**}

- Auti, Prashant S., Sakshi Jagetiya, and Atish T. Paul. "Chromone Containing Hybrid Analogs: Synthesis and Applications in Medicinal Chemistry." *Chemistry & Biodiversity* (2023): e202300587. {**Journal Publication; Impact Factor: 2.9**}

- Atish T. Paul and Auti, Prashant S., "A pancreatic lipase inhibitor comprising chromone-3-acrylic acid ester analogues and method of preparing the same" filed at Indian Patent Office (Application No: 202311075941), dated 7th November 2023 {**Patent Application**}

From Project Work:

- Auti, Prashant S., Ginson George, and Atish T. Paul. "Recent advances in the pharmacological diversification of quinazoline/quinazolinone hybrids." *RSC advances* (2020): 41353-41392. {**Journal Publication; Impact Factor: 3.9**}

- Auti, Prashant S., Nandi, Arijit and Atish T. Paul. "Design, synthesis, biological evaluation and molecular modelling studies of oxoacetamide warhead containing indole-quinazolinone based novel hybrid analogues as potential pancreatic lipase inhibitors." *New Journal of Chemistry* (2022): 11648-11661. {**Journal Publication; Impact Factor: 3.3**}

- Nandi, A., Auti, P. S., Jagtap, U. A., & Paul, A. T. "Investigating the Role of Indole and Quinazolinone-Based Hybrid Analogues with Ketoamide Fragment and Alkyl Extension for Potential PL Inhibition." *Journal of Molecular Structure* (2023): 137337. {**Journal Publication; Impact Factor: 3.8**}

Appendix I

Other Publications:

- George, Ginson, Prashant S. Auti, and Atish T. Paul. "Design, synthesis, in silico molecular modelling studies and biological evaluation of novel indole-thiazolidinedione hybrid analogues as potential pancreatic lipase inhibitors." *New Journal of Chemistry* (2021): 1381-1394. {**Journal Publication; Impact Factor: 3.3**}

- George, Ginson, Prashant S. Auti, and Atish T. Paul. "Design, synthesis and biological evaluation of N-substituted indole-thiazolidinedione analogues as potential pancreatic lipase inhibitors." Chemical Biology & Drug Design (2021): 49-59. {**Journal Publication; Impact Factor: 3.0**}

- George, Ginson, Yadav, Nisha, Prashant S. Auti, and Atish T. Paul. "Molecular modelling, synthesis and in vitro evaluation of quinazolinone hybrid analogues as potential pancreatic lipase inhibitors." Journal of Biomolecular Structure and Dynamics (2023): 9583-9601. {**Journal Publication; Impact Factor: 5.2**}

- Paul, A. T., George, G., Yadav, N., Jeswani, A., & Auti, P. S. "Pharmaceutical Application of Bio-actives from Alstonia Genus: Current Findings and Future Directions." Bioactive Natural Products for Pharmaceutical Applications (2021): 463-533. {**Book chapter**}

- Yadav, N., Auti, P., George, G., & Paul, A. T. "Design, synthesis and biological evaluation of O-alkyl umbelliferone derivatives as pancreatic lipase inhibitors." *J. Indian Chem. Soc* (2020): 1265-1271. {**Journal Publication; Impact Factor: 0.2**}

- Jagetiya, Sakshi, Prashant S. Auti, and Atish T. Paul. "Design, Synthesis, Molecular Modelling and in Vitro Evaluation of Indolyl Ketohydrazide-Hydrazone Analogs as Potential Pancreatic Lipase Inhibitors." *Chemistry & Biodiversity* (2023): e202301154. {**Journal Publication; Impact Factor: 2.9**}

- George, G., Auti, P. S., Sengupta, P., & Paul, A. T. "Design and Synthesis of Echitamine-inspired Hybrid Analogues Containing Thiazolidinediones as Potential Pancreatic Lipase Inhibitors." *Letters in Drug Design & Discovery* (2022): 956-968. {**Journal Publication; Impact Factor: 1.0**}

BRIEF BIOGRAPHY OF THE SUPERVISOR

Dr. Paul Atish Tulshiram is Associate Professor & Ex-Head (Department of Pharmacy). He completed his bachelor's in pharmacy from University of Pune (Maharashtra). He pursued M.S. (Pharmaceutical Sciences) and Ph.D. in Natural Products from National Institute of Pharmaceutical Education and Research (NIPER, S.A.S Nagar, Punjab). After completion of his doctorate, he joined the research group of Prof. Ikhlas Khan as Postdoctoral Research Associate at the National Center for Natural Product Research (University of Mississippi, USA). His current research interest is identification of pancreatic lipase inhibitory natural products and synthesis of their inspired analogues for obesity management. He has 03 ongoing research grants from agencies such as, DST (SEED), DBT, and Industry etc. and has completed 03 government and 01 industry projects. He has published 69 research articles in reputed international journals and has also contributed 24 official monographs on polyherbal formulations in The Ayurvedic Pharmacopoeia of India. He has guided 5 doctoral students and is currently supervising 8 doctoral candidates. He is a reviewer for various journals of reputed publishers such as ACS, Elsevier, Wiley, etc., and also for funding agencies such as DST-SERB and the South African Medical Research Council. He is also member of Standing committee [Chemical group] for FSSAI, New Delhi.

Appendix II

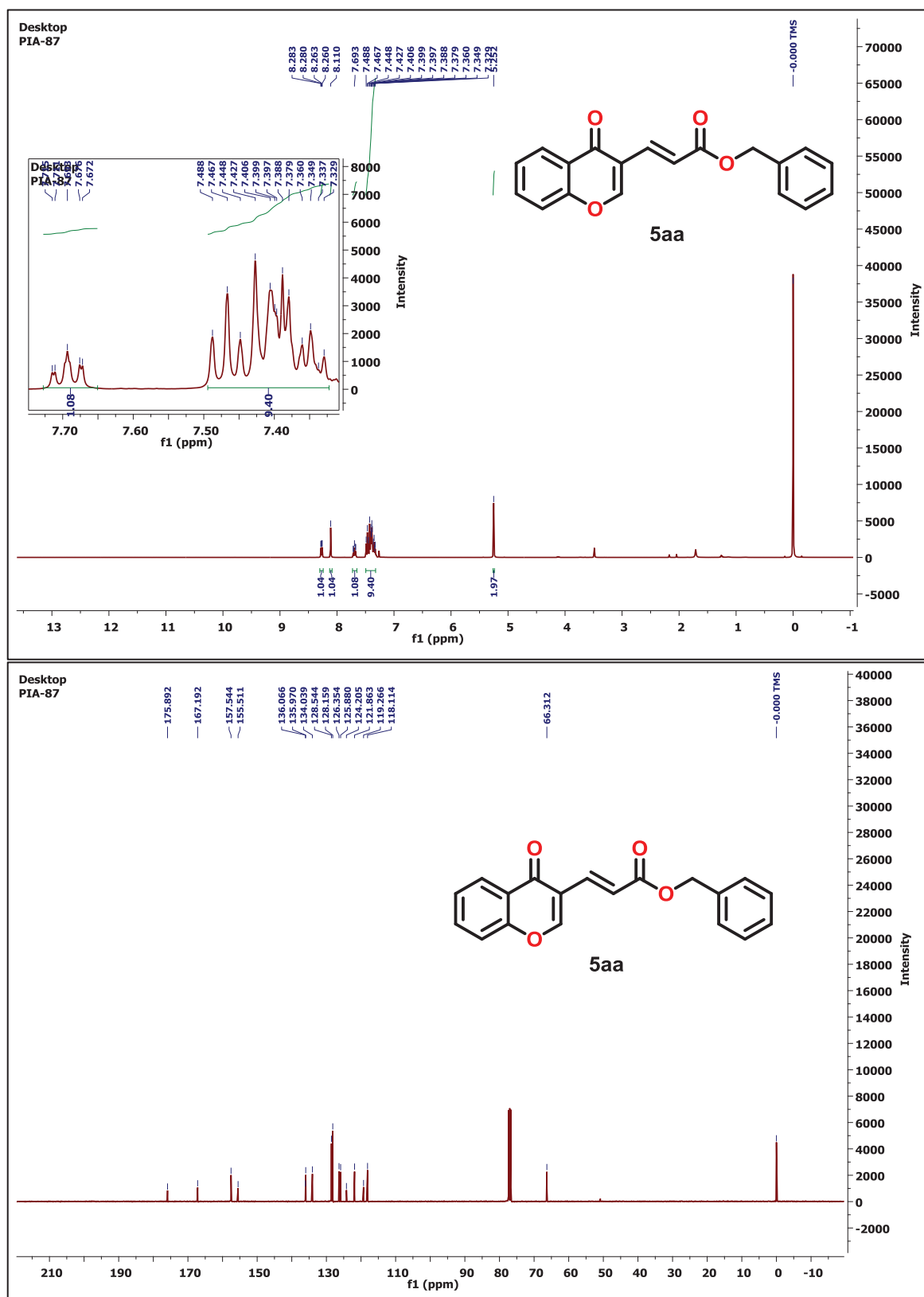**BRIEF BIOGRAPHY OF THE CANDIDATE**

Prashant Auti is pursuing Ph.D. degree in Pharmaceutical Chemistry from Birla Institute of Technology and Sciences, Pilani (BITS Pilani), Pilani campus, Rajasthan, India. He has completed B.Pharmacy in 2017, from Oriental College of Pharmacy, Maharashtra. He completed his M.S. (Pharm.) in Medicinal Chemistry with a gold medal from the National Institute of Pharmaceutical Education and Research, Ahmedabad (NIPER-A) 2019. In M.S., he has worked in the field of C-H activation under the guidance of Dr. Satyasheel Sharma, Assistant professor, NIPER-A. He joined Ph.D. programme at BITS Pilani, Pilani Campus, under the supervision of Dr. Atish Tulshiram Paul, Associate Professor, Department of Pharmacy, BITS Pilani, Pilani Campus in the year 2019. He is availing prestigious INSPIRE fellowship from the Department of Science & Technology, New Delhi. His research interest includes the use of molecular modelling tools in the design of analogues for the treatment of metabolic disorders. He has published several articles in peer reviewed journals. Apart from this, some of his works are filed for patent applications.
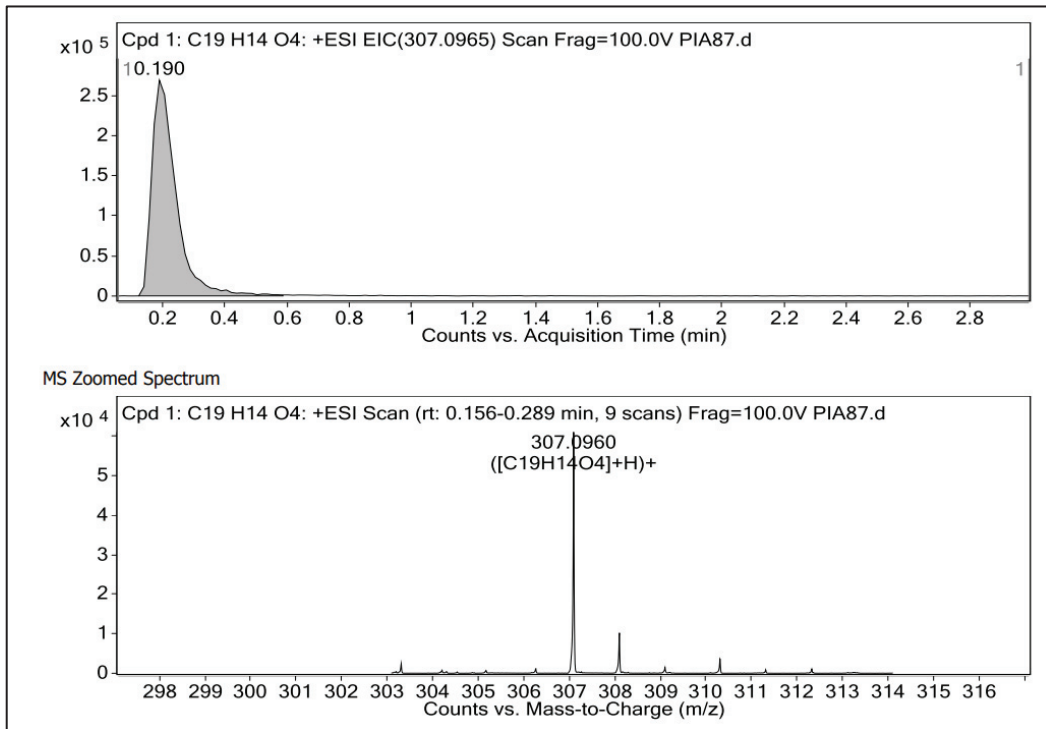
Representative NMR, HRMS Spectra and HPLC Chromatogram:

5aa: ^{1}H and ^{13}C NMR Spectra

5aa: HRMS Spectra

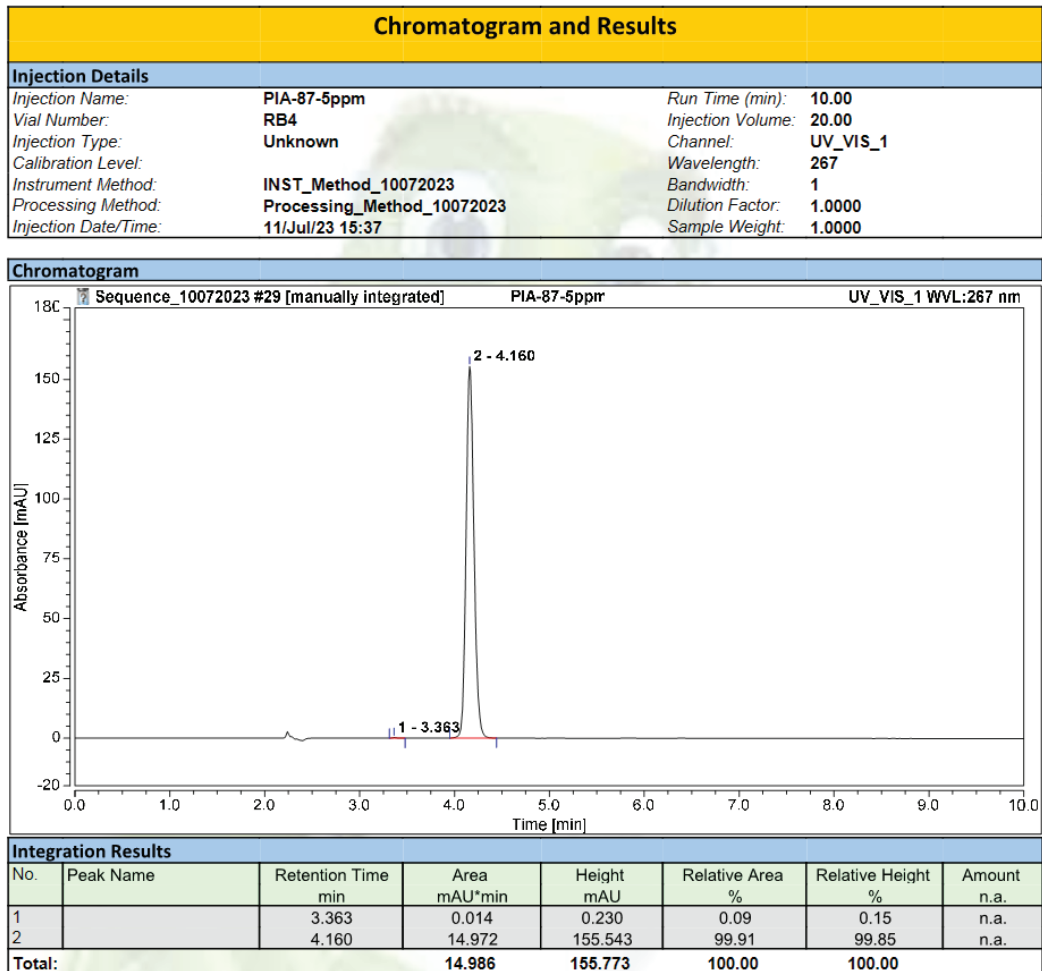Cpd 1: C19 H14 O4: +ESI EIC(307.0965) Scan Frag=100.0V PIA87.d

10.190

Counts vs. Acquisition Time (min)

MS Zoomed Spectrum

Cpd 1: C19 H14 O4: +ESI Scan (rt: 0.156-0.289 min, 9 scans) Frag=100.0V PIA87.d

307.0960
([C19H14O4]+H)+

Counts vs. Mass-to-Charge (m/z)

5aa: HPLC Chromatogram

Chromatogram and Results			
Injection Details			
Injection Name:	PIA-87-5ppm	Run Time (min):	10.00
Vial Number:	RB4	Injection Volume:	20.00
Injection Type:	Unknown	Channel:	UV_VIS_1
Calibration Level:		Wavelength:	267
Instrument Method:	INST_Method_10072023	Bandwidth:	1
Processing Method:	Processing_Method_10072023	Dilution Factor:	1.0000
Injection Date/Time:	11/Jul/23 15:37	Sample Weight:	1.0000

Chromatogram

Sequence_10072023 #29 [manually integrated]   PIA-87-5ppm   UV_VIS_1 WVL:267 nm

2 - 4.160

1 - 3.363

Time [min]

Integration Results

No.	Peak Name	Retention Time min	Area mAU*min	Height mAU	Relative Area %	Relative Height %	Amount n.a.
1		3.363	0.014	0.230	0.09	0.15	n.a.
2		4.160	14.972	155.543	99.91	99.85	n.a.
Total:			14.986	155.773	100.00	100.00	

Appendix III

6aa: ^{1}H and ^{13}C NMR Spectra
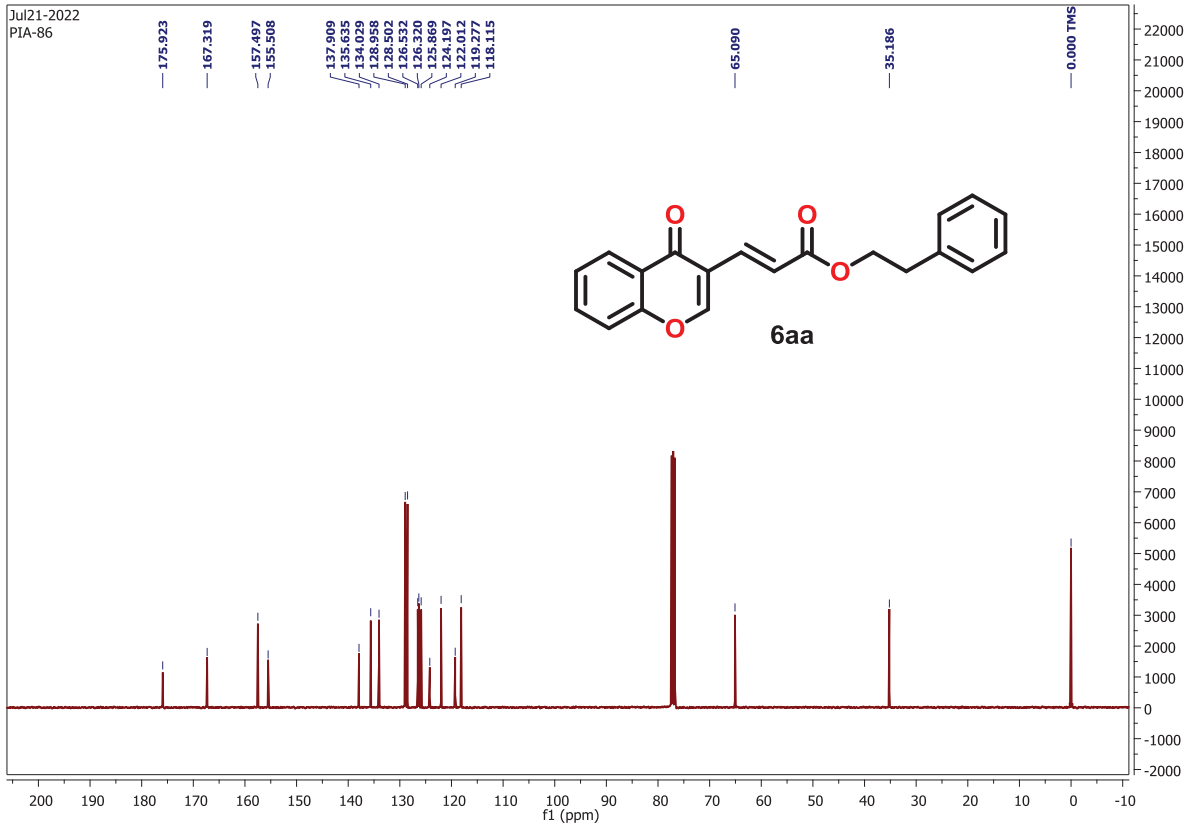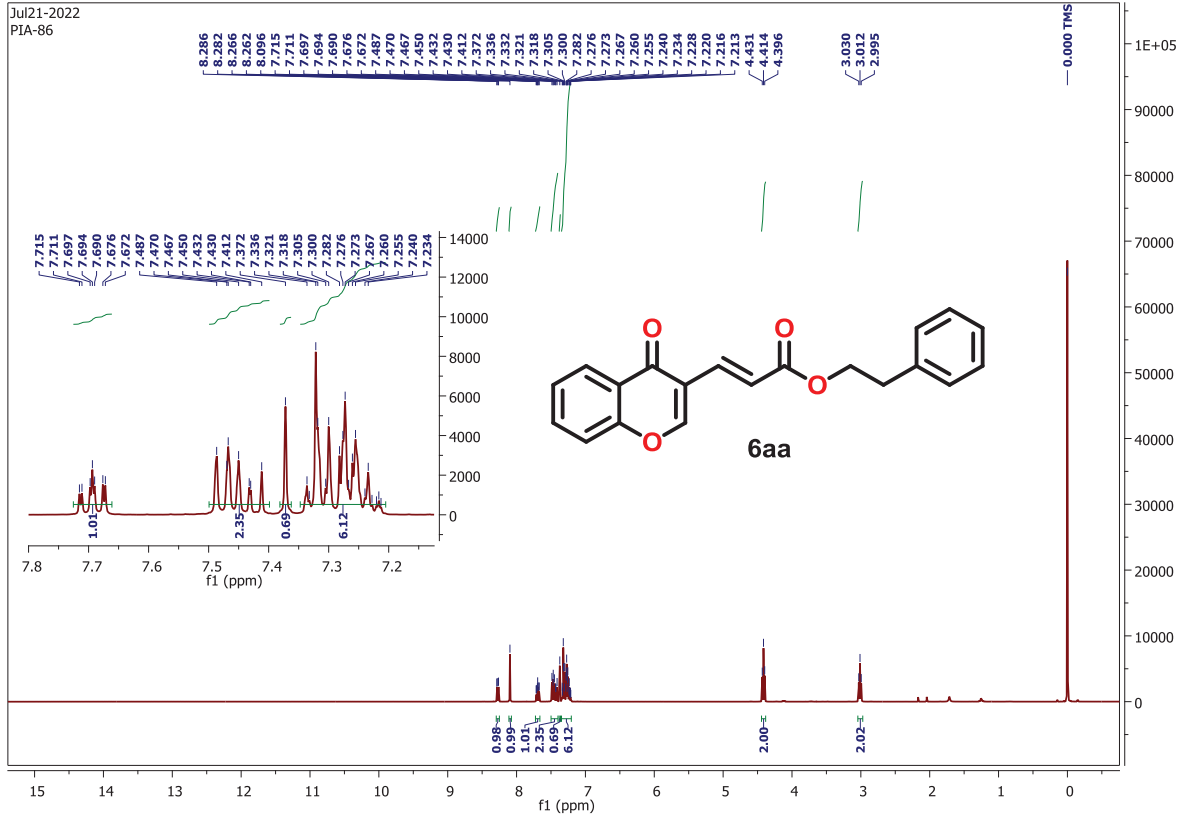
Appendix III

6aa: HRMS Spectra

Cpd 1: C20 H16 O4: +ESI EIC(321.1121, 343.0941) Scan Frag=100.0V PIA-86.d

MS Zoomed Spectrum

Cpd 1: C20 H16 O4: +ESI Scan (rt: 0.172-0.321 min, 10 scans) Frag=100.0V PIA-86.d

321.1115
([C20H16O4]+H)+

343.0927
([C20H16O4]+Na)+

6aa: HPLC Chromatogram

Chromatogram and Results

Injection Details

Injection Name:	PIA-86	Run Time (min):	15.00
Vial Number:	RE1	Injection Volume:	20.00
Injection Type:	Unknown	Channel:	UV_VIS_1
Calibration Level:		Wavelength:	267
Instrument Method:	INST_Method_10072023	Bandwidth:	1
Processing Method:	Processing_Method_10072023	Dilution Factor:	1.0000
Injection Date/Time:	13/Jul/23 14:50	Sample Weight:	1.0000

Chromatogram

Integration Results

No.	Peak Name	Retention Time min	Area mAU*min	Height mAU	Relative Area %	Relative Height %	Amount n.a.
1		2.237	0.093	1.198	0.31	0.42	n.a.
2		3.317	0.032	0.262	0.11	0.09	n.a.
3		4.590	29.716	284.439	99.58	99.49	n.a.
Total:			29.841	285.899	100.00	100.00	

A8

10ab: ^{1}H and ^{13}C NMR Spectra

Appendix III

10ab: HRMS Spectra

Cpd 1: C28 H22 O7: -ESI EIC(505.1060, 507.1044) Scan Frag=175.0V PIA-262.d

MS Zoomed Spectrum

Cpd 1: C28 H22 O7: -ESI Scan (rt: 0.165, 0.181, 0.198, 0.214 ... min, 7 scans) Frag=175.0V PIA-2...

505.1058
([C28H22O7]+Cl)-

507.1054
([C28H22O7]+Cl)-
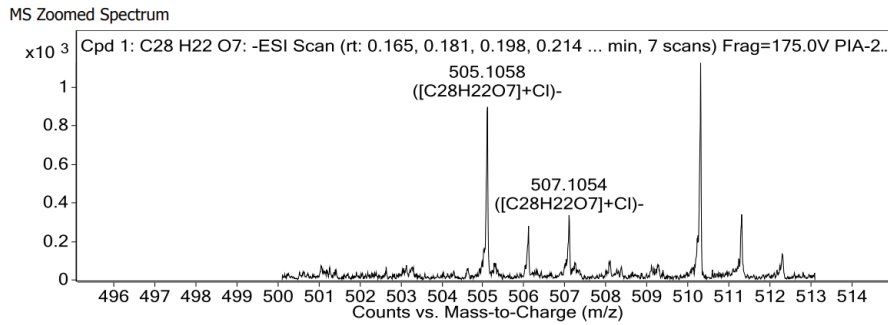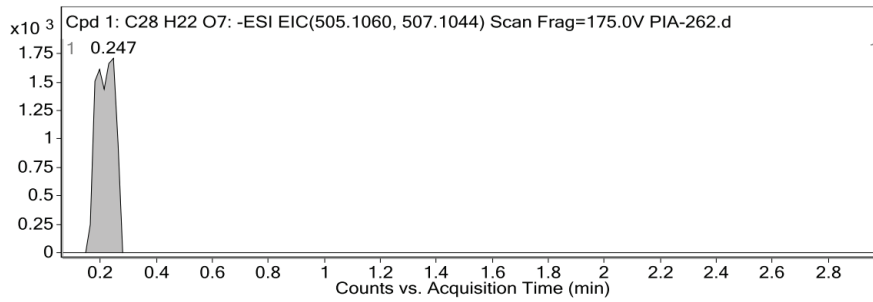
10ab: HPLC Chromatogram

Chromatogram and Results				

Injection Details

Injection Name:	PIA-262		Run Time (min):	15.00
Vial Number:	GA7		Injection Volume:	20.00
Injection Type:	Unknown		Channel:	UV_VIS_1
Calibration Level:			Wavelength:	262
Instrument Method:	10-02-2023		Bandwidth:	1
Processing Method:	Processing Method_Prash_10-02-2023		Dilution Factor:	1.0000
Injection Date/Time:	02/Oct/23 14:55		Sample Weight:	1.0000
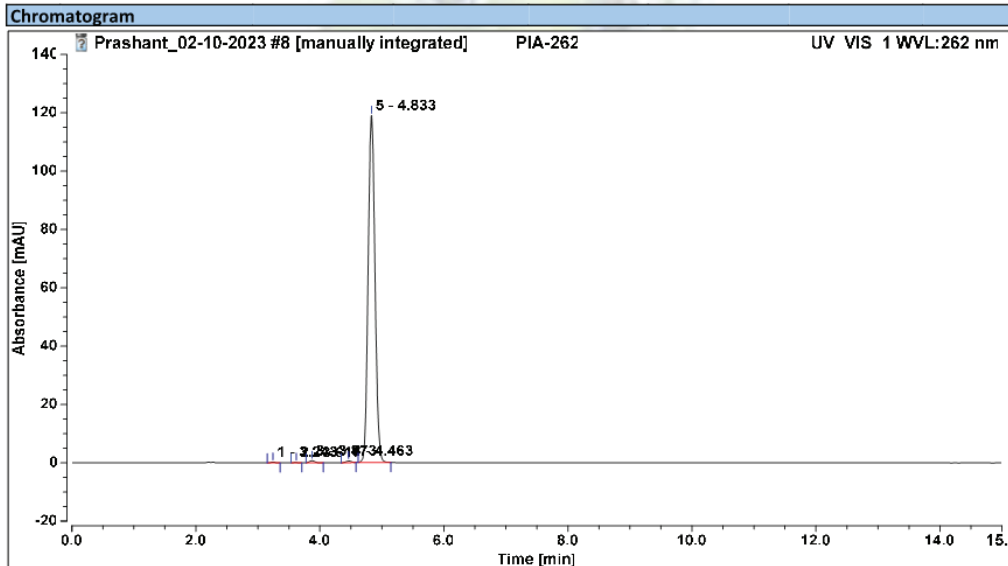
Chromatogram

Prashant_02-10-2023 #8 [manually integrated]   PIA-262   UV VIS 1 WVL:262 nm

5 - 4.833

Integration Results

No.	Peak Name	Retention Time min	Area mAU*min	Height mAU	Relative Area %	Relative Height %	Amount n.a.
1		3.243	0.019	0.231	0.13	0.19	n.a.
2		3.617	0.008	0.108	0.05	0.09	n.a.
3		3.873	0.071	0.736	0.46	0.61	n.a.
4		4.463	0.063	0.607	0.41	0.50	n.a.
5		4.833	15.127	119.006	98.94	98.61	n.a.
Total:			15.288	120.688	100.00	100.00	